

https://dspace.org/

Synthesis and characterisation of novel [PtII(phen)(Ln-S)2] complexes: exploring rare monodentate coordination of disubstituted acylthioureato ligands

Kangara, Edmore F.

2019

https://hdl.handle.net/10539/29474

Kangara Edmore Farayi (2019) Synthesis and characterisation of novel [PtII(phen)(Ln-kS)2] complexes:exploring rare monodentate coordination of disubstituted acylthiourea ligands, University of the Witwatersrand, Johannesburg, <http://hdl.handle.net/10539/29474>

Downloaded from a DSpace repository. https://dspace.org/

Synthesis and characterisation of novel $[Pt^{II}(phen)(L^{n}\text{-}\kappa S)_2]$ complexes: Exploring rare monodentate coordination of disubstituted acylthioureato ligands

A thesis submitted to the Faculty of Science, University of the Witwatersrand, Johannesburg, in fulfilment of the requirements for the degree of Doctor of Philosophy

By

Edmore F. Kangara

Student number:

751691

Supervised by:

Dr I A. Kotzé

Co-supervised by:

Dr J L. van Wyk

Prof. D C. Levendis

October 2019



WITS UNIVERSITY

Molecular Sciences Institute, School of Chemistry

University of the Witwatersrand

Private Bag 3, Wits, 2050

South Africa

Declaration

I, **Edmore F. Kangara**, declare that:

1. The research in this thesis, except where otherwise stated, is my original research.
2. This thesis has not been submitted for any degree or examination at other universities.
3. This thesis does not contain any other persons' data unless expressly acknowledged as being sourced from them.
4. This thesis does not contain any other persons' writing unless explicitly acknowledged as being sourced from other researchers.
5. This thesis does not contain text or graphics from the internet copied and pasted unless explicitly acknowledged, and the source being detailed in the thesis and the references section.

Edmore F. Kangara _  __ Edmore Farayi Kangara

Date 27/10/2019

Supervisor certification

This is to certify that this research is a record of original work carried out by **Edmore Farayi Kangara** under my supervision in the Coordination Chemistry Research laboratory of the School of Chemistry, at the University of the Witwatersrand in fulfilment of the requirements for the award of Doctor of Philosophy degree in Chemistry.

Supervisor _____ _____ Date__28/10/2019____

Dr Izak A. Kotzé

PhD (Stellenbosch University)

Dedication

I would like to dedicate this thesis to;

My late parents, Bothwell Kangara and Josephine Mapondera, for the love of science you instilled in me from birth,

My late grandmother (ambuya Maja) for being both father and mother to me and my siblings when our parents were taken away from us early in their lives. Your utmost trust, love and motivation inspired me to give my very best in everything I do,

My siblings: Christian and Wonderful, for their prayers, immense support and encouragement.

The good Lord never lets you down

Acknowledgements

Firstly, I would like to acknowledge, The Most-High, King of kings, God whose help, presence, guidance and mercies saw me through my studies at the University of the Witwatersrand and beyond.

My appreciation goes to my Supervisor, Dr Izak A. Kotzé, for the opportunity and privilege to work in his research area. I seize this opportunity to say, “Sir, I am extremely indebted to you”. I would also want to express my gratitude to my co-supervisors, Dr Juanita L. van Wyk and Professor Demetrius C. Levendis for their time, valued expertise and financial support. Special thanks go to the National Research Foundation (NRF) for the supervisor-linked bursary support system, and the University of the Witwatersrand, my Institution, which anchored the funding body and supplemented the funding for the period of study. Special recognition goes to Mr. Bill Dixon and my workmates at Battery Centre Kempton Park for the time you allowed me to work part-time to supplement my finances.

This medium also serves to acknowledge all members of staff of the School of Chemistry, at the University of the Witwatersrand. I also appreciate my colleagues in Coordination Chemistry Research (CCR) group. I am indebted to Professor Manuel Fernandes and Mr. Delbert Botes from the Structural Chemistry group at Gate House at the University of the Witwatersrand for their expertise and support in running and solving crystal structures of my complexes. An exceptional thank you to Dr Leonie Harmse and Miss Tebogo Peega from the Department of Pharmacy and Pharmacology, School of Therapeutic Sciences also at the University of the Witwatersrand for their help with preliminary antiproliferative studies.

I want to thank my wife for always standing by me, my siblings for your prayers, love and motivation. The good God almighty will continue to bless you. Lastly, I would like to appreciate my late father, mother, ambuya Maja and uncle (Brighton “Nodza” Kangara) by saying “Your sweat was not in vain. I would have loved you to see this research through with me; however, it was not to be, may your souls rest in eternal peace.”

List of publications and presentations

Publications

- Kangara, E.F., Peega, T., Harmse, L., van Wyk, J.L., Levendis, D.C. and Kotzé, I.A., **2019**. Conformational analysis and potential anticancer activity of [Pt(phen)(L^1-κ*S*)$_2$] studied by single-crystal X-ray diffraction and variable temperature ^{1}H and ^{195}Pt NMR spectroscopy. *New Journal of Chemistry*, 43(9), pp.3665-3672. (**front cover feature**)
- Kotzé, I.A., Smith, V.J., Kangara, E.F. and Koch, K.R., **2017**. Rare, hypodentate L-κ*S* coordination mode of *N*, *N*-dialkyl-*N*′-aroylthioureas leads to unprecedented mixed-ligand [Pt (phen)(L-κ*S*)$_2$] complexes. *New Journal of Chemistry*, 41(24), pp.14995-15002.

Presentations

- Oral presentation, "Synthesis and characterisation of novel [Pt^{II}(diimine)(acylthiourea)$_2$] complexes: Exploring the unusual monodentate coordination of monoanionic dialkyl - acylthiourea ligands." Wits-Sasol Academic Day, University of the Witwatersrand, Johannesburg, South Africa, 12th August 2016.
- Poster presentation, "Synthesis and characterisation of novel [Pt^{II}(phen)(ATU)$_2$] complexes: Exploring rare monodentate coordination of disubstituted acylthioureato (ATU) ligands." SACI Inorganic 2017 Conference, Cape Town, South Africa, 25-29th June 2017.
- Poster presentation, "Synthesis and characterisation of novel [Pt^{II}(phen)(L^n-κ*S*)$_2$] complexes: Exploring rare monodentate coordination of disubstituted acylthioureato (L^n) ligands." 43rd International Conference on Coordination Chemistry 2018 (ICCC 2018), Sendai, Japan, 30th July - 4th August 2018.

Abstract

This thesis describes a study directed towards the synthesis and full characterization of novel [Pt(phen)(L^n-κ*S*)$_2$] complexes where disubstituted acylthioureato ligands (**L^n**), (also referred herein as *N*,*N*-di(alkyl/aryl)-*N*'-acylthioureato ligands), coordinate to the platinum(II) metal centre in a monodentate fashion through the sulfur donor atom and establishing the driving factors behind this rare coordination mode. The study included a systematically chosen ligand library where the ligands varied mainly on the electronic influence of acyl substituents balanced with minor steric variations on the amino end of the ligand.

[Pt(phen)(L^n-κ*S*)$_2$] complexes were synthesized in excellent yields via a stepwise method where the ligands were first deprotonated using sodium hydride in anhydrous THF and subsequently reacting the resultant solvated salts with the [$PtCl_2$(phen)] precursor under reflux for one hour in a 1:2.2 (precursor/ligand) stoichiometric ratio. The complexes were characterised using FT-IR (ATR) spectroscopy, ^{1}H- and ^{13}C NMR spectroscopy, high-resolution mass spectrometry, UV-vis spectrophotometry, elemental analysis, and single-crystal X-ray diffraction. The complexes were also probed for their solution conformations in correlation with the solid-state structures obtained through single-crystal X-ray diffraction using variable temperature ^{1}H- and ^{195}Pt NMR spectroscopy in order to gain insight into the persistence of intramolecular π-π stacking interactions in solution as a stabilising factor directing the monodentate coordination. This study showed that [Pt(phen)(L^n-κ*S*)$_2$] complexes with acylthioureato ligands bearing aromatic acyl substituents could at least exist in three conformations while complexes with acylthioureato ligands that have non-aromatic acyl substituents could only have one structural conformation at -50 ° C. However, there is no conclusive evidence of the intramolecular π-π stacking interactions in solution at ambient and higher temperatures.

Investigations into whether the electronic effects of acyl substituents could influence the nucleophilicity of the other donor sites in the ligands, particularly oxygen, enough to render their reactivity towards platinum(II) ions more preferable was done using conceptual DFT. The study showed that the sulfur donor atom was tenfold more nucleophilic than any other donor atom in the acylthioureato ligands regardless of acyl substituents making it the most probable site to coordinate with platinum(II) ions.

Mechanistic insights into how the reaction proceeded were probed through a series of individual experiments that involved the metal precursor, the ligands, the [Pt(phen)(L^n-κ*S*)$_2$] complexes, the by-product [Pt(phen)(L^n-κ*O*,*S*)]$^+$ complexes and acids of different degrees of acidity. These experiments showed that the synthetic reaction proceeded most likely *via* solvolysis of the precursor resulting in a solvento complex and subsequent anation of the solvento complex with disubstituted acylthioureato

anions to get [Pt(phen)(L^n-κ*S*)$_2$]. [Pt(phen)(L^n-κ*S*)$_2$] could also be obtained by reacting the cationic by-product [Pt(phen)(L^n-κ*O*,*S*)]$^+$ with the ligand after deprotonation with base. It was also shown that the [Pt(phen)(L^n-κ*S*)$_2$] complexes dissociated under different acids resulting in different dissociation products *via* protonation-anation reactions. The nature of the dissociation products depended on the strength of the acid and the coordinating properties of the acids' conjugate bases. This coordination mode could be extrapolated to include platinum(II) complexes bearing other co-ligands like bipyridine and triphenylphosphine, however in medium to low yields.

A pilot study into the potential antiproliferative activity of [Pt(phen)(L^1-κ*S*)$_2$] and [Pt(phen)(L^2-κ*S*)$_2$] (where L^1 = *N*,*N*-di(ethyl)-*N*'-(1-naphthoylthioureato) and L^2 = *N*,*N*-di(butyl)-*N*'-(1-naphthoylthioureato) anions) against an A549 lung cancer line showed that these complexes are very active with IC_{50} values of 6.4 ± 0.9 and 2.4 ± 0.3 μM respectively, killing cancer cells *via* apoptosis. This study also revealed that these complexes could potentially interact with DNA as a major groove binder.

The knowledge obtained through this study should contribute to the fundamental understanding of the coordination chemistry of disubstituted acylthiourea ligands, chemical and physical properties of various platinum(II) complexes bearing disubstituted acylthiourea ligands coordinated in a monodentate fashion and explore possible applications in the fight against cancer.

Keywords: Disubstituted acylthioureato, Monodentate coordination, Platinum(II), Phenanthroline, Conformational analysis, Antiproliferative, Variable temperature-NMR, X-ray crystallography, Conceptual DFT

Table of Contents

Declaration.....ii

Supervisor Certification.....iii

Dedication.....iv

Acknowledgements.....v

List of Publications.....vi

Abstract.....vii

Table of Contents.....ix

List if Figures and Schemes.....xiii

List if Tables.....xix

Abbreviations.....xx

Chapter 1. ***Background and Context for the monodentate coordination of N,N-di(alkyl/aryl)-N'-acylthioureato ligands in [Pt(phen)(L^n-κS)$_2$] complexes***

1.1. Acylthiourea ligands.....1

1.1.1. Coordination chemistry of acylthiourea ligands.....3

1.1.2. Coordination behaviour of analogous compounds to acylthiourea ligands.....6

1.2. Platinum complexes in cancer therapy.....7

1.2.1. Biologically active platinum(II)-acylthiourea complexes.....8

1.3. Drug–DNA binding interaction modes.....9

1.3.1. Covalent drug–DNA binding.....9

1.3.2. Non-covalent drug–DNA binding.....10

1.4. Aims of this thesis.....13

1.4.1. Objectives.....13

1.5. Outline of this thesis.....13

1.6. References.....15

Chapter 2. ***Ligand and Complex Synthesis, Characterization and Experimental***

2.1. Introduction 19

2.2. Results and Discussion 21

2.2.1. Synthesis of *N*,*N*-di(alkyl/aryl)-*N*'-acylthiourea (HL^n) ligands 21

2.2.2. Synthesis of the $[PtCl_2(phen)]$ precursor 26

2.2.3. Synthesis of the $[Pt(phen)(L^n\text{-}\kappa S)_2]$ complexes 27

2.2.4. Single crystal X-ray crystallographic analysis of $[Pt(phen)(L^n\text{-}\kappa S)_2]$ complexes 33

(a) Crystal structure of *bis*(*N*,*N*-diethyl-*N*'-pivaloylthioureato-κ*S*)-phenanthrolineplatinum, water solvate, $[Pt(phen)(L^7\text{-}\kappa S)_2]$ (**7**) 34

(b) Crystal structure of *bis*(*N*,*N*-diethyl-*N*'-benzoylthioureato-κ*S*)-phenanthrolineplatinum, ethanol/water solvate, $[Pt(phen)(L^3\text{-}\kappa S)_2]$ (**3**) 36

(c) Crystal structure of *bis*(*N*,*N*-diethyl-*N*'-(4-chlorobenzoylthioureato)-κ*S*)-phenanthrolineplatinum, $[Pt(phen)(L^{12}\text{-}\kappa S)_2]$ (**12**) 38

(d) Crystal structure of *bis*(*N*,*N*-diethyl-*N*'-(1-naphthoylthioureato)-κ*S*)-phenanthrolineplatinum, $[Pt(phen)(L^1\text{-}\kappa S)_2]$ (**1**) 40

2.3. Conclusion 43

2.4. Experimental 44

2.4.1. General procedure for the synthesis of *N*,*N*-di(alky/aryl)-*N*'-acylthiourea ligands 45

(a) Synthesis of *N*,*N*-di(butyl)-*N*'-acetylthiourea (**HL^6**) and *N*,*N*-di(ethyl)-*N*'-(trichloro-acetylthiourea) (**HL^9**) 45

2.4.2. Synthesis of the $[PtCl_2(phen)]$ precursor complex 49

2.4.3. General procedure for the synthesis of $[Pt(phen)(L^n\text{-}\kappa S)_2]$ complexes 49

2.5. References 54

Chapter 3. ***Solution conformational analysis of $[Pt(phen)(L^n\text{-}\kappa S)_2]$ complexes, theoretical and experimental rationale into the monodentate coordination of N,N-di(alkyl/aryl)-N'-acylthioureato ligands***

3.1. Introduction 56

3.2. Results and Discussion 59

3.2.1. Solution-state conformational analysis of [Pt(phen)(L^n-κ*S*)$_2$] complexes using variable temperature ^{1}H and ^{195}Pt NMR spectroscopy 59

3.2.2. Investigation of the reactivity of O, N, N' and S donor sites in disubstituted acylthioureato ligands towards platinum(II) using conceptual DFT 65

3.2.3. Mechanistic insights into the monodentate coordination of disubstituted acylthioureato ligands in [Pt(phen)(L^n-κ*S*)$_2$] complexes 67

(a) Solvolysis of the [$PtCl_2$(phen)] precursor 67

(b) Reactions of neutral disubstituted acylthiourea ligands with [$PtCl_2$(phen)] in methanol of varying degrees of water wetness 69

(c) Interconversion between [Pt(phen)(L^n-κ*S*)$_2$] and [Pt(phen)(L^n-κ*O*,*S*)]$^+$ 71

3.2.4. Stepwise synthesis of the [Pt(phen)(L^n-κ*S*)$_2$] complexes using sodium hydride as base .. 74

3.2.5. Extrapolation of the monodentate coordination into complexes with different co-ligands or metal centres 75

3.3. Conclusion 78

3.4. Experimental 80

3.5. References 81

Chapter 4. ***Antiproliferation activity of [Pt(phen)(L^1-κ*S*)$_2$] and [Pt(phen)(L^2-κ*S*)$_2$] complexes***

4.1. Introduction 84

4.2. Results and discussion 86

4.2.1. Cell viability study 86

4.2.2. Morphological study 87

4.2.3. Molecular docking study 88

4.3. Conclusion 90

4.4. Experimental 91

4.4.1. Materials 91

4.4.2. Methodology 92

(a) Cell culture preparation and in vitro antiproliferative assays 92

(b) Cell morphology study 92

4.5. References 93

Chapter 5. *Conclusion*

5.1. Monodentate coordination chemistry of *N*,*N*-di(alkyl/aryl)-*N*'-acylthioureato ligands towards platinum(II) ions 95

5.2. Evaluation of the antiproliferative activity of [Pt(phen)(L^1-κ*S*)$_2$] and [Pt(phen)(L^2-κ*S*)$_2$] 98

5.3. Future Prospects 98

Supplementary Information

Appendix 1. ^{1}H-NMR and FT-IR spectroscopy data for [Pt(phen)(L^n-κ*S*)$_2$] complexes 100

Appendix 2. Uv-vis spectrophotometry and MS data for [Pt(phen)(L^n-κ*S*)$_2$] complexes 114

Appendix 3. Single crystal X-ray diffraction data for [Pt(phen)(L^n-κ*S*)$_2$] complexes 122

List of Figures and Schemes

Chapter 1

Figure 1: The structure of Thiourea depicting atom numbering according to the systematic nomenclature of organic chemistry. 1

Figure 2: Acylthiourea ligand system showing different degrees of substitution on the amino terminus. 2

Figure 3: General acylthiourea structures illustrating the most stable conformations of monosubstituted and disubstituted acylthiourea ligands. 2

Figure 4: Major coordination modes exhibited by disubstituted acylthiourea ligands. 4

Figure 5: Example of (i) neutral (water-insoluble) and (ii) cationic (water-soluble) platinum(II) complexes in which mono-anionic disubstituted acylthioureato ligands coordinate in a bidentate fashion. 4

Figure 6: Selected examples of a neutral disubstituted acylthiourea ligand coordinating in a monodentate and bidentate fashion with transition metal ions. 5

Figure 7: Monodentate coordination of monoanionic disubstituted acylthioureato ligands in bridged dimeric Cu(II) complexes. 5

Figure 8: Structural analogues of disubstituted acylthiourea ligands having a matching and a mismatch of chalcogen donor atoms. 6

Figure 9: Illustration of the delocalisation of the negative charge in 1,3-dichalcogenate and dichalcogenoimido-diphosphinate anions after deprotonation. 6

Figure 10: Monodentate coordination of 1,3-dichalcogenato and dichalcogenoimido-diphosphinato ligands. 7

Figure 11: Structures of clinically approved platinum(II) anticancer drugs. 8

Figure 12: Cisplatin mechanism of action from cellular uptake, aquation and ultimately to the interaction with DNA. 10

Figure 13: Chemical structures of some typical platinum(II) DNA intercalators. 11

Figure 14: Graphic illustration of DNA's major and minor grooves (with the red and green threads running in the major and minor grooves, respectively). 11

Figure 15: Structures of some metal complexes that interact with DNA via groove binding. 12

Chapter 2

Figure 1: Structures of ligands synthesised showing significant variations on the acyl substituents and minor variations on the amino end of the ligands. 23

Figure 2: ^{1}H-NMR spectrum of HL^3 in chloroform-*d* at 25°C assigned as per the numbering scheme indicated. 24

Figure 3: The COSY spectrum for HL^3 in chloroform-*d* at 25°C. 24

Figure 4: ^{13}C-Nmr spectrum for HL^3 in chloroform-*d* at 25°C with complete assignments and numbering scheme. 25

Figure 5: ^{1}H-NMR spectrum of $[PtCl_2(phen)]$ in DMSO-*d* at 25°C. 26

Figure 6: Stacked ^{1}H-NMR spectra (aromatic region) of the reaction mixture aliquots taken at different times during the reaction between *N*,*N*-di(ethyl)-*N*'-benzoylthiourea and $[PtCl_2(phen)]$ and recorded in chloroform-*d* at 25°C. 28

Figure 7: Stacked ^{1}H-NMR spectra (aromatic region) of the reaction mixture aliquots taken at different times during the reaction between *N*,*N*-di(ethyl)-*N*'-pivaloylthiourea and $[PtCl_2(phen)]$ and recorded in chloroform-*d* at 25°C. 29

Figure 8: ^{1}H-NMR spectrum for *N*,*N*-di(ethyl)-*N*'-benzoylthiourea and $[Pt(phen)(L^3\text{-}\kappa S)_2]$ in chloroform-*d* at 25°C with the complete numbering scheme. 31

Figure 9: COSY spectrum for $[Pt(phen)(L^3\text{-}\kappa S)_2]$ recorded in chloroform-*d* at 25°C. 31

Figure 10: ^{13}C-NMR spectra for *N*,*N*-di(ethyl)-*N*'-benzoylthiourea and the complex $[Pt(phen)(L^3\text{-}\kappa S)_2]$ recorded in chloroform-*d* at 25°C. 32

Figure 11: Crystal structures of the platinum(II) complexes, were at least one disubstituted acylthioureato ligand is coordinated in a monodentate fashion to the metal centre..... 33

Figure 12: Molecular structure of the $[Pt(phen)(L^7\text{-}\kappa S)_2]$ (**7**) solvate, with partial labelling of the coordinated atoms and the pendant carbonyl oxygen for clarity. 34

Figure 13: Packing diagram of the $[Pt(phen)(L^7\text{-}\kappa S)_2]$ (**7**) solvate showing intermolecular π-π stacking and a network of hydrogen bonds between the complex molecules and the solvated water molecules. 35

Figure 14: Molecular structure of the $[Pt(phen)(L^3\text{-}\kappa S)_2]$ (**3**) solvate, with partial labelling of the coordinated atoms and the pendant carbonyl oxygen for clarity. 36

Figure 15: Packing diagram of the $[Pt(phen)(L^3\text{-}\kappa S)_2]$ (**3**) solvate showing intermolecular π-π stacking and a network of hydrogen bonds between the complex molecules and the solvated ethanol and water molecules. 37

Figure 16: Molecular structure of [Pt(phen)(L^{12}-κ*S*)$_2$] (**12**), with partial labelling of the coordinated atoms and the pendant carbonyl oxygen for clarity. 38

Figure 17: 1D Packing array diagram of [Pt(phen)(L^{12}-κ*S*)$_2$] (**12**) showing intramolecular and intermolecular π-π stacking and aromatic C-H---O (carbonyl) hydrogen bonds between the complex molecules..... 39

Figure 18: Molecular structure of the [Pt(phen)(L^{1}-κ*S*)$_2$] (**1**) form I solvate, with partial labelling of the coordinated atoms and the pendant carbonyl oxygen for clarity..... 40

Figure 19: 1D Packing array diagram of the [Pt(phen)(L^{1}-κ*S*)$_2$] (**1**) form I solvate showing intramolecular and intermolecular π-π stacking and aromatic C-H---N and aromatic C-H---O hydrogen bonds between the complex molecules and solvent molecules..... 41

Figure 20: Molecular structure of the [Pt(phen)(L^{1}-κ*S*)$_2$] (**1**) form II solvate, with partial labelling of the coordinated atoms and the pendant carbonyl oxygen for clarity..... 42

Figure 21: Partial packing diagram of the solvate [Pt(phen)(L^{1}-κ*S*)$_2$] (**1**) form II showing intramolecular and intermolecular π-π stacking and aromatic C-H---O (carbonyl), OH2---O (carbonyl), MeOH---O (carbonyl) and solvent-solvent hydrogen bonds resulting in dimeric units of the complex.. 43

Scheme 1: Common routes to the synthesis of *N*,*N*-di(alkyl/aryl)-*N*'-acylthiourea ligands (HL^n). 19

Scheme 2: General illustration of ligand substitution reactions in square planar complexes. 20

Scheme 3: Effects of HCl acid on cis-[Pt(L^n-κ*O*,*S*)$_2$] according to Koch *et al*. 21

Scheme 4: General procedure for the synthesis of *N*,*N*-di(alkyl/aryl)-*N*'-acylthiourea ligands. 22

Scheme 5: Two possible nucleophilic attack of the carbonyl carbon and thiocarbonyl carbon by an amine. 22

Scheme 6: Thione-Thiol tautomerism is HL_3. 25

Scheme 7: Reaction scheme for the synthesis of [$PtCl_2$(phen)]. 26

Scheme 8: One-pot synthesis (method A) of [Pt(phen)(L^n-κ*S*)$_2$]complexes where the acylthioureato ligand was generated in-situ through deprotonation with sodium acetate. 27

Scheme 9: Method B- stepwise synthesis of [Pt(phen)(L^{3}-κ*S*)$_2$] where the ligand was deprotonated using sodium hydride. (final method adopted for all complexes). 30

Chapter 3

Figure 1: General structure of [Pt(phen)(L^n-κ*S*)$_2$] complexes illustrating molecular symmetry and the origins of conformational isomerism (red bonds = rotatable bonds). 60

Figure 2: Stacked variable temperature ^{1}H-NMR spectra of [Pt(phen)(L^1-κ*S*)$_2$] measured from 55 °C to -70 °C in methanol-*d*. 60

Figure 3: Stacked variable temperature ^{195}Pt-NMR spectra of [Pt(phen)(L^1-κ*S*)$_2$] measured from 55 °C to -50 °C in methanol-*d*. 62

Figure 4: Illustration of ring currents in the naphthyl rings of acylthioureato ligands that induces a magnetic field opposing the applied magnetic field B_0 at the platinum centre. ((i) [Pt(phen)(L^1-κ*S*)$_2$] form II and (ii) [Pt(phen)(L^1-κ*S*)$_2$] form I.) 63

Figure 5: Stacked variable temperature ^{1}H-NMR spectra of [Pt(phen)(L^7-κ*S*)$_2$] measured at 25 °C and -70 °C in methanol-*d*. 64

Figure 6: Stacked variable temperature ^{195}Pt-NMR spectra of [Pt(phen)(L^1-κ*S*)$_2$], [Pt(phen)(L^3-κ*S*)$_2$] and [Pt(phen)(L^7-κ*S*)$_2$] measured at -50 °C in methanol-*d*. 64

Figure 7: Highest occupied molecular orbitals (HOMO) diagrams for the various acylthioureato ligands studied. The molecular structures of the acylthioureato ligands were optimised at B3LYP level using ma-def2-TZVPP basis set in the gas phase courtesy of ORCA quantum chemistry software. 65

Figure 8: Solubility test of [$PtCl_2$(phen)] in 99% (blue) and 90% (red) methanol studied using UV-vis spectrophotometry in the region 290-600 nm. 68

Figure 9: ^{1}H-NMR spectrum for the solvolysis of [$PtCl_2$(phen)] in 99.9% methanol/water recorded in methanol-*d* for 78 hours. (* = the protons due to the phenanthroline moiety). 68

Figure 10: Stacked ^{1}H-NMR spectra of the products from the reactions between the precursor [$PtCl_2$(phen)] and *N*,*N*-(diethyl)-*N*'-(1-naphthoylthiourea) in wet methanol (99.9% and 85%) recorded in DMSO-*d*. 70

Figure 11: Variation of pH with time during the synthesis of [Pt(phen)(L^n-κ*S*)$_2$] from *N*,*N*-(diethyl)-*N*'-pivaloylthiourea (red) and *N*,*N*-(diethyl)-*N*'-(1-naphthoylthiourea) (blue) using the one-pot synthesis method A in methanol. (shaded region indicates when all the precursor had been consumed). 71

Figure 12: Chelate ring opening through heterolytic dissociation of the Pt – O bond in the conversion of [Pt(phen)(L^1-κ*O*,*S*)]$^+$ to [Pt(phen)(L^1-κ*S*)(L^2-κ*S*)]. (green arrow = [Pt(phen)(L^1-κ*S*)(L^2-κ*S*)] proton signals). 72

Figure 13: Protolytic dissociations of [Pt(phen)(L^3-κ*S*)$_2$] complexes showing different end products with varying acids in the ^{1}H-NMR spectra recorded in methanol-*d* 73

Figure 14: Crystal structure of; (a) [Pt(bipy)(L^{10}-κ*S*)$_2$] and (b) [Pt(PPh_3)(L^1-κ*O*,*S*)(L^1-κ*S*)]. (hydrogens omitted for clarity) 76

Figure 15: ^{1}H-NMR spectrum of [Pt(H_2O)(PPh_3)(L^1-κ*S*)$_2$] recorded at 25 °C in chloroform-*d*, showing only the presence of one triphenylphosphine ligand. 77

Figure 16: (a) Crystal structure of [Co^{II}(phen)(L^1-κ*O*,*S*)$_2$] showing an octahedral geometry with *N*,*N*-di(ethyl)-*N*'-(1-naphthoylthioureato) ligands coordinated in a bidentate fashion, (b) 1D packing array of [Co^{II}(phen)(L^1-κ*O*,*S*)$_2$] illustrating intermolecular π-π interactions. (The Hydrogens omitted for clarity)..... 78

Scheme 1: Resonance structures showing possible negative charge distribution on oxygen, nitrogen, and sulfur in the anionic disubstituted acylthiourea ligand..... 56

Scheme 2: Deprotonation of *N*,*N*-di(alkyl)-*N*'-acylthiourea ligands by water in wet methanol. 70

Scheme 3: Representations of chelate ring opening through heterolytic bond dissociation of the Pt – O bond in [Pt(phen)(L^n-κ*O*,*S*)]$^+$..... 73

Scheme 4: Comparisons of deprotonation of *N*,*N*-di(alkyl/aryl)-*N*'-acylthiourea ligands when sodium acetate and sodium hydride are used as bases..... 74

Scheme 5: Proposed mechanism for the synthesis of [Pt(phen)(L^n-κ*S*)$_2$] complexes using synthetic method A showing steps contributing to the formation and decomposition of [Pt(phen)(L^n-κ*S*)$_2$]. 75

Chapter 4

Figure 1: Examples of platinum(II) complexes (bearing a $[Pt(phen)]^{2+}$core) with significant preliminary antiproliferative activity. 84

Figure 2: Dose-response curves of $[Pt(phen)(L^1\text{-}\kappa S)_2]$ and $[Pt(phen)(L^2\text{-}\kappa S)_2]$ versus percentage cell viability against A549 lung cancer cell line treated for 48 hours respectively (with ●, ■ and ▲ representing replicate experiments). 87

Figure 3: Morphological changes of A549 cells treated with 50 mM of $[Pt(phen)(L^1\text{-}\kappa S)_2]$ for a period of 20 hours. Cells were stained with the Hoechst 33343 nuclear stain and ethidium bromide as indicators for necrosis. (Legend: N = nucleus, DC = dividing cell, M + cell membrane, V = vacuoles, AN = apoptotic nucleus, D = detached cell, R = round cell, yellow oval = filopodia). 88

Figure 4: The structure of the most stable binding mode of the $[Pt(phen)(L^1\text{-}\kappa S)_2]$ complex to DNA (C1), as assessed by molecular docking. (DNA pdb code:- 1BNA[26]). 89

Figure 5: The structures of the most stable binding modes of the $[Pt(phen)(L^1\text{-}\kappa S)_2]$ complex to DNA (C2-C9), as assessed by molecular docking. 90

Scheme 1: Mitochondrial reduction of MTT (yellow) to Formazan (purple). 85

List of Tables

Chapter 2

Table 1: Selected bond lengths and bond angles for [Pt(phen)(L^7-κ*S*)$_2$] (**7**) 35

Table 2: Selected bond lengths and bond angles for [Pt(phen)(L^3-κ*S*)$_2$] (**3**) 37

Table 3: Selected bond lengths and bond angles for [Pt(phen)(L^{12}-κ*S*)$_2$] (**12**) 39

Table 4: Selected bond lengths and bond angles for [Pt(phen)(L^1-κ*S*)$_2$] (**1**), form I 41

Table 5: Selected bond lengths and bond angles for [Pt(phen)(L^1-κ*S*)$_2$] (**1**), form II 43

Chapter 3

Table 1: Ionization Potential (*IP*), global nucleophilicity (*N*), and condensed Fukui function (f_k^-) for acylthioureato ligands. 66

Table 2: Local nucleophilicity indices (N_k) for acylthioureato ligands. 66

Abbreviations

1-D	One Dimensional
2-D	Two Dimensional
bipy	2,2-bipyridine
Chloroform-*d*	Deuterated chloroform
COSY	Correlated spectroscopy
CSA	Chemical Shift Anisotropy
DCM	Dichloromethane
DEPT	Distortions Enhancement by Polarisation Transfer
DFT	Density Functional Theory
DMSO-*d*	Deuterated dimethyl sulfoxide
DMSO	Dimethyl sulfoxide
DNA	Deoxyribonucleic acid
FT-IR	Fourier Transform Infra-Red
HMBC	Heteronuclear Multiple Bond Correlation
HOMO	Highest Occupied Molecular Orbital
HRMS	High Resolution Mass Spectrometry
HSQC	Heteronuclear single quantum correlation
MeOH	Methanol
Methanol-*d*	Deuterated methanol
MTT	3-(4-5-dimethylthioazol-2-yl)-2,5-diphenyl tetrazolium bromide
MS	Mass Spectrometry
m/z	Mass to charge ratio
NMR	Nuclear Magnetic Resonance
phen	1,10-phenanthroline
PPh_3	Triphenylphosphine
ppm	parts per million
sc-XRD	single crystal X-Ray Diffraction

THF	Tetrahydrofuran
Uv-vis	Ultraviolet-visible
VT-NMR	Variable Temperature Nuclear Magnetic Resonance

Chapter 1

Background and context for the monodentate coordination of N,N-di(alkyl/aryl)-N'-acylthioureato ligands in [Pt(phen)(L^n-κS)$_2$] complexes

1.1. Acylthiourea ligands

Acylthiourea ligands are organo-sulfur compounds with the core -C(O)NHC(S)N- derived from thiourea. Thiourea is an analogue of urea having the oxygen atom replaced with sulfur and numbered as indicated below (*Figure 1*).[1]

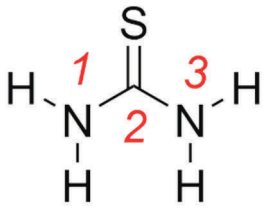


Figure 1: The structure of thiourea depicting atom numbering according to the systematic nomenclature of organic chemistry.

Thioureas can be classified into five categories based on the number of substituent R groups (R = phenyl, aryl, alkyl, cycloalkyl, heterocycle, acyl) attached to the thiourea moiety and the positions to which they are attached.[2] They are called mono-*N*-substituted thioureas when a substituent R group replaces one hydrogen of an amino moiety. When substituent R groups replace two hydrogens, either from the same amino group or one from each of the two amino groups, they classify as disubstituted thioureas (*1*,*1*-disubstituted or *1*,*3*-disubstituted thiourea). Trisubstituted thioureas result when substituent R groups replace two hydrogens from one amino group and one hydrogen from the other amino group giving *1*,*1*,*3*-trisubstituted thiourea. Substitution on the sulfur atom gives rise to pseudo-thioureas while when a substituent R group replaces one hydrogen of one amino group, and guanidine replaces one hydrogen of the other amino group we get guanyl-thiourea.[2] mono-*N*-substituted thioureas and trisubstituted thioureas can be viewed as a sub-group under the name acylthiourea on account of one substituent R group being an acyl group such that, depending on the extent of substitution on the amino moiety, they classify as un-substituted (**H_3L**), monosubstituted (**H_2L**) or disubstituted acylthiourea (**HL**) as illustrated in (*Figure 2*).[3]

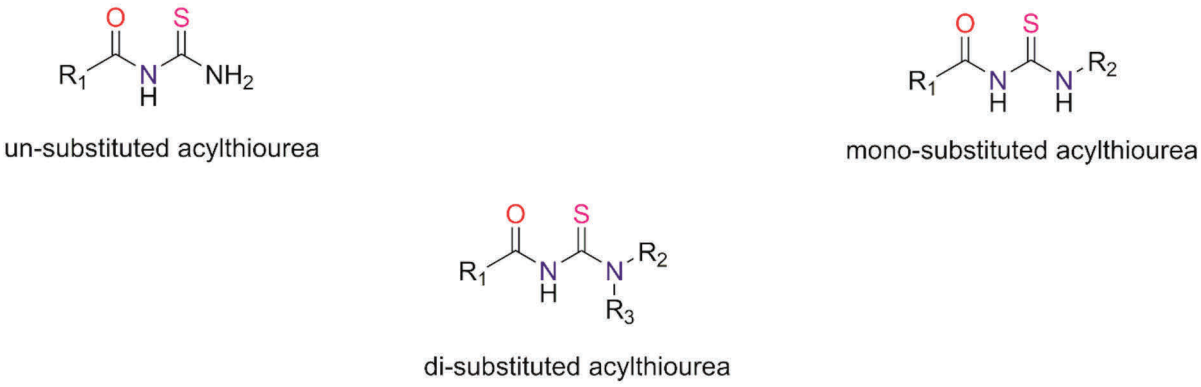


Figure 2: Acylthiourea ligand system showing different degrees of substitution on the amino terminus.

Conformational and structural analyses of these compounds in the CSD database have indicated that un-substituted and mono-substituted acylthiourea always adopts an **S** configuration with the carbonyl and thiocarbonyl groups *anti* to each other due to a strong intramolecular hydrogen bonding between the amino N-H group and carbonyl oxygen. Four conformations are, however, theoretically possible with disubstituted acylthiourea ligands (denoted as **S**, **U**, **M** and **Z** where these letters indicate the position of the C=O and C=S double bonds relative to the vertically drawn N-H bond)[4] as shown in (*Figure 3*).

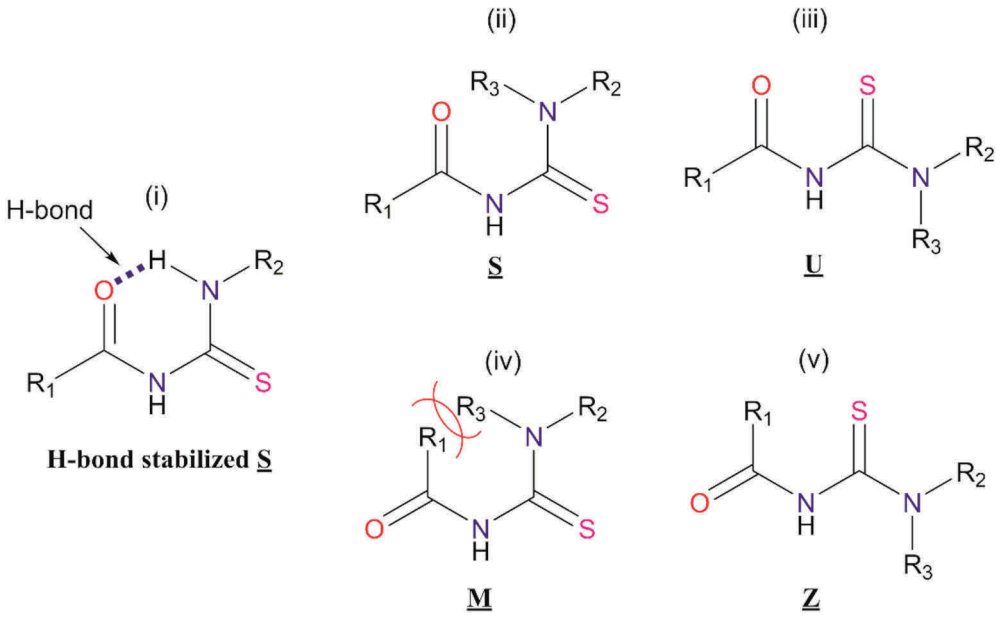


Figure 3: General acylthiourea structures illustrating the possible conformations of monosubstituted and disubstituted acylthiourea ligands.

The **S** and **U** conformations were observed to be the prevalent forms with the **S**-form being the preferred conformation in unsubstituted and monosubstituted acylthiourea ligands while the **U**-form preferred in disubstituted acylthiourea ligands.

Over the years, there has been an increased interest in the applications of acylthiourea ligands due to their high stability and facile synthesis. A wide variety of potential applications have been found: (i) in mineral extraction due to their selective complexation of soft metal ions,[5,6] (ii) as precursors for metal sulphide nanoparticles,[7,8] (iii) and in medicine as potential anti-viral, anti-bacterial, anti-fungal and anti-neoplastic agents.[9] The disubstituted variation of the acylthiourea ligand system has drawn remarkable attention as the substituents on the terminal nitrogen as well as the acyl-group can readily be varied to give different physical and chemical properties of the resultant complexes.

1.1.1. Coordination chemistry of acylthiourea ligands

While unsubstituted and monosubstituted acylthiourea ligands tend to coordinate predominantly in a monodentate fashion to transition metals through sulfur as result of intramolecular hydrogen bonding that locks oxygen in a six-membered ring with a hydrogen of the amino end, this type of intramolecular hydrogen bonding is not possible in disubstituted acylthiourea ligands.[10] Thus, disubstituted acylthiourea ligands act more as ambidentate ligands compared to the unsubstituted and monosubstituted variations because of multiple donor atoms positionally available for coordination. Disubstituted acylthiourea ligands exhibit a variety of coordination modes with transition metals, being: (a) mono-basic bidentate – through oxygen and sulfur donor atoms,[11,12] (b) neutral monodentate – through the sulfur donor atom only,[13] and (c) neutral bidentate[14] – through oxygen and nitrogen donor atoms (*Figure 4*). The structure of these ligands is similar to that of di-ketonates and have been shown to preferably form six-membered chelate structures to a metal centre through positionally preorganised chalcogen atoms following deprotonation of the central amidic hydrogen.

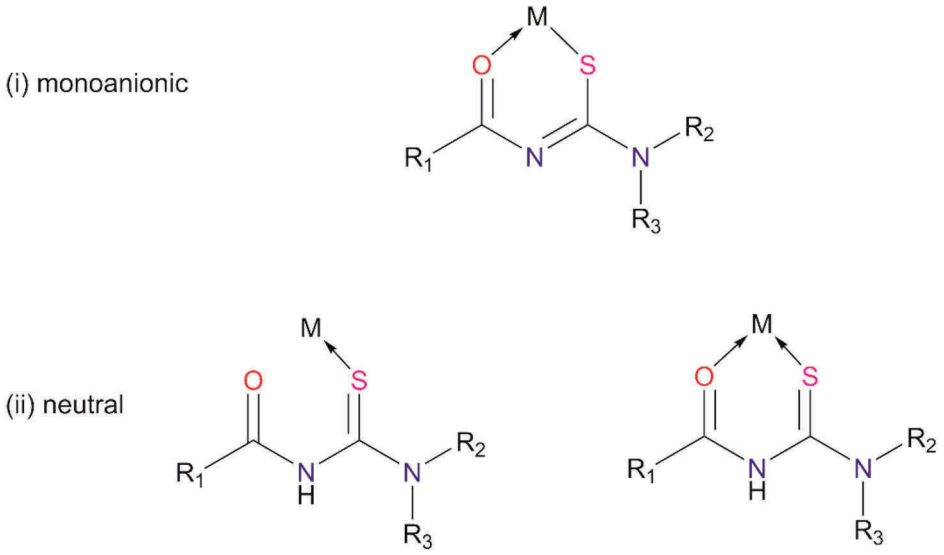


Figure 4: Major coordination modes exhibited by disubstituted acylthiourea ligands.

A CSD query (CSD version 5.39; using the transition metal-acylthiourea fragment with no exclusions and producing 296 hits) shows that most of the complexes exhibit a mono-basic bidentate coordination mode of acylthioureato ligands all of which coordination takes place through sulfur and oxygen to give a six-membered chelate.[15] Depending on the charges on the metal centre and the co-ligands, the resulting complexes can be neutral as well as cationic (*Figure 5*). One of the consequences of mono-anionic bidentate coordination of acylthioureato ligands in conjunction with neutral bidentate co-ligands on metals of +2 oxidation state is that it results in cationic complexes that are water-soluble.

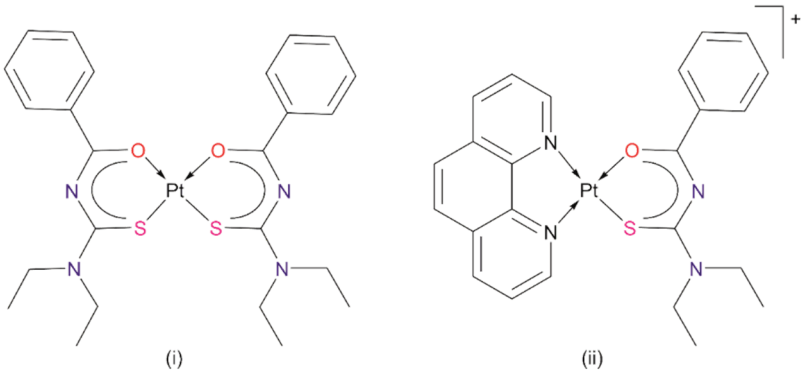


Figure 5: Example of (i) neutral (water-insoluble) and (ii) cationic (water-soluble) platinum(II) complexes in which mono-anionic disubstituted acylthioureato ligands coordinate in a bidentate fashion.

Bidentate coordination of disubstituted acylthioureato ligands may be as a result of the proximal arrangement of the oxygen and sulfur donor atoms ideal for the formation of a stable six-membered chelate ring with the metal centre and driven by the chelate effect. However, coordination of the neutral disubstituted acylthiourea ligand either in a monodentate or bidentate fashion is rare. Most of the

reported complexes involving neutral disubstituted acylthiourea ligands show a monodentate mode as the primary coordination mode, for example, (i) with Au(I), Ag(I) and Hg(II), (ii) with Cu(I), (iii) with Pt(II) in concentrated HCl or HI solutions and (iv) with Pd(II) .[13,16–20] There are only a few literature reports of bidentate coordination of neutral disubstituted acylthiourea ligands (*Figure 6(ii)*).

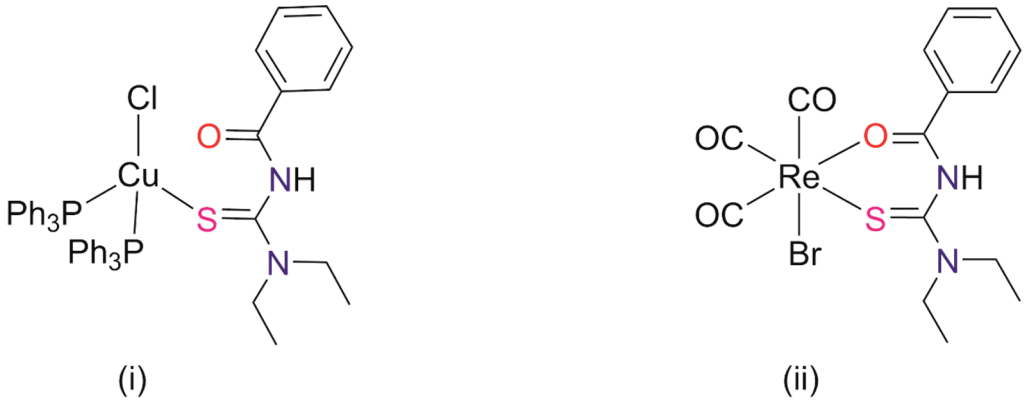


Figure 6: Selected examples of a neutral disubstituted acylthiourea ligand coordinating in a monodentate and bidentate fashion with transition metal ions.[13,14]

With the presence of multiple donor sites in disubstituted acylthiourea ligands, one would expect a multitude of coordination modes when they coordinate with transition metals; however, it is not the case. One other coordination mode of these ligands that is peculiarly scarce in the literature, of which other structurally similar ligands can form, is the monodentate coordination of the mono-anionic ligand. The only reported case of monodentate coordination of mono-anionic disubstituted acylthiourea ligands was in bridged dimeric copper(II) complexes by Che *et al*.[21] (*Figure 7*).

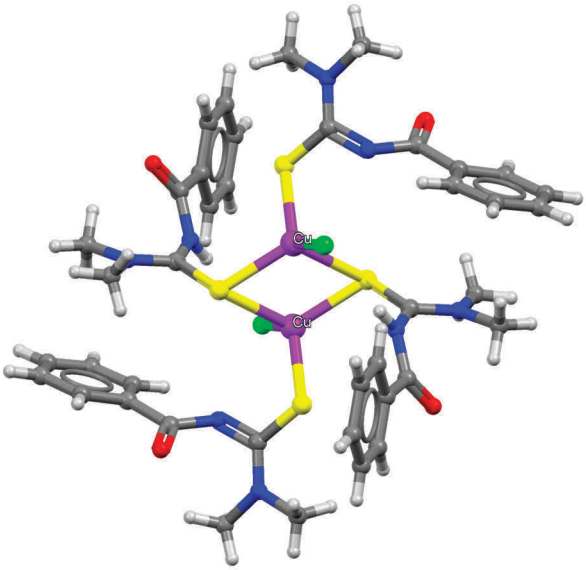


Figure 7: Monodentate coordination of mono-anionic disubstituted acylthioureato ligands in bridged dimeric copper(II) complexes.[21]

1.1.2. Coordination behaviour of analogous compounds to acylthiourea ligands

Since the outset of our study we noticed the absence of monodentate coordination of mono-anionic disubstituted acylthiourea ligands in literature, and therefore we decided to widen the search to structurally similar *1*,*3*-diketone and dichalcogenoimido-diphosphine ligands (*Figure 8*).



Figure 8: Structural analogues of disubstituted acylthiourea ligands having a matching and a mismatch of chalcogen donor atoms.

These ligands have two chalcogen atoms with a central carbon (in case of *1*,*3*-dichalcogen) or central nitrogen (in dichalcogenoimido-diphosphine) both of which have acidic protons. Deprotonation of the acidic protons in both ligand systems, results in anionic species with the negative charge delocalized across the chalcogen – C – C – C – chalcogen or chalcogen – P – N – P – chalcogen framework in the same way envisaged in disubstituted acylthiourea ligands (*Figure 9*).[22,23]



Figure 9: Illustration of the delocalisation of the negative charge in 1,3-dichalcogenate and dichalcogenoimido-diphosphinate anions after deprotonation.

Similarly, coordination in both ligand systems is dominated by the mono-basic bidentate mode through the chalcogen atoms following deprotonation of the acidic proton on the central carbon or nitrogen, the same way as with disubstituted acylthiourea ligands. However, a notable exciting observation was the existence of several examples of complexes in which the *1*,*3*-dichalcogenato and dichalcogenoimido-diphosphinato anions coordinated in a monodentate fashion through one of the chalcogens with transition metals (*Figure 10*). In these studies it was observed that in the most complexes exhibiting monodentate coordination, the *1*,*3*-dichalcogenato ligands (with the same or a mismatch in donor chalcogen atoms) have electron-withdrawing trifluoro-acetyl substituents (CSD-ACFCUA,[24] CSD-BOLTOL,[25] CSD-DUSRAM,[26] CSD-THFACE10,[27] CSD-GUXNES,[28] etc)[15] which may suggest the importance of the ligands' electronic properties in the coordination regioselective control of these ligands. Another attractive characteristic of these complexes, particularly $M(CO)_5L]^-$ (where M = Cr,

Mo, W and L = monothio-β-ketonate anions) as reported by Barnett *et al.*,[27] was that they were very unstable in the presence of a little trifluoro-acetic acid or sulfuric acid. Only two reports of monodentate coordination of dichalcogenoimido-diphosphinato anions (with matching or a mismatch of chalcogen donor atoms) exist on the Cambridge Crystallographic Data centre (CCDC) database (CSD-LOGNEA,[29] CSD-QABXOH[30]).[15]

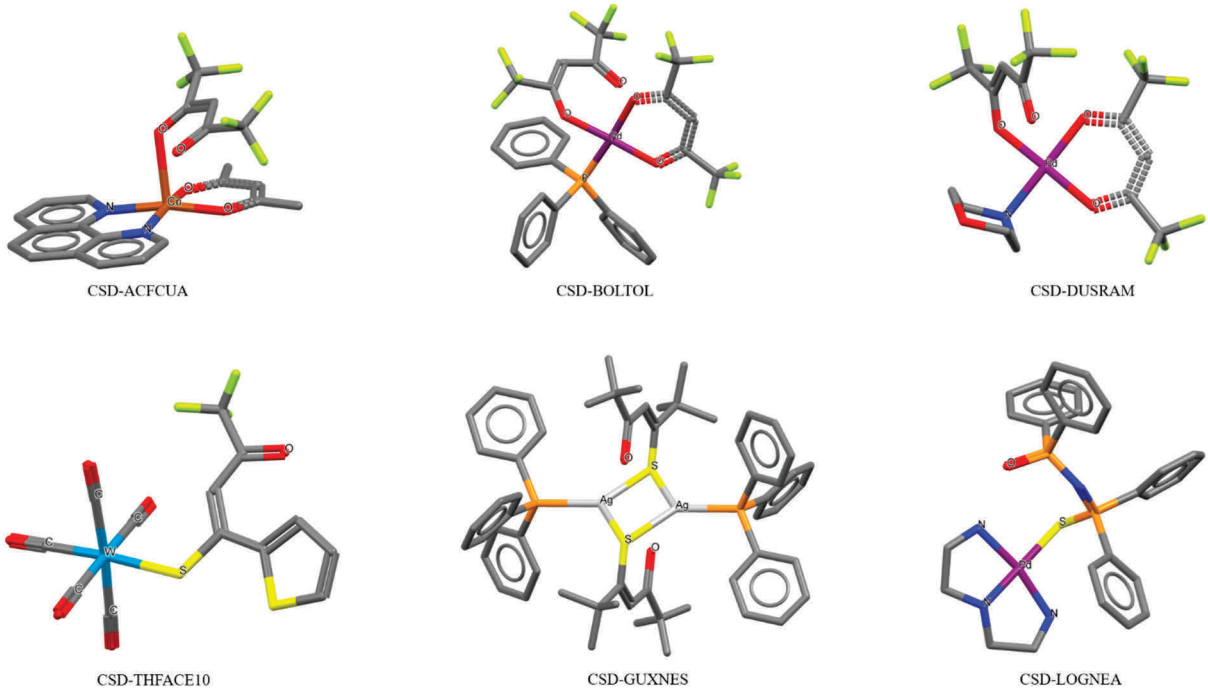


Figure 10: Monodentate coordination of 1,3-dichalcogenato and dichalcogenoimido-diphosphinato ligands.[15]

This exciting find reinforces the idea that our structurally similar disubstituted acylthioureato ligand system may be capable of exhibiting the same coordination mode where only one of the chalcogens coordinates to the metal centre.

1.2. Platinum complexes in cancer therapy

Metal complexes as therapeutic agents have increasingly become key due to their improved properties and mode of action compared to the free ligand.[31,32] They present a variety of tuneable attributes such as coordination spheres, ligand designs, oxidation states and redox potentials, giving them the ability to alter the kinetic and thermodynamic properties of these complexes towards biological receptors.[33–35] Complexation can also modify the bioavailability of the drug assisting in targeting specific tissues or enzymes, thereby enhancing bioactivity.[36,37] The early success of metal complexes in medicine came in the form of Cisplatin which triggered the interest in platinum(II) and other metal-containing compounds as anti-cancer agents.[38] Cisplatin and its second and third generation analogues (*Figure 11*) have successfully been used clinically in the treatment of different types of cancers that include: (i)

sarcoma cancers, and (ii) cancers of soft tissue, bones, muscles and blood vessels.[39] Use of cisplatin as a principal component of a combination regimen has rendered testicular cancer curable with typical doses ranging from 20 mg/m^2 to 100 mg/m^2, normally for up to 5 consecutive days.[40]

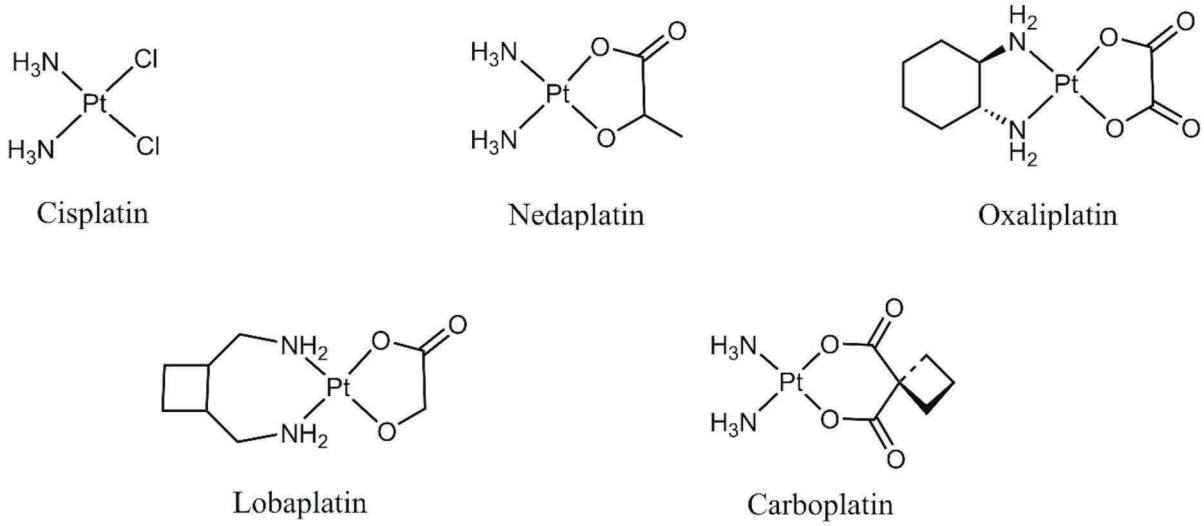


Figure 11: Structures of clinically approved platinum(II) anticancer drugs.

Regardless of these successes, there is still a limited range of cancers sensitive to cisplatin, and some cancers are inherently resistant.[41] A further disadvantage is an onset of acquired resistance after treatment and severe side effects that include dose-limiting nephrotoxicity, neurotoxicity, ototoxicity and emetogenesis; some of which the second and third generation analogues managed to some extent.[34,42–44] The usefulness of any drug is a balance between its toxicity and activity as alluded to in this great quote by Paracelsus, 1493-1541; "Everything is poisonous, and nothing is harmless. The dose (amount) alone defines whether something is not poison".[45]

Hence several efforts have been directed at managing the toxicity of cisplatin and other platinum-based drugs, which may derive from its metabolism and unwanted "random" protein interactions while maintaining activity. Such efforts have included changing the metal to other transition metals (such as copper(II), ruthenium(III), palladium(II)),[46–48] while other researchers have been probing complexes that proffer a different mechanism of action, such as intercalators, with promising results.[49,50]

1.2.1. Biologically active platinum(II)-acylthiourea complexes

The thiourea backbone (as found in acylthiourea ligands) is a very important pharmacophore that has been used by researchers in drug discovery.[51–53] Many transition metal complexes bearing acylthiourea ligands have been reported to have some bioactivity with even better cytotoxicity compared to the free acylthiourea ligand. Ruthenium(II)-acylthiourea complexes have been shown to have potential antiproliferative activity against a DU-145 prostate cancer cell line, an MCF-7 breast cancer cell line and an A549 lung cancer cell line.[54,55] Copper(I) and copper(II)-acylthiourea complexes have been

reported to have potent antibacterial and antitumor activity;[56,57] while some palladium(II)-acylthiourea complexes have been shown to have potential anticancer activity against an MCF-7 breast cancer line as well as anti-*Mycobacterium tuberculosis* and anti-*Trypanosoma cruzi* activity.[20,58] Platinum(II)-acylthiourea complexes have also been found to have various biological activities. In a study by Plutin *et al.*,[59] it was shown that some platinum(II)-disubstituted acylthiourea complexes had antimycobacterial activity against *M. tuberculosis H37Rv* strains. Egan *et al.* [60] reported on a series of 2,2'-bipyridyl- and 1,10-phenanthrolineplatinum(II)-benzoyl thiourea complexes with *in vitro* antimalarial activity. In another study more related to our study, a series of platinum(II)-acylthiourea complexes of the form $[Pt(phen)(L^n\text{-}\kappa O,S)]^+$ (where L^n = *N*,*N*-di(alkyl/aryl)-*N*'-acylthioureato ligands), were shown to have potent anticancer activity comparable to that of cisplatin against H1975 cell lines.[61]

1.3. Drug–DNA binding interaction modes

DNA is a critical target for several drug discovery and pharmaceutical development studies in the fight against the dreaded cancer scourge. Interactions of drug molecules with DNA often results in a significant alteration in the DNA properties and expression of genes impacting cell proliferation.[62] Hence, understanding the drug-DNA interactions is crucial in the fight against cancerous cell proliferation. Most chemotherapeutic anticancer drugs currently in use, which target DNA, interact with the DNA duplex by three general binding modes: (i) covalent binding, (ii) intercalation and (iii) non-covalent groove binding.[63]

1.3.1. Covalent drug–DNA binding

Covalent binding mode involves an irreversible interaction of the drug molecule with DNA base pairs resulting in the formation of strongly bound drug-DNA adducts via normal covalent bonding (alkylation) or coordination dative bonding (metalation).[64] This mode leads to complete inhibition of cellular processes and subsequent cell death. Platinum complexes are important examples of this class, particularly cisplatin as a metalating anticancer agent. Cisplatin and its analogues are square planar complexes that do not expand their coordination number easily but rather undergo ligand substitution reactions.[65] These complexes are taken up through the cell by either passive or active transport where they are aquated to give mono aquo and diaqua complexes (*Figure 12A*) which in turn reacts with the DNA.[32] They destroy malignant cells by interfering with DNA, *via* intra- and inter-strand crosslinks, were platinum primarily bonds to the adjacent guanine-N7 sites, thereby preventing cell division and growth (*Figure 12B*).[66]

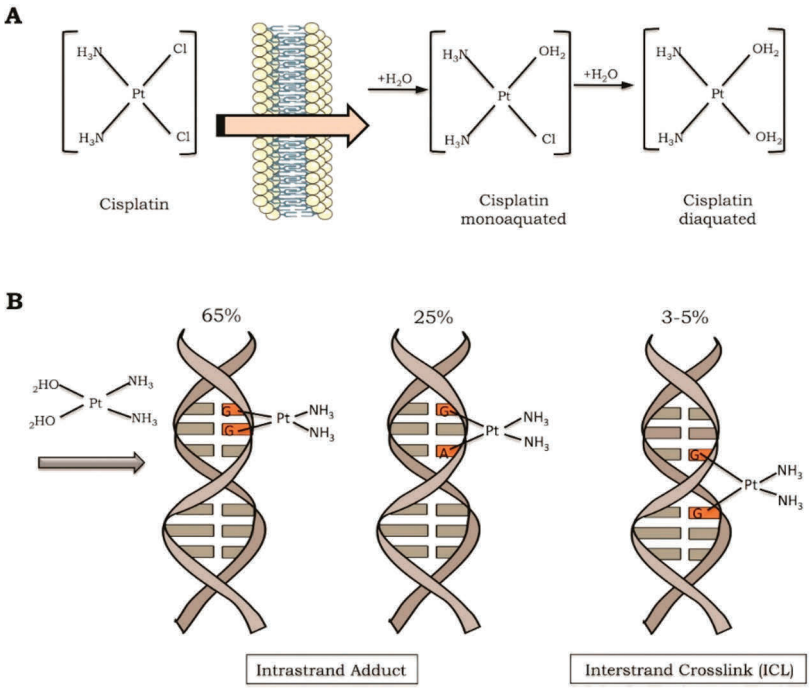


Figure 12: Cisplatin mechanism of action from cellular uptake, aquation and ultimately to the interaction with DNA.[67]

1.3.2. Non-covalent drug–DNA binding

This kind of binding involves reversible interaction between the drug molecule and DNA base pairs stabilised through noncovalent interactions such as π-π stacking or hydrogen bonding.

Intercalation: This takes place when planar molecules such as aromatic ring systems insert between base pairs and is generally independent of base-pair sequence. Several drugs containing planar aromatic ring systems have been reported as successful as intercalating cancer treatments (*Figure 13*).[68–70] Generally, intercalation requires changes in the sugar-phosphate torsional angles to accommodate the planar aromatic compound resulting in changes in helical parameters such as winding and bending.[71] Intercalation causes stabilisation, local unwinding, lengthening and some other structural changes to DNA with consequent alteration of biological functions which may have therapeutic implications. Van der Waals, electrostatic and hydrophobic forces stabilise the intercalation complexes.[72]

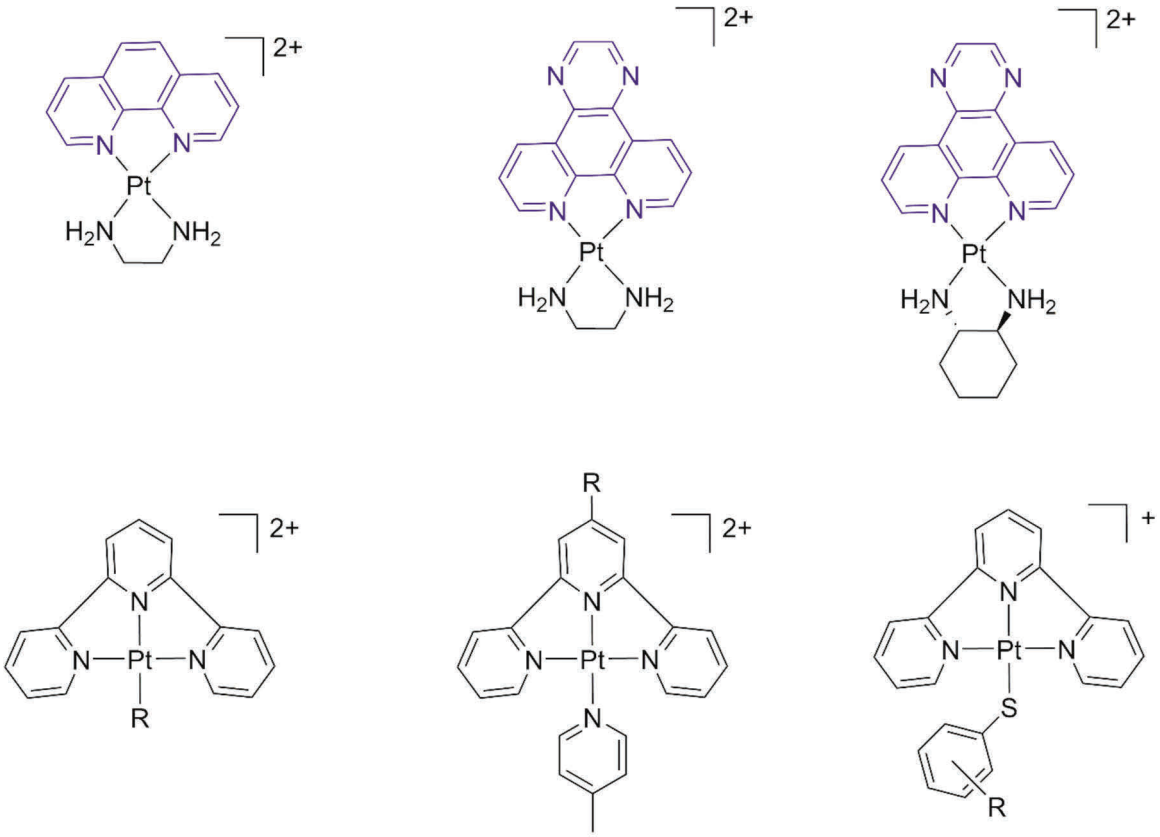


Figure 13: Chemical structures of some typical platinum(II) DNA intercalators.[70]

Groove binding: The most biologically prevalent form of DNA is the B-form characterised by a wide, deep major groove and a deep narrow minor groove.[73] These grooves differ in hydrogen bonding, electrostatic potential and degree of hydration.[74] Drugs usually approach DNA through one of the grooves and interact with either the backbone or nucleobases (*Figure 14*).

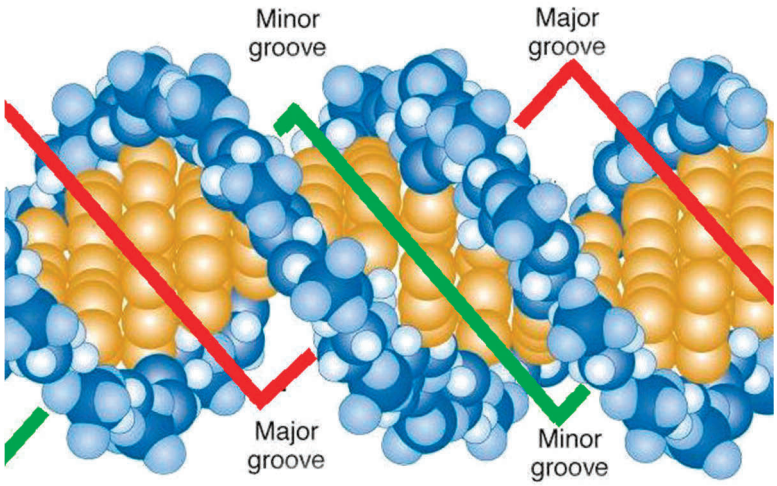


Figure 14: Graphical illustration of DNA's major and minor grooves (with the red and green threads running in the major and minor grooves, respectively).[75]

Groove binding DNA-drug interaction occurs through electrostatic interactions with the charged phosphate backbone, hydrogen bonding and van der Waals interactions with base pairs.[76] This kind of binding is considered more selective compared to intercalation. Groove binders might seem not to bring about substantial conformational changes in DNA; however, they block sites on DNA that otherwise interact with biomolecules (such as transcription proteins) in normal cellular processes thereby perturbing cell proliferation of cancerous cells.

Minor groove binding: These are usually crescent-shaped molecules which complement the shape of the groove and facilitate binding by promoting van der Waals interactions *(Figure 15)*.[77,78] They may typically have several aromatic rings such as pyrrole, furan or benzene connected by bonds with torsional freedom.[79] The drug fits snugly into the minor groove and replaces the hydration layer. Minor groove binders frequently show selectivity towards A - T rich grooves compared to G – C rich grooves due to a higher electrostatic potential in A – T rich grooves.[63]

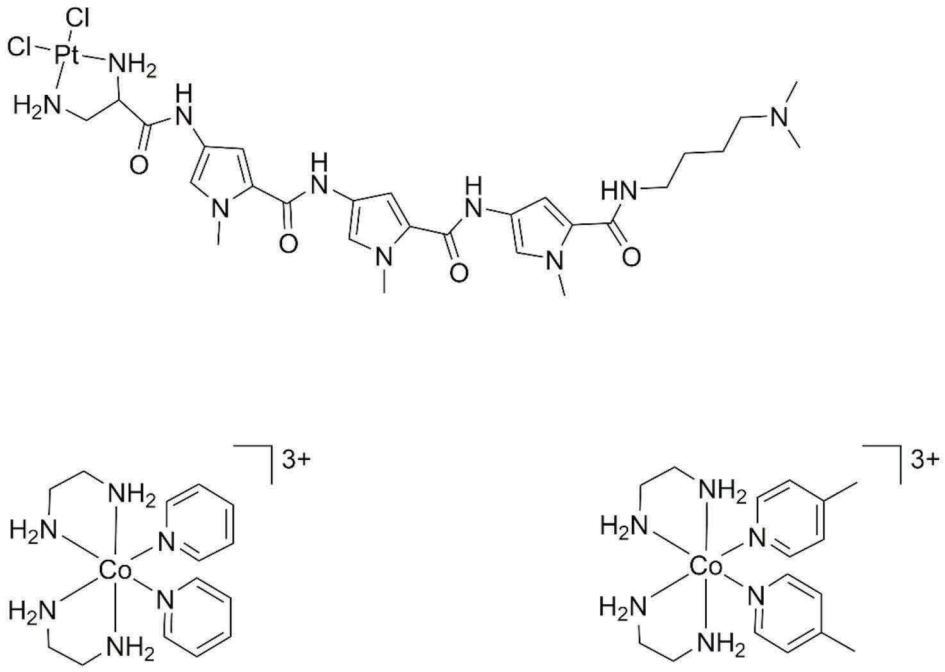


Figure 15: Structures of some metal complexes that interact with DNA via groove binding.[77,78]

Major groove binding: Most DNA groove binders target the minor groove; however, major groove binding arises due to the steric bulkiness of the drug that hinders interaction with the minor groove.[80] Usually, the major grooves are sites for the binding of DNA interacting proteins for transcriptive processes.[81] Drugs thus can be tailored to target these sites and inhibit these cellular transcriptive processes necessary for cell proliferation, making the major groove a potentially more attractive target.

1.4. Aims of this thesis

The primary objective of this thesis is to synthesize and fully characterize mixed ligand [Pt(phen)(L^n-κ*S*)$_2$] complexes where mono-anionic disubstituted acylthioureato ligands (**L^n**) coordinate to platinum(II) in a monodentate fashion through the sulfur donor atom and establish a rational explanation to what drives this rare coordination mode. The secondary aim of this thesis is to investigate the potential application of these complexes as anti-proliferative agents.

Motivation: The nature of this research is of both, academic interest, and potential applicability. This is brought about by the observation that *N*,*N*-di(alkyl/aryl)-*N*'-acylthiourea ligands exhibit many other coordination modes with platinum(II) ions (monobasic bidentate mode being the most common), except the monobasic monodentate mode. This observation suggested that there must be underlying factors that govern the coordination preference of these ligands and we were set to investigate these out. In hindsight, this research also opened avenues of potential applications, as the new coordination mode results in complexes with an interesting architecture that could be exploited in the development of anti-cancer metallodrugs. This was inspired by the success platinum(II) complexes have had in the fight against cancer. In this regard, a series of carefully chosen *N*,*N*-di(alkyl/aryl)-*N*'-acylthiourea ligands will be synthesised to evaluate the factors that may be responsible for these observed coordination preferences with platinum(II) ions. Ligand variations will derive mainly from the use of different acyl substituents that present different electronic characteristics since we suspect them to be a contributing factor to the observed coordination modes. We will also investigate a potential application of a select of the complexes as anti-proliferative agents.

1.4.1. Objectives

1) Synthesise and characterise a series of *N*,*N*-di(alkyl/aryl)-*N*'-acylthiourea (**HL^n**) ligands.
2) Synthesise and characterise the [$PtCl_2$(phen)] metal precursor.
3) Synthesise and characterise the respective [Pt(phen)(L^n-κ*S*)$_2$] complexes.
4) Investigate the driving force behind the monodentate coordination of *N*,*N*-di(alkyl/aryl)-*N*'-acylthioureato (**L^n**) ligands with platinum(II) through a solution-phase conformational analysis (using variable temperature ^{1}H and ^{195}Pt NMR studies), regioselectivity studies on the ligands using conceptual DFT and a series of experimental studies.
5) Evaluate the anti-proliferative activity of selected [Pt(phen)(L^n-κ*S*)$_2$] complexes against the A549 lung cancer cell line and potential DNA binding mode of these complexes.

1.5. Outline of this thesis

Chapter 1 introduces the acylthiourea ligand system, their applications, and critical aspects about the coordination chemistry of disubstituted acylthiourea ligands to metals both as neutral ligands and as

anionic ligands. Anionic disubstituted acylthiourea ligands being the most reported in literature preferentially coordinate in a bidentate fashion. They compare well with structurally similar ligands such as 1,3-dichalcogenato and dichalcogenoimido-diphosphinato ligand systems. They have mainly been reported as three-electron LX-type donors (coordinating through oxygen and sulfur) after deprotonation; while the neutral ligands have either been four-electron L_2-type donors or two-electron L-type ligands coordinating through the sulfur donor atom. Their monodentate coordination as one-electron X-type ligand is rare in literature with only a few ever been reported,[21] however, several complexes with 1,3-dichalcogenato and dichalcogenoimido-diphosphinato analogues as one electron X-type ligands have been reported. The monodentate coordination of these anionic disubstituted acylthiourea ligands with platinum(II) ions will be the target of consideration as we attempt to understand the coordination chemistry of these ligands further. Furthermore, platinum complexes (for example, anticancer agents such as cisplatin and its analogues) successfully kill cancer cells although with adverse side effects mainly caused by side reactions these complexes undergo after administration in the human body. Hence this study also explores the potential application of these new platinum complexes as anticancer agents with possibly a different mode of action to subvert the side effects.

C**hapter 2** presents the synthetic protocols for preparing various disubstituted acylthiourea ligands and their platinum(II) complexes along with spectroscopic and structural data for the complexes. Variation of the electronic effect of substituents on the acyl substituents of the ligands (from electron-withdrawing to electron-donating) with minor steric variations on the amino end of the ligands was investigated.

Chapter 3 investigates the solution-state conformations of a selection of the synthesised complexes for the existence of intramolecular π-π stacking in solution by studying their solution conformations with the use of variable-temperature ^{1}H and ^{195}Pt NMR spectroscopy and correlating these with their crystal structures. This particular study aims to answer the question of whether the ability of the co-ligands to form intramolecular π-π stacking interactions influence the way the ligands coordinate. Using a few select examples of the [Pt(phen)(L^n-κ*S*)$_2$] complexes, we also try and gain mechanistic insights into this rare coordination mode using conceptual DFT and some experimental analyses. The chosen compounds are of such a nature that the disubstituted acylthioureato ligands differ only in the electronic characteristic of the substituent groups on the acyl substituents since we suspect that the electronic properties of these substituents influence the propensity of the ligand to coordinate as a monodentate or bidentate ligand.

In **chapter 4**, Two complexes [Pt(phen)(L^1-κ*S*)$_2$] and [Pt(phen)(L^2-κ*S*)$_2$] (where L^1 and L^2 are the deprotonated form of *N*,*N*-(diethyl)-*N*'-(1-naphthoylthiourea) and *N*,*N*-(dibutyl)-*N*'-(1-naphthoylthiourea) respectively) are investigated for their antiproliferative activity against a lung cancer cell line A549. Further investigations are undertaken to verify the method of cell death (apoptosis or necrosis) and the potential mode of action.

Chapter 5 summarises the findings discussed in preceding chapters and ends with recommendations for the future work on this study.

1.6. References

[1] D. Hellwinkel, *Systematic Nomenclature of Organic Chemistry*, Springer-Verlag, Berlin, **2001**.

[2] A. Shakeel, A. A. Altaf, A. M. Qureshi, A. Badshah, *J. Drug Des. Med. Chem.* **2016**, *2*, 10–20.

[3] A. Saeed, U. Flörke, M. F. Erben, *J. Sulfur Chem.* **2014**, *35*, 318–355.

[4] M. G. Woldu, J. Dillen, *Theor. Chem. Acc.* **2008**, *121*, 71–82.

[5] L. Guang-Yi, Z. Hong, X. Liu-Yin, W. Shuai, X. Zheng-He, *Miner. Eng.* **2011**, *24*, 817–824.

[6] A. M. Alkherraz, Z. I. Lusta, A. E. Zubi, *Int. J. Chem. Nucl. Metall. Mater. Eng.* **2014**, *8*, 116–118.

[7] J. C. Bruce, N. Revaprasadu, K. R. Koch, *New J. Chem.* **2007**, *31*, 1647–1653.

[8] Z. Ali, N. E. Richey, D. C. Bock, K. A. Abboud, J. Akhtar, M. Sher, L. McElwee-White, *Dalton Trans.* **2018**, *47*, 2719–2726.

[9] Y. Wu, X. Rao, Z. Song, S.-B. Shang, Z.-D. Wang, *Med. Chem. Res.* **2011**, *20*, 333–338.

[10] K. R. Koch, *Coord. Chem. Rev.* **2001**, *216–217*, 473–488.

[11] S. San, A. A. Al-abbasi, M. Ibrahim, M. Tahir, M. B. Kassim, *Polyhedron* **2014**, *68*, 287–294.

[12] R. S. Correa, K. M. Oliveira, H. Pérez, A. M. Plutın, R. Ramos, R. Mocelo, E. E. Castellano, A. A. Batista, *Arab. J. Chem.* **2015**, 1–9.

[13] N. Gunasekaran, P. Ramesh, M. N. G. Ponnuswammy, R. Karvembu, *Dalton Trans.* **2011**, *40*, 12519–12526.

[14] U. Abram, S. Abram, R. Alberto, R. Schibli, *Inorg. Chim. Acta* **1996**, *248*, 193–202.

[15] C. R. Groom, I. J. Bruno, M. P. Lightfoot, S. C. Ward, *Acta Crystallogr. Sect. B Struct. Sci. Cryst. Eng. Mater.* **2016**, *72*, 171–179.

[16] R. C. Luckay, F. Mebrahtu, C. Esterhuysen, K. R. Koch, *Inorg. Chem. Commun.* **2010**, *13*, 468–470.

[17] U. Braun, R. Richter, J. Sieler, *Z. Anorg. Allg. Chem.* **1985**, *629*, 201–208.

[18] O. Estévez-Hernández, J. Duque, J. Rodríguez-Hernández, E. Reguera, *Polyhedron* **2015**, *97*, 148–156.

[19] K. R. Koch, S. Bourne, *J. Mol. Struct.* **1998**, *441*, 11–16.

[20] N. Selvakumaran, S. W. Ng, E. R. T. Tiekink, R. Karvembu, *Inorg. Chim. Acta* **2011**, *376*, 278–284.

[21] D. Che, G. Li, X. Yao, D. Zhou, *Dalton Trans.* **1999**, *16*, 2683–2687.

[22] P. Bhattacharyya, J. D. Woollins, *Polyhedron* **1995**, *14*, 3367–3388.

[23] C. Pettinari, F. Marchetti, A. Drozdov, in *Compr. Coord. Chem. II*, Elsevier, Toronto, **2004**, pp. 97–115.

[24] N. A. Bailey, D. E. Fenton, M. V Franklin, M. Hall, *Dalton Trans.* **1980**, 984–990.

[25] A. R. Siedle, R. A. Newmark, L. H. Pignolet, *J. Am. Chem. Soc.* **1982**, *104*, 6584–6590.

[26] A. L. Rheingold, M. Hampden-Smith, *CSD Commun.* **2015**, DOI 10.5517/cc1k7xf4.

[27] G. H. Barnett, M. K. Cooper, M. Mcpartlin, G. B. Robertson, *Dalton Trans.* **1978**, *6*, 587–592.

[28] S. C. Ngo, K. K. Banger, P. J. Toscano, J. T. Welch, *Polyhedron* **2002**, *21*, 1289–1297.

[29] A. M. Z. Slawin, M. B. Smith, *Polyhedron* **2000**, *19*, 695–704.

[30] I. Haiduc, A. Fischer, F. T. Edelmann, *Reveu Roum. Chim.* **1999**, *44*, 805–809.

[31] F. Téllez, R. Ramírez-Trejo, R. Vieto-Peña, G. V Suárez-Moreno, R. Colorado-Peralta, A. Flores-Parra, R. Contreras, N. Barba-Behrens, *Z. Anorg. Allg. Chem.* **2013**, *639*, 1438–1444.

[32] M. B. Baile, N. S. Kolhe, P. P. Deotarse, A. S. Jain, A. A. Kulkarni, *Int. J. Pharma Res. Rev.* **2015**, *4*, 59–66.

[33] L. Colina-Vegas, L. Luna-Dulcey, A. M. Plutín, E. E. Castellano, M. R. Cominetti, A. A. Batista, *Dalton Trans.* **2017**, *46*, 12865–12875.

[34] P. Jia, R. Ouyang, P. Cao, X. Tong, X. Zhou, T. Lei, Y. Zhao, N. Guo, H. Chang, Y. Miao, et al., *J. Coord. Chem.* **2017**, *70*, 2175–2201.

[35] U. Ndagi, N. Mhlongo, M. E. Soliman, *Drug Des. Dev. Ther.* **2017**, *11*, 599–616.

[36] S. Wanninger, V. Lorenz, A. Subhan, F. T. Edelmann, *Chem. Soc. Rev.* **2015**, *44*, 4986–5002.

[37] K. H. Thompson, C. Orvig, *Dalton Trans.* **2006**, 761–764.

[38] D. Chen, V. Milacic, M. Frezza, Q. P. Dou, *Curr. Pharm. Des.* **2009**, *15*, 777–791.

[39] A. Florea, D. Büsselberg, *Cancers* **2011**, *3*, 1351–1371.

[40] N. Farrell, in *Compr. Coord. Chem. II Appl. Coord. Chem.* (Ed.: M.D. Ward), Elsevier Ltd, Richmond, USA, **2004**, pp. 809–840.

[41] N. Martinho, T. C. B. Santos, H. F. Florindo, L. C. Silva, M. Saleem, L. C. Silva, *Front. Physiol.* **2018**, *9*, 1898.

[42] L. Kelland, *Nat. Rev. Cancer* **2007**, *7*, 573–584.

[43] A. M. Florea, D. Büsselberg, *BioMetals* **2006**, *19*, 419–427.

[44] B. Desoize, C. Madoulet, *Crit. Rev. Oncol.* **2002**, *42*, 317–325.

[45] M. Frezza, S. Hindo, D. Chen, A. Davenport, S. Schmitt, D. Tomco, Q. P. Dou, *Curr. Pharm. Des.* **2013**, *16*, 1813–1825.

[46] J. Li, Z. Tian, Z. Xu, S. Zhang, Y. Feng, L. Zhang, Z. Liu, *Dalton Trans.* **2018**, *47*, 15772–15782.

[47] M. Wang, X. Nan, G. Feng, H. Yu, G. Hu, Y. Liu, *Ind. Crop. Prod.* **2014**, *55*, 11–18.

[48] J. Wang, G. Xu, Y. Zhang, H. Luo, J. Li, L. Zhang, D. Jia, *New J. Chem.* **2019**, *43*, 2529–2539.

[49] M. Cusumano, M. Letizia, D. Pietro, A. Giannetto, P. A. Vainiglia, *J. Inorg. Biochem.* **2005**, *99*, 560–565.

[50] M. Cusumano, M. Letizia, D. Pietro, A. Giannetto, *Inorg. Chem.* **2006**, *45*, 230–235.

[51] M. M. Aslabban, R. A. Adigun, W. DeBenedetti, W. Mbiya, M. Mhike, K. Morakinyo, A. Otoikhian, T. Ruwona, R. H. Simoyi, *J. Phys. Chem. A* **2014**, *118*, 11145–11154.

[52] K. Chipiso, W. Mbiya, T. Tran, R. H. Simoyi, *S. Afr. J. Chem.* **2016**, *69*, 27–34.

[53] A. F. Shalas, Siswandono, M. Rudyanto, *Int. J. Pharm. Pharm. Sci.* **2016**, *8*, 297–298.

[54] J. P. Barolli, P. I. S. Maia, L. Colina-Vegas, J. Moreira, A. M. Plutin, R. Mocelo, V. M. Deflon, M. R. Cominetti, M. I. Camargo-Mathias, A. A. Batista, *Polyhedron* **2017**, *126*, 33–41.

[55] R. S. Correa, K. M. De Oliveira, F. G. Delolo, A. Alvarez, R. Mocelo, A. M. Plutin, M. R. Cominetti, E. E. Castellano, A. A. Batista, *J. Inorg. Biochem.* **2015**, *150*, 63–71.

[56] P. R. Chetana, B. S. Srinatha, M. N. Somashekar, R. S. Policegoudra, *J. Mol. Struct.* **2016**, *1106*, 352–365.

[57] J. Ferreira, M. Pavani, W. Hermindez, E. Spodine, L. Beyer, U. Schroder, R. Richter, *Bioinorg. Chem. Appl.* **2005**, *3*, 299–317.

[58] A. M. Plutín, R. Mocelo, A. Alvarez, R. Ramos, E. E. Castellano, M. R. Cominetti, A. E. Graminha, A. G. Ferreira, A. A. Batista, *J. Inorg. Biochem.* **2014**, *134*, 76–82.

[59] A. M. Plutín, A. Alvarez, R. Mocelo, R. Ramos, E. E. Castellano, M. M. Da Silva, L. Colina-Vegas, F. R. Pavan, A. A. Batista, *Inorg. Chem. Commun.* **2016**, *63*, 74–80.

[60] T. J. Egan, K. R. Koch, P. L. Swan, C. Clarkson, D. A. Van Schalkwyk, P. J. Smith, *J. Med. Chem.* **2004**, *47*, 2926–2934.

[61] R. N. Magwaza, Synthesis and characterization of novel $[Pt(diimine)(acylthiourea)]^{+}$ complexes as potential anticancer agents and exploring the use of Sulphobutyl-ether- β -cyclodextrin and surfactant micelles as a drug delivery system, MSc, University of the Witwatersrand, **2017**.

[62] M. M. Aleksić, V. Kapetanović, *Acta Chim. Slov.* **2014**, *61*, 555–573.

[63] M. Sirajuddin, S. Ali, A. Badshah, *J. Photochem. Photobiol. B Biol.* **2013**, *124*, 1–19.

[64] S. Puyo, D. Montaudon, P. Pourquier, *Crit. Rev. Oncol.* **2014**, *89*, 43–61.

[65] A. S. Abu-Surrah, M. Kettunen, *Curr. Med. Chem.* **2006**, *13*, 1337–1357.

[66] L. Fuks, E. Anuszewska, H. Kruszewska, A. Kro´wczyn´ski, J. Dudek, N. Sadlej-Sosnowska, *Transit. Met. Chem.* **2010**, *35*, 639–647.

[67] C. Rocha, M. Silva, A. Quinet, J. Cabral-Neto, C. Menck, *Clinics* **2018**, *73*, 1–10.

[68] D. Jaramillo, D. P. Buck, J. G. Collins, R. R. Fenton, F. H. Stootman, N. J. Wheate, J. R. Aldrich-Wright, *Eur. J. Inorg. Chem.* **2006**, 839–849.

[69] G. Lowe, A. S. Droz, T. Vilaivan, G. W. Weaver, J. J. Park, J. M. Pratt, L. Tweedale, L. R. Kelland, *J. Med. Chem.* **1999**, *42*, 3167–3174.

[70] B. J. Pages, D. L. Ang, E. P. Wright, J. R. Aldrich-Wright, *Dalton Trans.* **2015**, *44*, 3505–3526.

[71] M. F. Brana, M. Cacho, A. Gradillas, B. de Pascual-Teresa, A. Ramos, *Curr. Pharm. Des.* **2001**, *7*, 1745–1780.

[72] R. Martínez, L. Chacón-García, *Curr. Med. Chem.* **2005**, *12*, 127–151.

[73] J. C. García-Ramos, R. Galindo-Murillo, F. Cortés-Guzmán, L. Ruiz-Azuara, *J. Mex. Chem. Soc.* **2013**, *57*, 245–259.

[74] K. Nakamoto, M. Tsuboi, G. D. Strahan, *Drug-DNA Interactions: Structures and Spectra*, John Wiley & Sons, New Jersy, **2008**.

[75] S. M. Carr, "Major and Minor Grooves in a space-filling model of DNA," can be found under https://www.mun.ca/biology/scarr/MGA2_02-07.html, **2011**.

[76] S. U. Rehman, T. Sarwar, M. A. Husain, H. M. Ishqi, M. Tabish, *Arch. Biochem. Biophys.* **2015**, *576*, 49–60.

[77] V. Brabec, H. Loskotova, *Eur. J. Biochem.* **1999**, *266*, 392–402.

[78] P. Nagababu, D. A. Kumar, K. L. Reddy, K. A. Kumar, M. B. Mustafa, M. Shilpa, S. Satyanarayana, *Met. Drugs* **2008**.

[79] K. Mišković, M. Bujak, M. Baus Lončar, L. Glavaš-Obrovac, *Arch. Ind. Hyg. Toxicol.* **2013**, *64*, 593–602.

[80] M. Wang, Y. Yu, C. Liang, A. Lu, G. Zhang, *Int. J. Mol. Sci.* **2016**, *17*, 779.

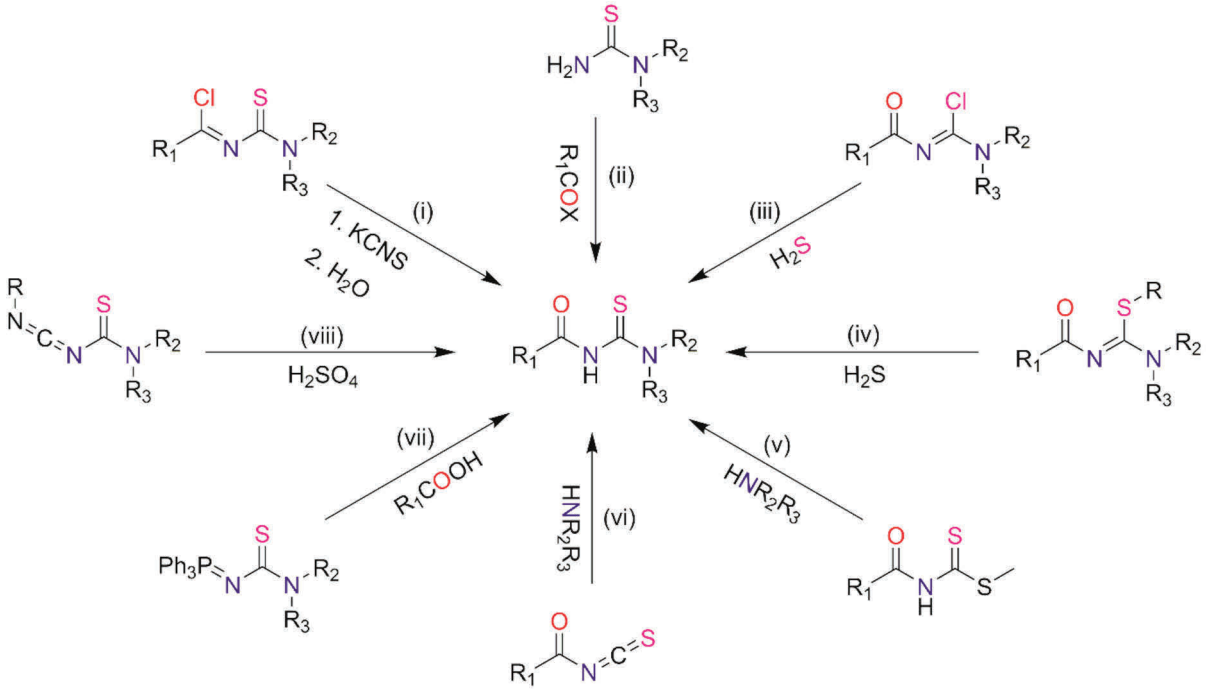
[81] Y. Xiong, M. Sundaralingam, *Encycl. Life Sci.* **2001**, 1–8.

Chapter 2

Ligand and Complex Synthesis, Characterization and Experimental

2.1. Introduction

Disubstituted acylthiourea ligands are valuable organo-sulfur compounds with interesting potential applications[1–5] given that their synthesis has thoroughly been investigated and continues to be of interest. There are several synthetic routes to disubstituted acylthiourea ligands (*Scheme 1*); however, the most commonly used method firstly involves the synthesis of an isothiocyanate from the reaction of an acyl chloride and a thiocyanate salt followed by a subsequent reaction with a secondary amine under inert conditions[6] (*Scheme 4*). This method was adopted for the synthesis of most of the ligands throughout this study.



*Scheme 1: Common routes to the synthesis of N,N-di(alkyl/aryl)-N'-acylthiourea ligands (**HL^n**).*[7]

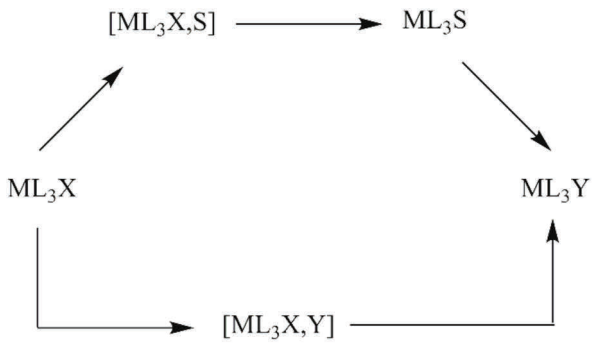
Complex synthesis, on the other hand, was not straight forward as these types of complexes had never been synthesised before. First attempts involved a modified literature method used for the synthesis of cationic $[Pt(phen)(L^n\text{-}\kappa O,S)]^+$ complexes,[8] by reacting a platinum(II) metal precursor $[PtCl_2(phen)]$ with 2.5 equivalents of a deprotonated disubstituted acylthiourea ligand where deprotonation happened *in-situ* through the use of sodium acetate as a base. A suspension of $[PtCl_2(phen)]$ in methanol was added slowly to a solution of 2.5 equivalents disubstituted acylthiourea ligand and 2.5 equivalents

sodium acetate in methanol and heated under reflux until the suspension cleared to give an orange solution. Generally platinum(II) undergoes mainly ligand substitution reactions, and it is reluctant to expand its coordination number since it prefers a square planar configuration.[9] These ligand substitutions usually occur *via* an associative (*A*) activation or at least an interchange mechanism under associative activation (I_a) due to unoccupied axial sites.[10,11] Substitution reactions in square planar complexes of the form(1), normally provide a simplified illustration of ligand substitutions (without the complexity of stepwise substitutions involved when there are more leaving ligands) and are frequently described by a two-term rate equation (2),[12]

$$ML_3X + Y \longrightarrow ML_3Y + X \quad (1)$$

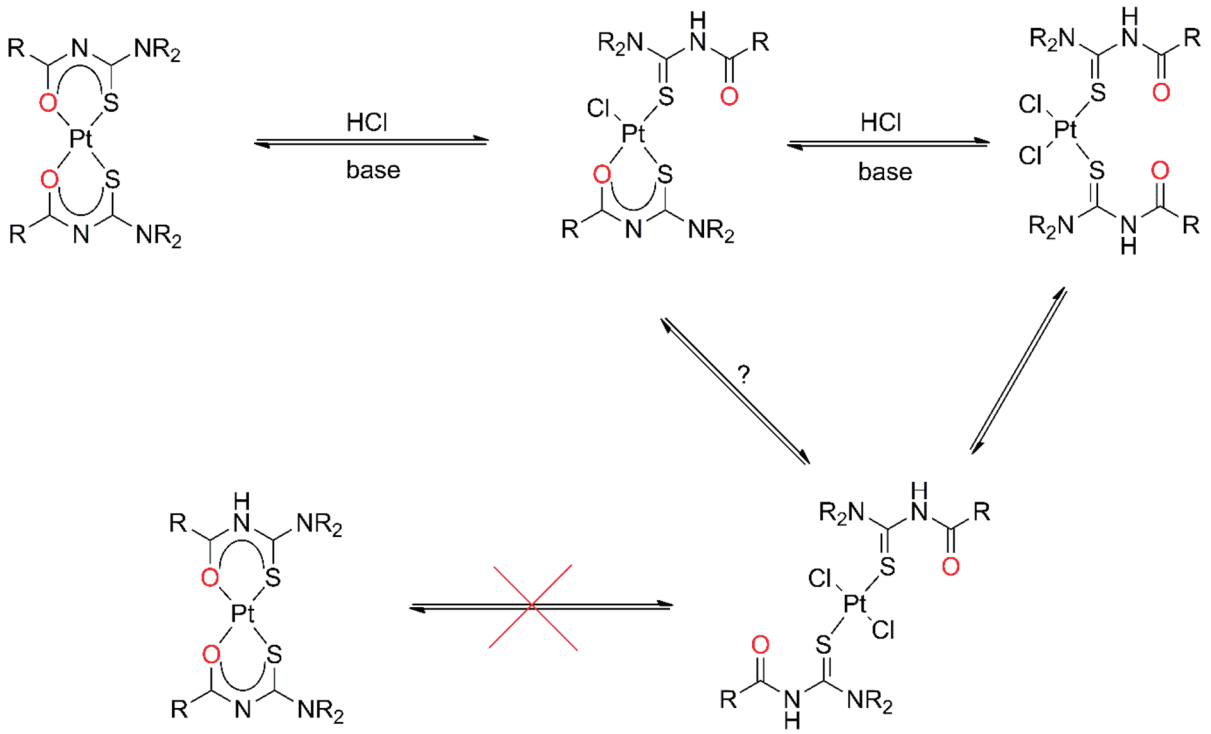
$$\text{Rate} = k_{obs}[ML_3X], \text{ where } k_{obs} = k_s + k_y[Y] \ldots\ldots.(2)$$

where k_s is the rate constant due to the displacement of X by the solvent and k_y is the rate constant due to the direct displacement of X by Y, which can be interpreted to be as a result of the operation of two parallel associative reaction paths (*Scheme 2*).



Scheme 2: General illustration of ligand substitution reactions in square planar complexes.[13]

It is with this model in mind that we anticipate the substitution of the chloro ligands with deprotonated disubstituted acylthiourea ligands to take place. Coordination of disubstituted acylthiourea ligands has been established to be pH-dependent where complexation to Pt(II), Pd(II) and Rh(III) in chloride rich solutions were reported to preferentially happen at pH<2 while complexation to Ni(II), Zn(II) and Co(II) occurred at pH>3.[14,15] In another study, Koch *et al.*[16] demonstrated the dependence of the coordination of disubstituted acylthiourea ligands on protonation. In their study addition of HCl to a solution of *bis*(platinum(II)-acylthiourea) chelate resulted in the protonation of the acylthioureato ligands with subsequent "anation" and isomerisation reactions affording a variety of species in solution (*Scheme 3*). As protonation of one ligand occurs, the ring-opening of the chelate takes place as a result of coordination by the halide. Further protonation affords equivalent results in the second chelating ligand. This interesting regulated "coordination switch", as will become apparent later (*chapter 3*), bears some resemblance to the explanation of acid stability exhibited by the [Pt(phen)(L^n-κ*S*)$_2$] complexes.

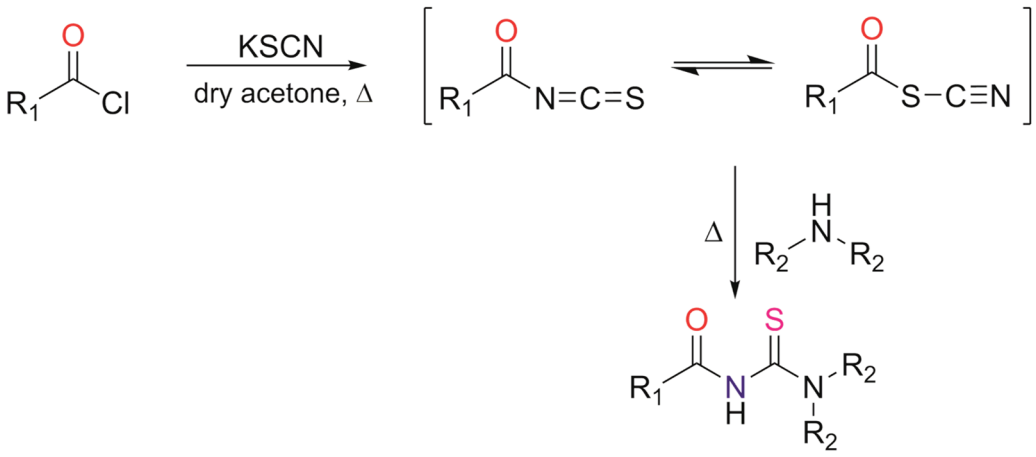


Scheme 3: Effects of HCl acid on cis-[Pt(L^n-κO,S)$_2$] according to Koch et al.[16]

2.2. Results and Discussion

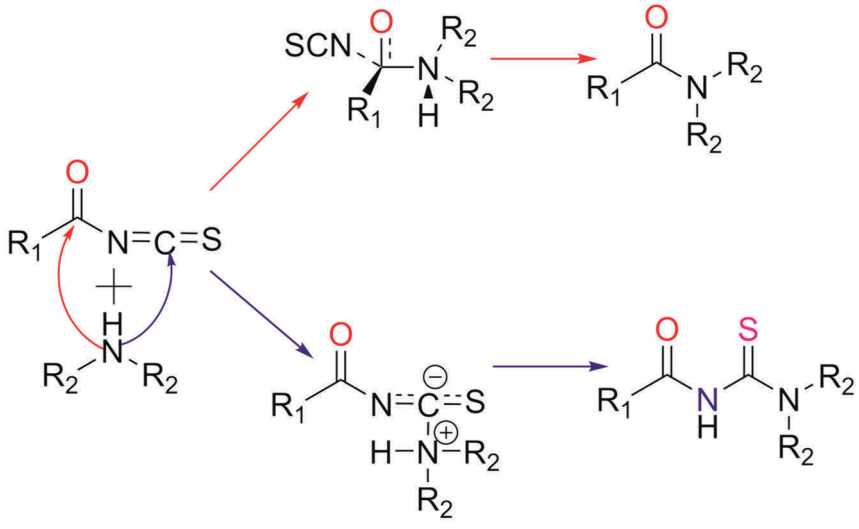
2.2.1. Synthesis of *N,N*-di(alkyl/aryl)-*N*'-acylthiourea (HL^n) ligands

We herein describe a wide range of *N,N*-di(alkyl/aryl)-*N*'-acylthiourea ligands synthesised with systematic variations in the R and R' substituents. These ligand variations hopefully allow for an extensive evaluation of factors that influence the coordination mode preference of these ligands to platinum(II) ions. *N,N*-di(alkyl/aryl)-*N*'-acylthiourea ligands have been prepared previously by a variety of methods, the most common of which is the facile one-pot synthesis described by Douglass and Dains[6] (*Scheme 4*). This method involves the addition of an acyl chloride to a solution of potassium thiocyanate in anhydrous acetone under inert conditions and refluxing the mixture for 45 minutes. In this step, the nucleophilic attack by the thiocyanate anion can either occur through the nitrogen or sulfur as the thiocyanate may exist in two mesomeric forms in acetone.[17] Theoretically, two products are possible depending on the thiocyanate isomer involved; however, in practice, only one product forms.



Scheme 4: General procedure for the synthesis of N,N-di(alkyl/aryl)-N'-acylthiourea ligands.[6,17]

The acyl thiocyanate formed then reacts with an appropriate amine with both the acyl carbon and the thiocarbonyl carbon being susceptible to electrophilic attack. Electronic as well as steric factors (with the latter being dominant) determines the preference as to which electrophilic centres between the two react.[18] Mechanistically attack at the carbonyl carbon is thought to occur via a tetrahedral intermediate in which both the carbonyl carbon and the nitrogen becomes sp^3 hybridised leading to a rather crowded transition state depending on the nature of the R substituents. However, attack at the thiocarbonyl carbon has been suggested to occur via a trigonal zwitterionic intermediate where the thiocarbonyl carbon becomes sp^2 hybridised, which is relatively less congested compared to the tetrahedral intermediate (*Scheme 5*).[19]



Scheme 5: Two possible routes to nucleophilic attack of the carbonyl carbon and thiocarbonyl carbon by an amine.[19]

Therefore, electron releasing R substituents that decrease the electrophilicity of the carbonyl carbon and sterically less bulk R_1 substituents that do not hinder access to the carbonyl carbon favour attack at this

carbon while electron-withdrawing R substituents and sterically bulk R substituents favour attack at the thiocarbonyl carbon. In this study, steric hindrance was introduced by either increasing the bulkiness of the R_1 substituents of the acyl group or increasing the bulkiness of the R_2 substituents of the amine. We synthesised the following ligand variations (*Figure 1*) and characterised them using ^{1}H, ^{13}C NMR, FTIR and elemental analysis.

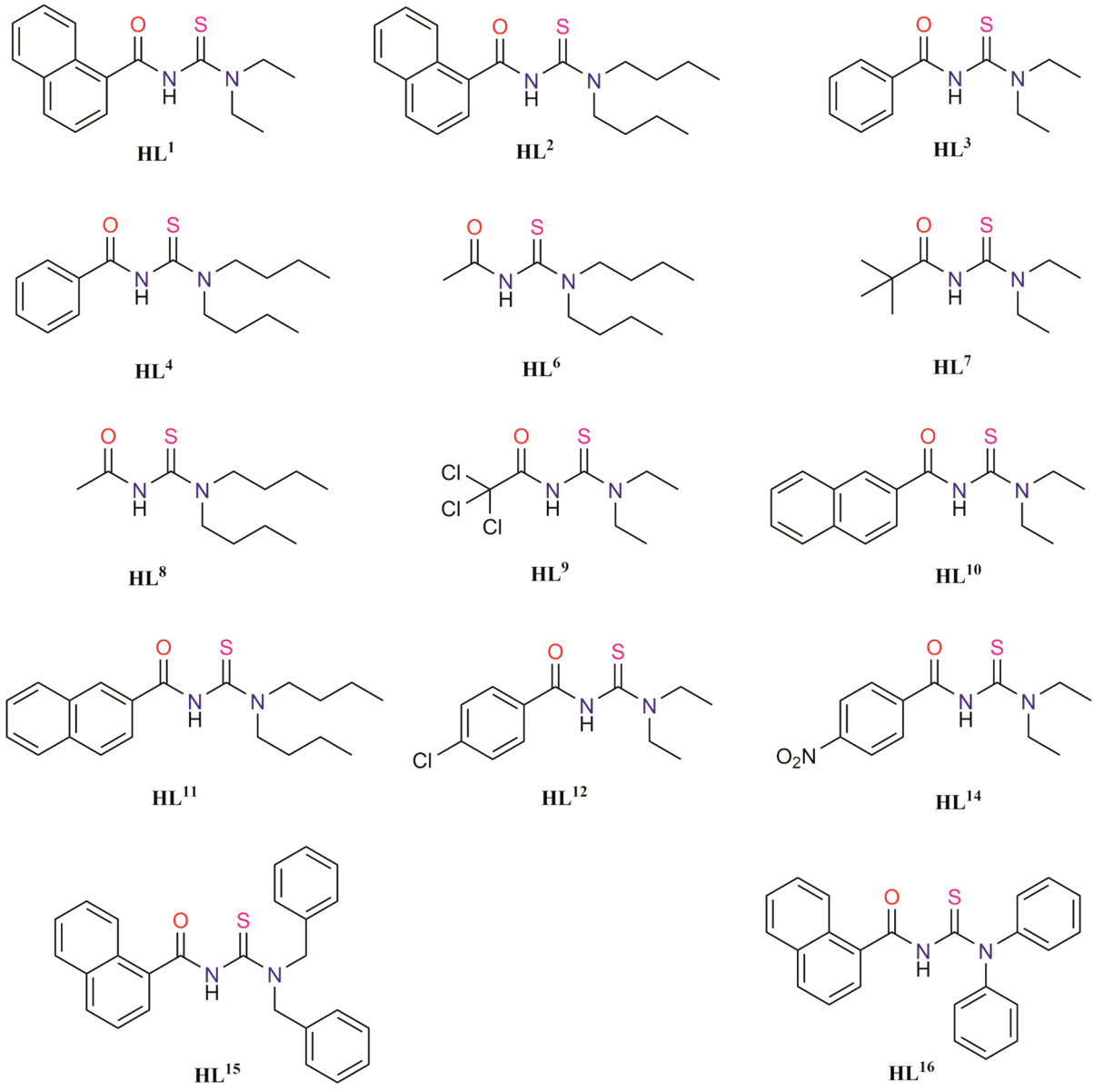


Figure 1: Structures of ligands synthesised showing significant variations on the acyl substituents and minor variations on the amino end of the ligands.

The ligand *N,N*-di(ethyl)-*N'*-benzoylthiourea (**HL^3**) is used to illustrate the spectroscopic characterisation in these ligands, unambiguously assigning ^{1}H and ^{13}C NMR signals with the aid of 2D-NMR techniques. The ^{1}H Nmr spectrum of **HL^3** (*Figure 2*) exhibited a broad singlet at 8.37 ppm, assigned as the amidic proton N-H in all the ligands. The aromatic signals $H^{2'+6'}$, $H^{3'+5'}$ and $H^{4'}$ were assigned with the aid of COSY NMR spectroscopy (*Figure 3*) with the most deshielded signal being $H^{2'+6'}$ due to the electron-withdrawing carbonyl group.

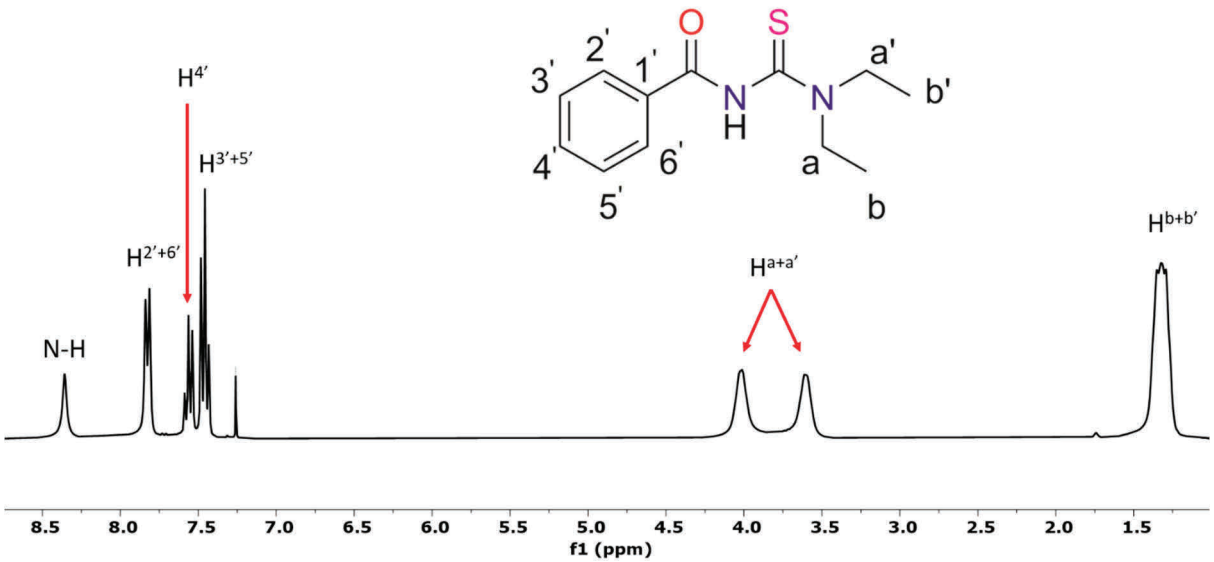


Figure 2: ^{1}H NMR spectrum of **HL^3** *in chloroform-d at 25°C assigned as per the numbering scheme indicated.*

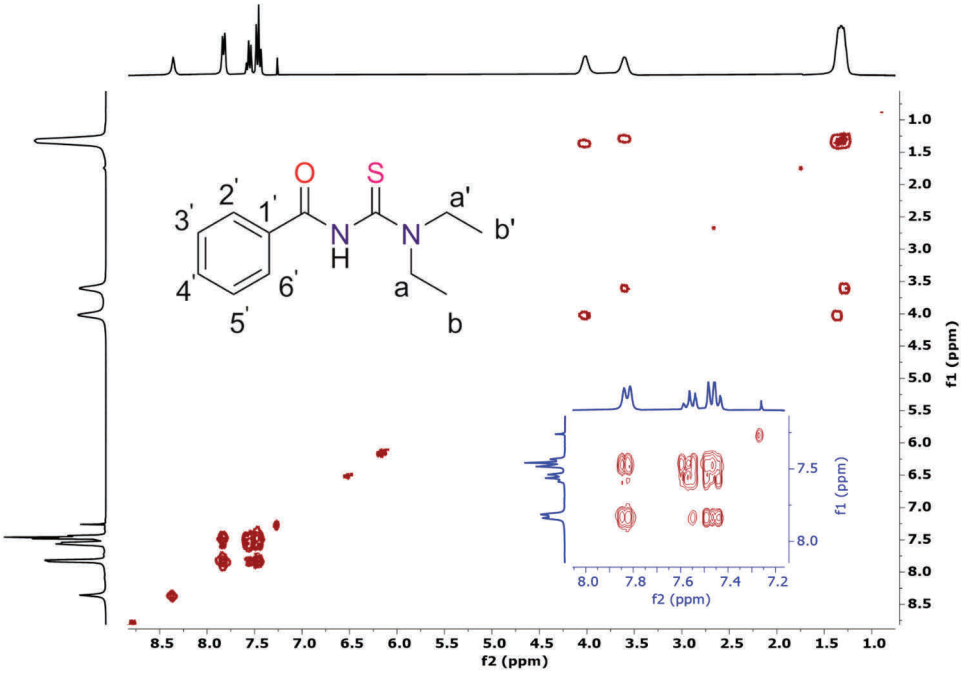
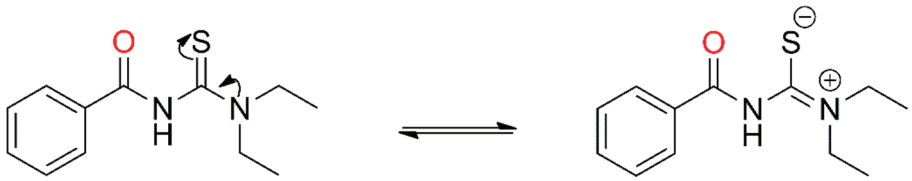


Figure 3: The COSY spectrum for **HL^3** *in chloroform-d at 25°C*

The most shielded aromatic ^{1}H resonance at 7.47 ppm could be assigned to $H^{3'+5'}$ as it shows three bond coupling with two different protons while the ^{1}H resonance at 7.57 ppm was assigned to $H^{4'}$ because it only shows strong three bond coupling to one proton (*Figure 3*). These assignments agree with the integrations observed. Another exciting feature of these ligands was seen in the methylene proton signals $H^{a+a'}$ which appear as two distinct peaks at 4.03 ppm and 3.62 ppm indicating two different proton environments and this observation is ascribed to the thione-thiol tautomerism (*Scheme 6*). This tautomerism effect renders the thioamidic C-N a partial double bond character restricting rotation around it at room temperature, hence the different proton environments.



Scheme 6: Thione-Thiol tautomerism is **HL^{3}**

The Carbonyl (C=O) and thiocarbonyl (C=S) signals in ^{13}C NMR (*Figure 4*) were assigned as the most deshielded peaks at 163.78 ppm and 179.34 ppm, respectively. The carbons bonded to protons were assigned with the help of an HSQC NMR spectrum while the quaternary carbons were distinguished using DEPT-135 NMR (*electronic supplementary information*).

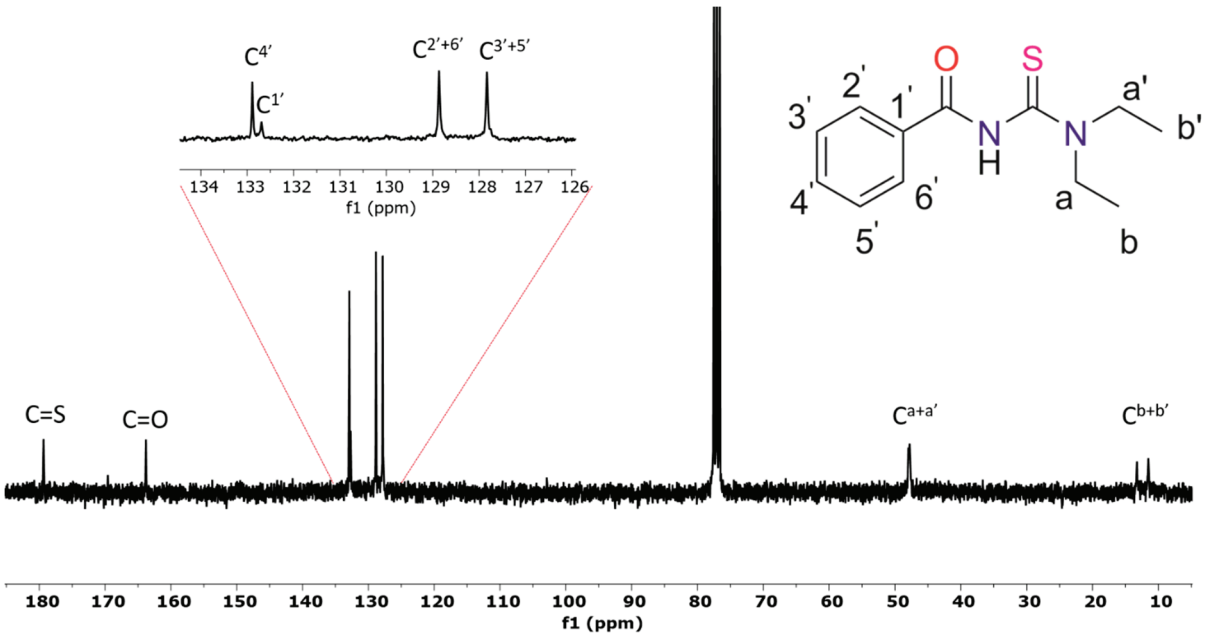
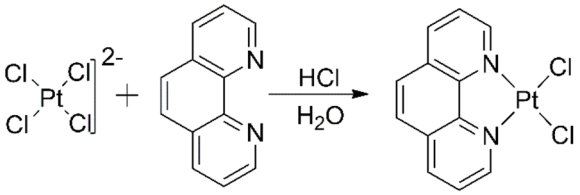


Figure 4: ^{13}C Nmr spectrum for **HL^{3}** *in chloroform-d at 25°C with complete assignments and numbering scheme.*

The ligand was also characterised using Fourier Transform Infrared spectroscopy (*Appendix 1 Figure A1-22*) with a characteristic weak N-H stretching band at 3267 cm^{-1}, a strong C=O stretching band at 1651 cm^{-1} and a strong C=N band at 1524 cm^{-1} while we could not assign the C=S stretching band with certainty. The C=O stretching band of these ligands is overly sensitive to substituents on the carbonyl carbon and it is shown to shift to lower wavenumbers with increasing electron releasing effect of substituent groups. Electron releasing substituents on the thioamidic nitrogen also seem to have the same impact on the carbonyl stretching frequency.

2.2.2. Synthesis of the [$PtCl_2$(phen)] precursor

The precursor [$PtCl_2$(phen)], was synthesised according to a literature method[20] whereby we heated, under reflux, a mixture of 1, 10-phenanthroline and potassium tetrachloroplatinate in distilled water acidified with six drops of concentrated HCl. The acidified water minimises the formation of dimeric hydroxo species of platinum(II). The reaction mixture was refluxed until the reddish mixture turned bright yellow (*ca.* 3 hours), the product washed with water and then small amounts of methanol and diethyl ether to remove unreacted material. Earlier studies suggested this reaction involves aquation of the [$PtCl_4^{2-}$] complex followed by substitution of the aqua ligands with 1, 10-phenanthroline to give a neutral chelate.[21–23] Characterisation of the product was done using ^{1}H-NMR and FT-IR spectroscopy and elemental analysis.



Scheme 7: Reaction scheme for the synthesis of [$PtCl_2$(phen)]

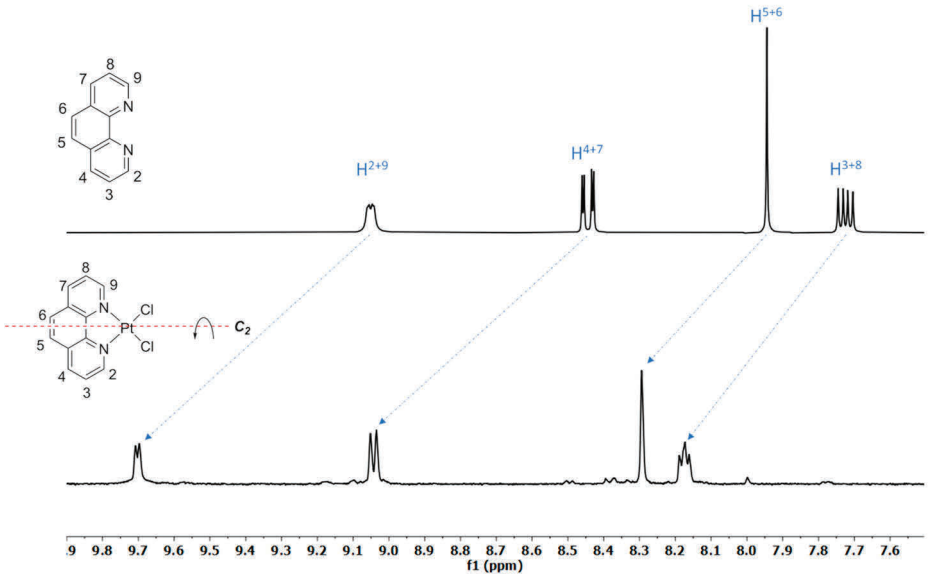


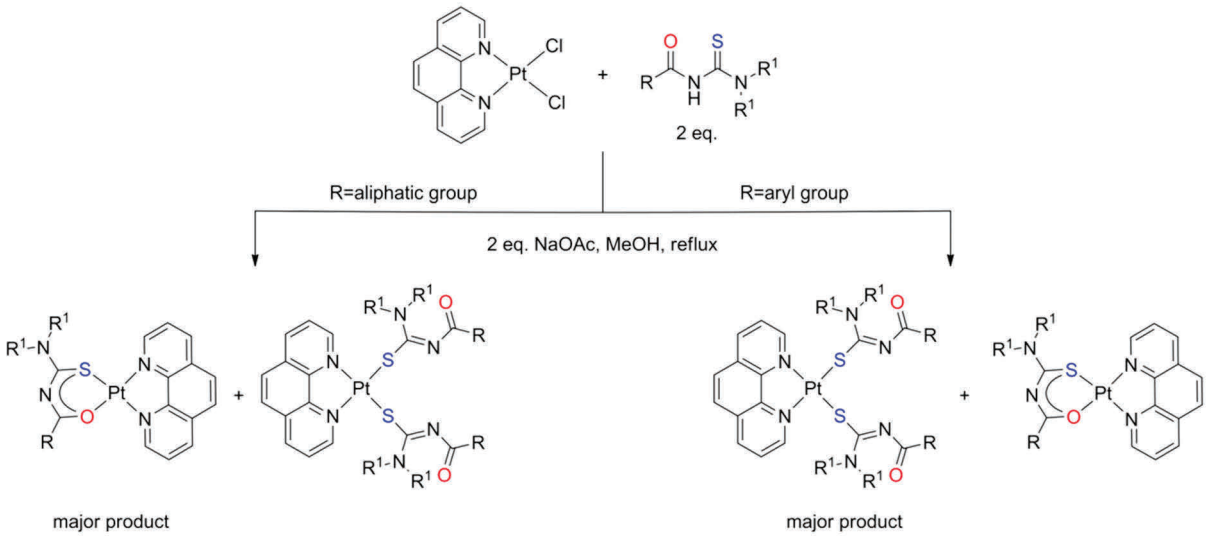
Figure 5: ^{1}H NMR spectrum of [$PtCl_2$(phen)] in DMSO-d at 25°C

The ^{1}H NMR spectrum of the precursor complex showed only four signals in the aromatic region as a result of C_2 symmetry in the molecule (*Figure 5*). The most deshielded proton signal was assigned to the protons H^{2+9} due to their proximity to nitrogen while the singlet at 8.31 ppm was assigned to protons H^{5+6} since they do not exhibit coupling with any other proton. The most shielded doublet of doublets at 8.18 ppm, which appear as an unresolved triplet due to three bond coupling with two protons from different environments, could be assigned to H^{3+8}. The remaining doublet of doublets at 9.05 ppm was assigned to H^{4+7}. The Infrared spectrum (*Appendix 1 Figure A1-29*) of the precursor complex showed typical bands at 3083 and 3059 cm^{-1} due to an aromatic C-H stretching vibration and at 1427 cm^{-1} due to a C=N stretching vibration.

2.2.3. Synthesis of the [Pt(phen)(L^n-κ*S*)$_2$] complexes

The synthesis of [Pt(phen)(L^n-κ*S*)$_2$] complexes (where L^n = deprotonated *N,N*-di(alkyl/aryl)-*N*'-acylthiourea) from [$PtCl_2$(phen)] was premised on the substitution of this precursor complex's two chloro ligands with two disubstituted acylthioureato ligands coordinated in a monodentate fashion against a seemingly thermodynamically favourable, chelation (through sulfur and oxygen) with only one acylthioureato ligand.

We considered a couple of approaches to the synthesis of [Pt(phen)(L^n-κ*S*)$_2$] complexes. The initial preference was a modification of the one-pot synthesis reported by Kotzé *et al*[8] where the generation of the acylthioureato anion happens *in situ* with subsequent substitution of the chlorides to give the corresponding [Pt(phen)(L^n-κ*S*)$_2$] complex (*Scheme 8*). However, this method only proved successful with acylthiourea ligands having a trichloroacetyl- or aryl- substituents on the acyl group with yields in the 70-90% range. Acylthioureas with aliphatic substituents (electron-donating, for example, acetyl and *tert*-butyl substituents) on the acyl moiety, instead, preferred chelate formation with yields higher than 90%.



*Scheme 8: One-pot synthesis (method A) of [Pt(phen)(L^n-κ*S*)$_2$]complexes where the acylthioureato ligand was generated in-situ through deprotonation with sodium acetate.*

In an attempt to understand how these two groups of disubstituted acylthiourea ligands behaved so differently under these conditions and in turn develop a new procedure that gives the desired complexes across the whole range of ligands, two reaction progress kinetics experiments were performed using *N,N*-di(ethyl)-*N*'-benzoylthiourea and *N,N*-di(ethyl)-*N*'-pivaloylthiourea ligands. In these experiments [$PtCl_2$(phen)] was added to a solution containing excess acylthiourea ligand dissolved in 5 ml methanol and refluxed while taking 50 µl aliquots at intervals for three and two hours respectively. The 50 µl aliquots were immediately trapped in chloroform-*d* and analysed using ^{1}H NMR to determine species distribution as the reaction progressed. From the series of spectra obtained, it is evident that in the reaction with *N,N*-di(ethyl)-*N*'-benzoylthiourea (*Figure 6*) that monodentate coordination of the acylthioureato ligand is preferred earlier, while chelate formation starts later in the reaction. We attributed this observation to result from possibly the depletion of the ligand as well as possible acidic instability of the complexes as acetic acid accumulates in the reaction mixture.

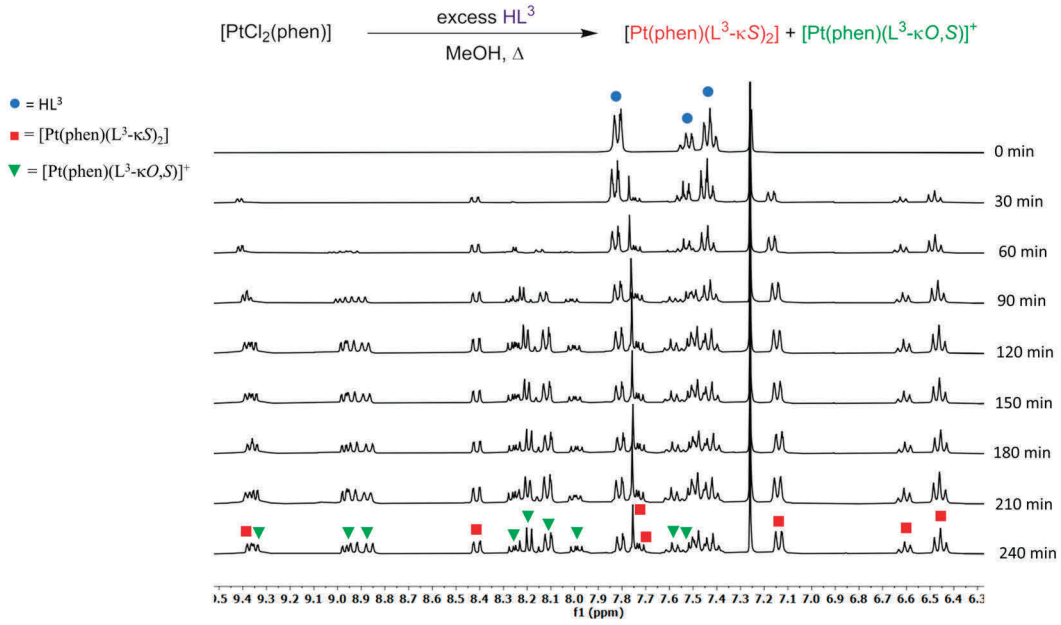


Figure 6: Stacked ^{1}H-NMR spectra (aromatic region) of the reaction mixture aliquots taken at different times during the reaction between N,N-di(ethyl)-N'-benzoylthiourea and [$PtCl_2$(phen)] and recorded in chloroform-d at 25°C.

However, during the synthesis of *N,N*-di(ethyl)-*N*'-pivaloylthiourea, none of the desired [Pt(phen)(L^7-κS)$_2$] complex seem to form at all as only the proton signals from the chelate are observed (*Figure 7*). This intriguing result may be due to the reduced acid stability of [Pt(phen)(L^7-κ*S*)$_2$]. The relative stabilities in an acidic medium between these two complexes [Pt(phen)(L^3-κ*S*)$_2$] and [Pt(phen)(L^7-κ*S*)$_2$] were deduced by inferring to the acid dissociation constants (hence pK_as) of the free ligands. Theoretically, we expect *N,N*-di(ethyl)-*N*'-pivaloylthiourea to be less acidic and thus have a stronger conjugate base compared to *N,N*-di(ethyl)-*N*'-benzoylthiourea, because a *tert*-butyl group is more

electron-donating than a phenyl group and also that the phenyl ring stabilises the conjugate base through extended conjugation. Hence [Pt(phen)(L^7-κ*S*)$_2$] is more likely to be less stable under even the slightest acidic conditions than [Pt(phen)(L^3-κ*S*)$_2$].

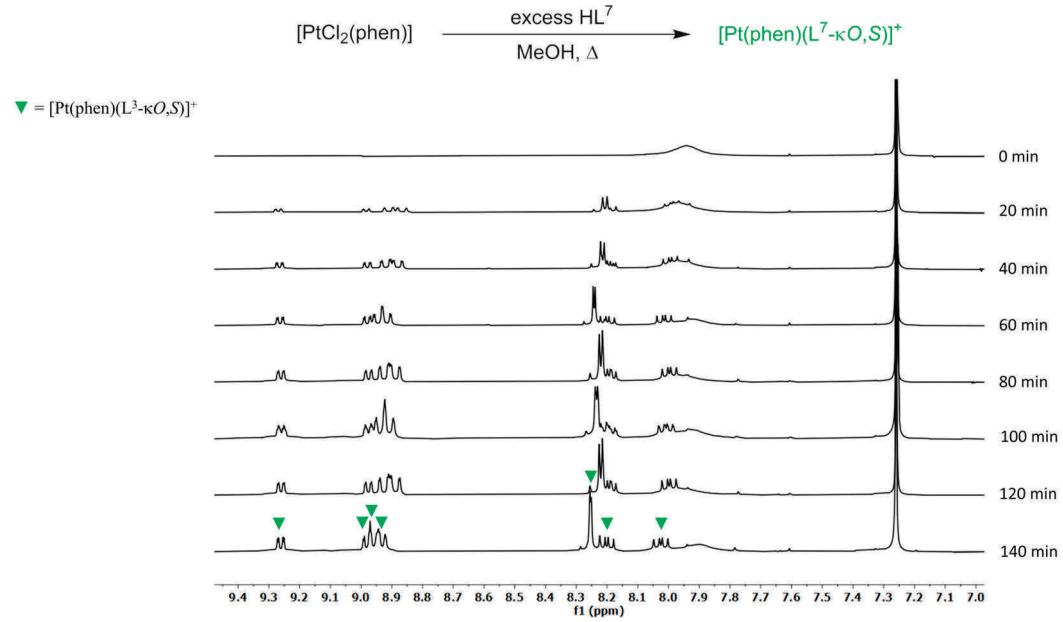
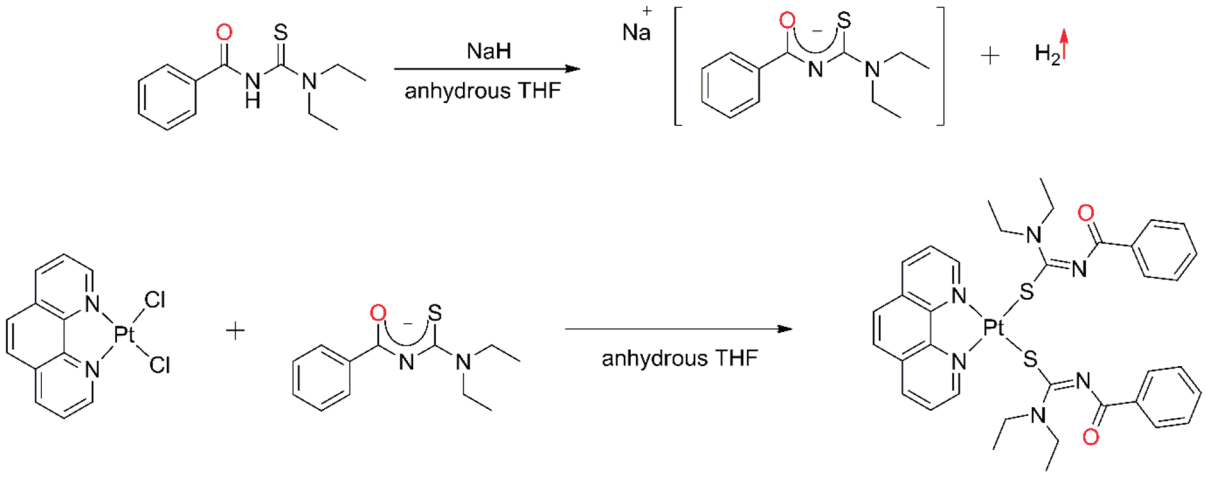


Figure 7: Stacked ^{1}H-NMR spectra (aromatic region) of the reaction mixture aliquots taken at different times during the reaction between N,N-di(ethyl)-N'-pivaloylthiourea and [PtCl$_2$(phen)] and recorded in chloroform-d at 25°C.

In light of these results, we decided to develop a reaction procedure where no acid was involved and came up with a method B (*Scheme 9*) which uses a salt of the acylthiourea ligand to react with the [PtCl$_2$(phen)] precursor. In this method, the ligands were deprotonated using sodium hydride as the base under anhydrous conditions in THF. 2.2 equivalents of the formed salt in solution then reacted with one equivalent of the precursor complex for one hour to obtain the desired product in excellent yields (greater than 80% yields depending on water content of the anhydrous solvents) across the whole ligand variations. Hence method B was adopted for the synthesis of [Pt(phen)(L^n-κ*S*)$_2$] complexes throughout this study. To illustrate the characterisation of these complexes, we have chosen [Pt(phen)(L^3-κ*S*)$_2$].



*Scheme 9: Method B- stepwise synthesis of [Pt(phen)(L^3-κ*S*)$_2$] where the ligand was deprotonated using sodium hydride. (final method adopted for all complexes)*

Structural characterisation of [Pt(phen)(L^3-κ*S*)$_2$] was achieved using ^{1}H- and ^{13}C NMR, FTIR, MS, single-crystal XRD and elemental analysis. The ^{1}H NMR spectrum of [Pt(phen)(L^3-κ*S*)$_2$] is relatively uncomplicated as the 1,10-phenanthroline (phen) and *N*,*N*-di(ethyl)-*N*'-benzoylthioureato (**L^3**) ^{1}H resonances appear separated in the aromatic region of the ^{1}H NMR spectrum (*Figure 8*). ^{1}H NMR spectrum for this complex shows firstly the disappearance of the N-H signal indicating a deprotonated acylthiourea ligand in the complex. We only observed seven aromatic proton environments (four due to the eight phenanthroline moiety protons from the [PtCl$_2$(phen)] precursor and three due to the five phenyl ring protons of the acylthiourea ligand) as a result of the presence of a C_2 symmetry axis in the molecule. Due to the clear separation of the aromatic ^{1}H resonances from the two ligand (phen and **L^3**), the protons were assigned as reported earlier in the free ligand (**HL^3**) and the [PtCl$_2$(phen)] precursor, and confirmed by three bond proton couplings observed in 2-D NMR COSY experiments (*Figure 9*). The proton signals from the phenyl ring of the *N*,*N*-di(ethyl)-*N*'-benzoylthioureato ligand shifted upfield compared to the free ligand (*Figure 8*). Another important observation was the coalescence of the methylene proton signals in the complex compared to free ligand at room temperature, which may indicate that coordination happened through the sulfur donor atom.

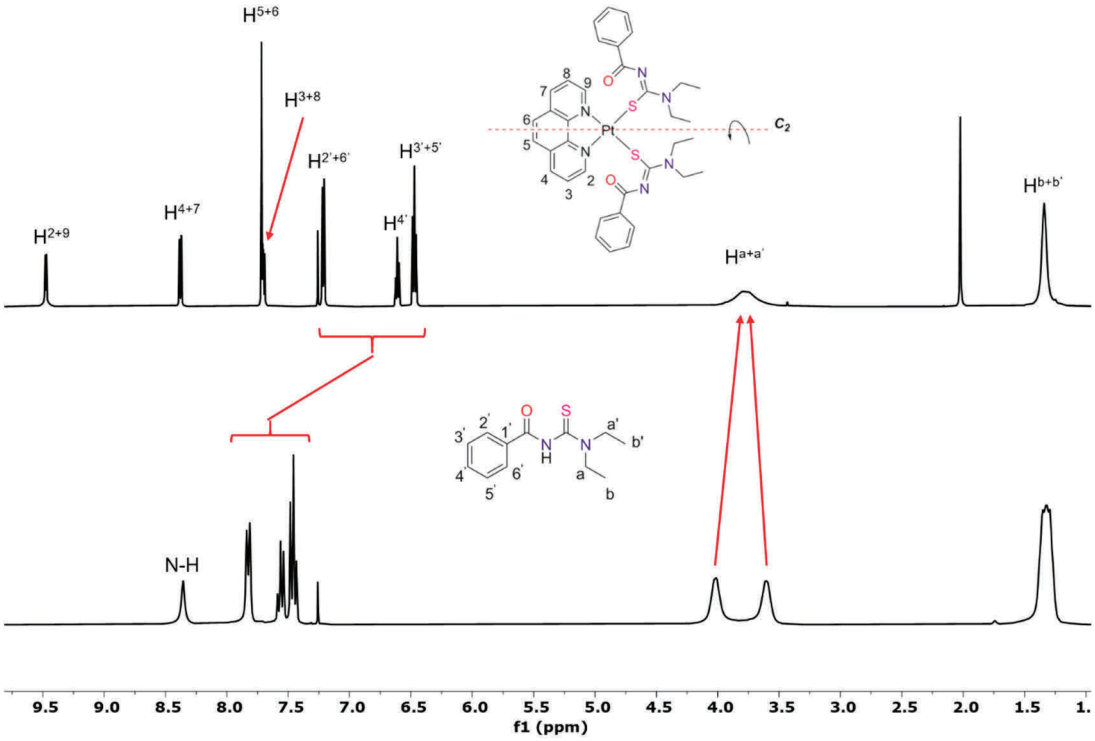


Figure 8: ^{1}H NMR spectrum for N,N-di(ethyl)-N'-benzoylthiourea and [Pt(phen)(L^{3}-κS)$_2$] in chloroform-d at 25°C with the complete numbering scheme.

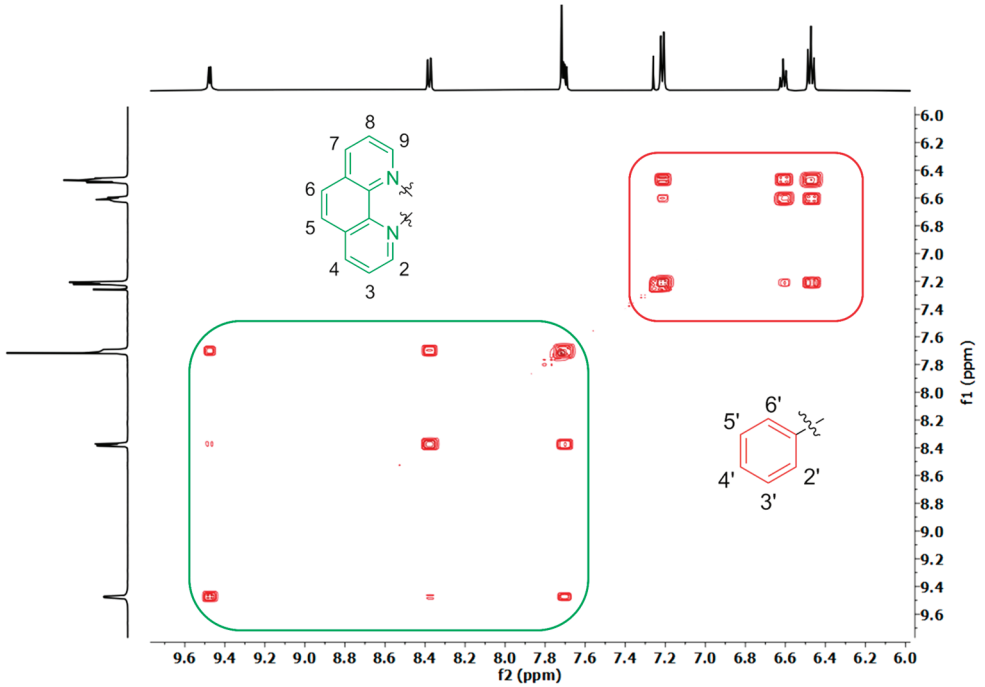


Figure 9: COSY spectrum for [Pt(phen)(L^{3}-κS)$_2$] recorded in chloroform-d at 25°C.

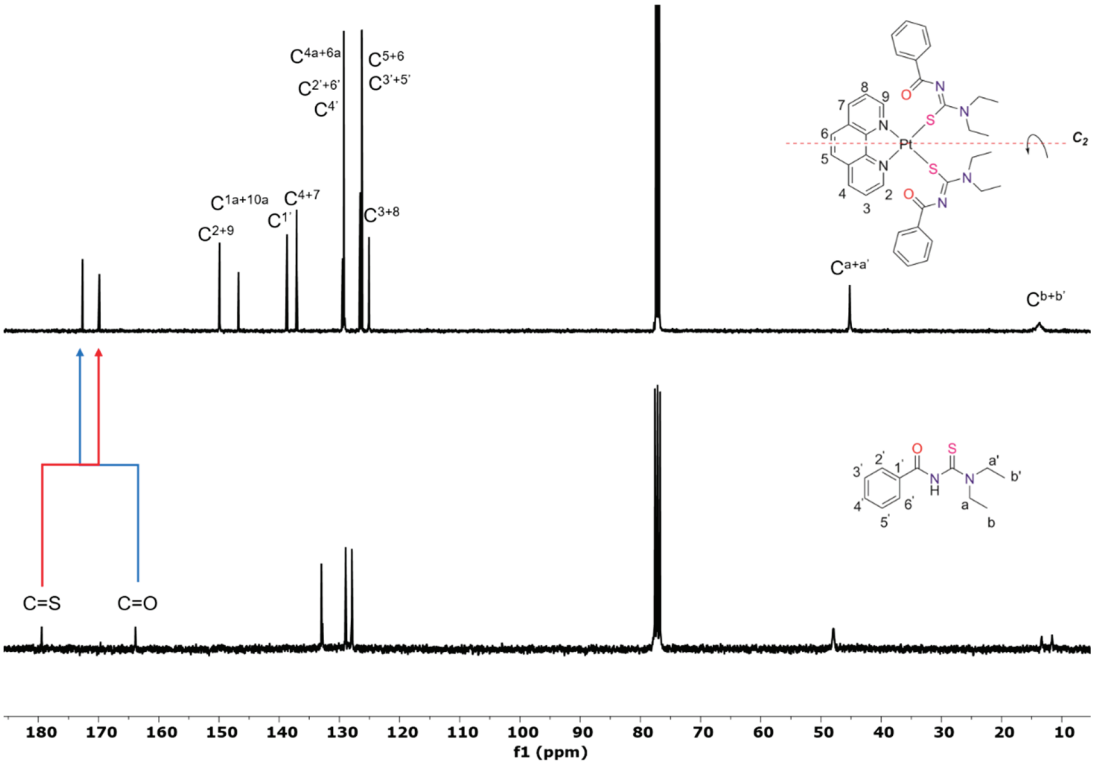


Figure 10: ^{13}C NMR spectra for N,N-di(ethyl)-N'-benzoylthiourea and the complex [Pt(phen)(L^3-κS)$_2$] in chloroform at 25°C.

We achieved the complete assignment of carbon atoms with the help of HSQC and HMBC 2-D NMR spectra, as well as DEPT-135 NMR (*electronic supplementary information*). Notably, in the ^{13}C NMR spectrum of the complex (*Figure10*), carbonyl and thiocarbonyl signals were observed at 172.54 ppm and 169.76 ppm respectively while the same resonances appear at 163.78 ppm and 179.34 ppm in the free ligand. There seem to be an interesting "symmetric swap" of the carbonyl and thiocarbonyl signals in the complex compared to the free ligand. This signal swap has been noticed in several chelate complexes of disubstituted acylthiourea ligands, though not this symmetric and has been vaguely explained as being due to extensive delocalisation of charge within the chelate ring.[24] Interpreting the observed trend in our complexes using the same argument seems counterintuitive as a different coordination mode is at play; however, the same concept may be at play for which we suggest that maybe further investigation is required to understand the observations fully.

The characteristic FT-IR absorption bands (*Appendix 1 Figure A1-29*) of the [Pt(phen)(L^3-κS)$_2$] complexes compared with those of the free ligand showed a disappearance of the N-H stretching frequency, indicating that the ligand is deprotonated in the complex. Also, in the IR spectrum of the complex, there is a shift of the carbonyl stretching frequency from an intense band at 1651 cm^{-1} in the free ligand to a signal at 1564 cm^{-1} of weak intensity in the complex. The observation may be as a result of the extensive conjugation introduced by the deprotonation of the ligand that in turn suppresses the

mesomeric electron-withdrawing effect of the amido group thereby reducing the dipole moment in the C=O bond and weakening it as well.

2.2.4. Single crystal X-ray crystallographic analysis of [Pt(phen)(L^n-κ*S*)$_2$] complexes

Single crystals suitable for single-crystal XRD analysis were grown using the slow evaporation, solvent diffusion, and vapour diffusion methods. In the slow evaporation method, [Pt(phen)(L^n-κ*S*)$_2$] complexes were dissolved in THF and left open in a cool place for the solvent to evaporate slowly. In the solvent diffusion method, water was carefully layered under a solution of the [Pt(phen)(L^n-κ*S*)$_2$] complexes dissolved in methanol or ethanol stoppered and left in a cool place for solvents to slowly diffuse across the interface. In the vapour diffusion method, a vial containing [Pt(phen)(L^n-κ*S*)$_2$] complexes dissolved in dichloromethane was placed in a beaker with 100 ml diethyl ether and covered so that no vapours could escape, and diethyl ether diffused into the dichloromethane solution resulting in crystal formation. Suitable crystals were analysed and provided crystal structures representative of [Pt(phen)(L^n-κ*S*)$_2$] complexes. Overall, we were able to successfully grow single crystals for at least twelve complexes for sc-XRD analysis as shown below (*Figure 11*) of which the crystallographic data and refinement parameters have been reported in *Appendix 3*; however, we have chosen to discuss only four of them that revealed some interesting conformational variations.

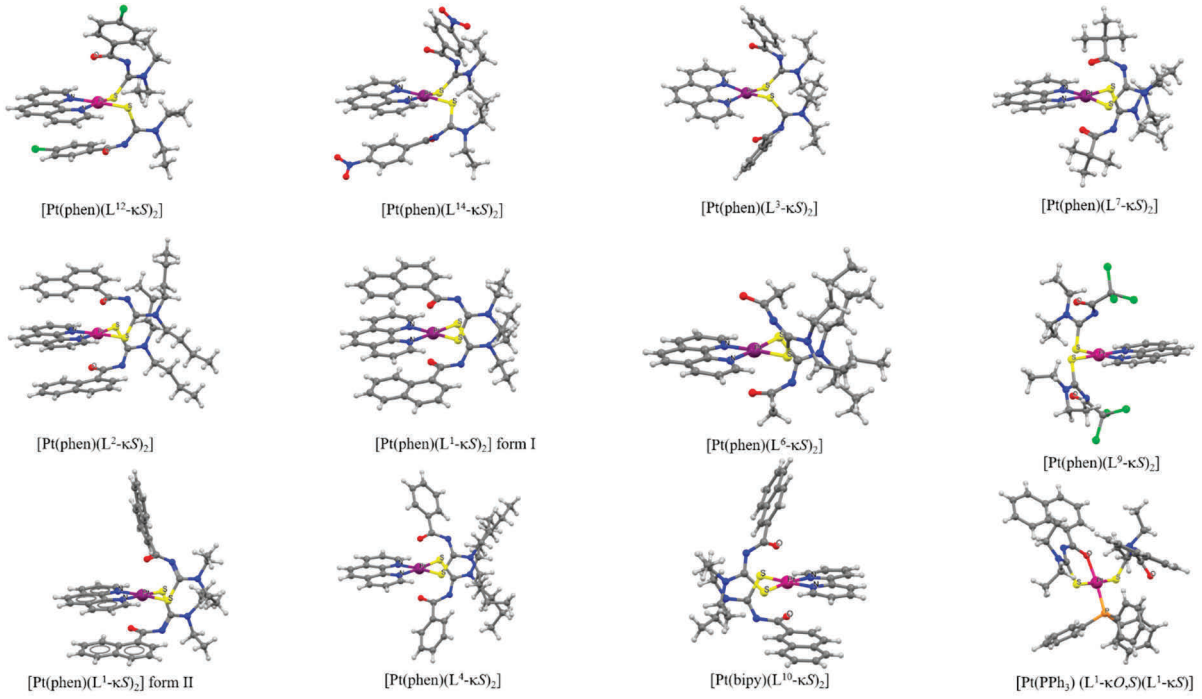


Figure 11: Crystal structures of the platinum(II) complexes, where at least one disubstituted acylthioureato ligand is coordinated in a monodentate fashion to the metal centre.

(a) Crystal structure of *bis*(*N*,*N*-diethyl-*N*'-pivaloylthioureato-κ*S*)-phenanthrolineplatinum, water solvate, [Pt(phen)(L^7-κ*S*)$_2$] (7)

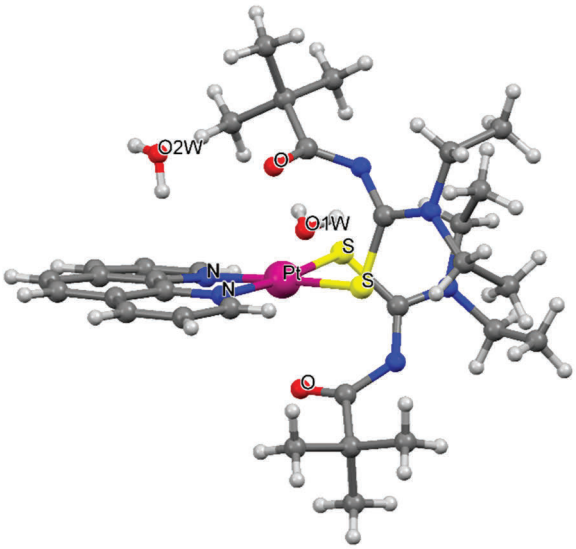


Figure 12: *Molecular structure of the [Pt(phen)(L^7-κ*S*)$_2$] (7) solvate, with partial labelling of the coordinated atoms and the pendant carbonyl oxygen for clarity*.

[Pt(phen)(L^7-κ*S*)$_2$] (**7**) crystallises as a solvate in the triclinic space group $P\bar{1}$, with one molecular complex and two water molecules in the asymmetric unit (*Figure 12).* The structure of the complex displays a square planar geometry with the acylthioureato ligands ligated to the platinum metal centre through sulfur donor atoms. Due to the steric bulkiness, the acylthioureato ligands arrange in an *anti*-conformation with the pendant acyl groups above and below the coordination plane. The average C=O bond length from the complex, 1.244(3) Å, is typically a double bond comparable with free ligand (HESLIB[25]), while there is shortening of the thioamidic $(CH_3)_3C(O)N$-C(S) bond to a double bond of average length 1.325(3) Å in the complex compared with free ligand. The bond lengths around the platinum centre, Pt-N and Pt-S, agree with literature where imine and thiolate ligands are involved (AREHIO[26]). The crystal packing (*Figure 13*) shows a network of hydrogen bonds between a water molecule, the carbonyl oxygens from two complex molecules and an aromatic C-H from a third complex molecule (H-bond set 1).

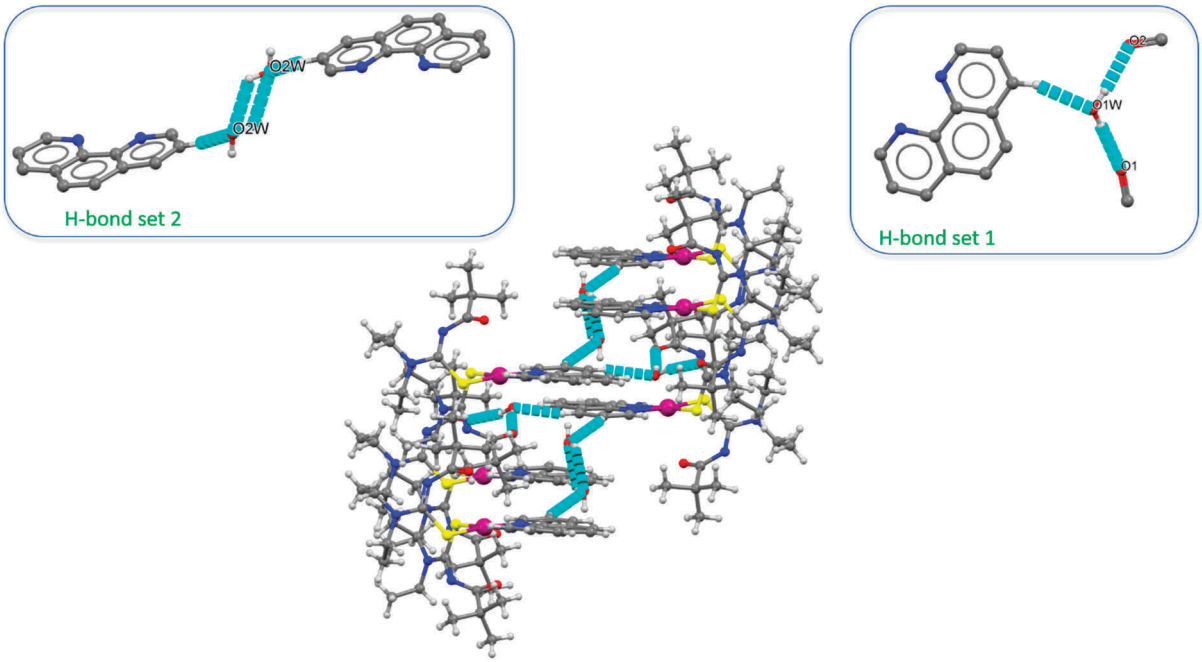


Figure 13: *Packing diagram of the [Pt(phen)(L^7-κS)$_2$] (**7**) solvate showing intermolecular π-π stacking and a network of hydrogen bonds between the complex molecules and the solvated water molecules.*

There is also hydrogen bonding involving two water molecules and two aromatic C-Hs from phenanthroline moieties of different molecules, (H-bond set 2). Further stabilisation of the crystal packing involves intermolecular offset π-π interactions between the phenanthroline moieties of the complexes.

*Table 1: Selected bond lengths and bond angles for [Pt(phen)(L^7-κS)$_2$] (**7**)*

Bond lengths (Å)			
Pt1 – S1	2.2799(8)	C6 – O2	1.258(4)
Pt1 – S2	2.2815(9)	C1 – S1	1.745(3)
Pt1 – N5	2.060(3)	C11 – S2	1.761(3)
Pt1 – N6	2.055(2)	C1 – N2	1.334(4)
C16 – O1	1.230(4)	C11 – N4	1.316(4)
Bond angles (°)			
S1 – Pt1 – S2	91.01(3)	Pt1 – S2 – C11	109.6(1)
N5 – Pt1 – N6	80.6(1)	C1 – N2 – C6	124.5(3)
Pt1 – S1 – C1	108.4(1)	C11 – N4 – C16	125.5(3)

(b) Crystal structure of *bis*(*N*,*N*-diethyl-*N*'-benzoylthioureato-κ*S*)-phenanthrolineplatinum, ethanol/water solvate, [Pt(phen)(L^3-κ*S*)$_2$] (3)

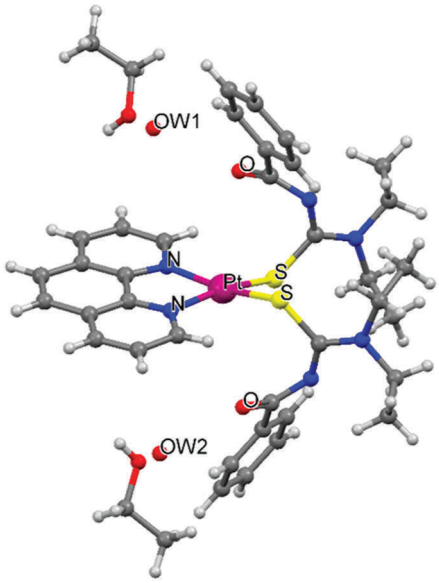


Figure 14: *Molecular structure of the [Pt(phen)(L^3-κ*S*)$_2$] (**3**) solvate, with partial labelling of the coordinated atoms and the pendant carbonyl oxygen for clarity*.

[Pt(phen)(L^3-κ*S*)$_2$] (**3**) crystallises as a solvate in the monoclinic space group *P2$_1$/c*, with one molecular complex and four solvent molecules (two ethanol and two water) in the asymmetric unit (*Figure 14*). The structure of the complex displays a distorted square planar geometry with the acylthioureato ligands ligated to the platinum metal centre through sulfur donor atoms. Due to the steric bulkiness, the acylthioureato ligands arrange in an *anti*-conformation with the pendant acyl groups above and below the coordination plane. The average C=O bond length from the complex, 1.236(4) Å, is typically a double bond comparable with free ligand (IJOQED01[27]), while there is shortening of the thioamidic (C_6H_5)C(O)N-C(S) bond to a double bond of average length 1.324(5) Å in the complex compared with free ligand. The bond lengths around the platinum centre, Pt-N and Pt-S, agree with literature where imine and thiolate ligands are involved (AREHIO[26]). The crystal packing (*Figure 15*) shows an intricate network of hydrogen bonds involving aromatic C-H donors and carbonyl oxygen acceptors interlinked with solvent molecules (ethanol and water) acting as both donors and acceptors. This hydrogen bond network forces a close approach of the complex molecules resulting in the "open sandwich" conformation, a non-offset intermolecular π-π interaction of the phenanthroline moieties and a distortion of the square planar geometry to compensate for the close approach. The sulfur donor atoms shifted 0.484 Å above and 0.541 Å below the plane containing the phenanthroline ring and platinum metal centre. There is also angular π-π interactions between the phenanthroline rings and the phenyl rings of the acylthioureato ligands that contribute to these aggregations stabilising the crystal packing.

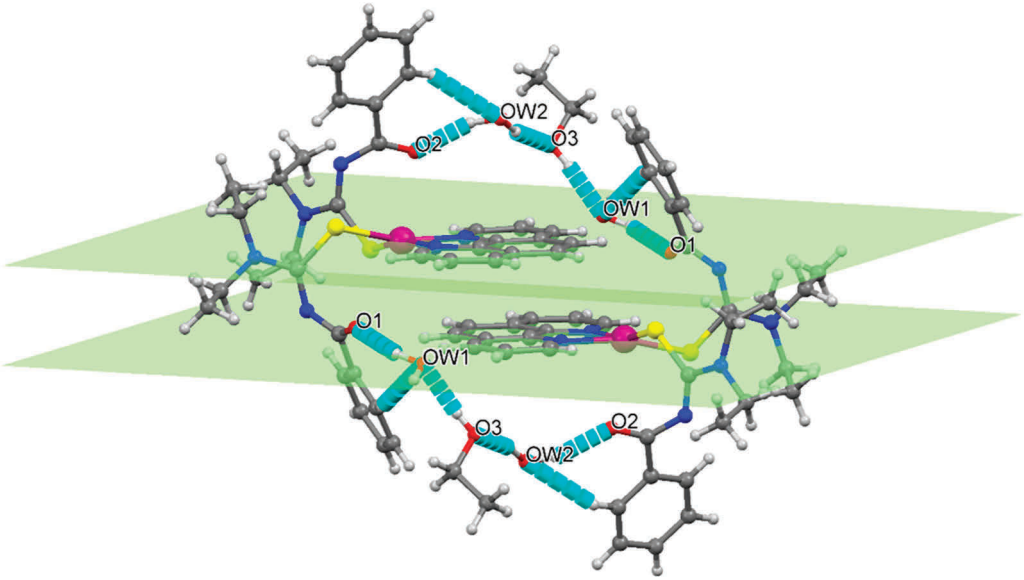


Figure 15: *Packing diagram of the [Pt(phen)(L^3-κS)$_2$] (**3**) solvate showing intermolecular π-π stacking and a network of hydrogen bonds between the complex molecules and the solvated ethanol and water molecules.*

*Table 2: Selected bond lengths and bond angles for [Pt(phen)(L^3-κS)$_2$] (**3**)*

Bond lengths (Å)			
Pt1 – S1	2.274(2)	C26 – O2	1.250(7)
Pt1 – S2	2.272(1)	C25 – S1	1.749(6)
Pt1 – N1	2.051(5)	C20 – S2	1.755(5)
Pt1 – N2	2.044(5)	C25 – N4	1.317(7)
C13 – O1	1.224(7)	C20 – N5	1.335(7)
Bond angles (°)			
S1 – Pt1 – S2	92.73(5)	Pt1 – S2 – C20	113.3(2)
N1 – Pt1 – N2	80.7(2)	C20 – N5 – C13	123.6(5)
Pt1 – S1 – C25	112.8(2)	C25 – N4 – C26	124.8(5)

(c) Crystal structure of *bis*(*N*,*N*-diethyl-*N*'-(4-chlorobenzoylthioureato)-κ*S*)-phenanthrolineplatinum, [Pt(phen)(L^{12}-κ*S*)$_2$] (12)

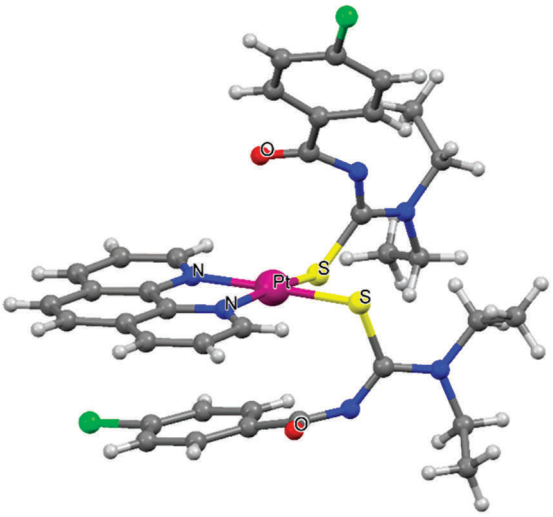


Figure 16: *Molecular structure of [Pt(phen)(L^{12}-κ*S*)$_2$]* ***(12)****, with partial labelling of the coordinated atoms and the pendant carbonyl oxygen for clarity*.

[Pt(phen)(L^{12}-κ*S*)$_2$] **(12)** (*Figure 16*), crystallised in the monoclinic space group *P2$_1$/n*, with four complex molecules in the unit cell. The structure of the complex displays a square planar geometry with the acylthioureato ligands ligated to the platinum metal centre through sulfur donor atoms. The acylthioureato ligands arrange in an *anti*-conformation with the pendant acyl groups above and below the coordination plane due to steric bulkiness. The average C=O bond length from the complex, 1.226(3) Å, is typically a double bond comparable with free ligand (WEPCIE[28]), while there is shortening of the thioamidic (4-C$_6$H$_5$Cl)C(O)N-C(S) bond to a double bond of average length 1.304(3) Å in the complex compared with free ligand. The bond lengths around the platinum centre, Pt-N and Pt-S, agree with literature where imine and thiolate ligands are involved (AREHIO[26]). The crystal packing (*Figure 17*) shows weak intermolecular aromatic C-H---O (carbonyl) hydrogen bonds and an extensive intramolecular and intermolecular π-π interactions to give a "half-open sandwich" conformation. There is evidence of intramolecular parallel π-π interactions between the chloro-benzoyl moiety and the phenanthroline moiety, both of which have intermolecular angular π-π interactions with the other chloro-benzoyl moiety of the other acylthioureato ligand. The chloro-benzoyl moieties from different molecules also π-stack in an anti-parallel orientation.

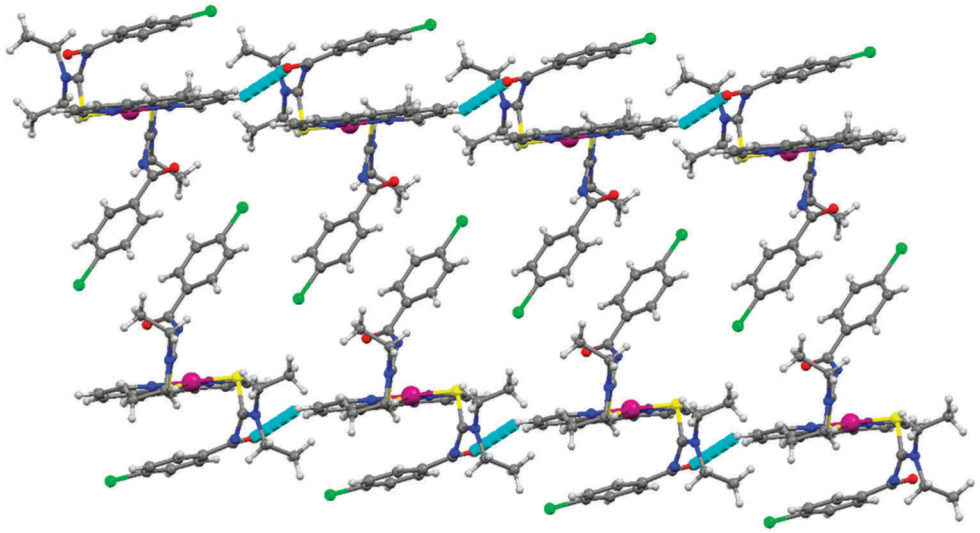


Figure 17: *1D Packing array diagram of [Pt(phen)(L^{12}-κS)$_2$] (**12**) showing intramolecular and intermolecular π-π stacking and aromatic C-H---O (carbonyl) hydrogen bonds between the complex molecules.*

*Table 3: Selected bond lengths and bond angles for [Pt(phen)(L^{12}-κS)$_2$] (**12**)*

Bond lengths (Å)			
Pt1 – S1	2.2864(9)	C52 – O2	1.225(4)
Pt1 – S2	2.2920(7)	C7 – S1	1.753(3)
Pt1 – N1	2.053(2)	C35 – S2	1.783(3)
Pt1 – N2	2.056(2)	C7 – N5	1.309(4)
C55 – O1	1.227(3)	C35 – N3	1.299(3)
Bond angles (°)			
S1 – Pt1 – S2	89.76(3)	Pt1 – S2 – C35	102.4(1)
N1 – Pt1 – N2	80.36(8)	C35 – N3 – C52	124.3(2)
Pt1 – S1 – C7	109.8(1)	C7 – N5 – C55	125.2(2)

(d) Crystal structure of *bis*(*N*,*N*-diethyl-*N*'-(1-naphthoylthioureato)-κ*S*)-phenanthrolineplatinum, [Pt(phen)(L^1-κ*S*)$_2$] (1)

(i) form I (tetrahydrofuran solvate)

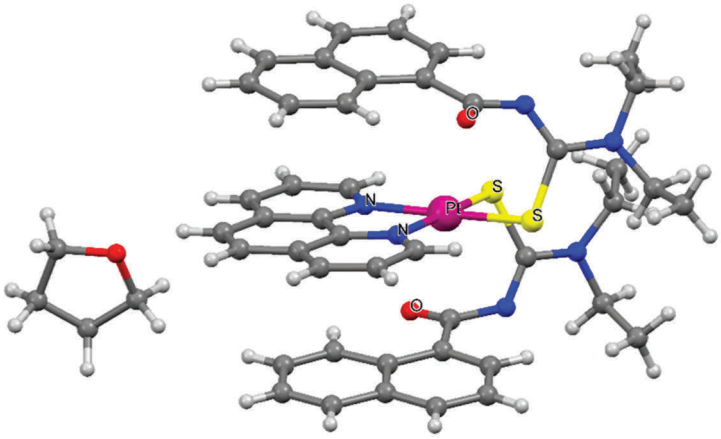


Figure 18: *Molecular structure of the [Pt(phen)(L^1-κ*S*)$_2$] **(1) form I** solvate, with partial labelling of the coordinated atoms and the pendant carbonyl oxygen for clarity*.

[Pt(phen)(L^1-κ*S*)$_2$] **(1) form I** (*Figure 18*), crystallised in the monoclinic space group *P2$_1$/n*, with one complex molecule and a THF solvent molecule in the asymmetric unit. The structure of the complex displays a square planar geometry with the acylthioureato ligands ligated to the platinum metal centre through sulfur donor atoms. The acylthioureato ligands arrange in an *anti*-conformation with the pendant acyl groups above and below the coordination plane due to steric bulkiness. The average C=O bond length from the complex, 1.225(2) Å, is typically a double bond comparable with free ligand (XATSAP[29]), while there is shortening of the thioamidic (1-$C_{10}H_8$)C(O)N-C(S) bond to a double bond of average length 1.292(2) Å in the complex compared with free ligand. The bond lengths around the platinum centre, Pt-N and Pt-S, agree with literature where imine and thiolate ligands are involved (AREHIO[26]). The crystal packing shows weak intermolecular aromatic C-H---N (acylthioureato imine), aromatic C-H---O (carbonyl) as well as aromatic C-H---S (thiolate) hydrogen bonds and an extensive intramolecular and intermolecular π-π interactions. There are intramolecular parallel π-π interactions between the two naphthoyl moieties and the phenanthroline moiety to give a "closed sandwich" conformation, which subsequently have perpendicular intermolecular π-π interactions with the other complexes resulting in a one-dimensional zig-zag chain (*Figure 19*). These chains are linked together via weak aromatic C-H---O (carbonyl) and aromatic C-H---S (thiolate) hydrogen bonds to give two-dimensional sheets which then stack on top of each other forming the three-dimensional packing.

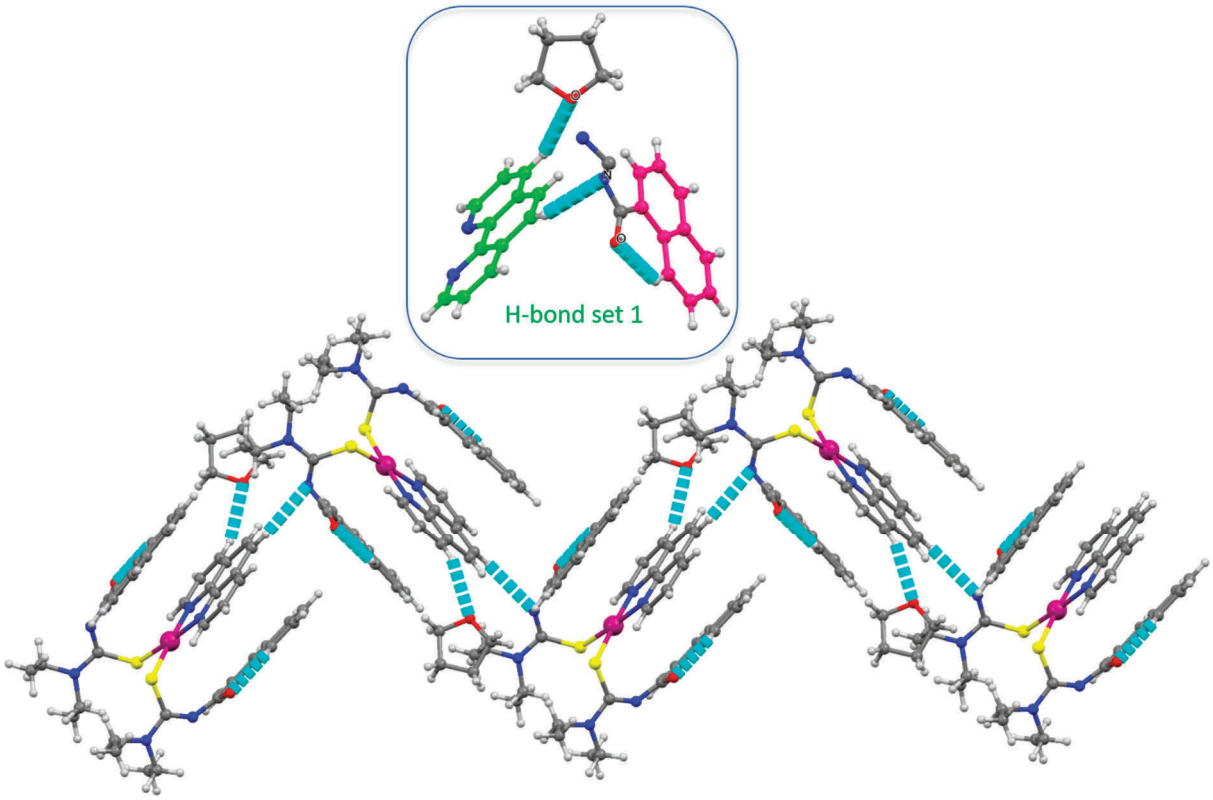


Figure 19: *1D Packing array diagram of the [Pt(phen)(L[1]-κS)$_2$] (**1**) **form I** solvate showing intramolecular and intermolecular π-π stacking and aromatic C-H---N and aromatic C-H---O hydrogen bonds between the complex molecules and solvent molecules.*

*Table 4: Selected bond lengths and bond angles for [Pt(phen)(L[1]-κS)$_2$] (**1**), (**form I**)*

Bond lengths (Å)			
Pt1 – S1	2.2914(7)	C24 – O2	1.223(3)
Pt1 – S2	2.2945(7)	C35 – S1	1.778(2)
Pt1 – N1	2.051(2)	C40 – S2	1.779(2)
Pt1 – N2	2.053(2)	C35 – N3	1.291(3)
C13 – O1	1.226(3)	C40 – N5	1.293(3)
Bond angles (°)			
S1 – Pt1 – S2	88.89(2)	Pt1 – S2 – C40	100.88(8)
N1 – Pt1 – N2	80.89(7)	C35 – N3 – C24	125.2(2)
Pt1 – S1 – C35	104.05(8)	C40 – N5 – C13	124.1(2)

(ii) form II (methanol solvate)

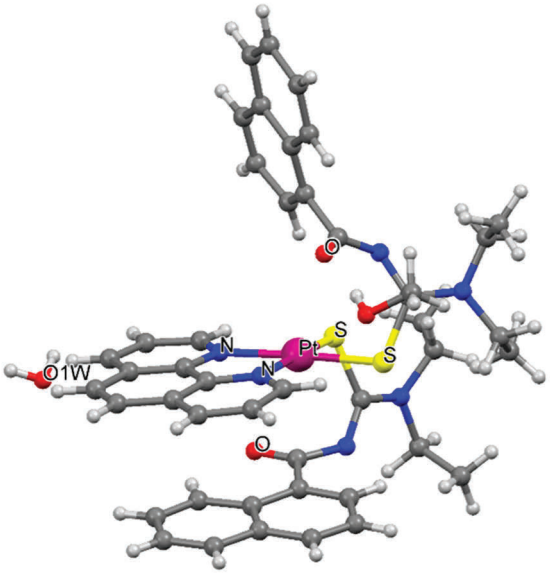


Figure 20: *Molecular structure of the [Pt(phen)(L[1]-κS)$_2$] **(1) form II** solvate, with partial labelling of the coordinated atoms and the pendant carbonyl oxygen for clarity*.

[Pt(phen)(L[1]-κS)$_2$] **(1) form II** (*Figure 20*), crystallised in the monoclinic space group *P21*, with two complex molecules with three methanol solvent molecules and one water molecule in the asymmetric unit. The structure of the complex displays a square planar geometry with the acylthioureato ligands ligated to the platinum metal centre through sulfur donor atoms. The acylthioureato ligands arrange in an *anti*-conformation with the pendant acyl groups above and below the coordination plane due to steric bulkiness. The average C=O bond length from the complex, 1.239(4) Å, is typically a double bond comparable with free ligand (XATSAP[29]), while there is shortening of the thioamidic (1-$C_{10}H_8$)C(O)N-C(S) bond to a double bond of average length 1.315(4) Å in the complex compared with free ligand. The bond lengths around the platinum centre, Pt-N and Pt-S, agree with literature where imine and thiolate ligands are involved (AREHIO[26]). The crystal packing shows weak intermolecular aromatic C-H---N (acylthioureato imine), aromatic C-H---O (carbonyl) as well as aromatic C-H---S (thiolate) hydrogen bonds and an extensive intramolecular and intermolecular π-π interactions. There are intramolecular parallel π-π interactions between the one naphthoyl moiety and the phenanthroline moiety to give a "half-open sandwich" conformation of the complex, which subsequently has perpendicular intermolecular π-π interactions with the other complex resulting in a dimeric unit (*Figure 21*). These dimeric units are linked together via weak aromatic C-H---O (carbonyl) hydrogen bonds as well as a hydrogen bond network involving solvent molecules (methanol and water) to give two-dimensional sheets which then stack on top of each other to form the three-dimensional packing.

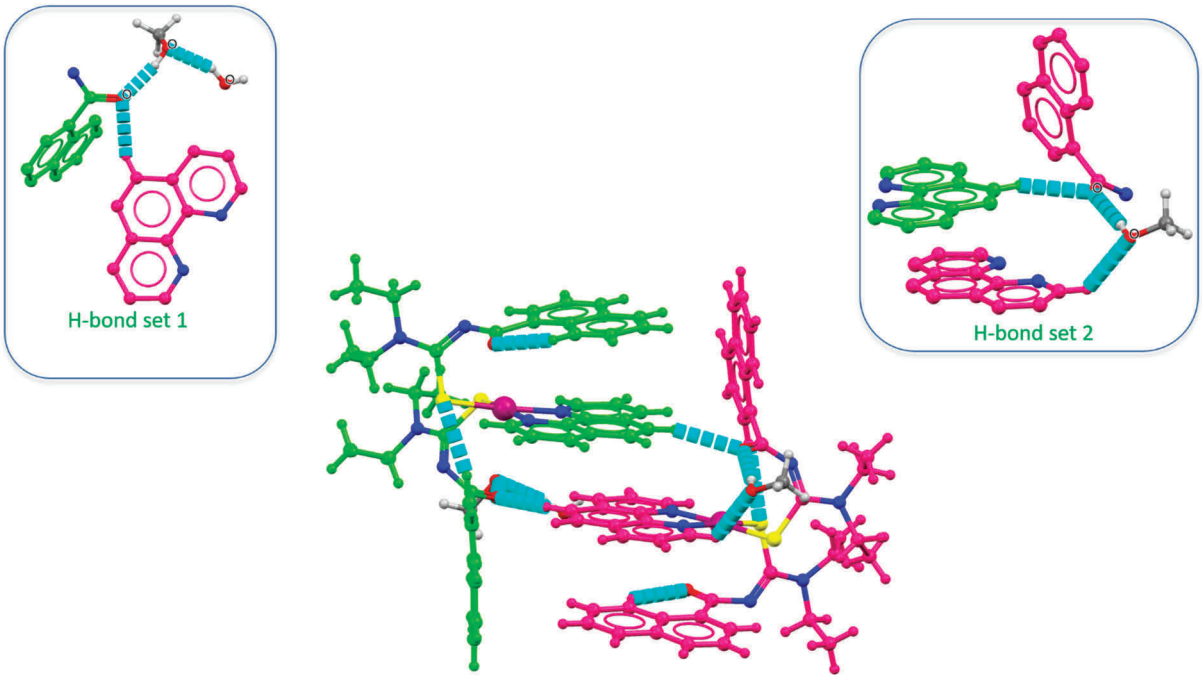


*Figure 21: Partial packing diagram of the solvate [Pt(phen)(L^1-κ*S*)$_2$] (**1**) **form II** showing intramolecular and intermolecular π-π stacking and aromatic C-H---O (carbonyl), OH_2---O (carbonyl), MeOH---O (carbonyl) and solvent-solvent hydrogen bonds resulting in dimeric units of the complex.*

*Table 5: Selected bond lengths and bond angles for [Pt(phen)(L^1-κ*S*)$_2$] (**1**), **form II***

Bond lengths (Å)			
Pt01 – S03	2.280(1)	C51 – O2	1.235(6)
Pt01 – S04	2.3017(9)	C46 – S03	1.757(4)
Pt01 – N024	2.066(3)	C52 – S04	1.765(5)
Pt01 – N025	2.061(4)	C46 – N021	1.339(6)
C45 – O1	1.262(6)	C52 – N023	1.315(6)
Bond angles (°)			
S1 – Pt1 – S2	88.32(4)	Pt1 – S2 – C40	104.8(2)
N1 – Pt1 – N2	80.4(1)	C35 – N3 – C24	122.7(4)
Pt1 – S1 – C35	105.0(1)	C40 – N5 – C13	122.6(4)

2.3. Conclusion

In this section of the thesis, we aimed to synthesise [Pt(phen)(L^n-κ*S*)$_2$] complexes from disubstituted acylthiourea ligands with different substituents and [$PtCl_2$(phen)] as precursor. The critical steps to achieving this were to synthesise the ligands and the precursor, and then use these in the synthesis of the [Pt(phen)(L^n-κ*S*)$_2$] complexes. The ligands and the precursor were successfully synthesised in high

yields and characterised using FT-IR spectroscopy, ^{1}H and ^{13}C NMR spectroscopy and elemental analysis.

[Pt(phen)(L^{n}-κ*S*)$_2$] complexes were then successfully synthesised in excellent yields using the stepwise synthetic method B (where the ligands were deprotonated using sodium hydride) across all ligand variations and characterised using FT-IR spectroscopy, ^{1}H and ^{13}C NMR spectroscopy, mass spectrometry, UV-vis spectrophotometry, single-crystal X-ray diffraction and elemental analysis. The crystal structures of these complexes show extensive intramolecular and intermolecular π-π stacking to be involved in the stabilisation of these solid-state structures. Our initial synthetic scheme (method A) successfully resulted in the formation of [Pt(phen)(L^{n}-κ*S*)$_2$] complexes in yields between 70-90% only for disubstituted acylthiourea ligands bearing a trichloroacetyl substituent or aromatic acyl substituents. Disubstituted acylthiourea ligands bearing alkyl acyl substituents favoured the formation of cationic [Pt(phen)(L^{n}-κ*O*,*S*)]$^{+}$ complexes using the same synthetic protocol. Analysis of species distribution during the synthesis of [Pt(phen)(L^{3}-κ*S*)$_2$] and [Pt(phen)(L^{7}-κ*S*)$_2$] complexes using the one-pot synthesis method (A) showed interesting ligand-dependent variations; with [Pt(phen)(L^{3}-κ*S*)$_2$] and [Pt(phen)(L^{3}-κ*O*,*S*)]$^{+}$ co-forming (though at different rates) when the ligand was *N*,*N*-di(ethyl)-*N*'-benzoylthiourea while only [Pt(phen)(L^{7}-κ*O*,*S*)]$^{+}$ formed with *N*,*N*-di(ethyl)-*N*'-pivaloylthiourea as ligand. These result from the method (A) supported by the crystal structures obtained seems to support suggestions by Kotzé *et al*.,[30] about the involvement of π-π stacking interactions in stabilising the [Pt(phen)(L^{n}-κ*S*)$_2$] complexes; as well as some electronic influence of acyl substituents in determining the disubstituted acylthioureato ligands' preferred coordination modes. Hence there is need to study whether these π-π stacking interactions we see in the solid-state persists in solution to influence the coordination behaviour of disubstituted acylthiourea ligands, and also investigate the electronic influence of acyl substituents in controlling the preferred coordination mode for us to explain successfully results from the synthetic method (A).

2.4. Experimental

All reagents and chemicals were purchased from Sigma Aldrich and SA Precious Metals and used without further purification. Anhydrous acetone, tetrahydrofuran (THF), dichloromethane (DCM) were prepared in accordance with literature methods[31] while we used the other solvents as received from commercial sources. Elemental analyses for C, H and N, were performed using a Flash2000 CHNS-O analyser fitted with an autosampler. Melting point measurements were done using a Stuart SMP30 melting point apparatus and were uncorrected. FT-IR spectra were obtained using a Bruker Tensor27 spectrometer in the range 4000-600 cm^{-1}. UV-vis absorption spectra of complexes were obtained in methanol using an Analytikjena Specord50 spectrophotometer in the range 1000-200 nm range. We recorded ^{1}H and ^{13}C NMR spectra on a Bruker Avance 300 MHz, Bruker Avance 400 MHz and Bruker

Avance III 500 MHz instruments in $CDCl_3$ and DMSO-*d*. We achieved the complete assignment of ^{1}H, and ^{13}C NMR spectra with the aid of COSY, DEPT, HSQC and HMBC NMR experiments.

Single crystal X-ray diffraction data (SC-XRD) for the complexes were collected on a Bruker Apex-II CCD diffractometer using Mo Ka radiation (l = 0.71073 A) at a temperature of 173(2) K. Intensities were integrated with SAINT and absorption corrections based on equivalent reflections were carried out using SADABS.6. The structure was solved using WinGx v2014 and refined using ShelXL and OLEX2. All of the nonhydrogen atoms were refined anisotropically, while all of the hydrogen atoms were located geometrically and refined using a riding model. Diagrams and publication materials were generated using PLATON and MERCURY. Experimental details of the X-ray analyses are provided in the appendix (*Appendix 3*).

2.4.1. General procedure for the synthesis of *N,N*-di(alky/aryl)-*N*'-acylthiourea ligands

We synthesised *N,N*-di(alkyl/aryl)-*N*'-acylthiourea ligands according to the method described by Douglass and Dains.[6] Equimolar amounts of potassium thiocyanate and an appropriate acid chloride were heated under reflux in anhydrous acetone under inert conditions for 45 minutes after which the reaction mixture was allowed to cool to room temperature; then an equimolar amount of a corresponding secondary amine added dropwise, with the reaction mixture heated under reflux for a further 45 minutes. The reaction mixture was again allowed to cool to room temperature before being poured into a beaker of icy water. Acetone was left to evaporate overnight, and solids (white to light yellow) were collected by suction filtration, washed with water, and recrystallized from ethanol. The *N,N*-di(alkyl/aryl))-*N'*-acylthiourea ligands were obtained in yields of 64-94% and characterised using ^{1}H, ^{13}C NMR spectroscopy, FT-IR spectroscopy, Mass spectrometry and elemental analysis.

(a) Synthesis of *N,N*-di(butyl)-*N*'-acetylthiourea (HL^6) and *N,N*-di(ethyl)-*N*'-(trichloro-acetylthiourea) (HL^9)

N,N-di(butyl)-*N*'-acetylthiourea **(HL^6)** was synthesised according to the method by Schuster *et al.* [32] with slight modifications. To a solution of KSCN (1.0670 g; 10.9 mmol) in 60 ml anhydrous cooled in an ice bath was added a solution of acetyl chloride (0.8680 g; 11.1 mmol) in 20 ml anhydrous acetone dropwise, and the mixture left stirring for 30 minutes while allowing the temperature to rise to room temperature. The precipitate of potassium chloride was filtered off, and the filtrate cooled again in an ice bath; a solution of diethylamine (0.8045 g; 11 mmol) in 20 ml anhydrous acetone added dropwise, and the mixture left stirring while allowing the temperature to rise to room temperature. The mixture was concentrated under vacuo and the residue taken up in diethyl ether after which crystalline solids resulted, in good yields. The product was characterised using FT-IR spectroscopy, ^{1}H, ^{13}C NMR spectroscopy, and elemental analysis.

N,N-di(ethyl)-*N*'-(trichloro-acetylthiourea) **(HL^9)** was synthesised using a slight modification of literature method,[33] in which a two-step method was used. In the first step, KSCN (1.5094 g; 15.5

mmol) was added into a 100 ml three-neck round-bottomed flask with 30 ml anhydrous dichloromethane under inert conditions. The flask was placed in an ice bath and trichloroacetyl chloride (1.7 ml; 15.2 mmol) in 15 ml anhydrous dichloromethane was added slowly over 20 minutes. The mixture was then slowly warmed to room temperature after which it was heated under reflux for 2 hours. The insoluble salts were filtered off and the filtrate concentrated under vacuo to get a reddish oil of trichloroacetyl isothiocyanate. Secondly, to the trichloroacetyl isothiocyanate (0.4000 g; 2 mmol) dissolved in 20 ml anhydrous dichloromethane, diethylamine (0.21 ml; 2 mmol) in 15 ml anhydrous dichloromethane was added dropwise. The mixture was heated under reflux for another 2 hours after which the solvent and excess amine were removed under vacuo. *N,N*-(diethyl)-*N*'-(trichloro-acetylthiourea) **(HL^{9})** was obtained as a deep red oil in relatively good yields and characterized using FT-IR spectroscopy, ^{1}H and ^{13}C NMR spectroscopy.

***N,N*-di(ethyl)-*N*'-(1-naphthoylthiourea) (HL^{1})**: Yield: 92%; mp (155.3-156.4 °C); $C_{16}H_{18}N_2OS$: calc.: C, 67.10; H, 6.33; N, 9.78. found: C, 67.16; H, 5.92; N, 9.79%; FT-IR (ATR): ν = 3174 (br. w, N-H), 2978 (w, aliphatic C-H), 1674 (m, C=O), 1593 (m, C=N), 1427 (m), 1279 (m), 1227 (s), 1135 (m), 788 (s) cm^{-1} ; ^{1}H NMR (300 MHz, Chloroform-*d*) δ 8.46 (d, 1H, H$^{8'}$), 8.27 (s, 1H, N-H), 7.99 (d, 1H, H$^{4'}$), 7.89 (d, 1H, H$^{2'}$), 7.77 (d, 1H, H$^{5'}$), 7.65 – 7.42 (m, 3H, H$^{3'+6'+7'}$), 4.05 (t, 2H, H^{a}), 3.75 (t, 2H, H$^{a'}$), 1.38 (t, 6H, H$^{b+b'}$) ppm; ^{13}C NMR (300 MHz, Chloroform-*d*): δ 164.5 (C=O), 179.0 (C=S), 133.9 (C$^{1'}$), 132.5 (C$^{4'}$), 131.6 (C$^{4a'}$), 130.3 (C$^{8a'}$), 128.6 (C$^{2'}$), 127.8, 126.8, 124.5 (C$^{3'+6'+7'}$), 126.4 (C$^{5'}$), 125.2, (C$^{8'}$), 46.6 (C$^{a+a'}$), 13.7, 11.4 (C$^{b+b'}$) ppm.

***N,N*-di(butyl)-*N*'-(1-naphthoylthiourea) (HL^{2})**: Yield: 94%; mp (95.3-96 °C); $C_{20}H_{26}N_2OS$: calc.: C, 70.14; H, 7.65; N, 8.18. found: C, 70.67; H, 7.83; N, 8.27%; FT-IR (ATR): ν = 3130 (br. w, N-H), 2958-2857 (w, aliphatic C-H), 1681 (m, C=O), 1543 (m, C=N), 1423 (m), 1206 (m), 1141 (m), 780 (s) cm^{-1} ; ^{1}H NMR (300 MHz, Chloroform-*d*) δ 8.45 (d, 1H, H$^{8'}$), 8.31 (s, 1H, N-H), 7.98 (d, 1H, H$^{4'}$), 7.88 (d, 1H, H$^{2'}$), 7.75 (d, 1H, H$^{5'}$), 7.63 – 7.43 (m, 3H, H$^{3'+6'+7'}$), 3.98 (t, 2H, H^{a}), 3.67 (t, 2H, H$^{a'}$), 1.78 (dq, 4H, H$^{b+b'}$), 1.41 (dp, 4H, H$^{c+c'}$), 0.97 (dt, 6H, H$^{d+d'}$) ppm; ^{13}C NMR (300 MHz, Chloroform-*d*): δ 165.2 (C=O), 179.4 (C=S), 133.9 (C$^{1'}$), 132.4 (C$^{4'}$), 131.7 (C$^{4a'}$), 130.3 (C$^{8a'}$), 128.5 (C$^{2'}$), 127.8, 126.7, 124.5 (C$^{3'+6'+7'}$), 126.3 (C$^{5'}$), 125.2, (C$^{8'}$), 52.5 (C$^{a+a'}$), 30.2, 28.5 (C$^{b+b'}$), 21.7 (C$^{c+c'}$), 12.0 (C$^{d+d'}$) ppm.

***N,N*-di(ethyl)-*N*'-benzoylthiourea (HL^{3})**: Yield: 84%; mp (99.9-100.5 °C); $C_{12}H_{16}N_2OS$: calc.: C, 60.99; H, 6.82; N, 11.85. found: C, 61.16; H, 6.71; N, 11.81%; FT-IR (ATR): ν = 3264 (br. w, N-H), 2873-2972 (w, aliphatic C-H), 1652 (m, C=O), 1525 (m, C=N), 1435 (m), 1284 (m), 1222 (m), 709 (s) cm^{-1} ; ^{1}H NMR (300 MHz, Chloroform-*d*) δ 8.37 (s, 1H, N-H), 7.83 (d, 2H, $^{2'+6'}$), 7.57 (t, 1H, H$^{4'}$), 7.47 (t, 2H, H$^{3'+5'}$), 4.02 (s, 2H, H^{a}), 3.62 (s, 2H, H$^{a'}$), 1.32 (dt, 6H, H$^{b+b'}$) ppm; ^{13}C NMR (300 MHz, Chloroform): δ 163.8 (C=O), 178.9 (C=S), 132.9 (C$^{4'}$), 132.7 (C$^{1'}$), 129.5 (C$^{2'+6'}$), 127.8 (C$^{3'+5'}$)), 46.9 (C$^{a+a'}$), 14.1, 11.4 (C$^{b+b'}$) ppm.

***N,N*-di(butyl)-*N'*-benzoylthiourea (HL^{4})**: Yield: 89%; mp (92.6-93.1 °C); $C_{16}H_{24}N_2OS$: calc.: C, 65.71; H, 8.27; N, 9.58. found: C, 65.47; H, 8.18; N, 9.55; FT-IR (ATR): v = 3169 (br. w, N-H), 2870-2960 (w, aliphatic C-H), 1689 (m, C=O), 1537 (m, C=N), 1425 (m), 1242 (m), 1200 (m), 1134 (m), 716 (s) cm^{-1} ; ^{1}H NMR (300 MHz, Chloroform-*d*) δ 8.39 (br. s, 1H, N-H), 7.82 (dd, J = 7.6 Hz, 2H, H$^{2'+6'}$), 7.56 (td, 1H, H$^{4'}$), 7.46 (td, J = 8.2, 6.7, 1.2 Hz, 2H, H$^{3'+5'}$), 3.96 (t, J = 7.8 Hz, 2H, H^{a}), 3.53 (t, 2H, H$^{a'}$), 1.72 (dq, J = 41.2, 7.6 Hz, 4H, H$^{b+b'}$), 1.34 (ddt, J = 46.2, 7.4 Hz, 4H' H$^{c+c'}$), 0.98 (dt, J = 23.8, 7.3 Hz, 6H, H$^{d+d'}$).ppm; ^{13}C NMR (300 MHz, Chloroform-*d*): δ 163.6 (C=O), 172.7(C=S), 179.8, 132.9 (C$^{4'}$), 132.8 (C$^{1'}$), 128.9 (C$^{3'+5'}$), 127.9 (C$^{2'+6'}$), 53.1 (C$^{a+a'}$), 30.2, 28.5 (C$^{b+b'}$), 20.1 (C$^{c+c'}$), 13.7, 13.9 (C$^{d+d'}$) ppm.

***N,N*-di(butyl)-*N'*-acetylthiourea (HL^{6})**: Yield: 64%; mp (54.6-55.2 °C); $C_{11}H_{22}N_2OS$: calc.: C, 57.35; H, 9.63; N, 12.16. found: C, 57.38; H, 9.94; N, 12.62%; FT-IR (ATR): v = 3233 (br. w, N-H), 2870-2955 (w, aliphatic C-H), 1657 (m, C=O), 1508 (m, C=N), 1456 (m), 1242 (m), 1200 (m), 1142 (m), 649 (s) cm^{-1} ; ^{1}H NMR (300 MHz, Chloroform-*d*) δ 8.51 (s, 1H, N-H), 3.90 (br. s, 2H, H^{a}), 3.46 (br. s, 2H, H$^{a'}$), 2.14 (s, 3H, H$^{1'}$), 1.64 (s, 4H, H$^{b+b'}$), 1.35 (s, 4H, H$^{c+c'}$), 0.94 (t, 6H, H$^{d+d'}$) ppm; ^{13}C NMR (300 MHz, Chloroform-*d*): δ 179.4 (C=S), 167.2 (C=O), 53.0 (C$^{a+a'}$), 30.0, 28.5 (C$^{b+b'}$), 24.0 (C$^{1'}$), 20.0 (C$^{c+c'}$), 13.8 (C$^{d+d'}$) ppm.

***N,N*-di(ethyl)-*N'*-pivaloylthiourea (HL^{7})**: Yield: 80%; mp (89.3-90.0 °C); $C_{10}H_{20}N_2OS$: calc.: C, 55.52; H, 9.32; N, 12.95. found: C, 55.68; H, 9.10; N, 12.98%; FT-IR (ATR): v = 3224 (w, N-H), 2870-2970 (w, aliphatic C-H), 1646 (m, C=O), 1498 (s, C=N), 1420 (m), 1231 (s), 1187 (m), 1132 (m), 789 (m) cm^{-1} ; ^{1}H NMR (300 MHz, Chloroform-*d*) δ 7.69 (br. s, 1H, N-H), 3.97 (br. s, 2H, H^{a}), 3.49 (br. s, 2H, H$^{a'}$), 1.42 – 1.14 (m, 15H, H$^{b+b'+2'}$) ppm; ^{13}C NMR (300 MHz, Chloroform-*d*): δ 174.7 (C=O), 179.7 (C=S), 48.0, 47.6 (C$^{a+a'}$), 13.2, 11.5 (C$^{b+b'}$), 39.7 (C$^{1'}$), 27.1 (C$^{2'}$) ppm.

***N,N*-di(butyl)-*N'*-pivaloylthiourea (HL^{8})**: Yield: 85%; mp (86.2-86.7 °C); $C_{14}H_{28}N_2OS$: calc.: C, 61.72; H, 10.36; N, 10.28. found: C, 61.74; H, 10.02; N, 10.39%; FT-IR (ATR): v = 3310 (br. w, N-H), 2864-2960 (w, aliphatic C-H), 1653 (m, C=O), 1516 (m, C=N), 1420 (m), 1258 (m), 1229 (m), 1198 (m), 1131 (m), 735 (m) cm^{-1} ; ^{1}H NMR (300 MHz, Chloroform-*d*) δ 7.65 (br. s, 1H, N-H), 3.90 (t, J = 7.7 Hz, 2H, H^{a}), 3.38 (t, J = 7.5 Hz, 2H, H$^{a'}$), 1.66 (dq, 4H, H$^{b+b'}$), 1.24 (m, 13H, H$^{c+c'+2'}$), 0.91 (dt, J = 10.2, 7.2 Hz, 6H, H$^{d+d'}$).ppm; ^{13}C NMR (300 MHz, Chloroform-*d*): δ 174.6 (C=O), 180.1 (C=S), 53.4, 52.9 (C$^{a+a'}$), 30.1, 28.5 (C$^{b+b'}$), 20.1 (C$^{c+c'}$), 13.8, 13.7 (C$^{d+d'}$), 39.7 (C$^{1'}$), 27.1 (C$^{2'}$) ppm.

***N,N*-(diethyl)-*N'*-(trichloro-acetylthiourea) (HL^{9})**: Yield: 77%; (deep red oil); FT-IR (ATR): v = 3416 (br. w, N-H), 2839-2981 (w, aliphatic C-H), 1719 (s, C=O), 1523 (m, C=N), 1446 (s), 1429 (m), 1282 (m), 1228 (m), 1121 (m), 814 (s) cm^{-1} ; ^{1}H NMR (300 MHz, Chloroform-*d*) δ 8.49 (s, 1H, N-H),

3.98 (br. s, 2H, H^{a}), 3.54 (br. s, 2H, $H^{a'}$), 1.33 (t, 6H, $H^{b+b'}$) ppm; ^{13}C NMR (300 MHz, Chloroform-*d*): δ 176.5 (C=S), 157.5 (C=O), 92.0 ($C^{1'}$), 48.3, 47.6 ($C^{a+a'}$), 13.4, 11.2 ($C^{b+b'}$) ppm.

***N,N*-di(ethyl)-*N'*-(2-naphthoylthiourea) (HL^{10})**: Yield: 90%; mp (105.5-106.3 °C); $C_{16}H_{18}N_2OS$: calc.: C, 67.10; H, 6.33; N, 9.78. found: C, 67.45; H, 6.72; N, 9.70%; FT-IR (ATR): *v* = 3225 (br. w, N-H), 2810-2970 (w, aliphatic C-H), 1650 (m), 1519 (m, C=N), 1447 (m), 1435 (m), 1283 (m), 1225 (s), 826 (m) cm^{-1} ^{1}H NMR (300 MHz, Chloroform-*d*) δ 8.63 (br. s, 1H, (N-H)), 8.36 (s, 1H, $H^{1'}$), 8.00 – 7.79 (m, 4H, $H^{3'+4'+5'+8'}$), 7.68 – 7.50 (m, 2H, $H^{6'+7'}$), 4.04 (s, 2H, H^{a}), 3.65 (s, 2H, $H^{a'}$), 1.35 (dt, 6H, $H^{b+b'}$) ppm; ^{13}C NMR (300 MHz, Chloroform-*d*): δ 164.0 (C=O), 179.5 (C=S), 135.9, 132.4, 130.4, 129.2, 129.0, 128.8, 128.4, 127.8, 127.1, 124.2 (aromatic), 47.8 ($C^{a+a'}$), 13.3, 11.6 ($C^{b+b'}$) ppm.

***N,N*-di(butyl)-*N'*-(2-naphthoylthiourea) (HL^{11})**: Yield: 93%; mp (108.4-109.0 °C); $C_{20}H_{26}N_2OS$: calc.: C, 70.14; H, 7.65; N, 8.18. found: C, 70.45; H, 7.91; N, 8.30%; FT-IR (ATR): *v* = 3256 (br. w, N-H), 2872-2959 (w, aliphatic C-H), 1684 (m, C=O), 1539 (m, C=N), 1416 (m), 1192 (m), 1133 (s), 773 (m) cm^{-1} ; ^{1}H NMR (300 MHz, Chloroform-*d*) δ 8.64 (br. s, 1H, (N-H)), 8.36 (s, 1H, $H^{1'}$), 7.97 – 7.82 (m, 4H, $H^{3'+4'+5'+8'}$), 7.65 – 7.52 (m, 2H, $H^{6'+7'}$), 3.98 (t, 2H, H^{a}), 3.58 (t, 2H, $H^{a'}$), 1.74 (dp, 4H, $H^{b+b'}$) 1.38 (ddq, 4H, $H^{c+c'}$), 0.95 (dt, 6H, $H^{d+d'}$) ppm; ^{13}C NMR (300 MHz, Chloroform-*d*): δ 163.7 (C=O), 178.9 (C=S), 135.32, 132.46, 129.86, 129.23, 128.81, 128.43, 127.81, 127.05, 123.75 (aromatic), 53.5 ($C^{a+a'}$), 30.66, 28.98 ($C^{b+b'}$), 20.71 ($C^{c+c'}$), 11.74 ($C^{d+d'}$) ppm.

***N,N*-di(ethyl)-*N'*-(4-chlorobenzoylthiourea) (HL^{12})**: Yield: 81%; mp (150.7-151.4 °C); $C_{12}H_{15}ClN_2OS$: calc.: C, 53.23; H, 5.58; N, 10.35. found: C, 53.38; H, 5.94; N, 10.12%; FT-IR (ATR): *v* = 3272 (br. w, N-H), 2980-2825 (w, aliphatic C-H), 1656 (m, C=O), 1600 (m), 1519 (s, C=N), 1468 (m), 1295(s), 1224 (m), 715 (s) cm^{-1}; ^{1}H NMR (300 MHz, Chloroform-*d*) δ 8.55 (s, 1H, N-H), 7.78 (d, 2H, $H^{2'+6'}$), 7.43 (d, 2H, $H^{3'+5'}$), 4.01 (s, 2H, H^{a}), 3.59 (s, 2H, $H^{a'}$), 1.32 (dt, 6H, $H^{b+b'}$) ppm; ^{13}C NMR (300 MHz, Chloroform-*d*): δ 163.0 (C=O), 179.7 (C=S), 139.3 ($C^{1'}$), 130.9 ($C^{4'}$), 129.4 ($C^{2'+6'}$), 129.1 ($C^{3'+5'}$), 47.9 ($C^{a+a'}$), 13.1, 10.4 ($C^{b+b'}$) ppm.

***N,N*-di(ethyl)-*N'*-(4-nitrobenzoylthiourea) (HL^{14})**: Yield: 89%; mp (160.0-161.0 °C); $C_{12}H_{15}N_3O_3S$: calc.: C, 51.23; H, 5.37; N, 14.94. found: C, 50.98; H, 5.64; N, 15.12%; FT-IR (ATR): *v* = 3277 (br. w, N-H), 2974-2872 (w, aliphatic C-H), 1645 (m, C=O), 1600 (m), 1524 (s, C=N), 1469 (m), 1283 (m), 1227 (m), 714 (s) cm^{-1} ; ^{1}H NMR (300 MHz, DMSO-d_6) δ 10.95 (s, 1H, N-H), 8.33 (d, 2H, $H^{3'+5'}$), 8.12 (d, 2H, $H^{2'+6'}$), 3.95 (q, 2H, H^{a}), 3.55 (q, 2H, $H^{a'}$), 1.23 (dt, 6H, $H^{b+b'}$) ppm; ^{13}C NMR (300 MHz, DMSO-d_6): δ 163.5 (C=O), 178.8 (C=S), 148.6 ($C^{4'}$), 138.7 ($C^{1'}$), 129.5 ($C^{2'+6'}$), 123.0 ($C^{3'+5'}$), 47.2, 46.6 ($C^{a+a'}$), 12.2, 8.9 ($C^{b+b'}$) ppm.

***N,N*-di(benzyl)-*N*'-(1-naphthoylthiourea) (HL^{15})**: Yield: 88%; mp (137.6-138.0 °C); $C_{26}H_{22}N_2OS$: calc.: C, 76.07; H, 5.40; N, 6.82. found: C, 75.88; H, 5.52; N, 7.04 %; FT-IR (ATR): ν = 3142 (br. w, N-H), 3043 (w, aromatic C-H), 1689 (m, C=O), 1526 (m, C=N), 1448 (m), 1422 (m), 1233 (m), 1185 (s), 778 (s) cm^{-1} ; ^{1}H NMR (300 MHz, Chloroform-*d*) δ 8.55 (s, 1H,N-H), 8.44 (d, 1H, H$^{8'}$), 7.97 (d, 1H, H$^{4'}$), 7.89 (d, 1H, H$^{2'}$), 7.74 – 7.04 (m, 7H, H$^{3'+5'+6'+7'+phenyl}$), 5.29 (s, 2H, H^{a}), 4.90 (s, 2H, H$^{a'}$). ppm; ^{13}C NMR (300 MHz, Chloroform-*d*): δ 166.4 (C=O), 181.6 (C=S), 135.4, 133.9, 132.7, 131.3, 130.2, 129.0, 128.6, 127.9, 126.8, 126.8, 125.2, 124.6 (aromatic), 57.2, 55.6 (C$^{a/a'}$) ppm.

***N,N*-di(phenyl)-*N*'-(1-naphthoylthiourea) (HL^{16})**: Yield: 78%; mp (141.0-142.6 °C); $C_{24}H_{18}N_2OS$: calc.: C, 75.37; H, 4.74; N, 7.32. found: C, 75.80; H, 4.44; N, 7.22%; FT-IR (ATR): ν = 3149 (br. w, N-H), 3047 (w, aromatic C-H), 1695 (m, C=O), 1490 (s, C=N), 1373 (s), 1213 (s), 1118 (m), 760 (s) cm^{-1}; ^{1}H NMR (300 MHz, Chloroform-*d*) δ 8.60(s, 1H, N-H), 7.92 (ddt, 2H, H$^{4'}$, H$^{8'}$), 7.88-7.76 (m, 1H, H$^{2'}$), 7.54-7.46 (m, 3H, H$^{3'}$, H$^{5'}$, H$^{6'}$), 7.45 – 7.31 (m, 9H, H^{b+c}, H^{d+e}, H$^{7'}$), 7.28 (dd, 2H, H^{f}) ppm; ^{13}C NMR (300 MHz, Chloroform-*d*): δ 163.6 (C=O), 182.4 (C=S), 145.9 (N-C^{a}), 133.6 (C$^{1'}$), 131.6 (C$^{4a'}$), 130.2 (C$^{8a'}$), 132.3, 129.3, 128.3, 128.3, 127.6, 127.5, 127.0, 126.7, 125.9, 125.0, 124.4 (aromatic) ppm.

2.4.2. Synthesis of the [PtCl$_2$(phen) precursor complex

The precursor was synthesised according to a literature method.[20] A mixture of equimolar amounts of potassium tetrachloroplatinate (K_2PtCl_4) and 1,10-phenanthroline (phen) in 50 ml distilled water acidified with six drops of concentrated hydrochloric acid was refluxed until a yellow precipitate resulted (*ca.* 3 hours). The resultant mixture was cooled to room temperature and washed firstly with three 10 ml aliquots of water and then two 5 ml aliquots of acetone using a centrifuge at 3000 rpm. The dried product which was obtained in excellent yields; characterised using ^{1}H NMR spectroscopy, FT-IR spectroscopy, and elemental analysis.

[PtCl$_2$(phen)]: Yield: 82%; $C_{12}H_8Cl_2N_2Pt$: calc.: C, 32.30; H, 1.81; N, 6.28. found: C, 31.98; H, 1.97; N, 6.12%; FT-IR (ATR): ν = 3057 (w, aromatic C-H), 2955-2862 (w, aliphatic C-H), 1578 (m, C=N), 1515 (m), 1427 (m), 1220 (m), 839 (s), 706 (s) cm^{-1} ; ^{1}H NMR (500 MHz, DMSO-d_6) δ 9.70 (dd, J = 5.6 Hz, 2H, H^{2+9}), 9.04 (dd, J = 8.4 Hz, 2H, H^{4+7}), 8.29 (s, 2H, H^{5+6}), 8.17 (dd, J = 8.2, 5.5 Hz, 2H, H^{3+8}) ppm.

2.4.3. General procedure for the synthesis of the [Pt(phen)(L^n-κ*S*)$_2$] complexes

5 ml THF was added to a mixture of *N,N*-di(alkyl/aryl)-*N*'-acylthiourea ligand and an equimolar amount of sodium hydride on an ice bath with continuous stirring under inert conditions. The stirring was stopped when no more bubbles were being evolved and the mixture was left to stand so that unreacted sodium hydride settled at the bottom. The solution was decanted carefully and 0.5 equivalents of the [PtCl$_2$(phen)] precursor complex was then added to it, and the reaction mixture refluxed for 1 hour. The

resultant orange mixture was filtered through cotton wool. The filtrate was evaporated to dryness and re-dissolved in dichloromethane with subsequent filtration to remove insoluble salts. The filtrate was then concentrated under vacuo and precipitated using hexane. The precipitate was washed with ice-cold diethyl ether except for the [Pt(phen)(L^7-κ*S*)$_2$] complex which was purified using a basic aluminium oxide column with a 1:15 methanol/dichloromethane solvent mixture. Products (yellow to orange) obtained in excellent yields, were characterized using ^{1}H and ^{13}C NMR spectroscopy, FT-IR spectroscopy, Mass spectrometry, UV-vis spectrophotometry, elemental analysis and single crystal X-ray diffraction.

[Pt(phen)(L^1-κ*S*)$_2$]: Yield 89%; m.p. (159.2-161.0 °C); $C_{44}H_{42}N_6O_2PtS_2$: calc.: C, 55.86; H, 4.47; N, 8.88 found: C, 54.31; H, 4.22; N, 6.56%; UV (MeOH), λ/nm (ε/dm^3 mol^{-1} cm^{-1}): 276 (31907), 350 (6400); FT-IR (ATR): *v* = 2864-2972 (w, aliphatic C-H), 1585 (m, C=O), 1533 (s, C=N), 1231 (s), 1105 (s), 876 (m), 789 (s) cm^{-1} ; ^{1}H NMR (500 MHz, Chloroform-*d*) δ 9.25 (dd, 2H, H^{2+9}), 8.44 (d, 2H, $H^{8'}$), 8.09 (dd, 2H, H^{4+7}), 7.93 (dd, 2H, $H^{2'}$), 7.51 (dd, 2H, H^{3+8}), 7.35 (s, 2H, H^{5+6}), 7.16 (d, 2H, $H^{4'}$), 7.03 – 6.94 (m, 4H, $H^{3'+5'}$), 6.61 (ddd, 2H, $H^{6'}$), 6.19 (ddd, 2H, $H^{7'}$), 3.83 (s, 8H, $H^{a+a'}$), 1.38 (t, 12H, $H^{b+b'}$) ppm; ^{13}C NMR (500 MHz, Chloroform-*d*): δ 174.3 (C=O), 169.0 (C=S), 148.8 (C^{2+9}), 146.1 (C^{1a+10a}), 136.5 (C^{4+7}), 134.9 ($C^{1'}$), 132.8 ($C^{4a'}$), 131.2 ($C^{8a'}$), 131.0 ($C^{2'}$), 129.7 ($C^{4'}$), 129.2 (C^{4a+6a}), 126.7 ($C^{5'+8'}$), 126.1 (C^{5+6}), 124.8 ($C^{7'}$), 124.5 (C^{3+8}), 124.1 ($C^{3'}$), 124.0 ($C^{6'}$), 45.1 ($C^{a+a'}$), 13.9 ($C^{b+b'}$) ppm; HRMS (ESI$^+$) *m/z* for $C_{44}H_{42}N_6O_2PtS_2$. found: 946.2521 $[M+H]^+$, 660.1384 $[M-L^1]^+$, 473.1291 $[M+2H]^{2+}$, 287.1210 $[L^1+2H]^+$.

[Pt(phen)(L^2-κ*S*)$_2$]: Yield 94%; m.p. (154.3-154.7°C); $C_{52}H_{58}N_6O_2PtS_2$: calc.: C, 59.02; H, 5.52; N, 7.94. found: C, 59.29; H, 5.12; N, 7.51%; UV (MeOH), λ/nm (ε/dm^3 mol^{-1} cm^{-1}): 218 (102626), 275 (35477); FT-IR (ATR): *v* = 3055 (w, aromatic C-H), 2860-2926 (w, aliphatic C-H), 1583 (m C=O), 1560 (m), 1529 (s, C=N), 1265 (m), 1201 (s), 1101 (s), 1103 (m) cm^{-1} ; ^{1}H NMR (500 MHz, Chloroform-*d*): δ 9.24 (dd, 2H, H^{2+9}), 8.41 (dd, 2H, $H^{8'}$), 8.02 (dd, 2H, H^{4+7}), 7.91 (dd, 2H, $H^{2'}$), 7.46 (dd, H^{3+8}), 7.23 (s, 2H, H^{5+6}), 7.15 (dd, 2H, $H^{4'}$), 7.00 (dd, 2H, $H^{5'}$), 6.93 (dt, 2H, $H^{3'}$), 6.62 (dt, 2H, $H^{6'}$), 6.20 (dt, 2H, $H^{7'}$), 3.74 (d, 8H, $H^{a+a'}$), 1.82 (br. s, 8H, $H^{b+b'}$), 1.45 (br. s, 8H, $H^{c+c'}$), 1.02 (br. s, 12H, $H^{d+d'}$) ppm; ^{13}C NMR (500 MHz, Chloroform-*d*): δ 174.2 (C=O), 169.8 (C=S), 148.9 (C^{2+9}), 146.1 (C^{1a+10a}), 136.7 (C^{4+7}), 135.1 ($C^{1'}$), 132.8 ($C^{4a'}$), 131.2 ($C^{8a'}$), 131.0 ($C^{2'}$), 129.8 ($C^{4'}$), 129.3 (C^{4a+6a}), 126.8 ($C^{5'+8'}$), 124.8 ($C^{7'}$), 124.6 (C^{3+8}), 124.2 ($C^{3'}$), 124.1 ($C^{6'}$), 51.0 ($C^{a+a'}$), 31.1, 30.4 ($C^{b+b'}$), 20.5 ($C^{c+c'}$), 14.2 ($C^{d+d'}$) ppm; HRMS (ESI$^+$) *m/z* for $C_{52}H_{58}N_6O_2PtS_2$. found: 1058.3801 $[M+H]^+$, 716.2021 $[(M-L^2)]^+$, 530.1931 $[M+2H]^{2+}$, 343.1838 $[L^2+2H]^+$.

[Pt(phen)(L^3-κ*S*)$_2$]: Yield 87%; m.p. (168.7-168.9 °C); $C_{36}H_{38}N_6O_2PtS_2$: calc.: C, 51.11; H, 4.53; N, 9.93. found: C, 50.35; H, 4.23; N, 9.69%; UV (MeOH), λ/nm (ε/dm^3 mol^{-1} cm^{-1}): 212 (66241), 274 (44842); FT-IR (ATR): *v* = 3055 (w, aromatic C-H), 2864-2933 (w, aliphatic C-H), 1564 (m, C=O),

1516 (m), 1497 (s, C=N), 1427 (s), 1244 (s), 1128 (m), 847 (m) cm^{-1} ; ^{1}HNMR (500 MHz, Chloroform-*d*): δ 9.48 (dd, 2H, H^{2+9}), 8.38 (dd, 2H, H^{4+7}), 7.73 – 7.68 (m, 4H, H^{5+6}, H^{3+8}), 7.21 (dd, 4H, $H^{2'+6'}$), 6.61 (dt, 2H, $H^{4'}$), 6.47 (dt, 4H, $H^{3'+5'}$), 3.78 (br. s, 8H, $H^{a+a'}$), 1.34 (br. s, 12H, $H^{b+b'}$) ppm; ^{13}C NMR (500 MHz, Chloroform-*d*): δ172.7 (C=O), 169.9 (C=S), 149.9 (C^{2+9}), 146.8 (C^{1a+10a}), 138.7 ($C^{1'}$), 137.1 (C^{4+7}), 129.5 (C^{4a+6a}), 129.3 ($C^{2'+6'}$), 129.1 ($C^{4'}$), 126.6 (C^{5+6}), 126.3 ($C^{3'+5'}$), 125.1 (C^{3+8}), 45.2 ($C^{a+a'}$), 13.7 ($C^{b+b'}$) ppm; HRMS (ESI^+) *m/z* for $C_{36}H_{38}N_6O_2PtS_2$. found: 847.2241 $[M+H]^+$, 610.1238 $[(M-L^3)]^+$, 424.1149 $[M+2H]^{2+}$, 237.1059 $[L^3+2H]^+$.

[Pt(phen)(L^4-κ*S*)$_2$]: Yield: 93%; mp (174.0-174.6 °C); $C_{44}H_{54}N_6O_2PtS_2$: calc.: C, 55.16; H, 5.68; N, 8.77. found: C, 54.84; H, 5.91; N, 8.49%; UV (MeOH), λ/nm (ε/dm^3 mol^{-1} cm^{-1}): 350 (6354), 400 (2836); FT-IR (ATR): *v* = 3058 (w, aromatic C-H), 2866-2958 (w, aliphatic C-H), 1599 (m C=O), 1564 (m), 1495 (s, C=N), 1423 (s), 1201 (s), 842 (m) cm^{-1}; ^{1}H NMR (500 MHz, Chloroform-*d*) δ 9.52 (dd, 2H, H^{2+9}), 8.41 (dd, 2H, H^{4+7}), 7.77 (s, 2H, H^{5+6}), 7.73 (dd, 2H, H^{3+8}), 7.22 (dd, 4H, $H^{2'+6'}$), 6.64 (dt, 2H, $H^{4'}$), 6.50 (dt, 4H, $H^{3'+5'}$), 3.66 (s, 8H, $H^{a+a'}$), 1.79 (s, 8H, $H^{b+b'}$), 1.43 (s, 8H, $H^{c+c'}$), 1.01 (s, 12H, $H^{d+d'}$) ppm; ^{13}C NMR (500 MHz, Chloroform-*d*): δ 173.5 (C=O), 169.5 (C=S), 150.0 (C^{2+9}), 146.8 C($^{1a+10a}$), 138.8 ($C^{1'}$), 136.8 (C^{4+7}), 129.4 (C^{4a+6a}), 129.3 ($C^{2'+6'}$), 128.9 ($C^{4'}$), 126.4 (C^{5+6}), 126.1 ($C^{3'+5'}$), 125.0 (C^{3+8})), 50.7 ($C^{a+a'}$), 30.5 ($C^{b+b'}$), 19.6 ($C^{c+c'}$), 14.1 ($C^{d+d'}$) ppm; HRMS (ESI^+) *m/z* for $C_{44}H_{54}N_6O_2PtS_2$. found: 958.3454 $[M+H]^+$, 666.1847 $[(M-L^4)+H]^+$, 480.1767 $[M+2H]^{2+}$, 315.1494 $[L^4+H+Na]^+$.

[Pt(phen)(L^6-κ*S*)$_2$]: Yield: 91%; mp (130.8-131.2 °C); $C_{34}H_{50}N_6O_2PtS_2$: calc.: C, 48.96; H, 6.04; N, 10.08. found: C, 49.03; H, 5.89; N, 9.49%; UV (MeOH), λ/nm (ε/dm^3 mol^{-1} cm^{-1}): 350 (4134), 400 (2452); FT-IR (ATR): *v* = 2868-2956 (w, aliphatic C-H), 1602 (m C=O), 1497 (s, C=N), 1429 (s), 1203 (s), 1126 (s), 850 (m) cm^{-1}; ^{1}H NMR (500 MHz, Chloroform-*d*) δ 9.91 (dd, 2H, H^{2+9}), 8.56 (dd, 2H, H^{4+7}), 7.94 – 7.86 (m, 4H, H^{5+6}, H^{3+8}), 3.64 (s, 8H, $H^{a+a'}$), 1.94 (s, 6H, $H^{1'}$), 1.72 (s, 8H, $H^{b+b'}$), 1.37 (q, 8H, $H^{c+c'}$), 0.96 (t, 12H, $H^{d+d'}$) ppm; ^{13}C NMR (500 MHz, $CDCl_3$, 298 K): δ 177.5 (C=O), 168.7 (C=S), 150.6 (C^{2+9}), 147.7 (C^{1a+10a}), 138.0 (C^{4+7}), 130.0 (C^{4a+6a}), 127.0 (C^{5+6}), 125.0 (C^{3+8})), 50.2 ($C^{a+a'}$), 30.1 ($C^{b+b'}$), 27.4 ($C^{1'}$) 20.3 ($C^{c+c'}$), 14.0 ($C^{d+d'}$) ppm; HRMS (ESI^+) *m/z* for $C_{34}H_{50}N_6O_2PtS_2$. found: 604.1705 $[(M-L^6)]^+$.

[Pt(phen)(L^7-κ*S*)$_2$]: Yield: 90%; mp (156.8-157.3 °C); $C_{32}H_{46}N_6O_2PtS_2$: calc.: C, 47.69; H, 5.75; N, 10.43. found: C, 47.68; H, 6.07; N, 10.58%; UV (MeOH), λ/nm (ε/dm^3 mol^{-1} cm^{-1}): 350 (5849), 400 (3134); FT-IR (ATR): *v* = 2870-2970 (w, aliphatic C-H), 1645 (m, C=O), 1497 (s, C=N), 1420 (m), 1231 (s), 1190 (s), 1132 (m), 789 (m) cm^{-1} ; ^{1}H NMR (300 MHz, Chloroform-*d*) δ 10.24 (dd, 2H, H^{2+9}), 8.58 (dd, 2H, H^{4+7}), 8.00 (dd, 2H, H^{3+8}), 7.95 (s, 2H, H^{5+6}), 3.68 (br. s, 8H, $H^{a+a'}$), 1.29 (dt, 12H, $H^{b+b'}$), 0.75 (s, 18H, $H^{2'}$) ppm; ^{13}C NMR (300 MHz, Chloroform-*d*): δ 183.3 (C=O), 171.2 (C=S), 151.6 (C^{2+9}),

147.3 (C^{1a+10a}), 137.5 (C^{4+7}), 129.7 (C^{4a+6a}), 126.8 (C^{5+6}), 125.7 (C^{3+8}), 51.0 ($C^{a+a'}$), 40.1 ($C^{1'}$), 29.9 ($C^{b+b'}$), 28.1 ($C^{2'}$) ppm; HRMS (ESI^+) *m/z* for $C_{32}H_{46}N_6O_2PtS_2$. found: 590.1532 $[(M\text{-}L^7)]^+$.

[Pt(phen)(L^8-κ*S*)$_2$]: Yield: 93%; mp (124.7-125.1 °C); $C_{40}H_{62}N_6O_2PtS_2$: calc.: C, 52.33; H, 6.81; N, 9.15. found: C, 52.67; H, 6.98; N, 9.43%; UV (MeOH), λ/nm (ε/dm^3 mol^{-1} cm^{-1}): 350 (6489), 400 (3531); FT-IR (ATR): *v* = 2866-2956 (w, aliphatic C-H), 1583 (m, C=O), 1494 (s, C=N), 1369 (m), 1103 (s), 852 (m) cm^{-1} ; ^{1}H NMR (500 MHz, Chloroform-*d*) δ 10.26 (dd, 2H, H^{2+9}), 8.57 (dd, 2H, H^{4+7})), 7.99 (dd, 2H, H^{3+8}), 7.93 (s, 2H, H^{5+6}), 3.59 (s, 8H, $H^{a+a'}$), 1.72 (s, 8H, $H^{b+b'}$), 1.36 (d, 8H, $H^{c+c'}$), 0.95 (t, 12H, $H^{d+d'}$), 0.76 (s, 18H, $H^{2'}$) ppm; ^{13}C NMR (500 MHz, Chloroform-*d*): δ 183.3 (C=O), 171.2 (C=S), 151.6 (C^{2+9}), 147.3 (C^{1a+10a}), 137.5 (C^{4+7}), 129.7 (C^{4a+6a}), 126.8 (C^{5+6}), 125.7 (C^{3+8}), 51.0 ($C^{a+a'}$), 40.1 ($C^{1'}$), 29.9 ($C^{b+b'}$), 28.1 ($C^{2'}$), 20.4 ($C^{c+c'}$), 14.0 ($C^{d+d'}$) ppm; HRMS (ESI^+) *m/z* for $C_{40}H_{62}N_6O_2PtS_2$. found: 646.2166 $[(M\text{-}L^8)]^+$.

[Pt(phen)(L^9-κ*S*)$_2$]: Yield: 97%; $C_{26}H_{28}Cl_6N_6O_2PtS_2$: calc.: C, 33.64; H, 3.04; N, 9.05. found: C, 33.58; H, 3.10; N, 8.82%; UV (MeOH), λ/nm (ε/dm^3 mol^{-1} cm^{-1}): 350 (2828), 400 (1615); FT-IR (ATR): *v* = 3050 (w, aromatic C-H), 2870-2974 (w, aliphatic C-H), 1602 (m, C=O), 1491 (s, C=N), 1409 (s), 1290 (s), 1147 (s), 1100 (m), 781 (m) cm^{-1} ; ^{1}H NMR (400 MHz, Chloroform-*d*): δ 9.98 (dd, 2H, H^{2+9}), 8.59 (dd, 2H, H^{4+7}), 8.03-7.84 (m, 4H, H^{3+8}, H^{5+6}), 3.97 (q, 4H, H^a), 3.49 (q, 4H, $H^{a'}$), 1.43 (t, 6H, H^b), 1.23 (t, 6H, $H^{b'}$) ppm; ^{13}C NMR (400 MHz, Chloroform-*d*): δ 182.5 (C=O), 160.2 (C=S), 151.0 (C^{2+9}), 147.3 (C^{1a+10a}), 138.2 (C^{4+7}), 129.9 (C^{4a+6a}), 126.9 (C^{5+6}), 125.6 (C^{3+8}), 46.6, 45.5 ($C^{a+a'}$), 13.2 ($C^{b+b'}$) ppm; HRMS (ESI^+) *m/z* for $C_{26}H_{28}Cl_6N_6O_2PtS_2$. found: 928.9487 $[M+H]^+$, 650.9854 $[(M\text{-}L^9)]^+$, 464.9791 $[M+2H]^{2+}$, 278.9691 $[L^9+2H]^+$.

[Pt(phen)(L^{10}-κ*S*)$_2$]: Yield: 88%; mp (182.3-183.4 °C); $C_{44}H_{42}N_6O_2PtS_2$: calc.: C, 55.86; H, 4.47; N, 8.88. found: C, 55.47; H, 4.86; N, 8.66%; UV (MeOH), λ/nm (ε/dm^3 mol^{-1} cm^{-1}): 350 (10373), 400 (3132); FT-IR (ATR): *v* = 2963-2882 (w, aliphatic C-H), 1602 (m, C=O), 1564 (m), 1500 (s, C=N), 1427 (s), 1250 (s), 1186 (s), 894 (m) cm^{-1} ; ^{1}H NMR (500 MHz, Chloroform-*d*) δ 9.11 (dd, 2H, H^{2+9}), 8.02 (dd, 2H, H^{4+7}), 7.56 (dd, 2H, $H^{1'}$), 7.47 (s, 2H, H^{5+6}), 7.28 – 7.20 (m, 6H, H^{3+8}, $H^{3'+5'}$), 7.19 (ddd, 2H, $H^{6'}$), 7.08 (ddd, 2H, $H^{7'}$), 7.01 (dd, 2H, $H^{8'}$), 6.82 (dd, 2H, $H^{4'}$), 3.83 (s, 8H, $H^{a+a'}$), 1.39 (s, 12H, $H^{b+b'}$) ppm; ^{13}C NMR (500 MHz, Chloroform-*d*): δ 173.2 (C=O), 168.5 (C=S), 148.7 (C^{2+9}), 146.0 (C^{1a+10a}), 136.2 (C^{4+7}), 136.1 ($C^{2'}$), 133.5 ($C^{4a'}$), 131.8 ($C^{8a'}$), 129.9 ($C^{1'}$), 128.9 (C^{4a+6a}), 128.7 ($C^{8'}$), 126.9 ($C^{5'}$), 126.6 ($C^{3'}$), 126.1 (C^{5+6}), 126.0 ($C^{6'}$), 125.4 ($C^{4'}$), 124.9 ($C^{7'}$), 124.3 (C^{3+8}), 45.1 ($C^{a+a'}$), 13.8 ($C^{b+b'}$) ppm; HRMS (ESI^+) *m/z* for $C_{44}H_{42}N_6O_2PtS_2$. found: 946.2533 $[M+H]^+$, 660.1384 $[(M\text{-}L^{10})]^+$, 473.6297 $[M+2H]^{2+}$, 287.1209 $[L^{10}+2H]^+$.

[Pt(phen)(L^{11}-κ*S*)$_2$]: Yield: 92%; mp (178.3-178.6 °C); $C_{52}H_{58}N_6O_2PtS_2$: calc.: C, 59.02; H, 5.52; N, 7.94. found: C, 58.81; H, 5.90; N, 7.50%; UV (MeOH), λ/nm (ε/dm^3 mol^{-1} cm^{-1}): 350 (12307), 400 (3579); FT-IR (ATR): *v* = 2869-2957 (w, aliphatic C-H), 1607 (m, C=O), 1600 (m), 1537 (m), 1495 (s, C=N)), 1425 (s), 1117 (s), 847 (m) cm^{-1} ; ^{1}H NMR (500 MHz, Chloroform-*d*) δ 9.11 (dd, 2H, H^{2+9}), 8.04 (dd, 2H, H^{4+7}), 7.57 (dd, 2H, $H^{1'}$), 7.48 (s, 2H, H^{5+6}), 7.30 – 7.16 (m, 8H, H^{3+8}, $H^{3'+5'+6'}$), 7.10 (ddd, 2H, $H^{7'}$), 7.03 (dd, 2H, $H^{8'}$), 6.82 (dd, 2H, $H^{4'}$), 4.23 – 3.30 (m, 8H, $H^{a+a'}$), 1.84 (s, 8H, $H^{b+b'}$), 1.48 (s, 8H, $H^{c+c'}$) 1.06 (dt, 12H, $H^{d+d'}$) ppm; ^{13}C NMR (500 MHz, Chloroform-*d*): δ 173.1 (C=O), 168.6 (C=S), 148.7 (C^{2+9}), 146.1 (C^{1a+10a}), 136.2 (C^{4+7}), ($C^{2'}$), 133.5 ($C^{4a'}$), 131.8 ($C^{8a'}$), 130.0 ($C^{1'}$), 128.9 (C^{4a+6a}), 128.7 ($C^{8'}$), 126.9 ($C^{5'}$), 126.6 ($C^{3'}$), 126.1 (C^{5+6}), 126.0 ($C^{6'}$), 125.4 ($C^{4'}$), 124.9 ($C^{7'}$), 124.4 (C^{3+8}), 50.7 ($C^{a+a'}$), 29.1 ($C^{b+b'}$), 20.5 ($C^{c+c'}$), 14.1 ($C^{d+d'}$) ppm; HRMS (ESI$^+$) *m/z* for $C_{52}H_{58}N_6O_2PtS_2$. found: 1058.3783 $[M+H]^+$, 716.2013 $[(M-L^{11})]^+$, 530.1928 $[M+2H]^{2+}$, 343.1834 $[L^{11}+2H]^+$.

[Pt(phen)(L^{12}-κ*S*)$_2$]: Yield: 90%; mp (163.8 °C and decomposed); $C_{36}H_{36}Cl_2N_6O_2PtS_2$: calc.: C, 47.27; H, 3.97; N, 9.19. found: C, 47.18; H, 3.77; N, 8.76%; UV (MeOH), λ/nm (ε/dm^3 mol^{-1} cm^{-1}): 350 (6298), 400 (2692); FT-IR (ATR): *v* = 3061 (w, aromatic C-H), 2866-2972 (w, aliphatic C-H), 1599 (m, C=O), 1491 (s, C=N), 1412 (s), 1126 (s), 845 (s) cm^{-1} ; ^{1}H NMR (500 MHz, Chloroform-*d*) δ 9.49 (dd, 2H, H^{2+9}), 8.50 (dd, 2H, H^{4+7}), 7.86 (s, 2H, H^{5+6}), 7.81 (dd, 2H, H^{3+8}), 7.15 (dd, 4H, $H^{2'+6'}$), 6.41 (dd, 4H, $H^{3'+5'}$), 3.82 (s, 8H, $H^{a+a'}$), 1.34 (s, 12H, $H^{b+b'}$) ppm; ^{13}C NMR (500 MHz, Chloroform-*d*): δ 171.4 (C=O), 170.0 (C=S), 149.6 (C^{2+9}), 146.6 (C^{1a+10a}), 137.3 ($C^{1'}$), 137.2 (C^{4+7}), 135.1 ($C^{4'}$), 130.7 ($C^{2'+6'}$), 129.5 (C^{4a+6a}), 126.6 (C^{5+6}), 126.3 ($C^{3'+5'}$), 125.2 (C^{3+8}), 45.2 ($C^{a+a'}$), 12.7 ($C^{b+b'}$) ppm; HRMS (ESI$^+$) *m/z* for $C_{36}H_{36}Cl_2N_6O_2PtS_2$. found: 915.1413 $[M+H]^+$, 645.0826 $[(M-L^{12})]^+$, 458.0741 $[M+2H]^{2+}$, 271.0660 $[L^{12}+2H]^+$.

[Pt(phen)(L^{14}-κ*S*)$_2$]: Yield: 86%; mp (160.0-160.8 °C); $C_{36}H_{36}N_8O_6PtS_2$: calc.: C, 46.20; H, 3.88; N, 11.97. found: C, 46.43; H, 4.11; N, 11.49%; UV (MeOH), λ/nm (ε/dm^3 mol^{-1} cm^{-1}): 350 (12167), 400 (2889); FT-IR (ATR): *v* = 3057 (w, aromatic C-H), 2871-2976 (w, aliphatic C-H), 1583 (m, C=O), 1510 (s, C=N), 1339 (s), 1236 (s), 1074 (s), 858 (s) cm^{-1} ; ^{1}H NMR (500 MHz, Chloroform-*d*) δ 9.53 (dd, 2H, H^{2+9}), 8.49 (dd, 2H, H^{4+7}), 8.30 (d, 2H,), 7.85 – 7.79 (m, 4H, H^{5+6}, H^{3+8}), 7.42 (dd, 4H, $H^{2'+6'}$), 7.35 (dd, 4H, $H^{3'+5'}$), 3.81 (d, 8H, $H^{a+a'}$), 1.34 (dt, 12H, $H^{b+b'}$) ppm; ^{13}C NMR (500 MHz, Chloroform-*d*): δ 173.0 (C=S), 168.7 (C=O), 149.9, (C^{2+9}), 147.7 ($C^{4'}$), 146.4 (C^{1a+10a}), 144.7 ($C^{1'}$), 137.7 (C^{4+7}), 129.7, (C^{4a+6a}), ($C^{2'+6'}$), 126.8 (C^{5+6}), 125.4 (C^{3+8}), 121.5 ($C^{3'+5'}$), 45.3 ($C^{a+a'}$), 13.0 ($C^{b+b'}$) ppm; HRMS (ESI$^+$) *m/z* for $C_{36}H_{36}N_8O_6PtS_2$. found: 936.1927 $[M+H]^+$, 655.1083 $[(M-L^{14})]^+$, 468.5995 $[M+2H]^{2+}$, 282.0906 $[L^{14}+2H]^+$.

[Pt(phen)(L^{15}-κ*S*)$_2$]: Yield: 93%; mp (178.0-178.5 °C); $C_{64}H_{50}N_6O_2PtS_2$: calc.: C, 64.36; H, 4.22; N, 7.04. found: C, 64.54; H, 4.27; N, 6.69%; UV (MeOH), λ/nm (ε/dm^3 mol^{-1} cm^{-1}): 350 (12211), 400

(3187); FT-IR (ATR): *v* = 3028 (w, aromatic C-H), 1587 (m, C=O), 1537 (s, C=N), 1452 (m), 1352 (m), 1175 (s), 1113 (s), 787 (s) cm^{-1} ; ^{1}H NMR (500 MHz, Chloroform-*d*) δ 9.23 (dd, 2H, H^{2+9})), 8.25 (dd, 2H, $H^{8'}$), 8.19 (dd, 2H, H^{4+7}), 7.93 (dd, 2H, $H^{2'}$), 7.58 (dd, 2H, H^{3+8}), 7.53 – 7.48 (m, 12H, H^{phenyl}), 7.47 (s, 2H, H^{5+6}), 7.30 (br. s, 8H, H^{phenyl}) 7.11 (d, 2H, $H^{4'}$), 6.97 – 6.88 (m, 2H, $H^{3'+5'}$), 6.56 (ddd, 2H, $H^{6'}$), 6.05 (ddd, 2H, $H^{7'}$), 4.94 (br. s, 8H, $H^{a+a'}$) ppm; ^{13}C NMR (500 MHz, Chloroform-*d*): δ 176.1 (C=O), 167.5 (C=S), 148.7 (C^{2+9}), 146.0 (C^{1a+10a}), 136.5 (C^{4+7}), 133.2 ($C^{2'}$), 132.9 ($C^{1'}$), 132.6 ($C^{4a'}$), 131.1 ($C^{8a'}$), 130.7 ($C^{4'}$), 129.3 (C^{4a+6a}), 128.5, 128.3, 127.0 (C^{phenyl}), 126.6 ($C^{5'}$), 126.2 (C^{5+6}), 126.0 ($C^{8'}$), 125.1 ($C^{7'}$), 124.5 (C^{3+8}), 124.2 ($C^{3'}$), 123.9 ($C^{6'}$), 52.3 ($C^{a+a'}$) ppm; HRMS (ESI^{+}) *m/z* for $C_{64}H_{50}N_6O_2PtS_2$. found: 1195.3166 $[M+H]^{+}$, 784.1697 $[(M-L^{15})]^{+}$, 598.1614 $[M+2H]^{2+}$, 411.1518 $[L^{15}+2H]^{+}$.

[Pt(phen)(L^{16}-κ*S*)$_2$]: Yield: 89%; mp (170.1-170.7 °C); $C_{60}H_{42}N_6O_2PtS_2$: calc.: C, 63.31; H, 3.72; N, 7.38. found: C, 63.46; H, 3.83; N, 7.49%; UV (MeOH), λ/nm (ε/dm^3 mol^{-1} cm^{-1}): 350 (18176), 400 (3525); FT-IR (ATR): *v* = 3051 (w, aromatic C-H), 1543 (m, C=O), 1489 (s, C=N), 1261 (m), 1219 (s), 1121 (s), 783 (s) cm^{-1} ; ^{1}H NMR (500 MHz, Chloroform-*d*) δ 9.27 (s, 2H, H^{2+9}), 8.32 (dd, 4H, $H^{4+7+8'}$), 7.96 (d, 2H, $H^{2'}$), 7.68 (s, 2H, H^{5+6}), 7.62 (dd, 2H, H^{3+8}), 7.48 (dd, 2H, $H^{4'}$), 7.36 – 6.73 (m, 26H, $H^{3'+5'+6'+ph}$), 6.36 (s, 2H, $H^{7'}$) ppm; ^{13}C NMR (500 MHz, Chloroform-*d*): δ 177.4 (C=O), 166.1 (C=S), 148.5 (C^{2+9}), 146.3 ($C^{1'}$), 137.0 (C^{4+7}), 133.0 ($C4^{a'}$), 132.5 ($C^{2'}$), 131.0 ($C^{4'}$), 131.1 ($C^{8a'}$), 129.5 (C^{4a+6a}), 128.4, 127.2, 125.4, 124.8, 124.4 ($C^{3'+5'+6'}$, C^{phenyl}), 126.5 (C^{5+6}), 126.2 ($C^{8'}$), 125.1 ($H^{7'}$), 124.9 (C^{3+8}) ppm; HRMS (ESI^{+}) *m/z* for $C_{60}H_{42}N_6O_2PtS_2$. found: 1139.2537 $[M+H]^{+}$, 756.1382 $[(M-L^{16})]^{+}$, 570.1300 $[M+2H]^{2+}$, 383.1205 $[L^{16}+2H]^{+}$.

2.5. References

[1] L. Guang-Yi, Z. Hong, X. Liu-Yin, W. Shuai, X. Zheng-He, *Miner. Eng.* **2011**, *24*, 817–824.

[2] A. M. Alkherraz, Z. I. Lusta, A. E. Zubi, *Int. J. Chem. Nucl. Metall. Mater. Eng.* **2014**, *8*, 116–118.

[3] J. C. Bruce, N. Revaprasadu, K. R. Koch, *New J. Chem.* **2007**, *31*, 1647.

[4] Z. Ali, N. E. Richey, D. C. Bock, K. A. Abboud, J. Akhtar, M. Sher, L. McElwee-White, *Dalton Trans.* **2018**, *47*, 2719–2726.

[5] A. Saeed, M. N. Mustafa, M. Zain-ul-Abideen, G. Shabir, M. F. Erben, U. Flörke, *J. Sulfur Chem.* **2018**, *5993*, 1–39.

[6] I. B. Douglass, F. B. Dains, *J. Am. Chem. Soc.* **1934**, *56*, 719–721.

[7] A. R. Katritzky, N. Kirichenko, B. V Rogovoy, J. Kister, H. Tao, *Synthesis* **2004**, *11*, 1799–1805.

[8] I. A. Kotzé, W. J. Gerber, J. M. Mckenzie, K. R. Koch, *Eur. J. Chem.* **2009**, 1626–1633.

[9] F. A. Cotton, G. Wilkinson, C. Murillo, M. Bochmann, *Advanced Inorganic Chemistry*, John Wiley & Sons, New York, **1999**.

[10] C. H. Langford, H. B. Gray, *Ligand Substitution Processes*, W. A. Benjamin, Inc., New York, **1966**.

[11] A. Bakac, *Physical Inorganic Chemistry: Reactions, Processes and Applications*, John Wiley & Sons, Inc, New Jersey, **2010**.

[12] J. R. Paxson, Ligand Substitution Reactions of Platinum(II) Complexes . Chloro (diethylenetriamine) Platinum(II)-Chloride Exchange, PhD, Iowa State University, **1970**.

[13] R. J. Mreinik, *Coord. Chem. Rev.* **1978**, *25*, 1–30.

[14] M. Schuster, E. Unterreitmaier, *Fresenius J. Anal. Chem.* **1993**, *346*, 630–631.

[15] M. Schuster, *Fresenius J. Anal. Chem.* **1992**, *342*, 791–792.

[16] K. R. Koch, T. Grimmbacher, C. Sacht, *Polyhedron* **1998**, *17*, 267–274.

[17] R. Koch, C. Wentrup, *J. Org. Chem.* **2013**, *78*, 1802–1810.

[18] D. T. Elmore, J. R. Ogle, *J. Am. Chem. Soc.* **1957**, 1141–1145.

[19] D. P. N. Satchell, R. S. Satchell, *J. Chem. Soc. Perkin Trans. 2* **1990**, *1415*, 1415–1420.

[20] T. J. Egan, K. R. Koch, P. L. Swan, C. Clarkson, D. A. Van Schalkwyk, P. J. Smith, *J. Med. Chem.* **2004**, *47*, 2926–2934.

[21] A. F. Palocsay, PART I - A Kinetic Study of Nitrosyl Exchange in Metal Nitrosyls. PART II - A Kinetic Study of the Reaction of Various Ortho- Phenanthrolines with Potassium Tetrachloroplatinate II, PhD, University of arizona, **1969**.

[22] L. I. Elding, I. Leden, *Acta Chem. Scand.* **1966**, *20*, 706–715.

[23] L. Drouge, L. I. Elding, L. Gustafson, *Acta Chem. Scand.* **1967**, *21*, 1647–1653.

[24] A. N. Mautjana, J. D. S. Miller, A. Gie, S. A. Bourne, K. R. Koch, *Dalton Trans.* **2003**, *10*, 1952–1960.

[25] J. Dillen, M. G. Woldu, K. R. Koch, *Acta Crystallogr. Sect. E Struct. Reports Online* **2006**, *62*, 5228–5229o.

[26] S. Kishi, M. Kato, *Inorg. Chem.* **2003**, *42*, 8728–8734.

[27] L. R. Gomes, L. Santos, J. Coutinho, B. Schroder, J. N. Low, *Acta Crystallogr. Sect. E Struct. Reports Online* **2010**, *66*, 870o.

[28] J. M. Mckenzie, R. Klaus, *Acta Crystallogr. Sect. E Struct. Reports Online* **2006**, *62*, 4263–4264o.

[29] S. Ashraf, A. Saeed, A. Malik, U. Flörke, M. Bolte, N. Haider, J. Akhtar, *Eur. J. Inorg. Chem.* **2014**, *3*, 533–538.

[30] I. A. Kotzé, V. J. Smith, E. F. Kangara, K. R. Koch, *New J. Chem.* **2017**, *41*, 14995–15002.

[31] D. B. G. Williams, M. Lawton, *J. Org. Chem.* **2010**, *75*, 8351–8354.

[32] M. Schuster, B. Kugler, *Fresenius J. Anal. Chem.* **1990**, *338*, 717–720.

[33] A. V Fokin, A. F. Kolomiets, A. I. Rapkin, V. I. Yakutin, S. Khimicheskaya, *Russ. Chem. Bull.* **1972**, *21*, 1172–1173.

Chapter 3

Solution conformational analysis of [Pt(phen)(L^n-κS)$_2$] complexes, theoretical and experimental rationale into the monodentate coordination of N,N-di(alkyl/aryl)-N'-acylthioureato ligands

3.1. Introduction

The versatility of disubstituted acylthiourea ligands stem from the presence of multiple donor sites in one ligand presenting several possible coordination modes; however, the bidentate coordination of the monoanionic ligand (through sulfur and oxygen) dominates coordination of these ligands to transition metals. The monoanionic ligand, in most of the reported synthetic procedures for these transition metal-acylthiourea complexes, is generated *in-situ via* deprotonation of the amidic proton using a mild base, a basic metal precursor or water in wet solvents.[1] The deprotonation of the thione tautomer (which is the most preferred tautomer of disubstituted acylthiourea ligands) is thought to produce a resonance stabilised anion which can be represented by three canonical forms (*Scheme 1*), that in turn coordinate to the metal centre always as an LX-type ligand in the case of bidentate coordination.[2]



Scheme 1: Resonance structures showing possible negative charge distribution on oxygen, nitrogen, and sulfur in the anionic disubstituted acylthiourea ligand.

Rarely has disubstituted acylthioureato ligands been seen to exhibit other coordination modes, particularly as monodentate X-type ligands, through the sulfur donor atom. We observed in *Chapter 2* that disubstituted acylthiourea ligands bearing aromatic acyl substituents or an electron-withdrawing trichloromethyl- group (CCl_3-) preferred monodentate coordination while those with disubstituted acylthiourea ligands bearing aliphatic acyl substituents favoured bidentate coordination when reacted in 1:2 metal to ligand ratio using the one-pot synthesis (Method A).

Guided by this result, we suspected intramolecular π-stacking interactions between aromatic moieties of acylthioureato ligands and the phenanthroline co-ligand as crucial in stabilising the [Pt(phen)(L^n-κS)$_2$] complexes as hinted to by the extensive intramolecular π-π stacking interactions in the solid-state structures. However, solid-state conformations may differ from solution conformations as observed by Kessler *et al.* [3] on two occasions; hence, there is a need to understand the conformations of these

complexes in solution and determine whether these π-π stacking interactions persist in solution. General solution NMR spectroscopy can enrich us with structural data of chemical compounds but falls short in the study of conformations of conformationally flexible molecules in solution when the interconversion between the conformations is faster than the NMR timescale. Dynamic NMR spectroscopy or variable temperature NMR spectroscopy is an excellent tool to manipulate these interconversion rates to observe the difficult species using NMR spectroscopy.

Variable temperature NMR spectroscopy is a spectroscopic method where the response of a nucleus with a non-zero spin to a perturbing magnetic field is detected at temperatures above and below ambient probe temperature.[4] It is a powerful tool for observing dynamic processes that may be occurring within or between molecules such as; (i) bond rotations about bond axes, (ii) ring inversions and (iii) fluxional properties of molecules.[5,6] These dynamic processes result in changes in chemical environments that will appear in the NMR spectra as changes in chemical shifts and coupling constants. The hunt for the solution-phase conformations is challenging, hence the importance of a correlation between conformations in solid-state and in solution.[7,8] Several nuclei can be investigated using variable-temperature NMR spectroscopy, however, in this study, we have focused only on ^{1}H and ^{195}Pt to investigate whether the intramolecular π-stacking observed in the solid-state structures of [Pt(phen)(L^{n}-*κS)*$_2$] complexes with acylthioureato ligands bearing aromatic acyl substituents also persist in solution.

We also suspected the electronic properties of substituent groups of having a significant influence on the way disubstituted acylthioureato ligands coordinated when reacted using the one-pot synthesis (method A). Understanding the electronic influence of substituents in a molecule and how thet affect the reactivity of many possible reactive sites within that molecule has over the years interested many researchers with some turning to theoretical chemistry, in particular, conceptual DFT for answers. Organic chemists have, on many occasions, used conceptual DFT as a tool to understand the electronic effects of substituent groups in a molecule on the reactivity of particular reactive sites within that molecule.[9,10] This tool has also been extended on numerous occasions to coordination chemistry.[11]

Conceptual DFT is a powerful quantum chemistry tool that quantifies the possible responses of a chemical system to various changes in electron density to a notion of chemical reactivity using the so-called response functions, which are reactivity descriptors or reactivity indicators for reactants in the ground state.[12,13] Electron density calculations offer crucial information about structural properties of molecules and materials.[14] Many studies have shown that the electron density, along with its response to perturbations contains valuable information about chemical reactivity.[13] The study of these response functions allows one to predict what sort of perturbations stabilises or destabilises the molecule the most or the least, thus allowing one to predict the regioselectivity, analyse and interpret reactions with those reagents.[15]

These response functions can be divided into three groups: global, local and non-local.[16] Global functions describe the global response against global perturbations and such quantities do not depend on spatial position within the molecular framework. They characterise the entire system as an entity and do not contain information about regioselectivity.[17] Local descriptors are position-dependent and are associated with global/local responses to a system against local/global perturbations.[18] These quantities vary from one position to another in a molecule and are thus important in making predictions about regioselectivity. Non-local indices, on the other hand, either measure a molecule's polarisation with respect to its environment or change in polarisation associated with charge transfer.[17] All these descriptors provide us with a way to understand experimental observations.

Local descriptors such as hardness (η), softness (*S*) and Fukui function allows us to distinguish between regions with different behaviour in a molecule and have been widely used within the quantum chemistry framework within DFT formalism.[15,19] Molecules containing multiple donor sites such as acylthioureato ligands present us with an optimal case for the testing of their reactivity criteria using conceptual DFT in a coordination chemistry framework in the same way Vivas-Reyes *et al.* reported.[20] This study explores these local quantities to rationalise the aspects of experimental observations which we noticed during the synthesis of [Pt(phen)(L^n-κ*S*)$_2$] complexes.

Since detailed presentations and derivations of various molecular reactivity descriptors have thoroughly been researched and reported elsewhere, only relevant expressions used for evaluation and discussion of different quantities are given below.[21–23]

Global nucleophilicity $\mathcal{N}$ is defined by Equation 1:

$$\mathcal{N} = E_{homo(Nu)} - E_{homo(TCE)} \quad \ldots\ldots\ldots\ldots\ldots\ldots\ldots\ldots 1$$

where $E_{homo(Nu)}$ is the HOMO energy of the acylthioureato ligand and $E_{homo(TCE)}$ is the HOMO energy of tetracyanoethylene (TCE) taken as reference. The Global nucleophilicity index $\mathcal{N}$ can be expressed as the sum of local nucleophilicities condensed to all atoms of the molecule:

$$\mathcal{N} = \sum \mathcal{N}_k \quad \ldots\ldots\ldots\ldots\ldots\ldots\ldots\ldots\ldots\ldots\ldots\ldots 2$$

where $\mathcal{N}_k$ is the local nucleophilicity index condensed to an atom k, and it is possible to define the local nucleophilicity through the nucleophilic Fukui function (f_k^-) using equation 3.

$$\mathcal{N}_k = \mathcal{N} f_k^- \quad \ldots\ldots\ldots\ldots\ldots\ldots\ldots\ldots\ldots\ldots\ldots\ldots 3$$

The Fukui function is defined in terms of the derivative of the electron density ρ(r) at point (r), with respect to the number of electrons in the system, *N*.

$$f(\mathrm{r}) = \left(\frac{\partial \rho(r)}{\partial N}\right)_{v(r)} \quad \ldots\ldots\ldots\ldots\ldots\ldots\ldots\ldots\ldots\ldots 4$$

The function $f(r)$ reflects the ability of a molecular site to accept or donate electrons. High values of $f(r)$ are related to a high reactivity at point (r). By applying the finite difference approximation to Equation 4, two definitions of the Fukui function depending on the electron densities are obtained.

$$f_{(r)}^{+} = \rho_{(N+1)}(r) - \rho_{(N)}(r) \quad \text{.....5}$$

$$f_{(r)}^{-} = \rho_{(N)}(r) - \rho_{(N-1)}(r) \quad \text{.....6}$$

where $\rho_{(N+1)}(r)$, $\rho_{(N)}(r)$ and $\rho_{(N-1)}(r)$ are the electronic densities at point (r) for a system with N+1, N and N-1 electrons, respectively. $f_{(r)}^{+}$ measures the reactivity at a site (r) towards nucleophilic reagents while $f_{(r)}^{-}$ measures the reactivity at a site (r) towards electrophilic reagents. These functions can be condensed to nuclei by using atomic charge partitioning scheme such as Mulliken population analysis, Lowdin population analysis or Hirshfeld population analysis to give equations 7 and 8.

$$f_{k}^{+} = q_{(k)}N - q_{(k)}(N+1) \quad \text{.....7}$$

$$f_{k}^{-} = q_{(k)}(N-1) - q_{(k)}N \quad \text{.....8}$$

where $q_{(k)}$ is the charge on atom (k) according to a charge partitioning scheme. Most researchers have adopted the Hirshfeld population analysis for charge partitioning since it is less basis set dependent compared to other charge partition schemes,[24] we have also focused on using Hirshfeld charges. The coordination modes of ambidentate ligands may vaguely be predicted via electronic and steric effects; however, they are also sensitive to various experimental factors such as central metals, oxidation states, co-ligands, reaction time, temperature and solvents.[25–29] such that an experimental mechanistic study is of the essence.

3.2. Results and Discussion

3.2.1. Solution-state conformational analysis of [Pt(phen)(L^n-κ*S*)$_2$] complexes using variable temperature ^{1}H and ^{195}Pt NMR spectroscopy

The [Pt(phen)(L^n-κ*S*)$_2$] complexes synthesised constitute a very symmetric system possessing a C_2 axis that divides the complexes into two with an acylthioureato ligand on each side (*Figure 1*). These complexes have at least 14 rotatable bonds; however, rotations about these bonds are restricted mainly due to steric hinderance leaving only a few bond rotation movements that give rise to the observed solid-state conformations.

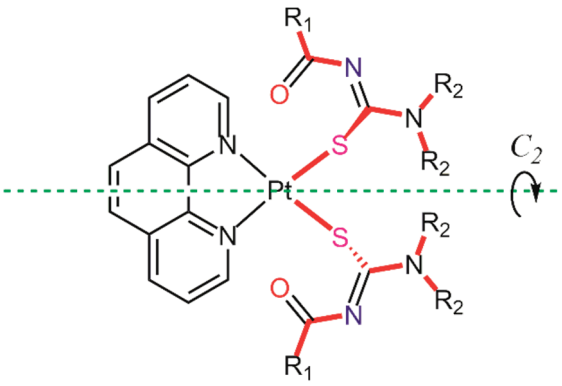


*Figure 1: General structure of [Pt(phen)(L^n-κ*S*)$_2$] complexes illustrating molecular symmetry and the origins of conformational isomerism (red bonds = rotatable bonds*

Four complexes ([Pt(phen)(L^1-κ*S*)$_2$], [Pt(phen)(L^3-κ*S*)$_2$] and [Pt(phen)(L^7-κ*S*)$_2$] were selected in order to study their solution conformational behaviour using variable temperature ^{1}H and ^{195}Pt NMR as they showed significant variations in their solid-state conformations. This study was triggered by the observation of two different solid-state conformations that [Pt(phen)(L^1-κ*S*)$_2$] exhibited when crystallised from two different solvents, methanol (a polar protic solvent) and tetrahydrofuran (a moderately polar aprotic solvent).[30]

The complexes were dissolved in deuterated methanol, and subsequently, ^{1}H and ^{195}Pt NMR experiments were performed varying the temperature from 55 °C to -70 °C with the first set of experiments being done using [Pt(phen)(L^1-κ*S*)$_2$].

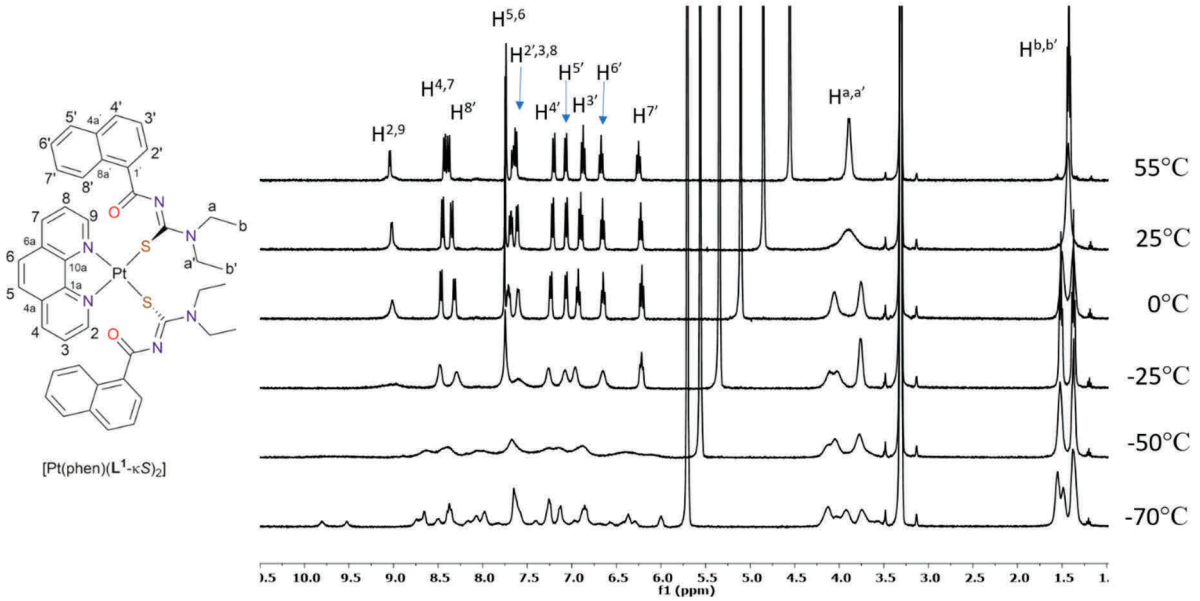


*Figure 2: Stacked variable temperature ^{1}H-NMR spectra of [Pt(phen)(L^1-κ*S*)$_2$] measured from 55 °C to -70 °C in methanol-d.*[30]

The ^{1}H NMR data (*Figure 2*) reveals a separation of overlapping signals, H^{4+7} and $H^{8'}$ as well as H^{3+8} and $H^{2'}$ as the temperature decreases with slight signal broadening at -25 °C. The resonances turned into overly broad and unresolved at -50 °C and then sharpen at -70 °C. As the temperature decreases new signals appear first, *via* decoalescence of the methyl- and methylene signals starting from 0 °C in the regions 1.0-1.8 ppm and 3.5-4.3 ppm due to restriction to rotation about the thioamidic (S)C-N$(C_2H_3)_2$ bond. This leads to these proton environments being non-equivalent, suggesting this bond rotation has the highest energy barrier. Tautomerism in the thio-amidic moiety, however, does not affect the overall symmetry of the complex as it affects both ligands. The overly broadening of the signals at -50 °C hints at the onset of the loss of C_2 symmetry in the molecule and arguably the advent of reversible conformational isomerism in the solution since the spectra recorded before and after the temperature change are identical. The loss in the C_2 symmetry may well be as a consequence a second fluxional processes; resulting from restriction to rotation about the amidic (O)C-N bond. Significantly downfield shifted ^{1}H resonances at 9.68 and 9.43 ppm could be due to the presence of a different conformer in solution in which substantial intramolecular π-π stacking interactions are absent. On the other hand, the new ^{1}H resonances emerging upfield in the aromatic region (around 6.0 ppm) intimates the existence of a conformer that exhibits significant π-π stacking interactions.

It was previously suggested that, ^{1}H NMR chemical shifts are extensively affected by the extent with which the moiety bearing the protons is involved in π-π stacking interactions during a study on $[Pt(phen)(L^{n}\text{-}O,S)]^{+}$ complexes. Shielding in those ^{1}H resonances was attributed to the shielding induced by the ring currents in the aromatic moieties of ligands in the complexes.[31] To confirm the possible presence of the proposed conformers in solution, we performed variable temperature ^{195}Pt NMR experiments since the ^{195}Pt chemical shift is highly sensitive to changes in the environment around the metal centre.[32] Species that are involved in slow exchange in the ^{1}H NMR frequency domain, as is the case for the complexes under investigation, could also be detected using ^{195}Pt NMR spectroscopy as the ^{195}Pt frequency is significantly lower (86.02 MHz) than ^{1}H (400.13 MHz).[33] Long data acquisition times were required (about 18 hours per spectrum) to overcome the broadening of ^{195}Pt resonances; typically observed for square planar complexes as a result of CSA relaxation. ^{195}Pt NMR data were collected at 55, 25, 0 and -50 °C (*Figure 3*).

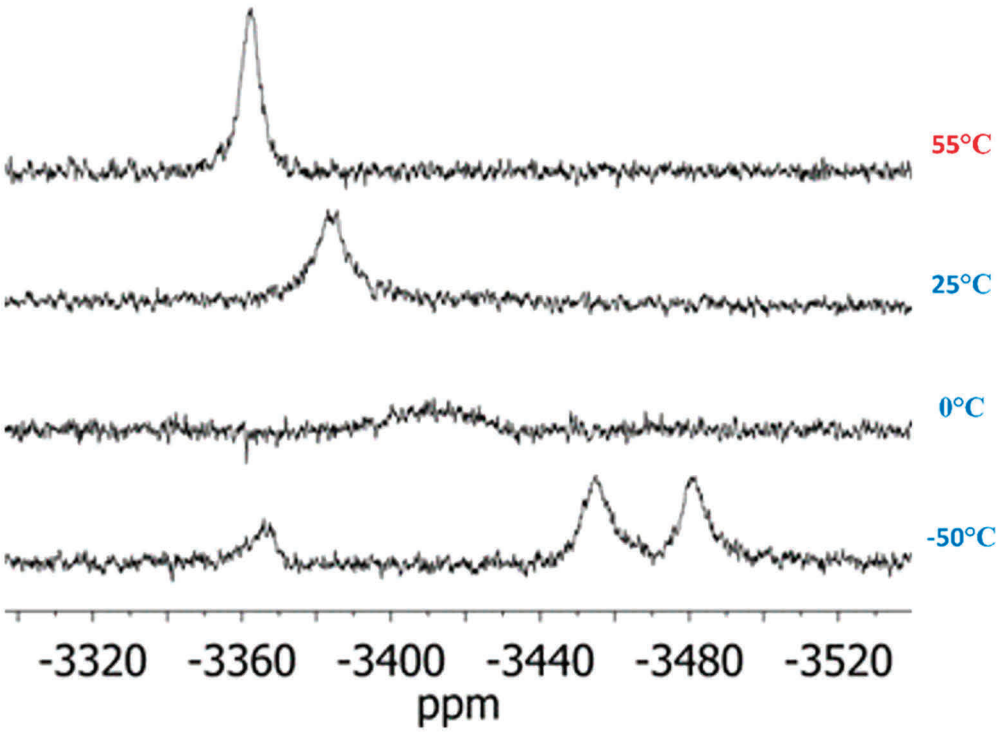


*Figure 3: Stacked variable temperature ^{195}Pt-NMR spectra of [Pt(phen)(L^1-κ*S*)$_2$] measured over the temperature range 55 °C to -50 °C, in methanol-d.*[30]

The ^{195}Pt NMR spectra obtained for variable temperature experiments, exhibit a single peak when recorded at 55°C and 25 °C. A very broad unresolved signal is observed at 0 °C while three well-resolved signals are observed at -50 °C (3376, 3461, 3485 ppm) with ratios 1 : 2.7 : 2.4 respectively and peak widths ($\nu_{1/2}$) = 634–637 Hz as determined from peak fitting analysis.[30] These observations allude to at least three platinum species in solution, with two out of the three appreciably shifted from the broad single peak seen at ambient temperature. The most shielded species could possibly be the "sandwich" structure (where the 1,10-phenanthroline rings are sandwiched by two naphthyl rings) (*Figure 4(ii)*), as reflected in the [Pt(phen)(L^1-κ*S*)$_2$] form II methanol solvate in the solid-state. In this case the intramolecular π-stacking of the naphthoyl moieties detected in this structure would have a substantial shielding effect on the platinum metal centre. The second most shielded species may well be the "half sandwich" structure (*Figure 4(i)*) as a result of only one naphthoyl moiety effectively shielding the platinum.

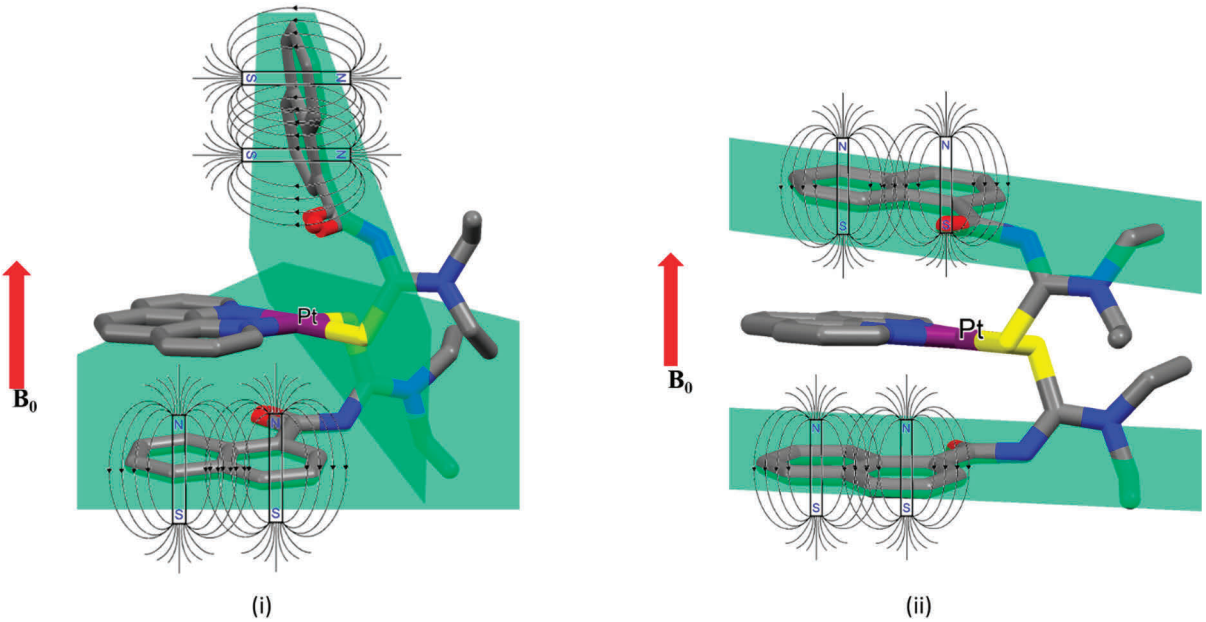


Figure 4: Illustration of ring currents in the naphthyl rings of acylthioureato ligands that induces a magnetic field opposing the applied magnetic field $\boldsymbol{B_0}$ *at the platinum centre. ((i) [Pt(phen)(L*^{1}*-κS)*$_2$*] form II and (ii) [Pt(phen)(L*^{1}*-κS)*$_2$*] form I.)*

The species that is present at 55 °C persists at -50 °C at only 16% of the total integration and could possibly be due to a completely open conformation similar to that in the [Pt(phen(L^3-κ*S*)$_2$] crystal structure (*Chapter 2, Figure 14*) with naphthoyl moieties that would not effectively shield the platinum metal centre. To ascertain the role of the aromatic rings in shielding the platinum metal centre, the same VT-NMR experiments were performed with a complex that has acylthiourea ligands that bear a "simple" aromatic ring, [Pt(phen)(L^3-κ*S*)$_2$] and a complex that has acylthiourea ligands that bear no aromatic rings, [Pt(phen)(L^7-κ*S*)$_2$].

The variable temperature ^{1}H NMR spectra for [Pt(phen)(L^3-κ*S*)$_2$] were similar to those of [Pt(phen)(L^1-κ*S*)$_2$], with small variations observed in their ^{195}Pt-NMR spectra. At -50°C, the ^{195}Pt-NMR spectrum showed three signals which thus meant three different platinum species in solution which could be correlated with the assignments made earlier in the case of [Pt(phen)(L^1-κ*S*)$_2$]. The notable variation was that the most deshielded signal appeared less shifted relative to the other two signals (*ca*. 62 ppm). This could possibly be attributed to the lower extent of shielding of the "simple" aromatic rings from the benzoyl moieties in [Pt(phen)(L^3-κ*S*)$_2$] compared to that of extended aromatic rings from the naphthoyl moieties in [Pt(phen)(L^1-κ*S*)$_2$] (*Figure 6*).

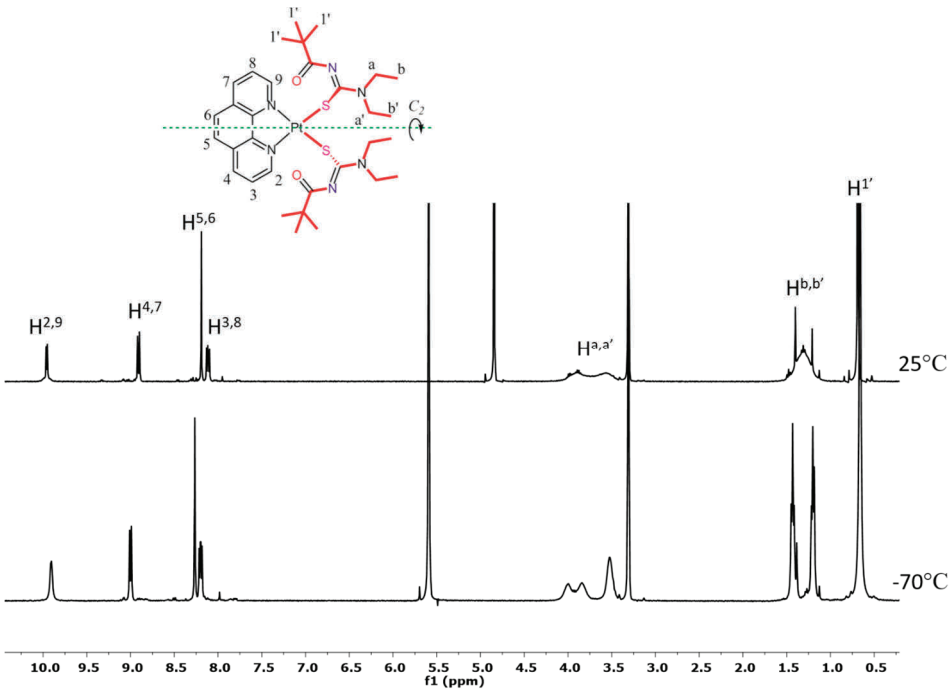


Figure 5: Stacked variable temperature ^{1}H-NMR spectra of [Pt(phen)(L^{7}-κS)$_2$] measured at 25 °C and -70 °C in methanol-d.

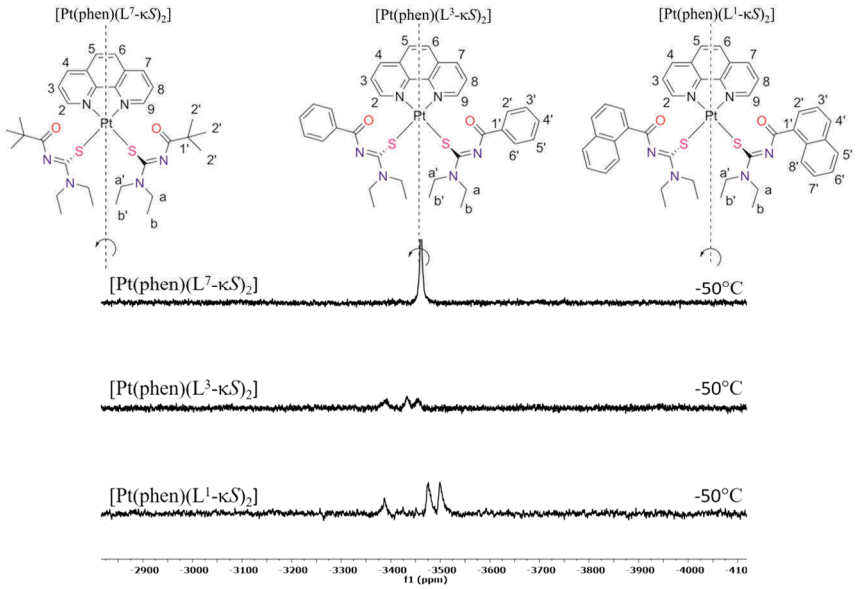


Figure 6: Stacked variable temperature ^{195}Pt-NMR spectra of [Pt(phen)(L^{1}-κS)$_2$], [Pt(phen)(L^{3}-κS)$_2$] and [Pt(phen)(L^{7}-κS)$_2$] measured at -50 °C in methanol-d.

On the other hand a VT-NMR study on [Pt(phen)(L^{7}-κS)$_2$] showed an interesting result; the first fluxional process was observed as in the [Pt(phen)(L^{1}-κS)$_2$] and [Pt(phen)(L^{3}-κS)$_2$] cases where there was restriction of bond rotation about the thioamidic (S)C-N(C$_2$H$_3$)$_2$ resulting in the non-equivalent proton environments in the ^{1}H-NMR spectra, however, no other changes were observed and in

particular, there was no loss of symmetry in the complex when varying the temperature from 25 °C to -70 °C (*Figure 5*). The ^{195}Pt-NMR spectra only showed the presence of one species in solution as only one signal was observed at -50 °C (*Figure 6*) suggesting that there is no detectable conformational isomerism due to the lack of aromatic rings in the acylthiourea ligands of the [Pt(phen)(L^7-κ*S*)$_2$] complex that can stabilise the other conformations through intramolecular π-π stacking interactions.

Above all, π-π interactions between the aromatic moieties of the complexes seem to stabilise conformations observed at -50 °C, that arises through rotations of (formally) single bonds which exhibit double bond character due to conjugation effects. However, at ambient temperature, there seems to be no persistence of the intramolecular π-π stacking interactions observed in solid-state. These assignments of the peaks in the ^{195}Pt NMR spectra are not final at the moment, as we are currently investigating this in a separate study where we are trying to use theoretical calculations in the DFT configuration as a tool in correlating the ^{195}Pt NMR signals observed with possible conformation.

3.2.2. Investigation of the reactivity of O, N, N' and S donor sites in disubstituted acylthioureato ligands towards platinum(II) using conceptual DFT

The construct of this study was such that a series of disubstituted acylthioureato ligands had their geometries optimised and studied using conceptual DFT. These ligands were chosen for their different electronic properties induced by different substituent groups on the acyl end of the ligands while keeping the rest of the ligand the same. Acylthioureato ligands have several sites that can function as potential donors such as N, N', S and O atoms. According to frontier molecular orbitals calculated the most reactive atomic site is sulfur across the whole range of six ligands studied as indicated by the largest highest occupied molecular orbital (HOMO) lobe being on the sulfur atom (*Figure 7*).

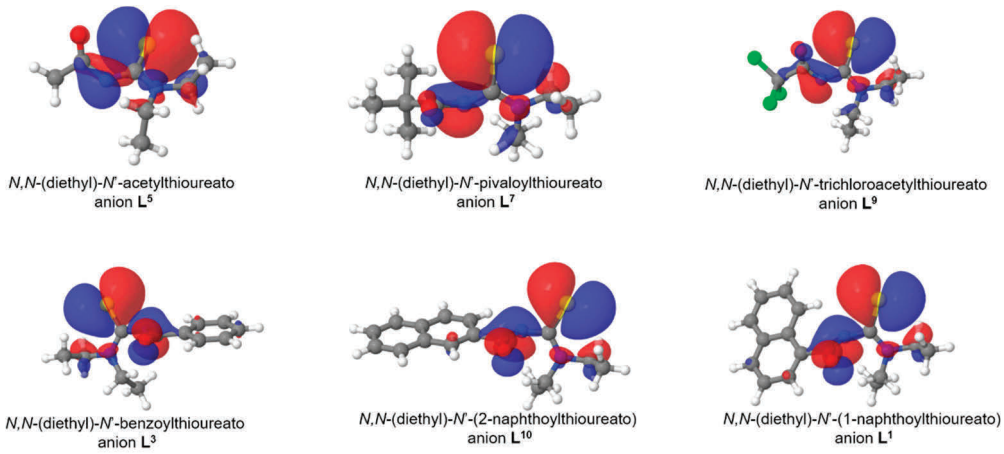


Figure 7: Highest occupied molecular orbitals (HOMO) diagrams for the various acylthioureato ligands studied. The molecular structures of the acylthioureato ligands were optimised at B3LYP level using ma-def2-TZVPP basis set in the gas phase courtesy of ORCA quantum chemistry software.[34]

Through the calculation of the Fukui function (f_k^-) (*Table 1*)) and the local nucleophilicity ($\mathcal{N}_k$) (*Table 2*), it is evident that there is a tenfold higher nucleophilic character on the sulfur atom than any other donor atoms in the ligand indicating sulfur as the most favourable donor site for possible coordination with platinum(II) ions regardless of different acyl substituent groups. This result agrees with experimental observations that platinum(II) selectively coordinated with acylthioureato ligands through sulfur as illustrated in synthetic method B.

Table 1: Ionization Potential (IP), global nucleophilicity ($\mathcal{N}$), and condensed Fukui function (f_k^-) for acylthioureato ligands.

			f_k^-			
Ligand	IP ≈ $-E_{homo}$(eV)	$\mathcal{N}$(eV)	S	O	N	N’
HL^9	1.6653	7.4531	0.48446	0.05291	0.02478	0.05816
HL^1	1.5594	7.5594	0.37647	0.08667	0.02107	0.07748
HL^{10}	1.5158	7.6026	0.39449	0.08948	0.02108	0.07426
HL^3	1.3943	7.7241	0.40328	0.09234	0.02161	0.07464
HL^7	1.1646	7.9538	0.48135	0.05834	0.02065	0.07385
HL^5	1.1072	8.0464	0.50053	0.06079	0.02152	0.07172

Table 2: Local nucleophilicity indices ($\mathcal{N}_k$) for acylthioureato ligands.

		$\mathcal{N}_k$			
Ligand	$\mathcal{N}$(eV)	S	O	N	N’
HL^9	7.4531	3.6107	0.3943	0.1847	0.4335
HL^1	7.5594	2.8459	0.6552	0.1593	0.5857
HL^{10}	7.6026	2.9991	0.6803	0.1603	0.5646
HL^3	7.7241	3.1150	0.7132	0.1669	0.5765
HL^7	7.9538	3.8286	0.4640	0.1642	0.5874
HL^5	8.0464	4.0275	0.4891	0.1732	0.5771

Conceptual DFT has successfully indicated the most reactive atomic site in the acylthiourea ligands towards platinum(II) ions; however, it did not account for the variations in products that were observed using synthetic method (A). Therefore, the electron distribution in the ligands alone is seemingly not able to account for the change in ligand behaviour during the synthesis of [Pt(phen)(L^n-κ*S*)$_2$] using the one-pot synthesis (method A), and the whole mechanism should be considered.

3.2.3. Mechanistic insights into the monodentate coordination of disubstituted acylthioureato ligands in [Pt(phen)(L^n-κ*S*)$_2$] complexes

Since the conceptual DFT study seemingly did not manage to explain the variations in ligand behaviour during the synthesis of [Pt(phen)(L-κ*S*)$_2$] using method (A), an experimental mechanistic probe was undertaken where a few individual experiments were performed that produced substantial accounts of the results from method A and some insights into a possible mechanism. Firstly, the synthesis was probed as to in which media the reaction took place (in solution or on the solid surface) since the reaction mixture was heterogeneous (a suspension). A suspension of [$PtCl_2$(phen)] in methanol being added to a methanol solution of the ligand and sodium acetate at different rates (added at once, added over 15 minutes and added over 30 minutes) and heating the mixture to reflux, no significant change in the yield or rate of reaction was observed. This finding suggested that the substitution reaction could not be taking place on the surface of the insoluble [$PtCl_2$(phen)] precursor but in solution, as it will become apparent later.

(a) Solvolysis of the [$PtCl_2$(phen)] precursor

Substitution reactions in square planar complexes are usually dominated by the associative mechanism.[35] Among these reactions are solvolysis, aquation and anation reactions. Anation reactions in solution are thought to first undergo the solvolysis/aquation step before proceeding with the actual ligand substitution.[36] This first step has been implicated in the mechanism of action of cisplatin; the aquation of cisplatin into its active species *cis*-[$Pt(H_2O)_2(NH_3)_2]^{2+}$.[37] The solvolysis/aquation step may also be viewed as an essential step responsible for the improved "dissolution" of some insoluble metal complexes if it results in ionic species that can be solvated. In the framework of this experiment, we investigated the solvolysis of [$PtCl_2$(phen)] to gain insight into the form of the reacting metal species in solution.

[$PtCl_2$(phen)] was added to two flasks, containing 20 ml of 99% methanol and 90% methanol/water solvents respectively, and then heated with stirring for 10 minutes. The undissolved precursor was filtered off, and the remaining very pale-yellow solutions were analysed for the presence of chloride ions in solution while parts of the solutions were studied using UV-vis spectrophotometry, ^{1}H-NMR spectroscopy, and high-resolution mass spectrometry.

Both solutions tested positive for chloride ions in solution as indicated by the solutions turning cloudy upon addition of silver nitrate. Controls (solvents alone) remained clear on addition of silver nitrate.

These results suggest that [$PtCl_2$(phen)] "dissolves" by forming a solvento complex via solvolysis/aquation with solvent molecules substituting either one or both chloro ligands resulting in a charged species that are then solvated. The mechanism responsible for this "dissolution" may be attributed to aquation, because methanol is a poor coordinating solvent for soft metals like platinum as indicated by its low donor strength compared to water.[38] An increase in the amount of water in the methanol solvent was shown to result in increased solubility of [$PtCl_2$(phen)] (*Figure 8*).

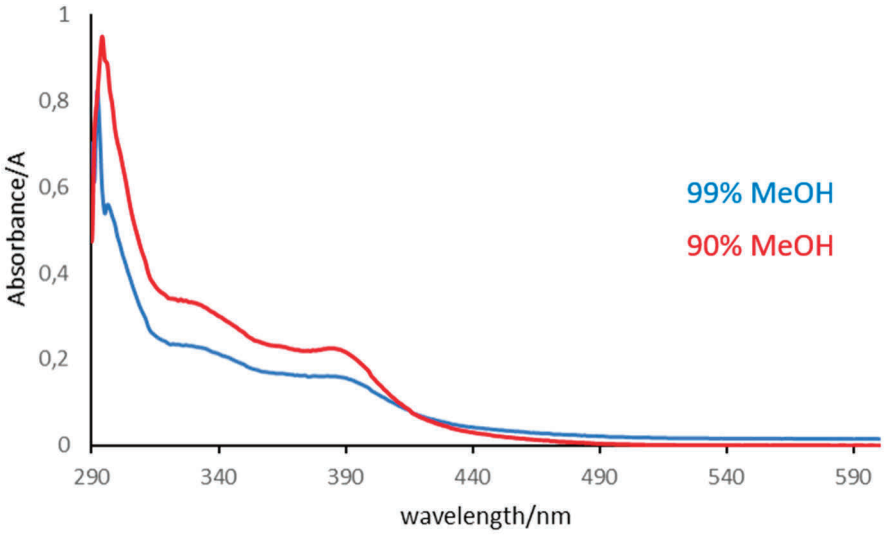


Figure 8: *Solubility test of [$PtCl_2$(phen)] in 99% (blue) and 90% (red) methanol studied using UV-vis spectrophotometry in the region 290-600 nm.*

The ^{1}H-NMR spectrum of [$PtCl_2$(phen)] "dissolved" in 99.9% MeOH/water solution was recorded in methanol-*d* for 78 hours due to the extremely low solubility of [$PtCl_2$(phen)]. The ^{1}H-NMR spectrum showed at least four clear signals that could be attributed to the symmetric $[Pt(phen)(solvent)_2]^{2+}$ complex and the other signals possibly to the unsymmetric solvolysis product $[PtCl(phen)(solvent)]^+$ (*Figure 9*).

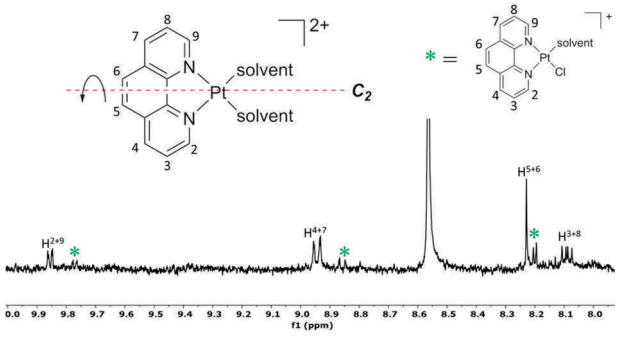


*Figure 9: ^{1}H-NMR spectrum for the solvolysis of [$PtCl_2$(phen)] in 99.9% methanol/water recorded in methanol-d for 78 hours. * = extra protons possibly due to the unsymmetrical $[PtCl_2(phen)(solvent)]^+$.*

Mass spectrum for the solution of the precursor (*Appendix Figure A2-20*) revealed the presence of two major species at 439.01 and 452.03 *m/z* possibly corresponding to [PtCl(phen) + acetonitrile]$^{+}$ and [(phen)Pt(μ-Cl)$_2$Pt(phen)]$^{2+}$ ions. From all this evidence we could summarily say [PtCl$_2$(phen)] undergoes solvolysis in wet methanol to give [PtCl(phen)(solvent)]$^{+}$ which dimerises to the [(phen)Pt(μ-Cl)$_2$Pt(phen)]$^{2+}$ complex. The symmetric species observed in the ^{1}H NMR spectrum for the solvolysis of the [PtCl$_2$(phen)] precursor could as well be this dimeric species instead of the [Pt(phen)(solvent)$_2$]$^{2+}$ complex since it is also symmetrical hence further investigations are required.

(b) Reactions of neutral disubstituted acylthiourea ligands with [PtCl$_2$(phen)] in methanol with varying amounts of water

An attempt was made to determine whether the neutral ligands could coordinate to the precursor without deprotonation and evaluating the influence of the water as a base or solvent or both. Coordination of neutral disubstituted acylthiourea ligands with transition metals either monodentate or bidentate is seldom encountered in literature. Most research has focused on the monodentate coordination of the neutral disubstituted acylthiourea ligands,[39,40] with only two reporting on bidentate coordination of the same ligands.[41,42] The scarcity of this coordination mode may indicate that it is probably difficult to achieve. However, our research intends to use this reaction to explain and rationalize reaction results we obtained from the method (A) and possibly answer the question, "does deprotonation take place before or after coordination in our reaction?".

The reaction of [PtCl$_2$(phen)] with a slight excess of *N*,*N*-di(ethyl)-*N*'-(1-naphthoylthiourea) was performed in wet methanol solvents (99.9% and 85%) and refluxed until a clear yellow solution resulted. The reaction mixtures were taken up in dichloromethane and filtered to remove insoluble salts. Notably, the reactions took about 2.5 hrs (for the reaction in 99.9% methanol) and 40 minutes (for the reaction in 85% methanol) to complete. From ^{1}H-NMR spectral analysis (*Figure 10*), we can see the presence of a very deshielded signal at 10.78 ppm integrating for two protons and other aromatic signals that integrate for twenty protons. The most deshielded signal could tentatively be assigned to the amidic N-H proton, and from integration and the symmetry in the phenanthroline proton signals, there is evidence of the presence of the di-cationic [Pt(phen)(HL^{1}-κ*S*)$_2$]$^{2+}$ complex in both reactions. The extra peaks, mainly showing in the ^{1}H-NMR spectrum for the reaction in 85% methanol solvent (*Figure 10*), could be due to the mono-cationic [Pt(phen)(L^{1}-κ*O,S*)]$^{+}$ complex formed after deprotonation of the *N*,*N*-di(ethyl)-*N*'-(1-naphthoylthiourea) ligand with water.

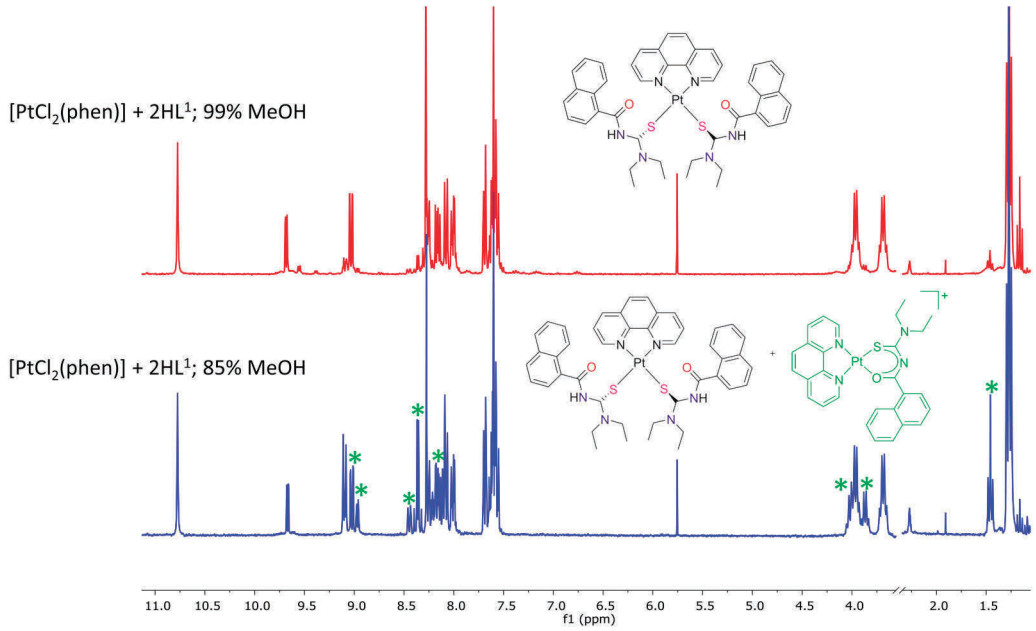
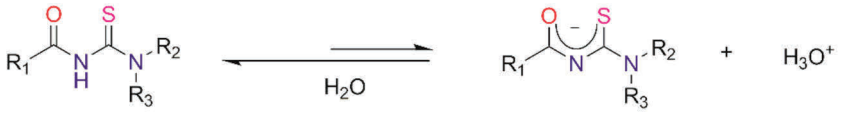


Figure 10: *Stacked* ^{1}*H-NMR spectra of the products from the reactions between the precursor [PtCl*$_2$*(phen)] and N,N-di(ethyl)-N'-(1-naphthoylthiourea) in wet methanol (99.9% and 85%) recorded in DMSO-d.*

Coordination of the protonated ligand took place slowly depending on how wet the methanol was, with the reaction in 85% MeOH faster than in 99.9% MeOH. Coordination of the anionic ligand starts to be seen when the water content in the solvent increased as indicated by the formation of an additional $[Pt(phen)(L^1\text{-}\kappa O,S)]^+$ complex from the reaction in 85% MeOH. The formation of the $[Pt(phen)(L^1\text{-}\kappa O,S)]^+$ complex maybe because enough water was now available to act as a ligand for the solvolysis of the precursor as well as a base for the deprotonation of the weakly acidic ligand *via* an aqueous acid-base equilibrium. According to the reported pK_as,[43,44] the disubstituted acylthioureato ligands only dissociate very slightly in aqueous solution (*Scheme 2*).



Scheme 2: *Deprotonation of N,N-di(alkyl)-N'-acylthiourea ligands by water in wet methanol.*

These observations suggest the importance of at least water or possibly other good coordinating solvents for the solvolysis/aquation step that precedes the substitution (anation) step so that the coordination of the neutral ligand or anionic ligand can occur. Under the conditions of synthetic method A, 99.9% MeOH was used as solvent and from the species distribution study using ^{1}H-NMR alluded to in *Chapter 2*, there is no evidence of the formation of the cationic species $[Pt(phen)(HL^1\text{-}\kappa S)_2]^{2+}$ in the presence of

a stronger base (sodium acetate). Hence, we can speculate that deprotonation takes place before coordination at least in the presence of sodium acetate.

(c) Interconversion between [Pt(phen)(L^n-κ*S*)$_2$] and [Pt(phen)(L^n-κ*O*,*S*)]$^+$

Interconversion reactions between co-products are not uncommon as highlighted in the reactions reported by Morris *et al*.[45,46] They may mechanistically offer additional pathways for formation or decomposition of the desired product. In this study, the first hints of interconversion between [Pt(phen)(L-κ*S*)$_2$] (the product) and [Pt(phen)(L-κ*O*,*S*)]$^+$ (the by-product), were seen from the continual drop in pH well after the precursor had been depleted (particularly in the synthesis with *N,N*-di(ethyl)-*N*'-pivaloylthiourea) as evidenced from the in-situ reaction progress analysis (*Figure 11*) monitoring pH change with time.

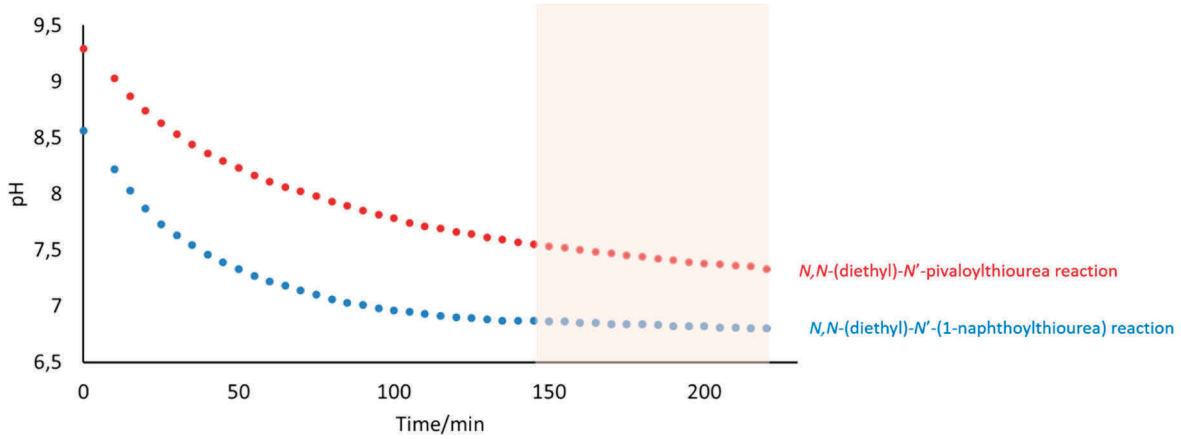


Figure 11: *Variation of pH with time during the synthesis of [Pt(phen)(L^n-κ*S*)$_2$] from N,N-di(ethyl)-N'-pivaloylthiourea (red) and N,N-di(ethyl)-N'-(1-naphthoylthiourea) (blue) using the one-pot synthesis method A in methanol. Shaded region indicates when all the precursor had been consumed.*

Two experiments were set up to investigate the interconversion and can be summarised as: (i) Conversion of [Pt(phen)(L^1-κ*O*,*S*)]$^+$ to [Pt(phen)(L^1-κ*S*)(L^2-κ*S*)] (*Figure 12*) and (ii) Conversion of [Pt(phen)(L^3-κ*S*)$_2$] back to [Pt(phen)(L^3-κ*O*,*S*)]$^+$ or [PtCl$_2$(phen)]. (*Figure 13*). Different ligands were used because they introduce structural changes to the final product that makes it easier to trace using ^{1}H-NMR spectroscopy; Use of different ligands in the conversion of [Pt(phen)(L^1-κ*O*,*S*)]$^+$ to [Pt(phen)(L^1-κ*S*)(L^2-κ*S*)] introduces slight asymmetry in the phenanthroline proton signals and the characteristic shielded aromatic protons from the acylthioureato ligand in the final product making it easy to distinguish from just a mixture of [Pt(phen)(L^1-κ*O*,*S*)]$^+$ and [Pt(phen)(L^2-κ*S*)$_2$] complexes, however, in the conversion of [Pt(phen)(L^3-κ*S*)$_2$] back to [Pt(phen)(L^3-κ*O*,*S*)]$^+$ or [PtCl$_2$(phen)] there is need for the resultant ^{1}H-NMR spectrum to be less crowded for less complications in visualizing the changes.

(i) Conversion of [Pt(phen)(L^1-κO,S)]$^+$ to [Pt(phen)(L^1-κS)(L^2-κS)]

[Pt(phen)(L^1-κ*O*,*S*)]$^+$ was dissolved in methanol and then the ligand *N*,*N*-di(butyl)-*N*'-(1-naphthoylthiourea) (**HL^2**) and sodium acetate as base were added such that the complex [Pt(phen)(L^1-κ*O*,*S*)]$^+$ was in slight excess. The reaction mixture was heated under reflux until no ligand was present and analysed using ^{1}H-NMR spectroscopy in chloroform-*d*.

The NMR spectra clearly shows a conversion of [Pt(phen)(L^1-κ*O*,*S*)]$^+$ to an unsymmetrical [Pt(phen)(L^1-κ*S*)(L^2-κ*S*)] complex through the appearance of additional butyl protons as well as typically shielded naphthyl protons in the region 6.0 – 7.2 ppm (*Figure 12*). The conversion of [Pt(phen)(L^1-κ*O*, *S*)]$^+$ to [Pt(phen)(L^1-κ*S*)(L^2-κ*S*)] was achieved presumably through chelate ring-opening by heterolytic dissociation of the Pt – O bond.

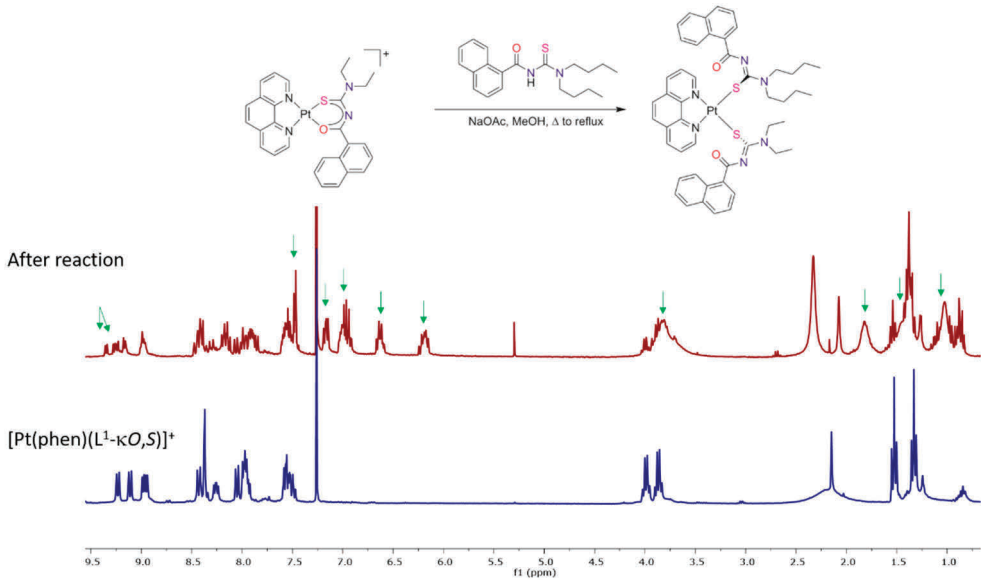
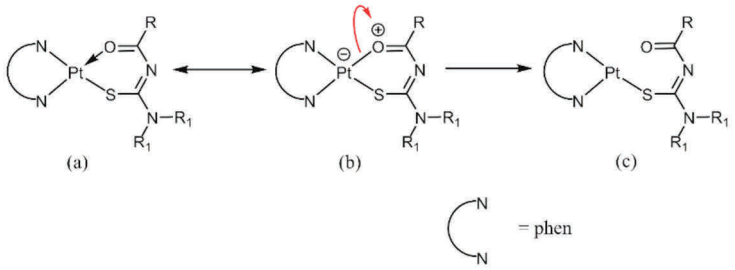


Figure 12: *Chelate ring opening through heterolytic dissociation of the Pt – O bond in the conversion of [Pt(phen)(L^1-κ*O*,*S*)]$^+$ to [Pt(phen)(L^1-κ*S*)(L^2-κ*S*)]. (green arrow = [Pt(phen)(L^1-κ*S*)(L^2-κ*S*)] proton signals).*

The six-membered chelate ring of the [Pt(phen)(L^n-κ*O*,*S*)]$^+$ complex can be represented by the following valence bond structure (*Scheme 3(b)*) where one bond is dative, and the other is simple covalent.[47]



Scheme 3: *Representations of chelate ring opening through heterolytic bond dissociation of the Pt – O bond in [Pt(phen)(L^n-κ*O*,*S*)]$^+$.*

The chelate opening reaction is possible in this complex through heterolytic bond dissociation of the Pt – O bond as it formally reduces charge separation in the molecule (*Scheme 3(b)*) and also as a result of a possibly weaker platinum - oxygen interaction (soft acid – hard base interaction).

(ii) Conversion of [Pt(phen)(L^3-κS)$_2$] back to [Pt(phen)(L^3-κO,S)]$^+$ and [PtCl$_2$(phen)]

The conversion of [Pt(phen)(L^3-κ*S*)$_2$] back to [Pt(phen)(L^3-κ*O*,*S*)]$^+$ and [PtCl$_2$(phen)] was studied by adding a drop of concentrated acid to solutions of [Pt(phen)(L^3-κ*S*)$_2$] in methanol-*d* which were then analysed using ^{1}H-NMR spectroscopy (*Figure 13*). The ^{1}H-NMR spectra show different dissociation products upon addition of acids with different strengths and conjugate bases.

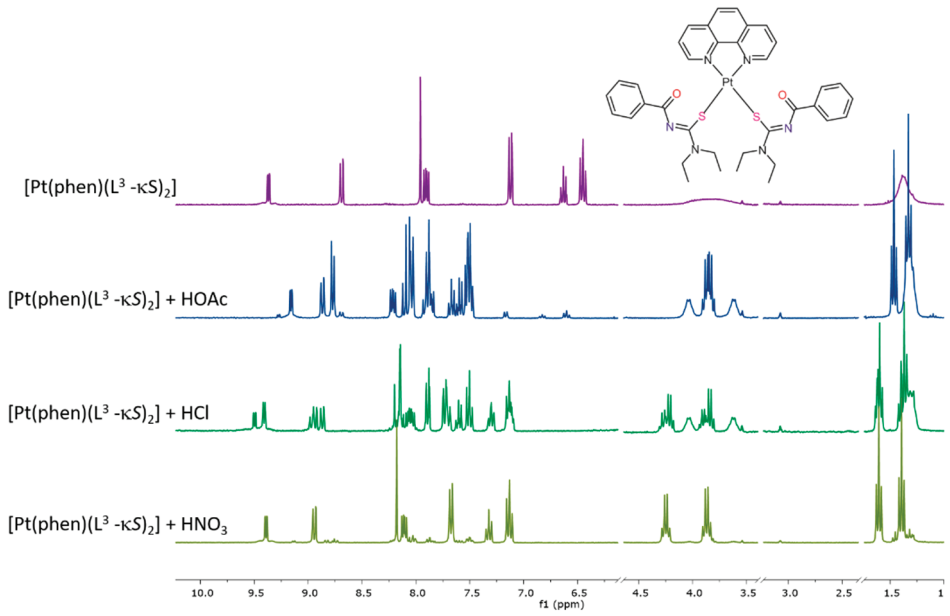


Figure 13: *Protolytic dissociations of [Pt(phen)(L^3-κ*S*)$_2$] complexes showing different end products with varying acids in the ^{1}H-NMR spectra recorded in methanol-d.*

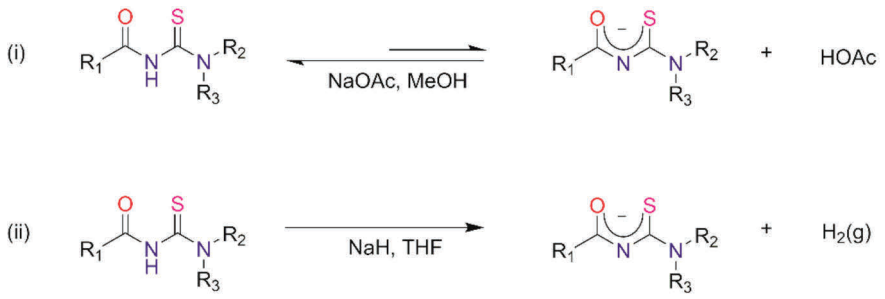
Addition of acetic acid (a weak acid with a poorly coordinating conjugate base) resulted in the dissociation of [Pt(phen)(L^3-κ*S*)$_2$] into the cationic complex [Pt(phen)(L^3-κ*O*,*S*)]$^+$ and free ligand *N*,*N*-di(ethyl)-*N*'-benzoylthiourea (**HL^3**). Stronger acids (concentrated hydrochloric acid and concentrated

nitric acid) gave various products as a result of the different coordinating properties of their conjugate bases, chloride (Cl^-) and nitrate (NO_3^-). Addition of hydrochloric acid presumably caused protonation of [Pt(phen)(L^3-κ*S*)$_2$] to [Pt(phen)(HL^3-κ*S*)$_2$]$^{2+}$ and a substitution of one acylthioureato ligands with a chloride in some of the protonated complex to give [PtCl(phen)(HL^3-κ*S*)]$^+$ while nitric acid only resulted in protonation of the complex [Pt(phen)(L^3-κ*S*)$_2$] to [Pt(phen)(HL^3-κ*S*)$_2$]$^{2+}$.

From these experiments, we can see that [Pt(phen)(L^n-κ*S*)$_2$] complexes can also be synthesised starting from [Pt(phen)(L^n-κ*O*,*S*)]$^+$, however, they are not acid-stable. These observations prompted us to search for synthetic methods in which the base does not produce a conjugate acid that might interfere with product formation such as sodium hydride, whose conjugate acid ($H_{2(g)}$) escapes the reaction thereby not interfering with product formation.

3.2.4. Stepwise synthesis of the [Pt(phen)(L^n-κ*S*)$_2$] complexes using sodium hydride as base

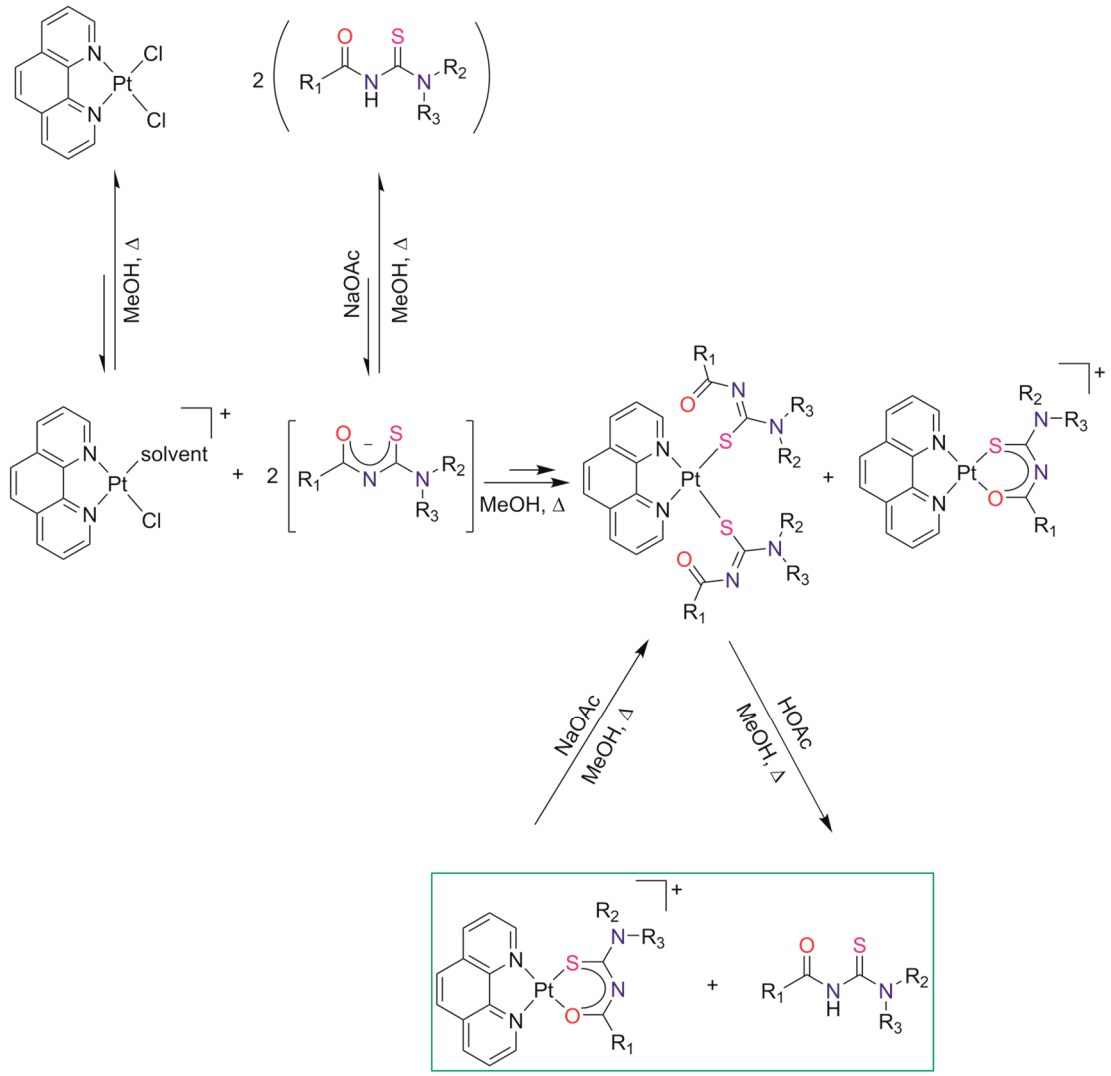
To obtain better yields from method A with ligands such as *N,N*-di(ethyl)-*N*'-pivaloylthiourea (**HL^6**), several bases were used but did not produce the desired outcome (i.e. solely monodentate coordination). As shown earlier the deprotonation step is vital in the coordination of disubstituted acylthiourea ligands starting from the [$PtCl_2$(phen)] precursor and thus a study on the deprotonation of the ligands using different bases was undertaken to find the optimal base for our desired coordination. Disubstituted acylthiourea ligands are very weak acids that dissociate slightly in solution[43], and their acid-base chemistry is best described with the following equilibria (*Scheme 4 (i) and (ii)*) when sodium acetate and sodium hydride are used as a base.



Scheme 4: *Comparisons of deprotonation of N,N-di(alkyl/aryl)-N'-acylthiourea ligands when sodium acetate and sodium hydride are used as bases.*

An interesting and positive reproducible result only came when the base was changed to sodium hydride and this was achieved by performing the experiment in a stepwise manner: deprotonation of the ligand using sodium hydride in anhydrous THF (at room temperature) followed by the addition of the metal precursor to the resulting solution with stirring under reflux. Regardless of the substituent groups on the acylthioureato ligands, this method always gave the desired product [Pt(phen)(L^n-κ*S*)$_2$] indicating the deprotonation step is critically important. The deprotonation reaction (*Scheme 4 (ii)*) is shifted far

to the right (products) by the evolution of the formed hydrogen gas compared to the equilibrium that favours the protonated acylthiourea ligand species in (*Scheme 4 (i*). The deprotonation using sodium hydride thus presents a sufficient concentration of the coordinating anionic species in the solution for encounters with the metal precursor to yield the desired product [Pt(phen)(L^n-κ*S*)$_2$]. To summarise the findings of this experimental study, we propose the following mechanism (*Scheme 5*) to be taking place when we synthesise [Pt(phen)(L^n-κ*S*)$_2$] complexes via method A.



*Scheme 5: Proposed mechanism for the synthesis of [Pt(phen)(L^n-κ*S*)$_2$] complexes using synthetic method A showing steps contributing to the formation and decomposition of [Pt(phen)(L^n-κ*S*)$_2$].*

3.2.5. Extrapolation of the monodentate coordination into complexes with different co-ligands or metal centres

Co-ligands or central metals may also dictate coordination modes.[29,46] In these cases, steric and electronic factors may play important roles in determining the relative stability of the resultant complexes. With this regard our study was extended to find out if the monodentate coordination of *N*,*N*-

di(alkyl/aryl)-*N*'-acylthioureato ligands is also possible with platinum(II) complexes bearing different co-ligands (in this case we tried bipyridine (bipy) and triphenylphosphine (PPh_3) as co-ligands) as well as using different metal centres (palladium (II) and cobalt (II) as metal centres).

Reactions of *N*,*N*-di(ethyl)-*N*'-(2-naphthoylthiourea) (**HL^{10}**) and *N*,*N*-di(ethyl)-*N*'-(1-naphthoylthiourea) (**HL^{1}**) with the metal precursors [Pt(bipy)Cl_2] and *cis*-[$PtCl_2(PPh_3)_2$] respectively were attempted using synthetic method B. Two molar equivalence of the ligands were deprotonated using equimolar amounts of sodium hydride in anhydrous THF at room temperature after which the one molar equivalents of respective the precursors were added and refluxed (*c.a* 1 hrs). The products were worked up and analysed using ^{1}H-NMR spectroscopy and single-crystal X-ray diffraction.

The reaction of *N*,*N*-di(alkyl/aryl)-*N*'-acylthioureato ligands with [Pt(bipy)Cl_2] was difficult as, in most cases, it resulted in the substitution of the bipyridine ligand to give a *bis*-[Pt(L^n-κ*O*,*S*)$_2$] complex as the major product indicating that the acylthioureato ligand is a better ligand than bipyridine under these conditions. However, we managed to get a reasonable yield of the [Pt(bipy)(L^{10}-κS)$_2$] complex with *N*,*N*-di(ethyl)-*N*'-(2-naphthoylthiourea) from which single crystals were grown and analysed (*Figure 14(a)*). The reaction with *cis*-[$PtCl_2(PPh_3)_2$] produced an interesting mixed coordination mode complex in moderate yields, with one *N*,*N*-di(ethyl)-*N*'-(1-naphthoylthiourea) ligand coordinated in a monodentate fashion through sulfur while the other *N*,*N*-di(ethyl)-*N*'-(1-naphthoylthiourea) ligand was coordinated in a bidentate mode through oxygen and sulfur to yield [Pt(PPh_3)(L^1-κ*O*,*S*)(L^1-κ*S*)] (*Figure 14(b)*).

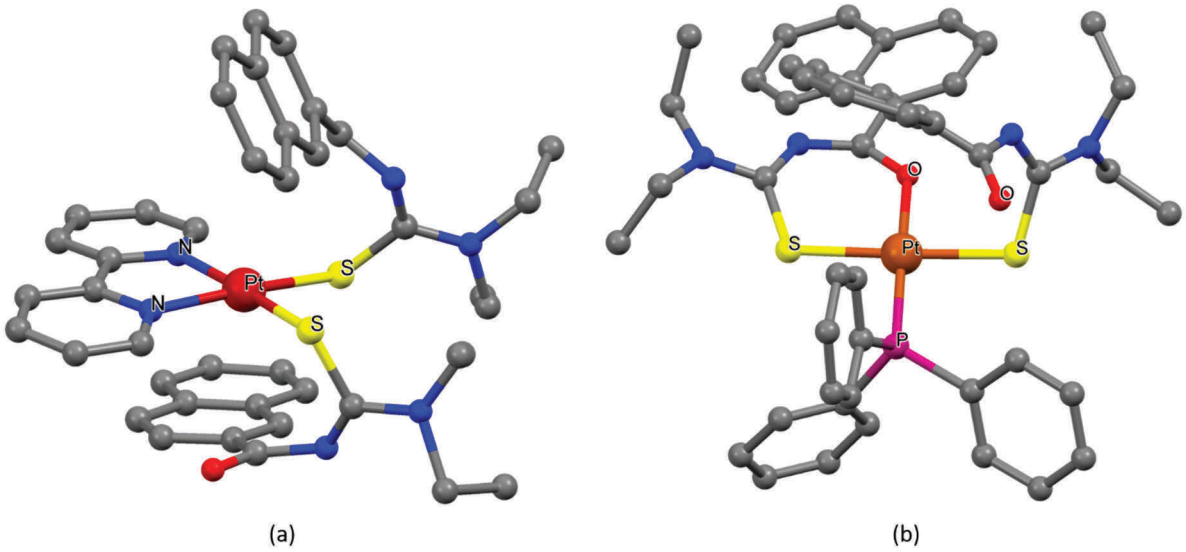


Figure 14: *Crystal structure of; (a) [Pt(bipy)(L^{10}-κS)$_2$] and (b) [Pt(PPh_3)(L^1-κO,S)(L^1-κS)]. (hydrogens omitted for clarity*)

^{1}H-NMR spectrum of the bulk product from the reaction of *N*,*N*-di(ethyl)-*N*'-(1-naphthoylthiourea) with *cis*-[$PtCl_2(PPh_3)_2$] via method B (*Figure 15*), before crystallization, suggest that one triphenylphosphine ligand came off to form [$Pt(THF)(PPh_3)(L^1$-κ*S*$)_2$] as an intermediate followed by arguably a subsequent substitution of the THF with water during work-up which then further underwent chelate ring closure during crystallization to give the complex [$Pt(PPh_3)(L^1$-κ*O*,*S*$)(L^1$-κ*S*$)$].

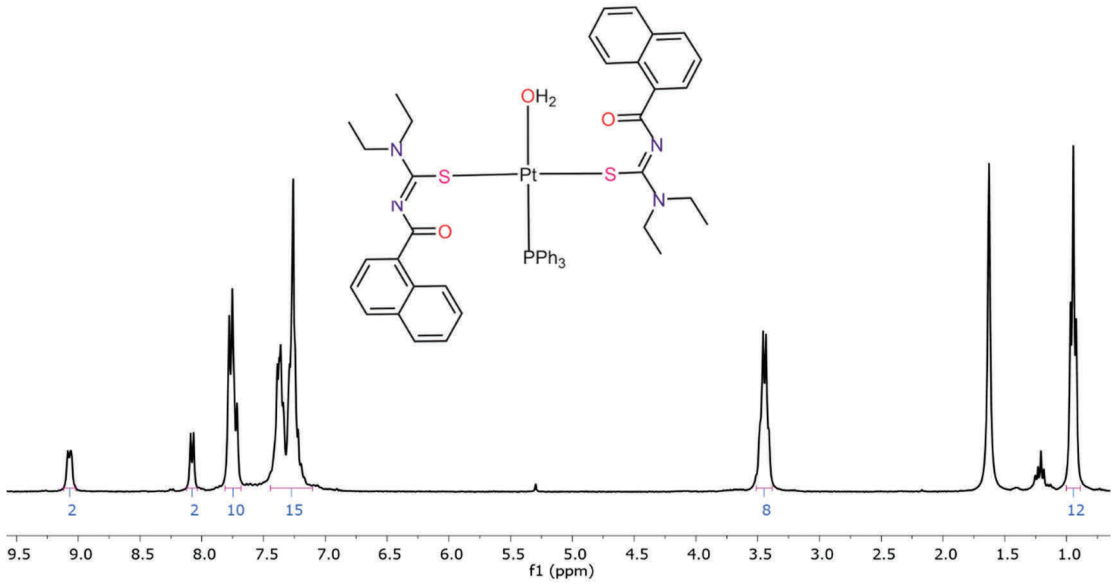


Figure 15: *^{1}H-NMR spectrum of [$Pt(H_2O)(PPh_3)(L^1$-κ*S*$)_2$] recorded at 25 °C in chloroform-d, showing only the presence of one triphenylphosphine ligand.*

Another exciting aspect of this reaction was that we started with a *cis*-[$PtCl_2(PPh_3)_2$] precursor; however, we ended up with the incoming ligands' sulfur donor atoms *trans* to each other. The observed result might be because of a temperature-dependent interconversion between the *cis* and *trans* isomers of the solvento complex species[48] before the substitution. This interconversion consequently influenced the final product as two *trans* directing ligands (PPh_3) labilised each other resulting in one being lost.

Attempts were made to coordinate the *N*,*N*-di(ethyl)-*N*'-(1-naphthoylthioureato) ligand to palladium(II) and cobalt(II) in a monodentate fashion starting from [$PdCl_2$(phen)] and [$CoCl_2$(phen)] respectively using the same synthetic method B with no success. Two molar equivalence of the *N*,*N*-di(ethyl)-*N*'-(1-naphthoylthiourea) ligand were deprotonated using sodium hydride in anhydrous THF at room temperature after which the one molar equivalence of the [$CoCl_2$(phen)] precursor was added and refluxed (*c.a* 1 hrs). The same procedure was repeated with [$PdCl_2$(phen)], however, at room temperature. The products were worked up and analysed using ^{1}H-NMR spectroscopy and single-crystal X-ray diffraction. The reaction with [$PdCl_2$(phen)] resulted in the elimination of phenanthroline

to give a *bis*-[Pd(L^1-κ*O*,*S*)$_2$] complex while the reaction with [$CoCl_2$(phen)] gave an octahedral *tris*-chelate (*Figure 16*).

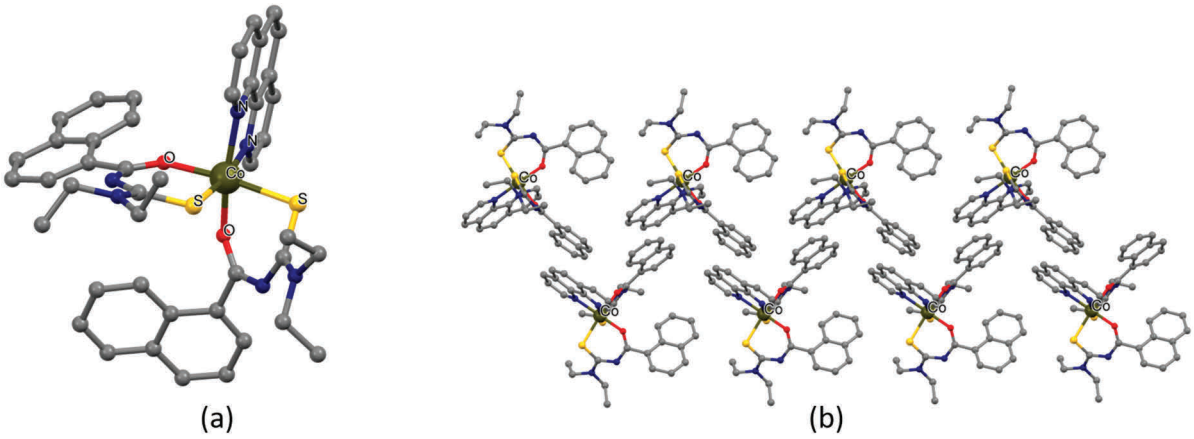


Figure 16: *(a) Crystal structure of [Co^{II}(phen)(L^1-κ*O*,*S*)$_2$] showing an octahedral geometry with N,N-di(ethyl)-N'-(1-naphthoylthioureato) ligands coordinated in a monodentate fashion, (b) 1D packing array of [Co^{II}(phen)(L^1-κ*O*,*S*)$_2$] illustrating intermolecular π-π interactions. The Hydrogens omitted for clarity.*

3.3. Conclusion

The one-pot synthesis of [Pt(phen)(L^n-κ*S*)$_2$] (method A) reported in *Chapter 2*, indicated that disubstituted acylthiourea ligands with an electron-withdrawing substituent (R_1 = -CCl_3) or aromatic acyl substituents favoured monodentate coordination while the acylthiourea ligands bearing non-aromatic acyl substituents (*e.g.* R_1 = -$C(CH_3)_3$) preferred chelate formation. We initially rationalised this result as being due to the stabilising effect of intramolecular π-π stacking interactions or the electronic influence of acyl substituents on disubstituted acylthioureato ligands or both.

Initially, we thought the preference of disubstituted acylthiourea ligands bearing aromatic acyl substituents to coordinate preferably in a monodentate fashion using this synthetic method was due to the stabilising effect of intramolecular π-π stacking interactions between the disubstituted acylthiourea ligands and 1,10-phenanthroline. A study into the persistence of the intramolecular π-π stacking interactions in solution was undertaken using VT-NMR spectroscopy and it showed that [Pt(phen)(L^n-κ*S*)$_2$] complexes bearing acylthioureato ligands with aromatic acyl substituents could have at least three low energy conformations; the "open", the "half-open" sandwich, and "closed" sandwich conformations. However, the "open" conformation was found to be preferred at ambient temperature. [Pt(phen)(L^n-κ*S*)$_2$] complexes with acylthioureato ligands bearing non-aromatic acyl substituents could only have one conformation. Although the intramolecular π-π stacking interactions may be seen to persist in solution at very low temperatures as evidenced by the existence of the "half-open" and

"closed" sandwich conformations, there seem to be no conclusive evidence of this at ambient temperature. Hence, we cannot speculate their role in why disubstituted acylthioureato ligands with aromatic acyl substituents favour monodentate coordination while disubstituted acylthioureato ligands with non-aromatic acyl substituents favour bidentate coordination under synthetic method A.

The theoretical study into the electronic effect of acyl substituents on the reactivity of donor sites within disubstituted acylthioureato ligands in a coordination chemistry framework (coordination regioselectivity) was initiated that showed that regardless of what acyl substituents the ligands may bear, the sulfur donor atom is the most nucleophilic site for coordination with platinum(II) metal ions. In an effort to understand why ligands bearing electron-donating acyl substituents produced very low [Pt(phen)(L^n-κ*S*)$_2$], an acid stability test was conducted on the synthesized [Pt(phen)(L^n-κ*S*)$_2$] complexes as we suspected the reaction to be poisoned by the acetic acid by-product. Indeed, the test showed that the complexes were not stable under acidic condition, with acetic acid decomposing the [Pt(phen)(L^n-κ*S*)$_2$] complexes to the cationic $[Pt(phen)(L^n\text{-}\kappa O,S)]^+$ complex and free ligand.

This result drove us into looking for bases that did not produce conjugate acids that could react with the [Pt(phen)(L^n-κ*S*)$_2$] complexes and we found sodium hydride. Sodium hydride forms a gaseous conjugate acid (H_2) as it deprotonates acidic protons, that eventually escapes the reaction such that it does not interfere with product formation. When sodium hydride was used as a base to deprotonate *N*,*N*-di(alkyl/aryl)-*N*'-acylthiourea ligands and the resulting solvated salt reacted with [$PtCl_2$(phen)] in the ratio 2:1 (method B), all the ligands produced the [Pt(phen)(L^n-κ*S*)$_2$] complexes in excellent yields regardless of what acyl substituents they had. This result correlated well with the result of the theoretical study and was adopted as the synthetic method of choice throughout the thesis; however, it did not explain why or how we were getting different results with method A.

A series of experiments were conducted that gave a better understanding of what was happening when disubstituted acylthiourea ligands reacted with [$PtCl_2$(phen)] using synthetic method (A). These experiments showed that the precursor undergoes solvolysis in wet methanol to give $[PtCl(H_2O)(phen)]^+$ species which then reacts with the deprotonated ligand in an "anation" type of reaction replacing the aqua ligand with acylthioureato ligands. The cycle is presumably repeated until the second ligand is substituted. Importantly, deprotonation of the acylthiourea ligands takes precedence before coordination in the presence of sodium acetate as the presence of acetate ions suppresses substitution of the coordinated water with the neutral acylthiourea ligand and that it is the availability of anionic species (deprotonated acylthiourea ligand) in solution that ultimately determines whether to coordinate in a monodentate fashion or to chelate. It was also shown that the product and by-product ([Pt(phen)(L^n-κ*S*)$_2$] and $[Pt(phen)(L^n\text{-}\kappa O,S)]^+$ respectively) can interconvert providing parallel reactions with which the product yield can be positively or negatively affected.

Extension of this coordination mode to complexes with different co-ligands or metal centres was only successful with the [Pt(bipy)Cl_2] and *cis*-[$PtCl_2(PPh_3)_2$] precursors when *N*,*N*-di(ethyl)-*N*'-(2-naphthoylthiourea) (**HL^{10}**) and *N*,*N*-di(ethyl)-*N*'-(1-naphthoylthiourea) (**HL^{1}**) were used resulting in a [Pt(bipy)(L^{10}-κ*S*)$_2$] complex and a mixed coordination modes [$Pt(PPh_3)(L^1$-κ*O*,*S*)(L^1-κ*S*)] complex. Successful monodentate coordination of disubstituted acylthiourea ligands in other complexes seems to depend on how strongly the co-ligands are bound to the metal centres and the presence of vacant coordination sites that the oxygen donor atom can use to chelate. Above all, the monodentate coordination of *N*,*N*-di(alkyl)-*N*'-acylthiourea ligands with platinum(II) ions (using [$PtCl_2$(phen)] as a precursor) seems to follow an "anation" type of reaction with solvolysis/aquation and the deprotonation of the ligand as important initial steps.

3.4. Experimental

[$Pt(PPh_3)(L^1$-κ*O*,*S*)(L^1-κ*S*)]: The precursor, *cis*-[$PtCl_2(PPh_3)_2$], was synthesised according to literature. *N,N*-di(ethyl)-*N*'-1-naphthoylthiourea (**HL^{1}**) (0.0172 g, 0.060 mmol) was added to a round-bottomed flask with sodium hydride (0.0032 g, 0.133 mmol) in anhydrous THF (4 ml) on an ice bath and stirred under inert conditions. The stirring was stopped when no more bubbles were being evolved and the mixture was left to stand so that unreacted sodium hydride settled at the bottom. The solution was decanted carefully and *cis*-[$PtCl_2(PPh_3)_2$] (0.0200 g, 0.025 mmol) was then added to it, and the reaction mixture refluxed for 1 hour. The resultant yellow mixture was filtered through cotton wool. The filtrate was evaporated to dryness and re-dissolved in dichloromethane with subsequent filtration to remove insoluble salts. The filtrate was then concentrated under *vacuo* and precipitated using hexane. The precipitate was washed with ice-cold diethyl ether to give a yellow powder.

Yield 61%; FT-IR (ATR): ν = 3057 (w, aromatic C-H), 2975-2867 (w, aliphatic C-H), 1603-1585 (m, C=O), 1493 (s, C=N), 1411 (s), 1237 (s), 1103 (s), 784 (s) cm^{-1} ; ^{1}H NMR (300 MHz, Chloroform-*d*) δ 9.15 (dd, 2H, $H^{7+7'}$), 8.10 (dd, 2H, $H^{3+3'}$), 7.75 (m, 10H, $H^{1+1'}$, $H^{2+2'}$, $H^{4+4'}$, $H^{6+6'}$, H^{ph}), 7.23 (m, 15H, $H^{5+5'}$, H^{ph}), 3.47 (q, 8H, $H^{a+a'}$), 0.98 (t, 12H, $H^{b+b'}$) ppm; HRMS (ESI^+) *m/z* for $C_{50}H_{49}N_4O_2PtPS_2$. Expected: 1028.2755 $[M+H]^+$; found: 1028.2745 $[M+H]^+$.

[Co(phen)(L^1-κ*O*,*S*)$_2$]: The precursor, [$CoCl_2$(phen)], was synthesised according to literature. *N,N*-di(ethyl)-*N*'-1-naphthoylthiourea (**HL^{1}**) (0.0381 g, 0.133 mmol) was added to a round-bottomed flask charged with sodium hydride (0.0047 g, 0.196 mmol) in anhydrous THF (4 ml) on an ice bath and stirred under inert conditions. The stirring was stopped when no more bubbles were being evolved and the mixture was left to stand so that unreacted sodium hydride settled at the bottom. The solution was decanted carefully and [$CoCl_2$(phen)] (0.0200 mg, 0.065 mmol) was then added to it, and the reaction mixture refluxed for 1 hour. The resultant mixture was filtered through cotton wool. The filtrate was evaporated to dryness and re-dissolved in dichloromethane with subsequent filtration to remove

insoluble salts. The filtrate was then concentrated under *vacuo* and precipitated using hexane. The precipitate was washed with ice-cold diethyl ether to give a brown powder.

Yield 83%; FT-IR (ATR): ν = 3086-3054 (w, aromatic C-H), 2924-2854 (w, aliphatic C-H), 1659 (m, C=O), 1630 (m, C=O), 1578 (m, C=N), 1412 (s), 1231 (s), 1351 (m), 851 (s), 720 (s) cm^{-1} ; HRMS (ESI^+) *m/z* for $C_{44}H_{42}N_6O_2CoS_2$. Expected: 809.21372 $[M]^+$; found: 809.1561 $[M]^+$.

3.5. References

[1] M. Dörner, J. M. Rautiainen, J. Rust, C. W. Lehmann, F. Mohr, *Eur. J. Inorg. Chem.* **2016**, 1–10.

[2] A. Saeed, U. Flörke, M. F. Erben, *J. Sulfur Chem.* **2014**, *35*, 318–355.

[3] H. Kessler, G. Zimmermann, H. Forster, J. Engel, G. Oepen, W. S. Sheidrick, *Angew. Chem. Int. Ed. Engl.* **1981**, *20*, 1053–1055.

[4] EMBL-EBI, "variable-temperature nuclear magnetic resonance spectroscopy," can be found under https://www.ebi.ac.uk/ols/search?q=VT+nmr&ontology=chmo, **2018**.

[5] F. L. Switzer, J. E. J. Toomey, R. Murugan, in *Compr. Heterocycl. Chem. II*, Elsevier Ltd., **1996**, pp. 784–794.

[6] J. W. Faller, in *Compr. Organomet. Chem. III*, Elsevier Ltd., New Haven, **2007**, pp. 407–427.

[7] K. R. Back, R. J. Davey, T. Grecu, C. A. Hunter, L. S. Taylor, *Cryst. Growth Des.* **2012**, *12*, 6110–6117.

[8] G. P. Migliaccio, S. R. Byrn, *J. Pharm. Sci.* **1981**, *70*, 284–287.

[9] R. A. Miranda-Quintana, M. M. González, D. Hernández-Castillo, L. A. Montero-Cabrera, P. W. Ayers, C. Morell, *J. Mol. Model.* **2017**, *23*, 1–15.

[10] M. Martínez González, D. Hernández-Castillo, L. A. Montero-Cabrera, R. A. Miranda-Quintana, *Int. J. Quantum Chem.* **2017**, *117*.

[11] W. Lamine, S. Boughdiri, L. Christ, C. Morell, H. Chermette, *J. Comput. Chem.* **2019**, *40*, 717–725.

[12] P. Geerlings, S. Fias, T. Stuyver, P. Ayers, R. Balawender, F. De Profit, in *Density Funct. Theory* (Ed.: D. Glossman-Mitnik), IntechOpen, **2018**, pp. 1–29.

[13] P. K. Chattaraj, *Chemical Reactivity Theory*, CRC Press, Taylor & Francis Group, London, **2009**.

[14] F. Neese, *Coord. Chem. Rev.* **2009**, *253*, 526–563.

[15] J. Frau, F. Muñoz, D. Glossman-Mitnik, *Quim. Nova* **2017**, *40*, 402–406.

[16] P. Fuentealba, E. Chamorro, C. Cardenas, *Int. J. Quantum Chem.* **2006**, *107*, 37–45.

[17] R. K. Roy, S. Saha, *Annu. Reports Prog. Chem. Sect. C* **2010**, 118–162.

[18] S. Saha, Density Functional Theory Based Studies of Reactivity Descriptors to Predict the Regioselectivity of Chemical and Biological Systems, PhD, Birla Institute of Technology and Science, Pilani India, **2010**.

[19] F. Boukli-Hacene, M. Merad, S. Ghalem, W. Soufi, *J. Chem. Eng.* **2014**, *8*, 1009–1017.

[20] R. Vivas-Reyes, E. Espinosa-Fuentes, J. Forigua, A. Arias, R. Gaitán, E. Arguello, *J. Mol. Struct. THEOCHEM* **2008**, *862*, 92–97.

[21] R. G. Parr, W. Yang, *J. Am. Chem. Soc.* **1984**, *106*, 4049–4050.

[22] W. Yang, R. G. Parr, R. Pucci, *J. Chem. Phys.* **1984**, *81*, 2862.

[23] P. Geerlings, F. De Proft, W. Langenaeker, *Chem. Rev.* **2003**, *103*, 1793–1873.

[24] G. Berger, *Comput. Theor. Chem.* **2013**, *1010*, 11–18.

[25] D. A. Buckingham, *Coord. Chem. Rev.* **1994**, *1351/136*, 587–621.

[26] H. A. Ankersmit, P. T. Witte, H. Kooijman, M. T. Lakin, A. L. Spek, K. Goubitz, K. Vrieze, G. Van Koten, *Inorg. Chem.* **1996**, *35*, 6053–6063.

[27] T. G. Appletorq, J. F. J. Pescb, M. Wienken, S. Menzer, B. Lippert, *Inorg. Chem.* **1992**, *31*, 4410–4419.

[28] Y. Lee, *Bull. Korean Chem. Soc.* **2005**, *26*, 1627–1630.

[29] P. Ghosh, P. Mondal, R. Ray, A. Das, S. Bag, S. M. Mobin, G. K. Lahiri, *Inorg. Chem.* **2014**, *53*, 6094–6106.

[30] E. F. Kangara, T. Peega, L. Harmse, J. L. van Wyk, D. C. Levendis, I. A. Kotzé, *New J. Chem.* **2019**, *43*, 3665–3672.

[31] I. A. Kotzé, W. J. Gerber, J. M. Mckenzie, K. R. Koch, *Eur. J. Chem.* **2009**, 1626–1633.

[32] J. R. L. Priqueler, I. S. Butler, F. D. Rochon, *Appl. Spectrosc. Rev.* **2007**, *41*, 185–226.

[33] "NMR Frequencies vs. Bruker Field Strengths-sorted by increasing atomic number 1 H," DOI 10.00can be found under http://kodu.ut.ee/~laurit/AK2/NMR_tables_Bruker2012.pdf, **2012**.

[34] F. Neese, *Wiley Interdiscip. Rev. Comput. Mol. Sci.* **2012**, *2*, 73–78.

[35] S. Asperger, *Inorganic Reaction Mechanisms Chemical Kinetics and Inorganic Reaction Mechanisms*, Springer Science+Business Media, LLC, Zagreb, **2003**.

[36] J. S. Chauhan, M. J. Solanki, in *Basics React. Mech. Inorg. Chem.*, Educreation Publishing, New Delhi, **2018**, pp. 54–57.

[37] L. Cubo, A. G. Quiroga, J. Zhang, D. S. Thomas, A. Carnero, C. Navaro-Ranninger, S. J. Berners-price, *Dalton Trans.* **2009**, *9226*, 3365–3616.

[38] P. Lindqvist-Reis, Structure of Solvated Metal Ions, PhD, Royal Institute of Technology Stockholm

Sweden, **2000**.

[39] B. Schmitt, T. I. A. Gerber, E. Hosten, R. Betz, *Inorg. Chem. Commun.* **2012**, *24*, 136–139.

[40] N. Gunasekaran, P. Ramesh, M. N. G. Ponnuswammy, R. Karvembu, *Dalton Trans.* **2011**, *40*, 12519–12526.

[41] A. Roodt, J. G. Leipoldt, K. R. Koch, M. Matoetoe, *Rhodium express* **1994**, 39–7.

[42] U. Abram, S. Abram, R. Alberto, R. Schibli, *Inorg. Chim. Acta* **1996**, *248*, 193.

[43] M. A. V Ribeiro, D. M. C. Ribeiro, C. M. Silva, F. Dietze, E. Hoyer, L. Beyer, B. Schröder, M. Damas, J. F. Liebman, *J. Chem. Soc. Perkin Trans. 2* **2001**, 2174–2178.

[44] M. Schuster, B. Kugler, *Fresenius J. Anal. Chem.* **1990**, *338*, 717–720.

[45] R. Morris, A. Habtemariam, Z. Guo, S. Parsons, P. J. Sadler, *Inorg. Chim. Acta* **2002**, *339*, 551–559.

[46] K. R. Koch, S. Bourne, *J. Mol. Struct.* **1998**, *441*, 11–16.

[47] H. S. Rzepa, "Aromaticity as a controlling influence on a ligand dissociation mechanism for Λ/Δ Interconversion in Metal tris Chelates," can be found under http://www.ch.ic.ac.uk/rzepa/tris-chelates/.

[48] F. P. Fanizzi, F. P. Intini, L. Maresca, G. Natile, D. F.- Chimico, G. Amendola, I.- Bari, *Dalton Trans.* **1990**, *1*, 199–202.

Chapter 4

*Antiproliferation activity of [Pt(phen)(L^1-κ*S*)$_2$] and [Pt(phen)(L^2-κ*S*)$_2$] complexes*

4.1. Introduction

In order to reduce the side effects of current platinum base metallodrugs, most efforts have focused on changing the metal to other transition metals such as copper(II), ruthenium(III), palladium(II), *etc*,[1–3] while other researchers have been probing complexes that proffer a different mechanism of action such as intercalators with auspicious results.[4,5] Platinum(II) complexes with a $[Pt(phen)]^{2+}$ core (*Figure 1*) have particularly sparked the interests of many researchers as they offer a potentially different or an additional (intercalating) mode of action due to their planar diimine moiety compared to cisplatin and its analogues.[6–9]

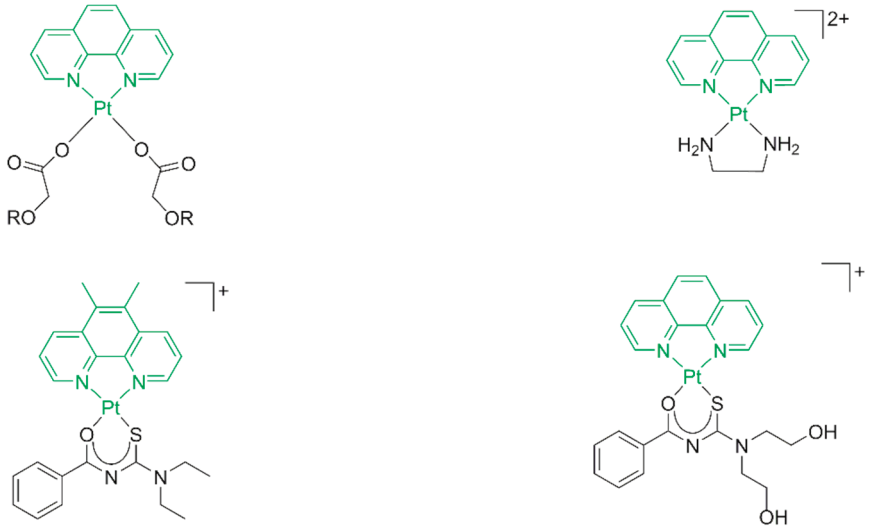
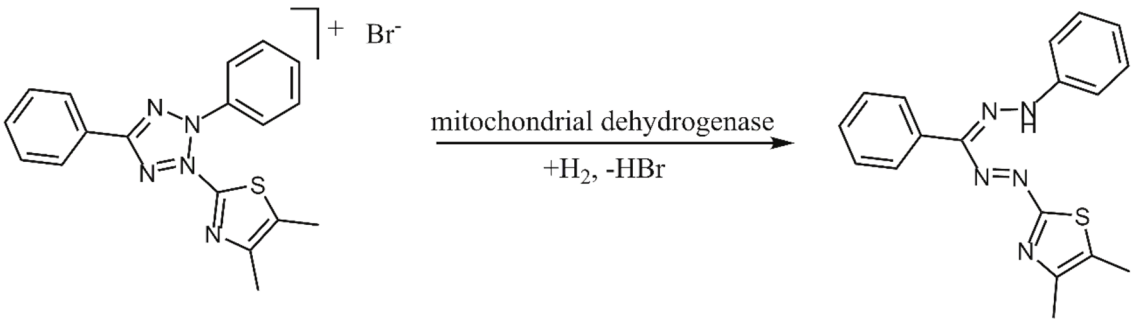


Figure 1: Examples of platinum(II) complexes (bearing a $[Pt(phen)]^{2+}$core) with significant preliminary antiproliferative activity.[6,9–11]

Due to the limited solubility of these complexes, ancillary ligands have been modelled to improve their solubility and activity while possibly reducing toxicity.[6] Our study has drawn its interest from the possible application of these new [Pt(phen)(L^n-κ*S*)$_2$] complexes as anti-cancer agents targeting DNA, that might have a different mechanism of action and hopefully be very active and less toxic. Mono- and bifunctional thiourea derivatives have already successfully been reported as alternative coordinating carrier ligands in platinum(II) anticancer complexes.[12] Several positive attributes inspired our antiproliferation studies on [Pt(phen)(L^n-κ*S*)$_2$] complexes. These complexes have planar phenanthroline rings that can intercalate between DNA base pairs providing an alternative mode of

action. Their axial sites are hindered such that side reactions with other biomolecules or aquation reactions are minimised. The acylthiourea ligands themselves are also known to have some bio-activity[13], and they can be tailored to have groups that bring additional intercalation capabilities or improve water solubility if need be. The [Pt(phen)(L^n-κ*S*)$_2$] complexes may provide a firmly bound complex architecture (*i.e.* no leaving group) because of the strong platinum-sulfur interaction thus reducing side reactions with biomolecules. Lastly, the complexes could be tuned to be more lipophilic by using appropriate substituent R-groups on the acylthioureato ligand, which may enhance their migration across cell membranes. To investigate the potential of our complexes as antiproliferative agents, we selected two complexes, [Pt(phen)(L^1-κ*S*)$_2$] and [Pt(phen)(L^2-κ*S*)$_2$].

Most prospective therapeutic agents are tested in tissue culture on a suitable model to gain useful information on the cytotoxicity of the agents, for example, *in vitro* proliferation or colony formation assays.[14] The MTT assay is a colorimetric assay commonly used as a screening method to examine the antiproliferation activity of drug candidates. The test quantifies the extent of 3-(4,5-dimethylthiazol-2-yl)-2,5-diphenyltetrazolium bromide (MTT) reduction to formazan by mitochondrial dehydrogenase (*Scheme 1*).[15]



Scheme 1: *Mitochondrial reduction of MTT (yellow) to Formazan (purple).*

In viable cells, MTT (yellow) is reduced to formazan (purple) which precipitates onto the surfaces of the wells. The precipitate dissolves in DMSO to give a purple solution from which the amount of formazan in each well can then be measured spectrophotometrically to determine the number of viable cells in each well. The absorbance values read at each concentration are divided by the absorbance values of the control and plotted against concentration to give plots where IC_{50} (which is the concentration at which the number of viable cells is 50% that of the control) values can be determined.

There are different pathways by which cell death occurs in response to a variety of external and physiological stimuli. Apoptosis (programmed cell death) is the normal way of development and maintenance of the health of multi-cellular organisms.[16] During apoptosis, cell death is controlled and regulated, whereas, under necrotic (unprogrammed cell death) pathways, there is no control and leads to serious health issues and side effects.[17] So there is a need for every prospective drug candidate to be

assessed for the cell death they induce upon uptake. Fluorescence microscopy is one technique that is commonly employed in morphological staining methods to detect apoptosis.[18] In this method, the untreated cells, as well as cells treated with prospective drug candidates, are treated with dyes such as a mixture of Hoechst 33342 and ethidium bromide dyes and incubated after which they are viewed under a fluorescence microscope for morphology changes. Tell-tale signs of apoptosis include a condensed nucleus, blebbing cell membrane, and clear cytoplasm.[19]

Structure-activity studies are fundamental to many aspects of drug discovery ranging from primary screening to lead optimisation.[20] They present chemical information relative to biological activity for the twin purposes of generating insight into the mechanism of action and predicting the potential activities of new chemicals.[21] Molecular docking is the most common in *silico* method used to unravel these structure-activity relationships. Molecular docking can be used to model the interaction between a drug candidate and target macromolecule at the binding site as well as to elucidate fundamental biochemical processes.[22] The docking process involves prediction of the drug conformation as well as its position and orientation within the binding site. In this study, molecular docking was used to investigate possible binding modes between the [Pt(phen)(L^1-κ*S*)$_2$] complex and DNA.

4.2. Results and discussion

4.2.1. Cell viability study

[Pt(phen)(L^1-κ*S*)$_2$] and [Pt(phen)(L^2-κ*S*)$_2$] were tested for their effect on the viability of a malignant A549 lung cancer cell line using an MTT assay. These cells were chosen because lung cancer is the leading cause of cancer deaths in the world, hence their study is of great importance. A549 cells were treated with the two complexes at increasing concentrations from 0.5 to 50 μM for 48 hours. Cells treated with both complexes showed a similar trend of a decrease in cell viability when the concentrations of the complexes increased; while at a maximum concentration of 50 μM, no cells survived (*Figure 2*).

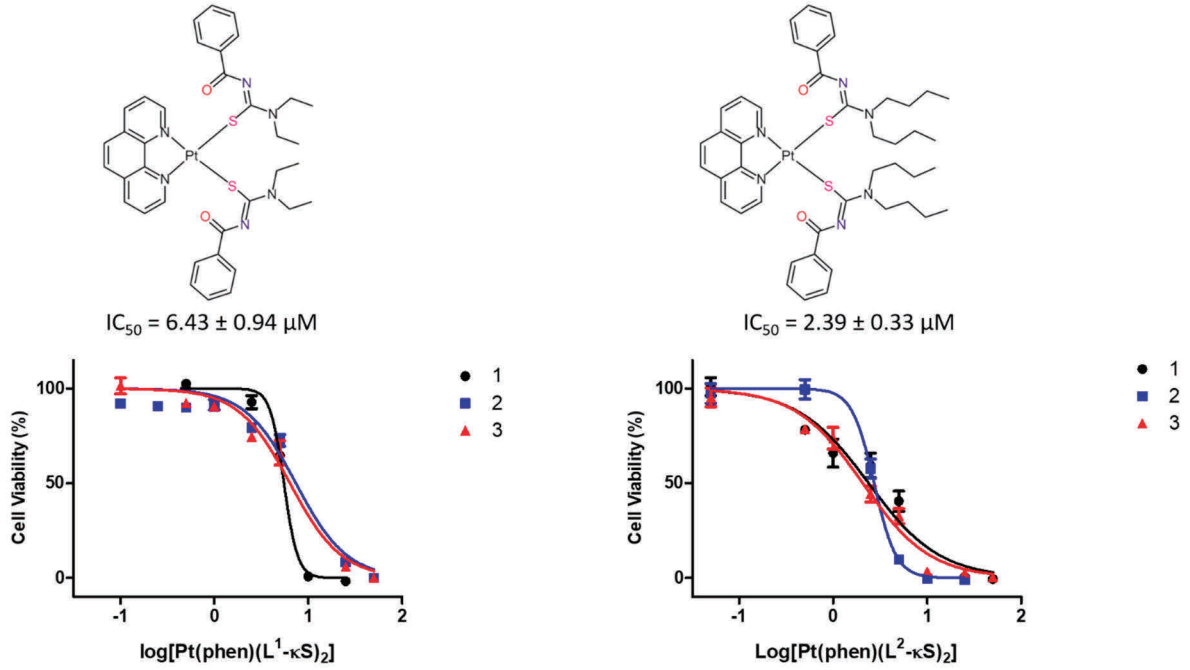


*Figure 2: Dose-response curves of [Pt(phen)(L^1-κ*S*)$_2$] and [Pt(phen)(L^2-κ*S*)$_2$] versus percentage cell viability against A549 lung cancer cell line treated for 48 hours respectively (with ●, ■ and ▲ representing replicate experiments).*

Subsequent calculations to determine the IC_{50} values (50 % inhibitory concentration) of the [Pt(phen)(L^1-κ*S*)$_2$] and [Pt(phen)(L^2-κ*S*)$_2$] complexes showed it to be 6.4 ± 0.9 µM and 2.4 ± 0.3 µM, respectively. Interestingly, the [Pt(phen)(L^2-κ*S*)$_2$] complex, with an extended hydrophobic chain on the amino terminus of the acylthioureato ligand, is more effective in killing the A549 cancer cells. This result, we suspect, may be attributed to better cellular uptake of [Pt(phen)(L^2-κ*S*)$_2$] compared to [Pt(phen)(L^1-κ*S*)$_2$]. These IC_{50} values are comparable with the cisplatin IC_{50} value of 5.1 ± 1.69 against an A549 lung cancer cell line treated for 48 hours reported by Kaplan *et al*.[23] With these encouraging results, the [Pt(phen)(L^1-κS)$_2$] complex was studied further for the kind of cell death it induces by analysing changes in cellular morphology after the cells were treated with the complex.

4.2.2. Morphological study

A549 cells were treated with 50 µM of the [Pt(phen)(L^1-κ*S*)$_2$] complex for 20 hours. The cells were viewed under a phase-contrast microscope, stained with Hoechst 33342 and ethidium bromide and examined again under a fluorescent microscope. When contrasted, cells treated with the [Pt(phen)(L^1-κ*S*)$_2$] complex exhibited notable changes in cell morphology when compared with the untreated cells (control).

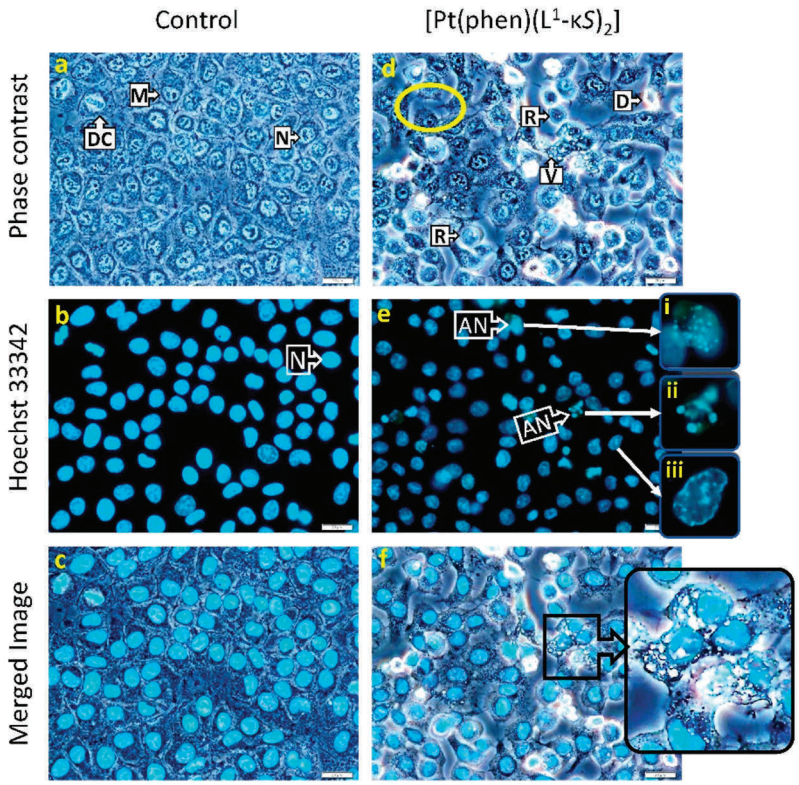


*Figure 3: Morphological changes of A549 cells treated with 50 mM of [Pt(phen)(L^1-κ*S*)$_2$] for 20 hours. Cells were stained with the Hoechst 33343 nuclear stain and ethidium bromide as indicators for necrosis. (Legend: N = nucleus, DC = dividing cell, M + cell membrane, V = vacuoles, AN = apoptotic nucleus, D = detached cell, R = round cell, yellow oval = filopodia).*[24]

The phase-contrast images (*Figure 3 panel d and f*) displayed some cells that were detached, with an irregular shape; while others assumed a round shape. Because of these transformations, the nucleus of each cell was no longer clearly visible using the phase contrast viewing mode. Filopodia-like protrusions were evident, as an indication of cells detaching from the growth surface (*Figure 3 panel d, yellow oval*). Additionally, the manifestation of cytoplasmic vacuoles indicated the spectre of cell stress (*Figure 3, panel d, inset panel f*). All these observations suggest that the [Pt(phen)(L^1-κS)$_2$] complex induces cell death in A549 cancer cells via apoptosis, prompting us to investigate the possible mechanism of action using molecular docking.

4.2.3. Molecular docking study

A molecular docking study was performed to evaluate the potential binding mode of the [Pt(phen)(L^1-κ*S*)$_2$] complex to DNA (assuming it reaches the target DNA still intact). It has been suggested that addition or inclusion of intercalating moieties (the $[Pt(phen)]^{2+}$ core in our case) in platinum(II) complexes improves their interaction with DNA,[8] hence docking studies were performed on DNA among the biomolecules found in the human body.

The graphical user interface program AutoDock Vina was used to set up the ligand ([Pt(phen)(L^1-κ*S*)$_2$]) and the macromolecule (DNA): all hydrogens were added, Gasteiger charges calculated and non-polar hydrogens merged to carbon atoms. The platinum force field parameters were set as; r_{ii} = 2.75 Å, esp_{ii} = 0.080 kcal/mol, *vol* = 12.000 Å^3 and *solpar* = -0.00110.[25,26] In the adduct illustrated in *Figure 4*, there is a hydrogen bond between the DNA's (N – H) and a carbonyl (C = O) group of the metal complex coupled with offset π – π interactions between the DNA's bases and the complex's aromatic rings result in a major-groove binding mode in an (AT) rich region of the DNA.

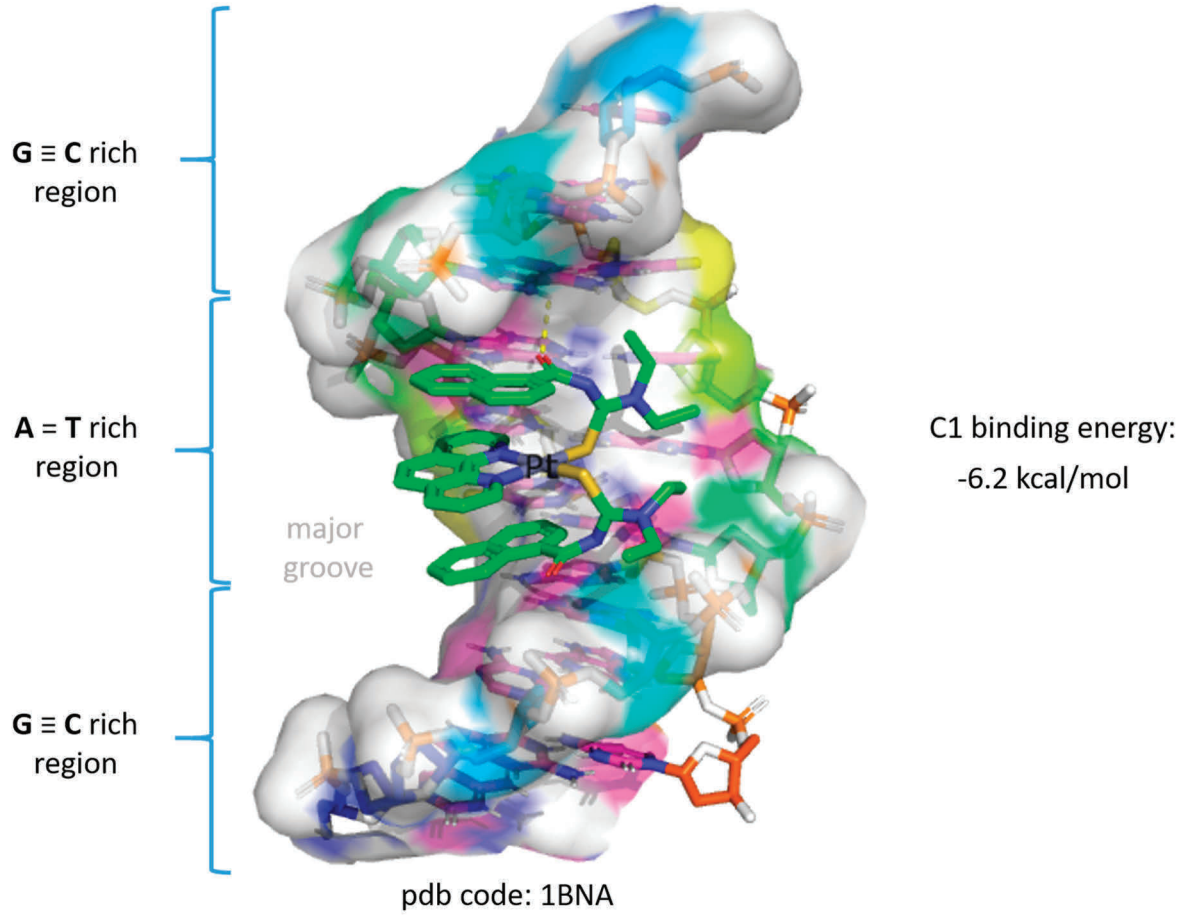


*Figure 4: The structure of the most stable binding mode of the [Pt(phen)(L^1-κ*S*)$_2$] complex to DNA (C1), as assessed by molecular docking. (DNA pdb code:- 1BNA*[27]*).*

The complex preferentially binds in the (AT) rich region for all adducts except for the C7 adduct where the complex bind in a (CG) rich region of the DNA (*Figure 5*), with binding energies of the most stable adducts (C1 – C9) in the range from −5.90 to −6.20 kcal mol^{-1}. The complex seems to prefer major groove binding, possibly due to its bulkiness.

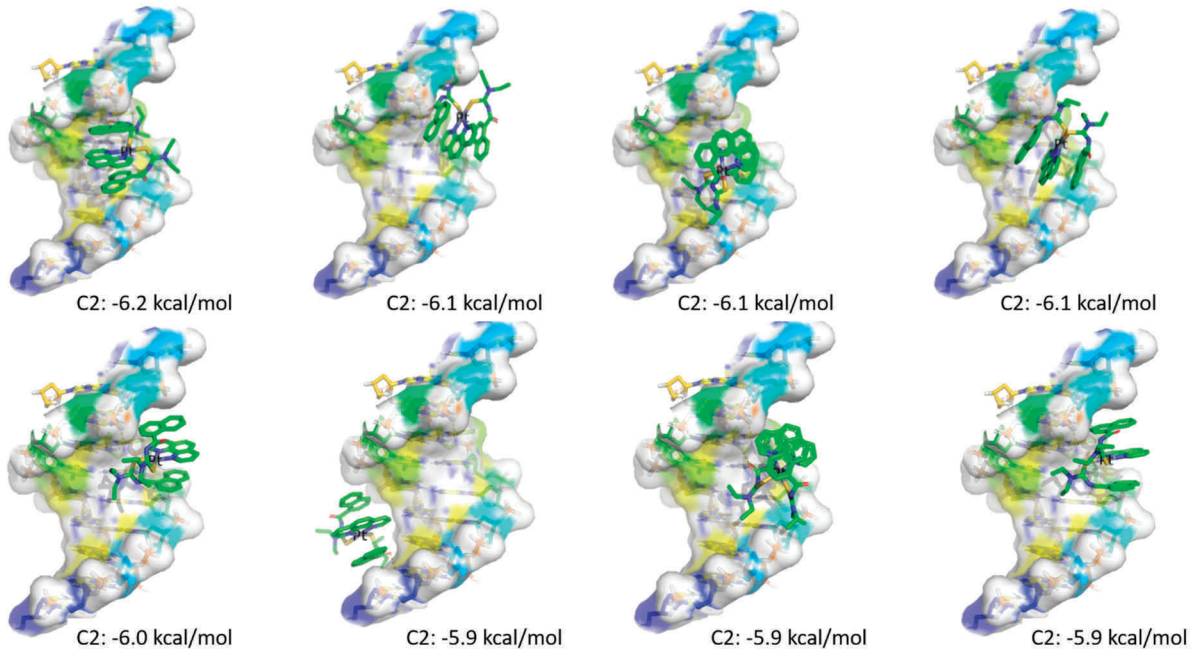


*Figure 5: The structures of the most stable binding modes of the [Pt(phen)(L^1-κ*S*)$_2$] complex to DNA (C2-C9), as assessed by molecular docking.*

In order to substantiate the results from the docking model and ascertain the binding mode of [Pt(phen)(L^1-κS)$_2$] to DNA, a number of experiments could be conducted. Electronic absorption titrations constitute one of the most important means of studying metal complexes binding with DNA. Complexes interactions with DNA are characterised by the change in intensity and wavelength of the absorption spectrum.[28] A complex bound to DNA via intercalation is characterised by hypochromism and red shift of the absorption bands due to the strong interaction between an aromatic chromophore and the base pairs of DNA,[29] while no red shifts and sharp isosbestic points is characteristic of groove binding.[30] Viscosity measurements may also be used to confirm intercalative or non-intercalative binding mode of complexes to DNA, since it is sensitive to variations in the DNA length accustomed with complex-DNA interactions. In order to distinguish between minor and major groove binders, competitive binding assays can be carried out via steady-state fluorescence emission analysis. In this experiment two different site markers are employed, for example, ethidium bromide (major groove marker) and 4',6-diamidino-2-phenylindole (minor groove marker).[31]

4.3. Conclusion

MTT assays have shown that [Pt(phen)(L^1-κ*S*)$_2$] and [Pt(phen)(L^2-κ*S*)$_2$] significantly suppressed the proliferation of an A549 cell line in a dose-dependent manner. The IC_{50} values for the A549 cell line after 48 hours of treatment with [Pt(phen)(L^1-κ*S*)$_2$] and [Pt(phen)(L^2-κ*S*)$_2$] were 6.4 ± 0.9 μM and 2.4 ± 0.3 μM, respectively. Substitution of an ethyl group with a more hydrophobic butyl chain at the amino terminus of the acylthioureato ligands lowers the IC_{50} significantly possibly due to an improved cellular

uptake since we do not think it plays a significant role in binding the target site. Apoptosis is evidenced by cytoplasmic enlargement, rupture of the plasma membrane, swelling of cytoplasmic organelles particularly mitochondria, and some condensation of nuclear chromatin.[19] The morphological studies suggest that [Pt(phen)(L^1-κ*S*)$_2$]] induced cell death on A549 primarily through apoptosis. However, morphological studies alone can only provide a rough estimation of the mode of action of the [Pt(phen)(L^1-κ*S*)$_2$] complex and more research in the mechanism is needed to conclude. The DNA docking experiment suggests that these complexes prefer to interact with an (A = T) rich region in the major groove of the target DNA if they manage to reach it. Above all, the results obtained from this preliminary antiproliferative studies are encouraging, and further studies are required on these types of complexes.

4.4. Experimental

4.4.1. Materials

Cell Cultures

A549, human lung carcinoma cell cultures were obtained from American Tissue Culture Collection (ATCC) and verified by STR. These cultures were grown in Dulbecco's Modified Eagle's Medium (DMEM) media with 1% (v/v) L-glutamine, 1% (v/v) sodium pyruvate and 10% (v/v) foetal bovine serum.

Preparation of reagents

Dulbecco's Modified Eagle's Medium (DMEM)

DMEM powder (Sigma-Aldrich, JHB, SA) was dissolved in sterile water with the aid of a sterile stirrer. The pH of the solution was adjusted to 4 with 1 N HCl to ensure complete solubilisation. Thereafter 2 g of $NaHCO_3$ was added to each litre of the medium. The pH was readjusted to 7.1 through the addition of either 1N HCl or 1 N NaOH. The solution was supplemented with 1% (v/v) L-glutamine, 1% (v/v) sodium pyruvate and 10% (v/v) fetal bovine serum at 37 °C and 5% CO_2 in a humified incubator.The medium was stored at 4 ºC until used.

MTT solution

A stock solution was prepared by dissolving 200 mg of 3-(4,5-dimethylthiazol-2-yl)-2,5-diphenyltetrazolium bromide (MTT), (Sigma-Aldrich, JHB, SA) in 40 ml PBS solution. After solubilising the light sensitive solution was filter sterilized using a 0.2 µm syringe filter and stored (covered in tin foil) at 4 ºC until use.

Phosphate buffered saline (PBS)

Using the manufacturers recommendations, 0.923 g of buffer powder (The Scientific Group, JHB, SA) was dissolved in 100 ml of deionised water. The pH was adjusted to 7.2.

Trypan blue

A 0.2% w/v stock solution was made in PBS.

4.4.2. Methodology

(a) Cell culture preparation and *in vitro* antiproliferative assays

All handling of cultures and experiments were conducted sterile within an ISO particle count certified High Efficiency Particulate Air (HEPA) filtered laminar flow cabinet.

Cultures of the respective cell lines were established using standard *in vitro* methods and the suppliers recommended media in 25 - 175 cm^2 plastic culture flasks (AEC-Amersham P/L, JHB, SA) to achieve the required cell numbers for each assay. Cultures were incubated at 37 °C in a humidified atmosphere with 5% CO_2. 10 000 cells were seeded per well on two 96 well plates and incubated for 24 hours at 37 °C and 5% CO_2 to allow adherence on the plate surface. 10 mM stock solutions of [Pt(phen)(L^1-κ*S*)$_2$] and [Pt(phen)(L^2-κ*S*)$_2$] were prepared in dimethyl sulfoxide (25%) and ethanol mixture (75%) and diluted with cell media to a concentrations range of 0.05-50 μM. Cells were then treated with [Pt(phen)(L^1-κ*S*)$_2$] and [Pt(phen)(L^2-κ*S*)$_2$] respectively with subsequent incubation for 46 hours. This was followed by the addition of 40 μL of MTT solution (5mg/ml) which was exposed to the cells for 2 hours. During this period MTT was metabolized into purple formazan crystals by succinate dehydrogenase in the mitochondria of viable cells.[15] Thereafter, the cell media with test compounds and MTT solution were carefully removed from each well and 200 μL of DMSO was added to dissolve formazan crystals formed. The two 96 well plates were then placed on an mrc thermoshaker for 5 minutes and the absorbance were measured using a microplate Labsystems iEMS Reader at 540 nm using 690 nm as reference. All measurements were conducted in quadruplicates for each dose of the complexes and the experiment was repeated three times. The absorbance values were used to determine the relative percentage of viable cells compared to untreated controls.

(b) Cell morphology study

Cells were seeded on sterile glass coverslips in a six-well culture plate at 5 x 10^4 per coverslip and incubated for 24 hours. Cells were treated with 50 μM of [Pt(phen)(L^1-κ*S*)$_2$] for 20 hours followed by three gentle washes with phosphate buffered saline. The cells were then incubated with 1 mL of dye mixture of Hoechst 33342 (5 μgmL^{-1}) and ethidium bromide for 30 minutes in the dark. This was followed by a gentle rinse of the coverslips with PBS and the mounting the coverslips, cell side facing downwards, on a microscope slide in a drop of Fluoromount mounting media (Sigma). The slides were

viewed, and images captured using an Olympus BX41 fluorescent microscope fitted with an Olympus DP72 digital camera at a 400 times magnification. Images were captured in colour mode using an ISO 400 and a fixed exposure time for each fluorochrome. An Olympus U-MWU2 filter cube was used to observe the Hoechst 33342 images and an Olympus U-MWIG2 filter cube was used to observe the ethidium bromide. Images were merged using the Olympus CellSens® software programme and adjusted for brightness where required.

4.5. References

[1] J. Li, Z. Tian, Z. Xu, S. Zhang, Y. Feng, L. Zhang, Z. Liu, *Dalton Trans.* **2018**, *47*, 15772–15782.

[2] M. Wang, X. Nan, G. Feng, H. Yu, G. Hu, Y. Liu, *Ind. Crop. Prod.* **2014**, *55*, 11–18.

[3] J. Wang, G. Xu, Y. Zhang, H. Luo, J. Li, L. Zhang, D. Jia, *New J. Chem.* **2019**, *43*, 2529–2539.

[4] M. Cusumano, M. Letizia, D. Pietro, A. Giannetto, P. A. Vainiglia, *J. Inorg. Biochem.* **2005**, *99*, 560–565.

[5] M. Cusumano, M. Letizia, D. Pietro, A. Giannetto, *Inorg. Chem.* **2006**, *45*, 230–235.

[6] Y. Sun, H. Wei, Q. Zhang, X. Zhao, *Chem. Biodivers.* **2019**, *16*, p.e1800373.

[7] N. S. Ng, P. Leverett, D. E. Hibbs, Q. Yang, J. C. Bulanadi, M. Jie Wu, J. R. Aldrich-Wright, *Dalton Trans.* **2013**, *42*, 3196–3209.

[8] L. Gude, M. Fernandez, K. B. Grant, A. Lorente, *Bioorganic Med. Chem. Lett.* **2002**, *12*, 3135–3139.

[9] Y. Wu, K. R. Koch, V. R. Abratt, H. H. Klump, *Arch. Biochem. Biophys.* **2005**, *440*, 28–37.

[10] J. R. Aldrich-Wright, *Metallointercalators: Synthesis and Techniques to Probe Their Interactions* ., SpringerWienNewYork, Sydney, **2011**.

[11] R. N. Magwaza, Synthesis and characterization of novel [Pt(diimine)(acylthiourea)]$^{+}$ complexes as potential anticancer agents and exploring the use of Sulphobutyl-ether- β -cyclodextrin and surfactant micelles as a drug delivery system, MSc University of the Witwatersrand, **2017**.

[12] U. Bierbach, T. W. Hambley, N. Farrell, *Inorg. Chem.* **2002**, *37*, 708–716.

[13] B. O'Reilly, A. M. Plutín, H. Pérez, O. Calderón, R. Ramos, R. Martínez, R. A. Toscano, J. Duque, H. Rodríguez-Solla, R. Martínez-Alvarez, et al., *Polyhedron* **2012**, *36*, 133–140.

[14] N. Farrell, in *Compr. Coord. Chem. II Appl. Coord. Chem.* (Ed.: M.D. Ward), Elsevier Ltd, Richmond, USA, **2004**, pp. 809–840.

[15] T. Mosmann, *J. Immunol. Methods* **1983**, *65*, 55–63.

[16] T. Vo, A. Letai, in *BCL-2 Protein Fam. Adv. Exp. Med. Biol.* (Ed.: C. Hetz), Springer, New York, NY, **2010**, pp. 49–50.

[17] S. Elmore, *Toxicol. Pathol.* **2007**, *35*, 495–516.

[18] D. Ribble, N. B. Goldstein, D. A. Norris, Y. G. Shellman, *BMC Biotechnol.* **2005**, *5*, 12.

[19] J. E. Coligan, *Current Protocols in Immunology*, J. Wiley, New York, **1996**.

[20] R. Guha, *Methods Mol Biol.* **2013**, *993*, 81–94.

[21] A. M. Richard, in *Chem. Mech. Toxic. Basic Knowl. Des. Safer Chem.*, Basel, Switzerland, **2000**.

[22] M. Cui, M. Mihaly, Z. Hong-Xing, X.-Y. Meng, *Curr. Comput.-Aided Drug Des.* **2011**, *7*, 146–157.

[23] A. Kaplan, G. A. Ciftci, H. M. Kutlu, *Tumor Biol.* **2017**, 1–12.

[24] E. F. Kangara, T. Peega, L. Harmse, J. L. van Wyk, D. C. Levendis, I. A. Kotzé, *New J. Chem.* **2019**, *43*, 3665–3672.

[25] R. Huey, "Adding new atom parameters to AutoDock — AutoDock," can be found under http://autodock.scripps.edu/faqs-help/how-to/adding-new-atom-parameters-to-autodock, **2011**.

[26] D. Suplatov, "AutoDock - ADL: Parameters for docking with metal ions in receptor," can be found under http://autodock.1369657.n2.nabble.com/ADL-Parameters-for-docking-with-metal-ions-in-receptor-td2505649.html, **2009**.

[27] H. R. Drew, R. M. Wingt, T. Takano, C. Broka, S. Tanaka, K. Itakura, R. E. Dickerson, *Proc. Natl. Acad. Sci.* **1981**, *78*, 2179–2183.

[28] A. Arunadevi, J. Porkodi, L. Ramgeetha, N. Raman, *Nucleosides, Nucleotides and Nucleic Acids* **2019**, 1–24.

[29] M. Zhu, X. Cui, F. Zhao, X. Ma, Z. Han, E. Gao, *RSC Adv.* **2015**, *5*, 47798–47808.

[30] K. Suntharalingam, O. Mendoza, A. A. Duarte, D. J. Mann, R. Vilar, *Metallomics* **2013**, 5, 514-523.

[31] A. Luiza, D. A. Querino, J. Thayanne, J. Teixeira, S. Gustavo, M. Alvarenga, C. Hahn, M. Torquato, Q. De Magalhães, O. Augusto, *JBIC J. Biol. Inorg. Chem.* **2019**, 1-17.

Chapter 5

Conclusion

5.1. Monodentate coordination chemistry of *N*,*N*-di(alkyl/aryl)-*N*'-acylthioureato ligands towards platinum(II) ions

The primary aim of this thesis was to synthesize and fully characterize the platinum(II) complexes of the form [Pt(phen)(L^n-κ*S*)$_2$], with disubstituted acylthioureato ligands (L^n) coordinated in a monodentate fashion through the sulfur donor atom and to establish the factors important in achieving this coordination mode. The syntheses of these novel complexes presented great insight into possibly overlooked aspects of coordination chemistry. Initial attempts focused on the facile one-pot synthesis from a platinum(II) source ([$PtCl_2$(phen)]) in methanol with sodium acetate as a base for *in-situ* deprotonation of the acylthiourea ligand. The [Pt(phen)(L^n-κ*S*)$_2$] complexes could be synthesised in particularly good yields with disubstituted acylthiourea ligands bearing a (trichloroacetyl-) or aromatic acyl substituents and only in extremely low yields with disubstituted acylthiourea ligands bearing electron-donating non-aromatic acyl substituents. Variations of substituents on the amino end of the ligands did not introduce any meaningful change in the yields. On the other hand when the synthetic method was changed to a step-wise synthesis where the ligand was firstly deprotonated with sodium hydride in anhydrous THF, and the resultant salt reacted with [$PtCl_2$(phen)], remarkably high yields of the [Pt(phen)(L^n-κ*S*)$_2$] complexes were obtained across all the ligands regardless of the substituents on the disubstituted acylthiourea ligands.

The first evidence of monodentate coordination of two *N*,*N*-di(alkyl/aryl)-*N*'-acylthioureato ligands in [Pt(phen)(L^n-κ*S*)$_2$] complexes was seen from the ^{1}H-NMR spectra of these complexes which showed characteristic symmetry in the phenanthroline protons as a result of a C_2 symmetry in the molecule. The ^{1}H-NMR spectra also showed a characteristic upfield shifting of aromatic protons of the acylthioureato ligands which may be attributed to a change in the electronic influence of the amido group on the aromatic ring of acylthioureato ligands. In the free ligand, the amido group function as an electron-withdrawing group via the mesomeric effect while in [Pt(phen)(L^n-κ*S*)$_2$] complexes, the mesomeric electron-withdrawing effect is suppressed. Unambiguous assignment of the protons and carbons of the complexes was done with the help of 2D-NMR (COSY, HSQC, and HMBC) as well as DEPT-135 NMR spectroscopy. Further evidence and confirmation of monodentate coordination of disubstituted acylthioureato ligands in [Pt(phen)(L^n-κ*S*)$_2$] complexes were obtained through single-crystal XRD.

Several single crystals of the complexes were grown and analysed which showed that the acylthioureato ligand coordinated as an X-type ligand to the platinum metal centre only through the sulfur donor atom with the acyl group pendant. Due to steric bulkiness, the ligands arranged in an anti-configuration where pendant acyl groups from the two acylthioureato ligands lie above and below the square planar coordination plane, with intramolecular π-π interactions stabilising this arrangement in complexes bearing aromatic acyl substituents. Diverse types of π-π interactions (parallel, offset parallel, perpendicular T-shaped and perpendicular L-shaped π-stacking) and hydrogen bonding interactions (aromatic C-H----O, O-H----O hydrogen bonding) seems to stabilise crystal packing in these complexes. One notably interesting observation during the single-crystal XRD study was the obtaining of two solvates of [Pt(phen)(L^1-κ*S*)$_2$] crystallised from methanol (a polar protic solvent) and THF (a medium polar aprotic solvent) that showed two different conformations of the complex. This finding prompted the study of the possible solution conformations of these conformationally flexible complexes, thereby investigating whether the extensive intramolecular π-π stacking interactions observed in the solid-state also persist in solution.

The [Pt(phen)(L^1-κ*S*)$_2$] complexes' solution conformations study was done using dynamic ^{1}H- and ^{195}Pt NMR spectroscopy in correlation with the solid-state structures obtained using single-crystal XRD. From this study we concluded that the complexes with acylthioureato ligands that bear aromatic acyl substituents might at least have three possible low energy conformations in methanol as evidenced by the three platinum species observed in their ^{195}Pt-NMR spectra at -50 °C, with the "open" conformation being the most stable at ambient temperature. However, with complexes that do not have acylthioureato ligands bearing aromatic acyl substituents, at least one solution conformation was possible. This finding may be attributed to the various ways in which the aromatic moieties of the two acylthioureato and the phenanthroline ligands may interact via π-stacking and hydrogen bonding interactions involving the solvent resulting in low energy conformations, which is not possible in the case of complexes where the acylthioureato ligands do not have aromatic substituents. The absence of the "half-closed" and the "closed" sandwich conformations, at ambient temperatures and higher, suggest that the intramolecular π-π stacking interactions that stabilise those conformations might not persist in solution at these temperatures. This study is still under investigation with regards to the unambiguous assignment of the three signals observed in the ^{195}Pt-NMR spectra at -50 °C through the use of theoretical calculations of the DFT-B3LYP-GIAO configuration.

After complete characterisations of the complexes, efforts were directed at establishing whether the electronic influence of acyl substituents was the driving factor, deriving possible mechanistic insights into this monodentate coordination of disubstituted acylthioureato ligands in [Pt(phen)(L^n-κ*S*)$_2$] complexes. The reactivity of nucleophilic sites in the acylthioureato ligands varying only on the acyl substituents was probed using conceptual DFT to establish whether the electronic effects of these substituents had any influence on the nucleophilicity of possible donor sites in the ligands. The results

showed that the most reactive donor site was sulfur as the largest HOMO lobe was on sulfur regardless of the acyl substituents (from electron-donating to electron-withdrawing). The Fukui function for the nucleophilic attack was tenfold greater on sulfur than on the other donor sites (oxygen and nitrogen) also indicating the most reactive nucleophilic site in these ligands regardless of acyl substituents. This finding prompted the investigation into the reaction conditions as they also have a significant role in directing reactions.

A series of reactions were performed that pointed out the most critical steps during the synthesis of [Pt(phen)(L^n-κ*S*)$_2$] complexes. Since our synthetic protocols involved reactants in heterogeneous phases (solid and solution), we wondered whether the reactions were happening in solution or on the surface of the solid reactant ([$PtCl_2$(phen)]). Attempts were made to unravel this ambiguity. Using the one-pot synthesis method, with a suspension of [$PtCl_2$(phen)] in methanol being added to a methanol solution of the ligand and sodium acetate at different rates (added at once, added over 15 minutes and added over 30 minutes) and heating the mixture to reflux, no significant change in the rate and yields was observed. However, when the precursor [$PtCl_2$(phen)] was reacted with neutral disubstituted acylthiourea ligands in methanol with varying amounts of water (distilled MeOH, 99.9% MeOH and 85% MeOH), were the rate reaction to completion changed significantly as; > 22 hrs in distilled MeOH, 2.5 hrs in 99.9% MeOH and 40 minutes in 85% MeOH. An increase in the water content of the solvent increased the rate of solvolysis of the precursor since water is a good coordinating solvent, thereby increasing the overall rate for the substitution reaction. These findings suggest the reactions were happening mainly in solution. These results also highlighted two things; (i) that solvents, particularly suitable coordinating solvents, are essential for this reaction through a solvolysis step as alluded to by subsequent analyses of the solution species of the precursor (solvento complex) and (ii) to some extent the importance of the ligand deprotonation step.

Deprotonation of the acylthioureato ligand was proven key when the reaction protocol changed to a stepwise synthesis deprotonating the ligand with sodium hydride. This experiment produced many anionic ligand species in solution that substituted the solvent in the solvento complex to get the desired [Pt(phen)(L^n-κ*S*)$_2$] complex across all ligands *via* an anation type of reaction. Other bases only produced small quantities of the deprotonated ligand species in solution *via* an equilibrium that disfavours the neutral disubstituted acylthiourea ligand species since these ligands are very weak acids.

Attempts were made to get insights into the interconvertibility between the [Pt(phen)(L^n-κ*S*)$_2$] complexes and the by-product of the synthesis [Pt(phen)(L^n-κ*O*,*S*)]$^+$ complexes, in order to understand the stability of our complexes of interest as well as finding other routes of getting the [Pt(phen)(L^n-κ*S*)$_2$] complexes. [Pt(phen)(L^n-κ*S*)$_2$] complexes were found to decompose under acidic conditions to different decomposition products depending on the acid used. Weak acids like acetic acid resulted in the decomposition to [Pt(phen)(L^n-κ*O*,*S*)]$^+$ and free ligand. Strong acids like hydrochloric acid resulted in

the total decomposition to a $[PtCl(phen)(HL^n\text{-}\kappa S)]^+$ complex and free ligand; while, nitric acid only resulted in the protonation of the acylthioureato ligands to give $[Pt(phen)(HL^n\text{-}\kappa S)_2]^{2+}$ complexes. These acids reacted with $[Pt(phen)(L^n\text{-}\kappa S)_2]$ complexes firstly by protonating the highly basic sites in the acylthioureato ligands followed by chelate ring closure or anation or no further reaction depending on the coordinating strength of the acid's conjugate base. Conversion of the by-product $[Pt(phen)(L^n\text{-}\kappa O,S)]^+$ to $[Pt(phen)(L^n\text{-}\kappa S)_2]$ was successful presumably via chelate ring opening.

Extrapolation of the monodentate coordination of disubstituted acylthioureato ligands to complexes bearing different co-ligands or metal centres was attempted and was not successful with other metal centres to date, but proved successful when bipyridine (bipy) and triphenylphosphine (PPh_3) were used as co-ligands giving complexes $[Pt(bipy)(L^{10}\text{-}\kappa S)_2]$ and $[Pt(PPh_3)(L^1\text{-}\kappa O,S)(L^1\text{-}\kappa S)]$ respectively only in low to moderate yields. The different metal precursors tried ($[PdCl_2(phen)]$ and $[CoCl_2(phen)]$) might have failed because $[PdCl_2(phen)]$ could easily lose the 1,10-phenanthroline ligand while $[CoCl_2(phen)]$ could easily expand its coordination sphere from four coordinate to six-coordinate through chelation.

5.2. Evaluation of the antiproliferative activity of $[Pt(phen)(L^1\text{-}\kappa S)_2]$ and $[Pt(phen)(L^2\text{-}\kappa S)_2]$

The secondary aim of this thesis was to evaluate the antiproliferative activity of $[Pt(phen)(L^1\text{-}\kappa S)_2]$ and $[Pt(phen)(L^2\text{-}\kappa S)_2]$ as a pilot experiment for potential further study. It was found out that the two complexes were highly active against an A549 lung cancer line with IC_{50} values of 6.43 ± 0.94 and 2.39 ± 0.33 respectively, killing the cancer cells *via* apoptotic cell death. $[Pt(phen)(L^2\text{-}\kappa S)_2]$ was almost threefold more effective in killing cancer cells than $[Pt(phen)(L^1\text{-}\kappa S)_2]$ which could potentially be attributed to better cellular uptake as a result of the extended hydrophobic butyl chain. Furthermore, an investigation on the potential mode of interaction of $[Pt(phen)(L^1\text{-}\kappa S)_2]$ with the DNA using molecular docking, showed that the complex preferably interacted as a major groove binder with an A=T rich region of DNA. These remarkable results encourage a further investigation with a more extensive library of complexes.

5.3. Future Prospects

The current study remarkably describes synthetic and mechanistic insights into the monodentate coordination of *N*,*N*-di(alkyl/aryl)-*N*'-acylthioureato ligands with platinum(II) ions in $[Pt(phen)(L^n\text{-}\kappa S)_2]$ complexes. This system can be extended to other complexes as was shown with complexes bearing different co-ligands. We also positively think that the monodentate coordination of disubstituted acylthioureato ligands can as well be extrapolated into complexes with varying metal centres although our first attempts failed. This monodentate coordination of acylthioureato ligands may be achieved by

carefully choosing metal precursors that will be strongly coordinated on three, four or five coordination sites leaving only one on two sites available to accommodate one or two acylthioureato ligands in a monodentate fashion. Currently, further studies are directed support assignments of the three platinum resonances observed at -50 °C for the complexes with acylthioureato ligands bearing aromatic acyl substituents.

The applicability outcome of this study revealed that these complexes could serve as a lead for the development of new antiproliferative agents. Further investigations into the complex-DNA interactions, cellular uptake potential, *in-vivo* complex stabilities and water solubility improvements should be conducted to gain insight into the structure-activity relationships of these complexes, on a more extensive library of complexes.

Above all, this research was based on the synthesis of [Pt(phen)(L^n-κ*S*)$_2$] complexes, where the disubstituted acylthioureato ligands coordinated in a monodentate fashion, and evaluation of the factors that could have influence on this coordination behaviour. It was also aimed at performing preliminary anti-proliferative tests on a select of these complexes. The aims were successfully achieved as evidenced by the successful synthesis of the [Pt(phen)(L^n-κ*S*)$_2$] complexes for all the ligand variations. The concentration of the deprotonated ligand in solution was found to be the major contributing factor in achieving this coordination mode. Preliminary anti-proliferative tests were encouraging as the tested complexes were shown to be active against the A549 cancer cell line.

Supplementary Information

Appendix 1. ^{1}H-NMR and FT-IR spectroscopy data for [Pt(phen)(L^{n}-κ*S*)$_2$] complexes

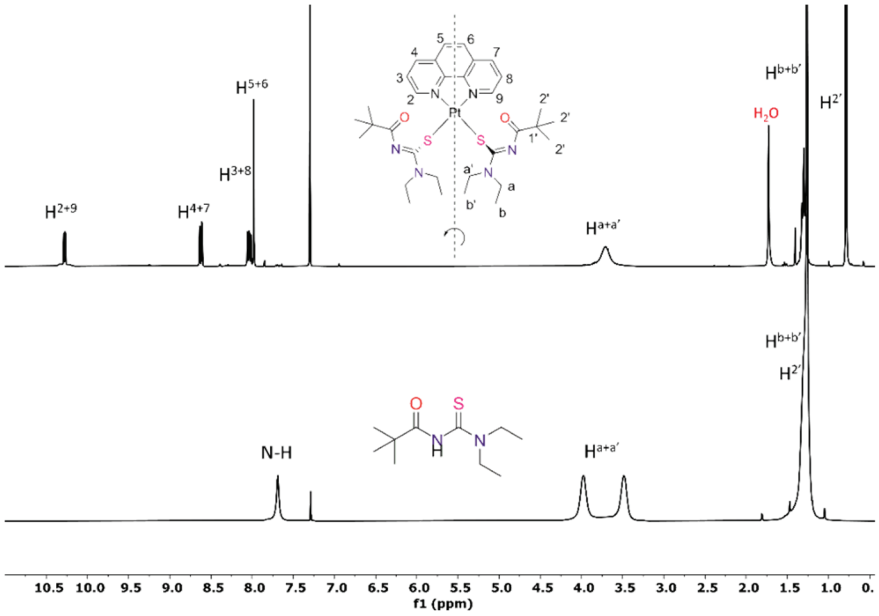


*Figure A1-1: Assigned stacked ^{1}H-NMR spectra for [Pt(phen)(L^{16}-κ*S*)$_2$] and HL^{16} complete with a numbering scheme.*

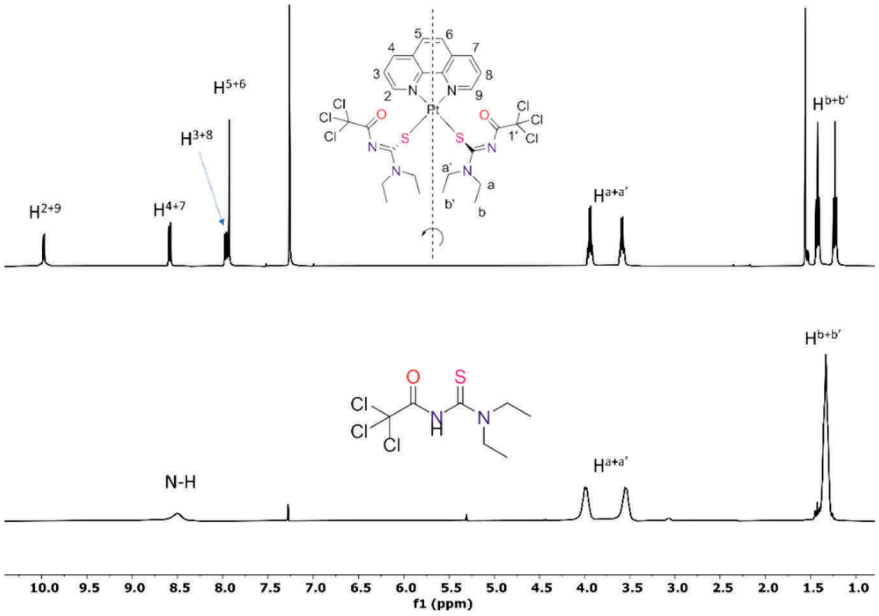


*Figure A1-2: Assigned stacked ^{1}H-NMR spectra for [Pt(phen)(L^{9}-κ*S*)$_2$] and HL^{9} complete with a numbering scheme.*

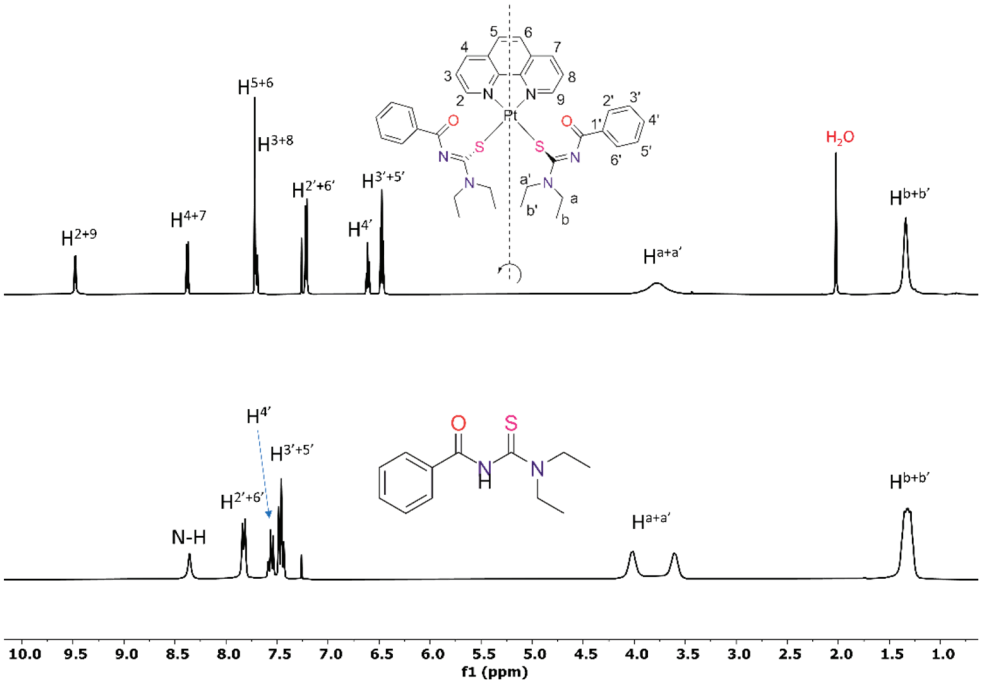


Figure A1-3: Assigned stacked ^{1}H-NMR spectra for [Pt(phen)(L^{3}-κS)$_2$] and HL^{3} complete with a numbering scheme.

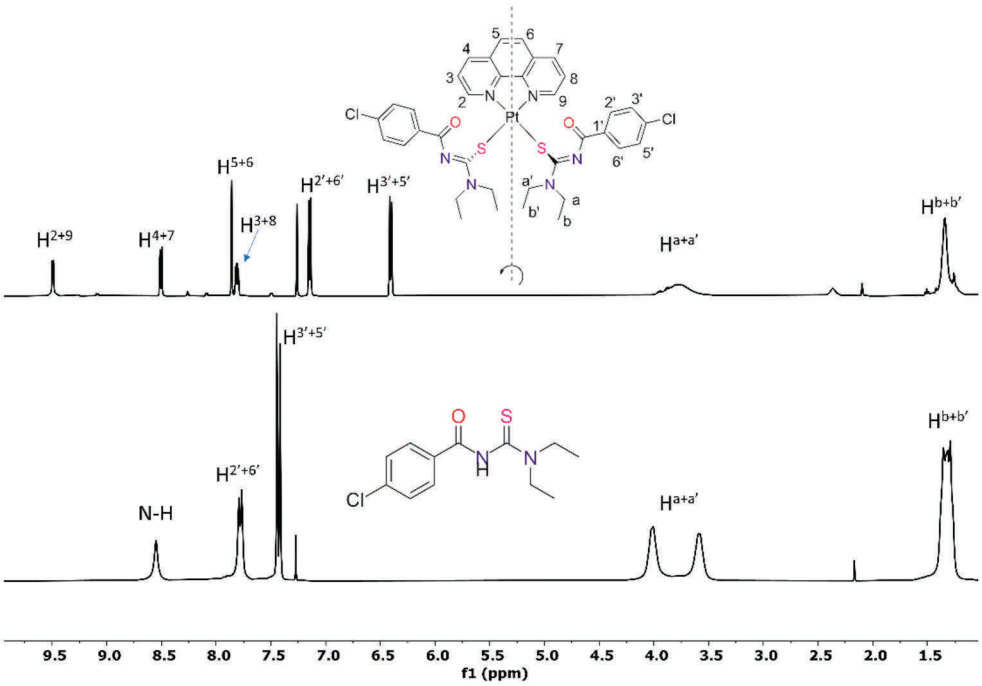


Figure A1-4: Assigned stacked ^{1}H-NMR spectra for [Pt(phen)(L^{12}-κS)$_2$] and HL^{12} complete with a numbering scheme.

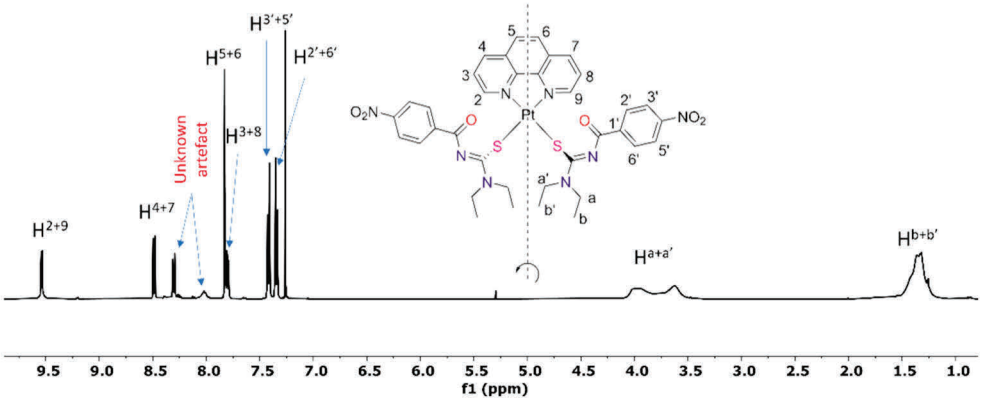


Figure A1-5: Assigned [1]H-NMR spectra for [Pt(phen)(L[14]-κS)$_2$] and HL[14] complete with a numbering scheme.

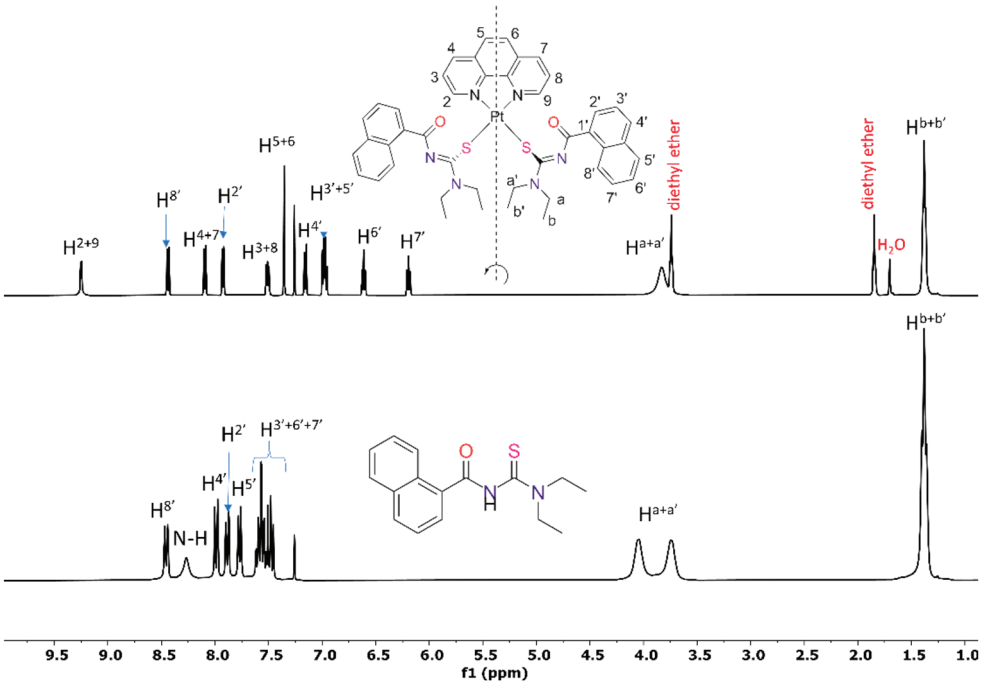


Figure A1-6: Assigned stacked [1]H-NMR spectra for [Pt(phen)(L[1]-κS)$_2$] and HL[1] complete with a numbering scheme.

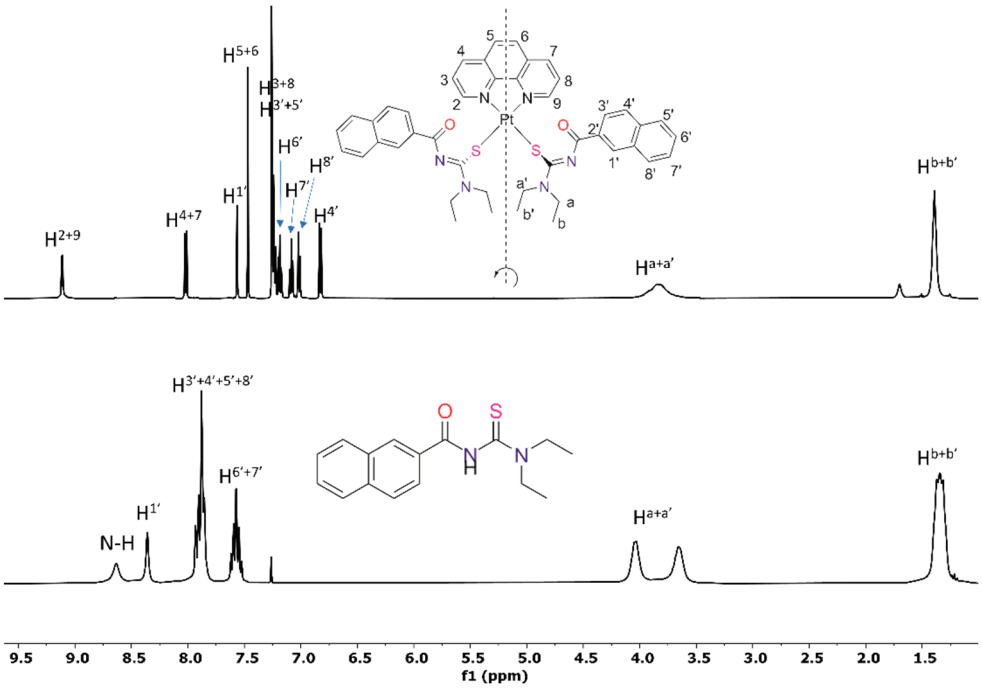


Figure A1-7: Assigned stacked ^{1}H-NMR spectra for [Pt(phen)(L^{10}-κS)$_2$] and HL^{10} complete with a numbering scheme.

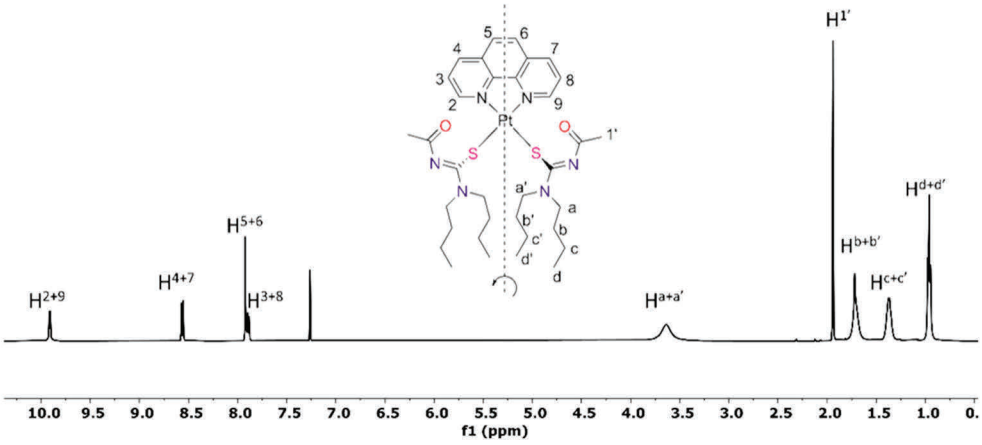


Figure A1-8: Assigned stacked ^{1}H-NMR spectra for [Pt(phen)(L^{6}-κS)$_2$] and HL^{6} complete with a numbering scheme.

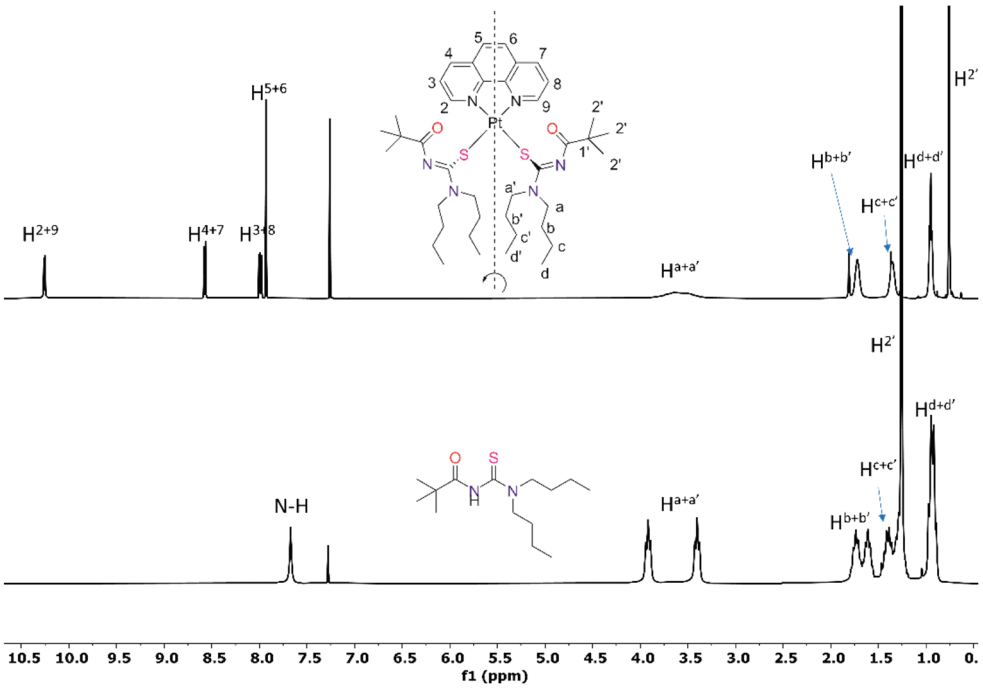


Figure A1-9: Assigned stacked ^{1}H-NMR spectra for [Pt(phen)(L^{8}-κS)$_2$] and HL^{8} complete with a numbering scheme.

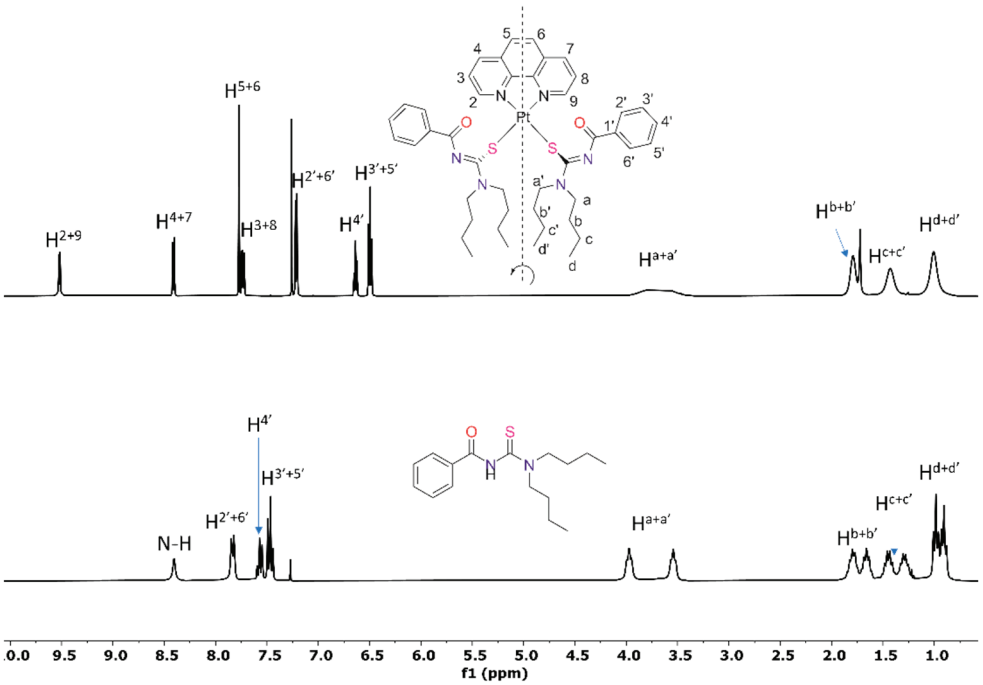


Figure A1-10: Assigned stacked ^{1}H-NMR spectra for [Pt(phen)(L^{4}-κS)$_2$] and HL^{4} complete with a numbering scheme.

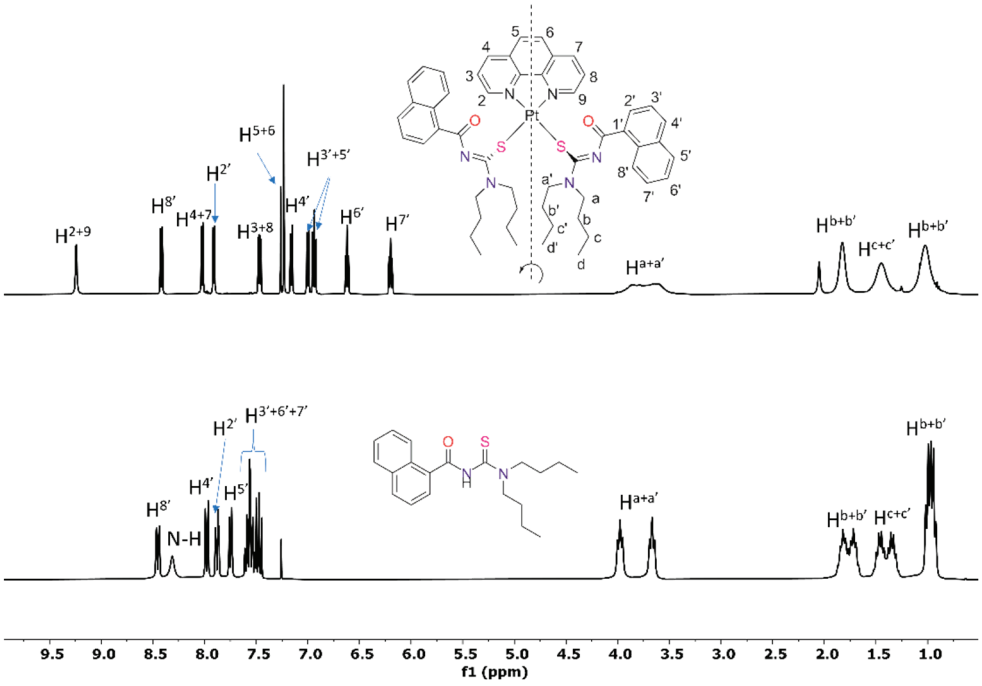


Figure A1-11: Assigned stacked ^{1}H-NMR spectra for [Pt(phen)(L^{2}-κS)$_2$] and HL^{2} complete with a numbering scheme.

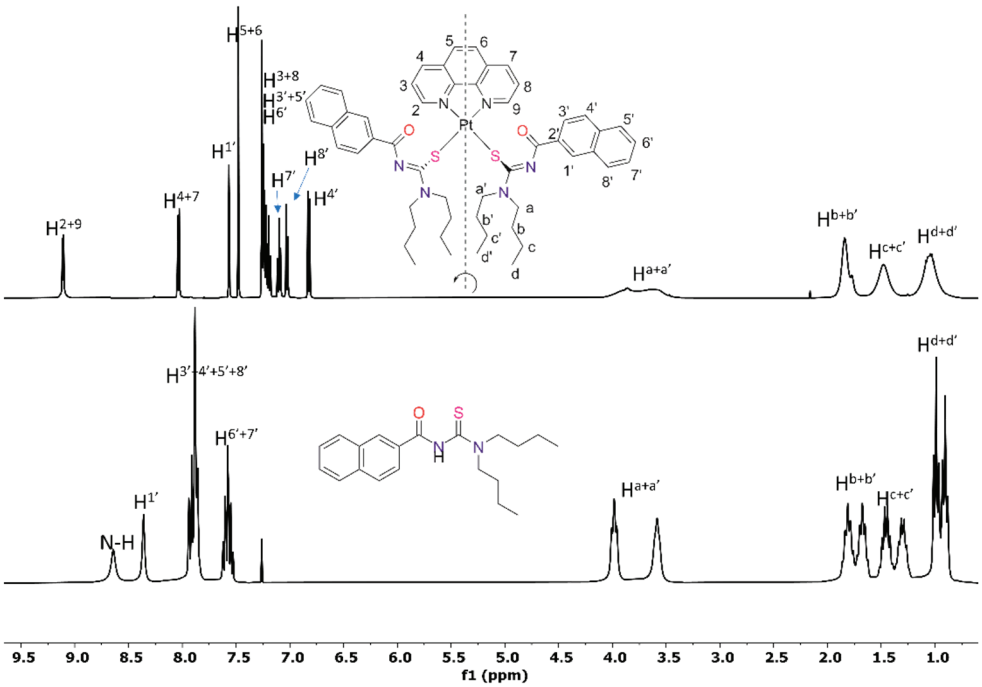


Figure A1-12: Assigned stacked ^{1}H-NMR spectra for [Pt(phen)(L^{11}-κS)$_2$] and HL^{11} complete with a numbering scheme.

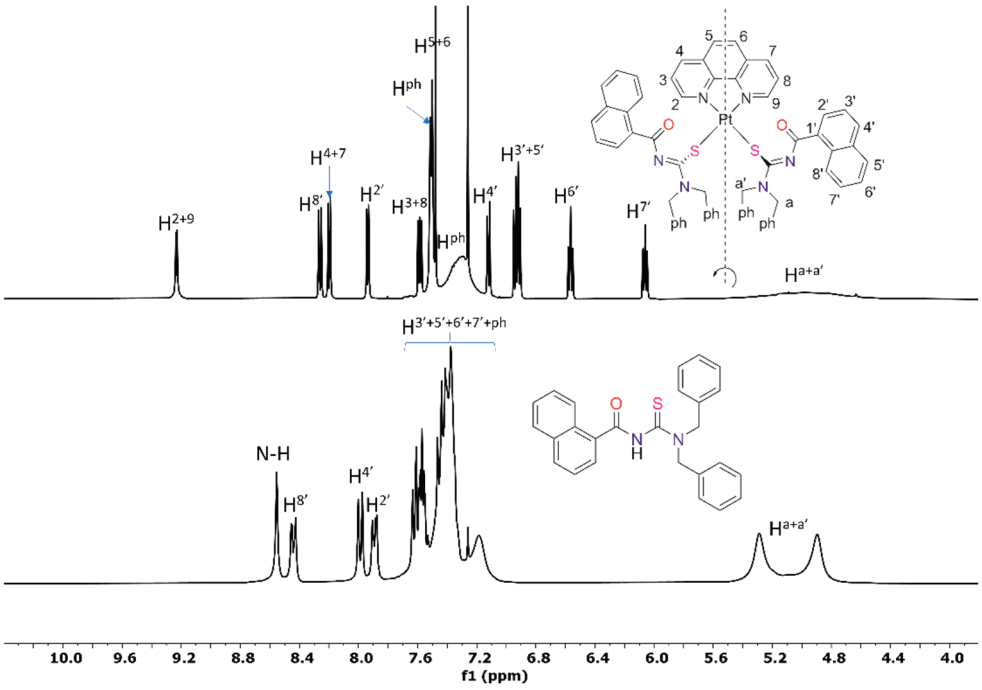


Figure A1-13: Assigned stacked ^{1}H-NMR spectra for [Pt(phen)(L^{15}-κS)$_2$] and HL^{15} complete with a numbering scheme.

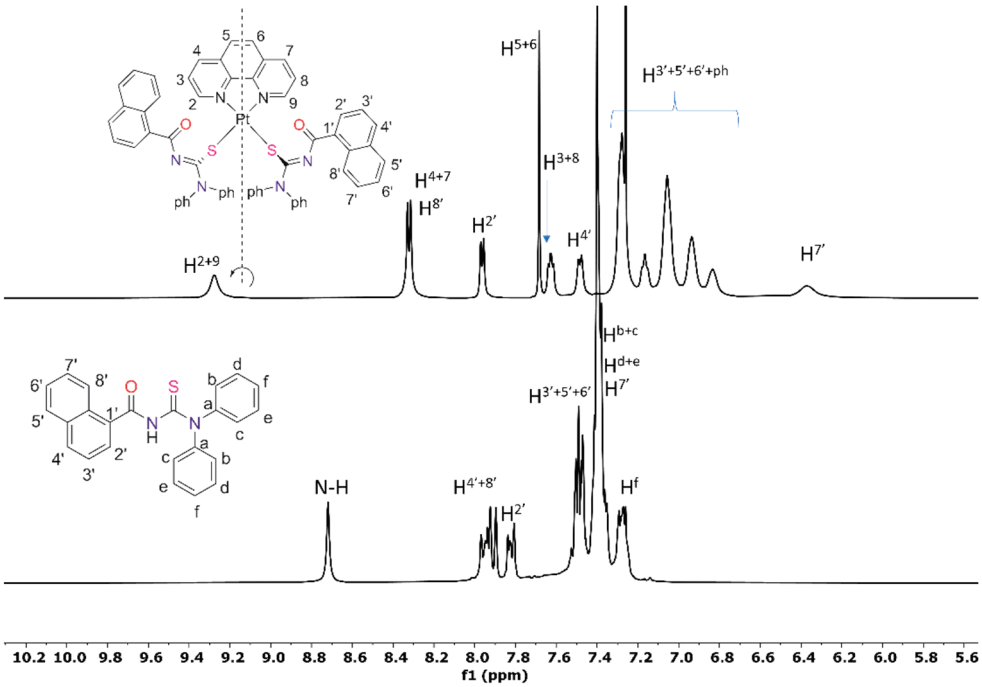


Figure A1-14: Assigned stacked ^{1}H-NMR spectra for [Pt(phen)(L^{16}-κS)$_2$] and HL^{16} complete with a numbering scheme.

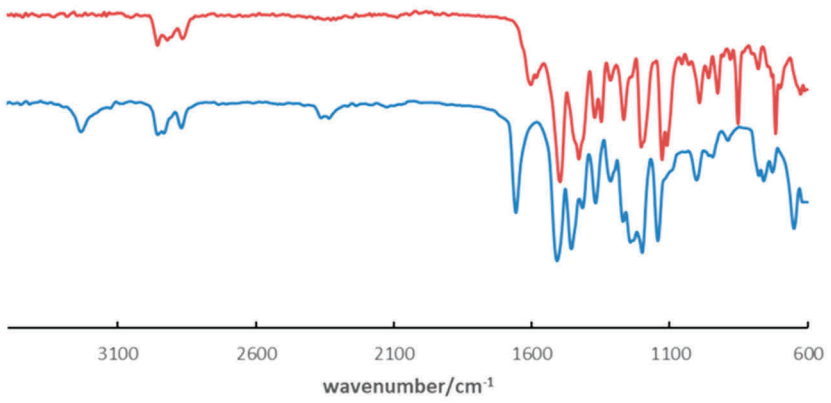


Figure A1-15: Stacked FT-IR spectra for [Pt(phen)(L^6-κS)$_2$] and HL^6.

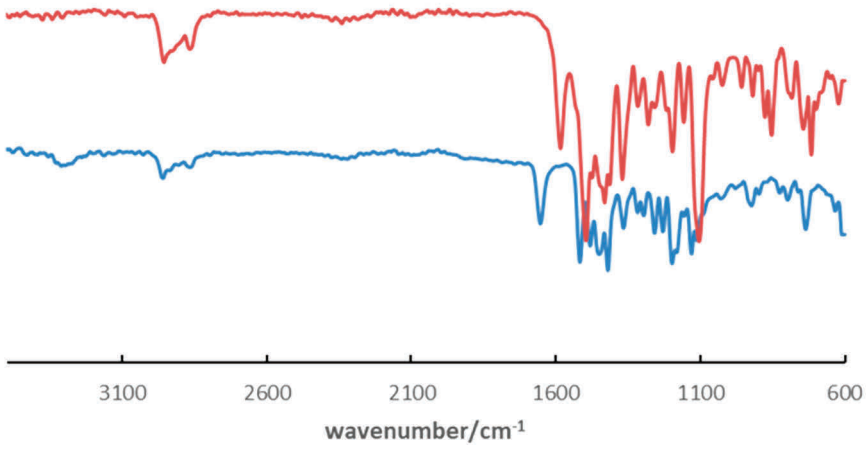


Figure A1-16: Stacked FT-IR spectra for [Pt(phen)(L^8-κS)$_2$] and HL^8.

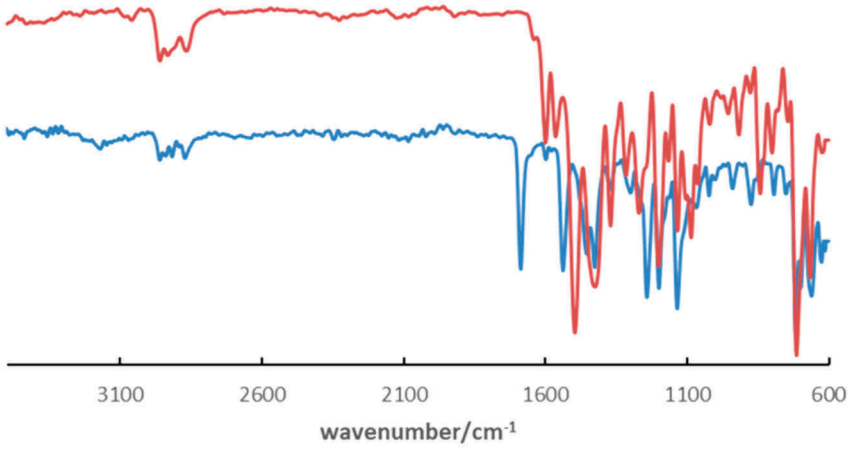


Figure A1-17: Stacked FT-IR spectra for [Pt(phen)(L^4-κS)$_2$] and HL^4.

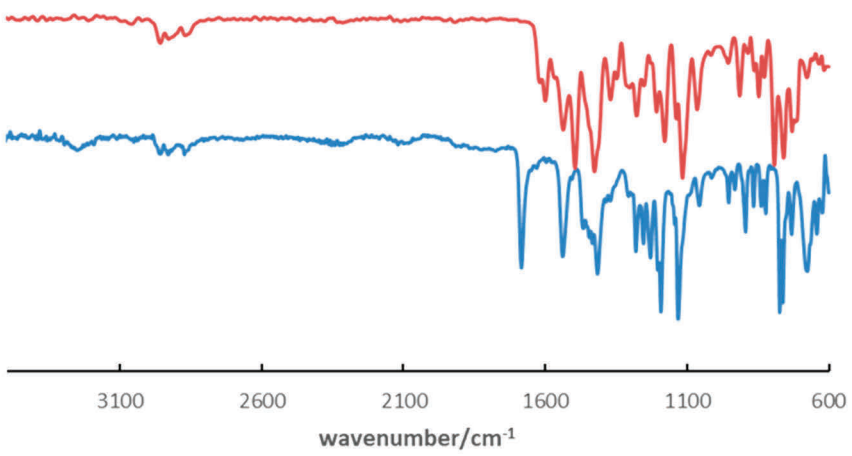


Figure A1-18: Stacked FT-IR spectra for [Pt(phen)(L^{11}-κS)$_2$] and HL^{11}.

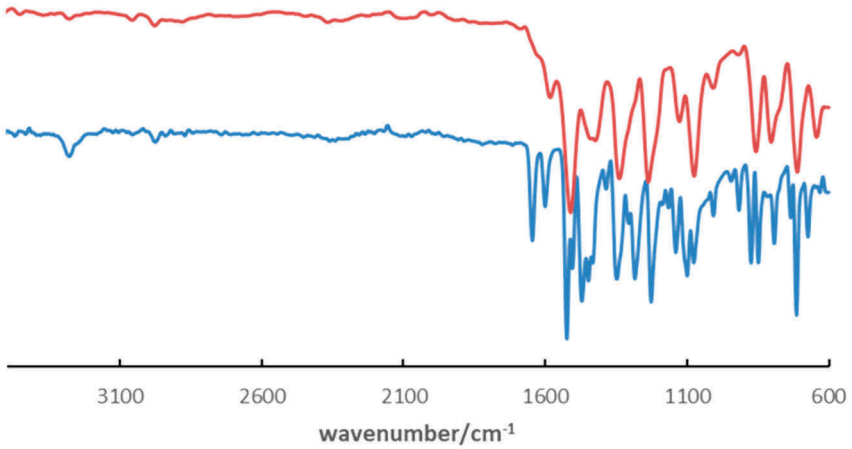


Figure A1-19: Stacked FT-IR spectra for [Pt(phen)(L^{14}-κS)$_2$] and HL^{14}.

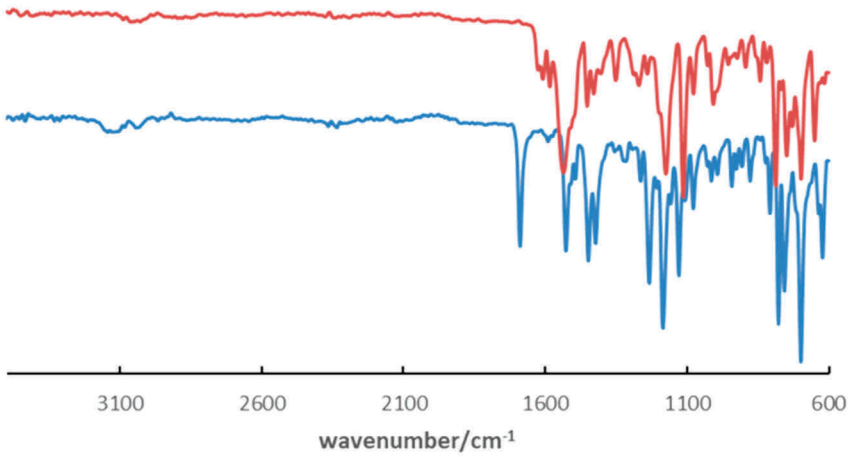


Figure A1-20: Stacked FT-IR spectra for [Pt(phen)(L^{15}-κS)$_2$] and HL^{15}.

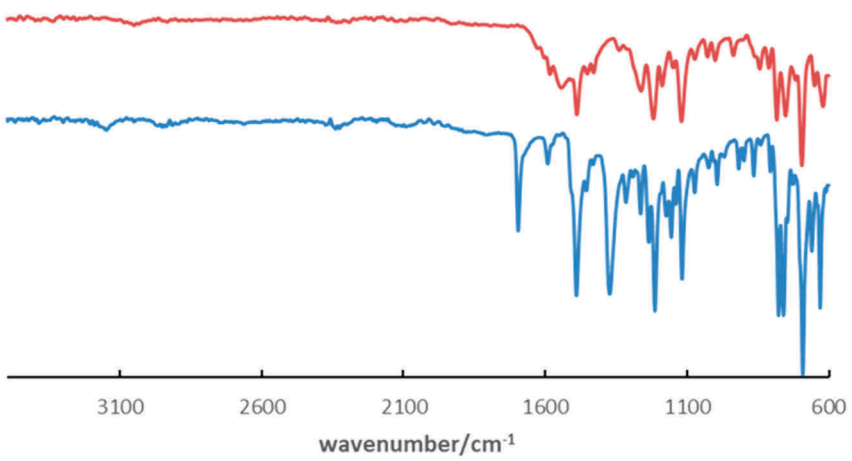


Figure A1-21: Stacked FT-IR spectra for [Pt(phen)(L^{16}-κS)$_2$] and HL^{16}.

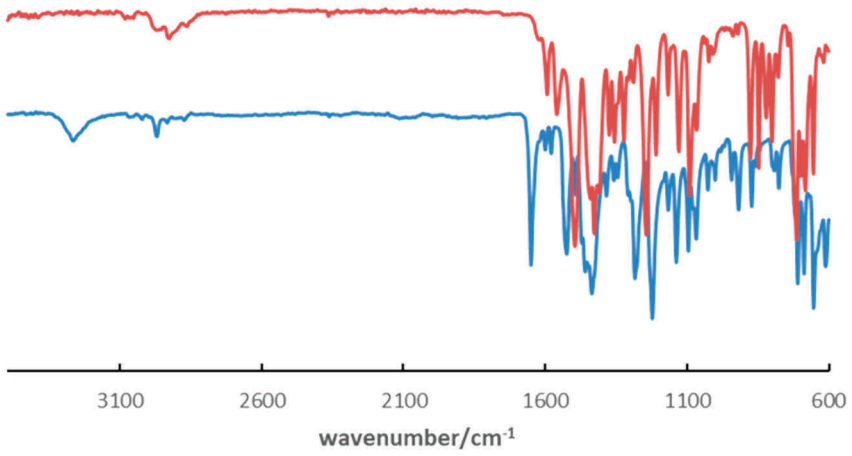


Figure A1-22: Stacked FT-IR spectra for [Pt(phen)(L^{3}-κS)$_2$] and HL^{3}.

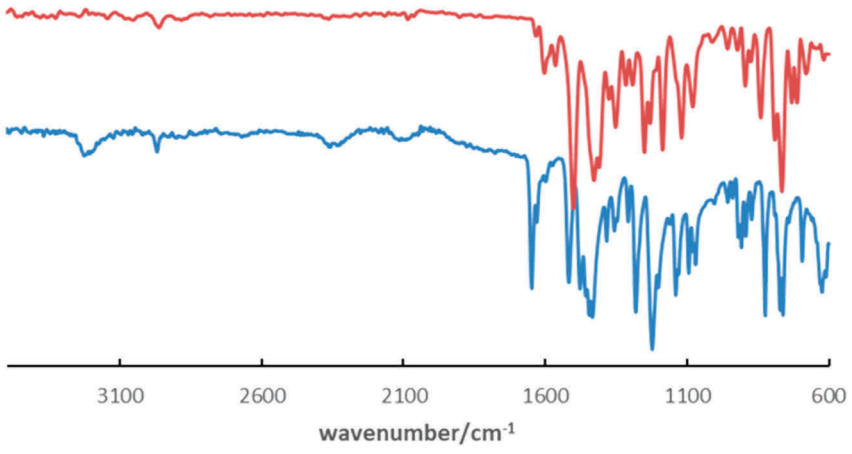


Figure A1-23: Stacked FT-IR spectra for [Pt(phen)(L^{10}-κS)$_2$] and HL^{10}.

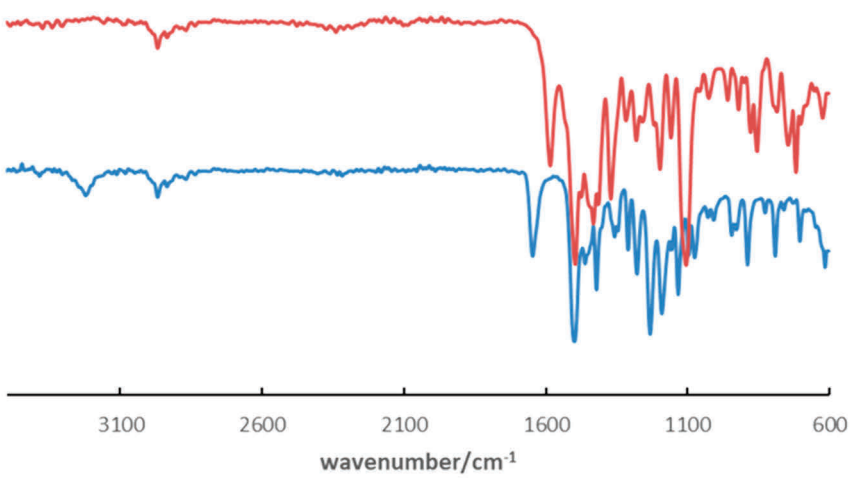


Figure A1-24: Stacked FT-IR spectrum for [Pt(phen)(L^7-κS)$_2$] and HL^7.

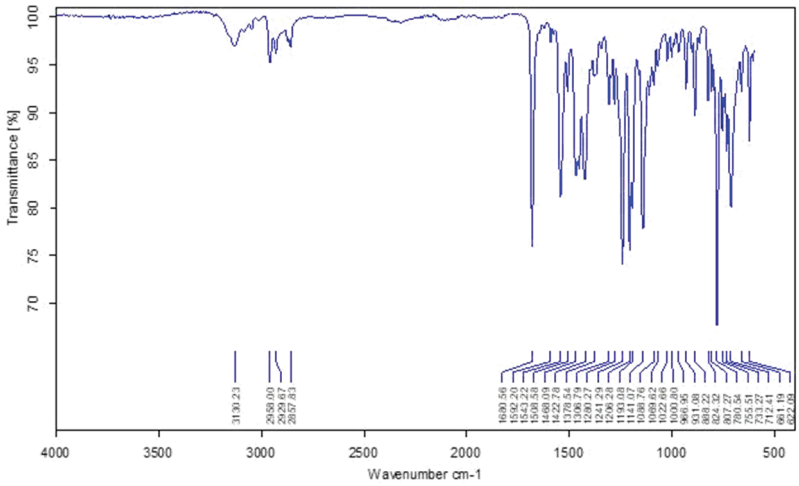


Figure A1-25a: FT-IR spectrum for HL^2.

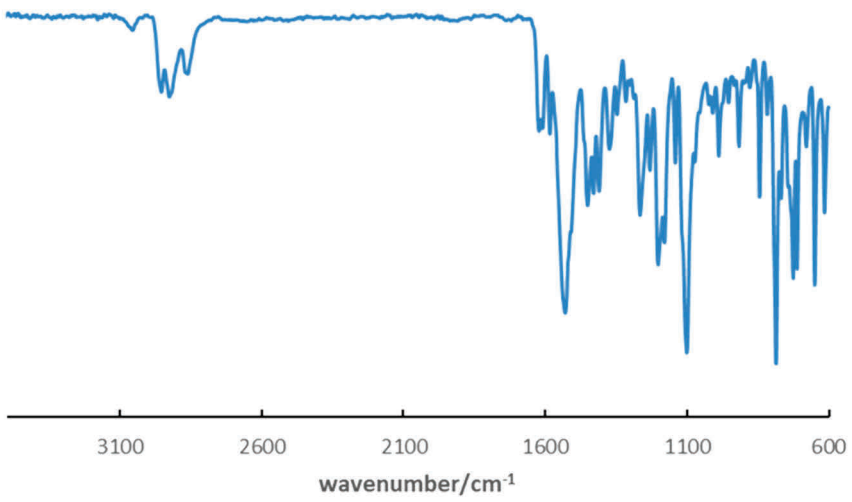


Figure A1-25b: FT-IR spectrum for [Pt(phen)(L^2-κS)$_2$].

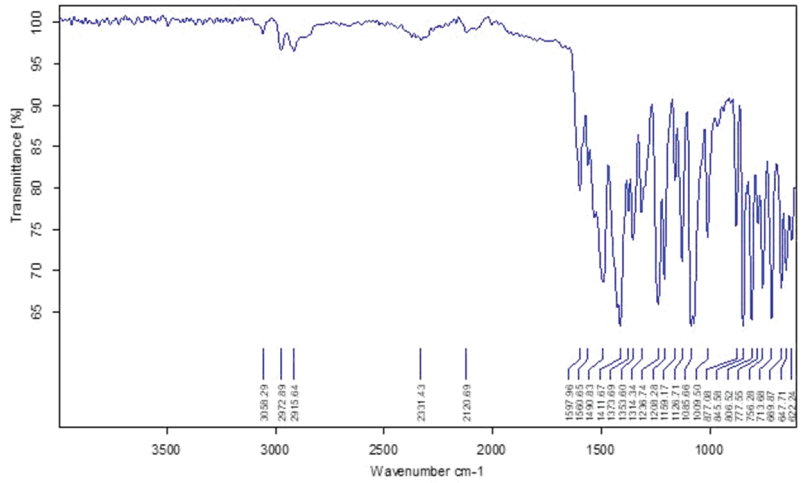


Figure A1-26a: FT-IR spectrum for HL^{12}.

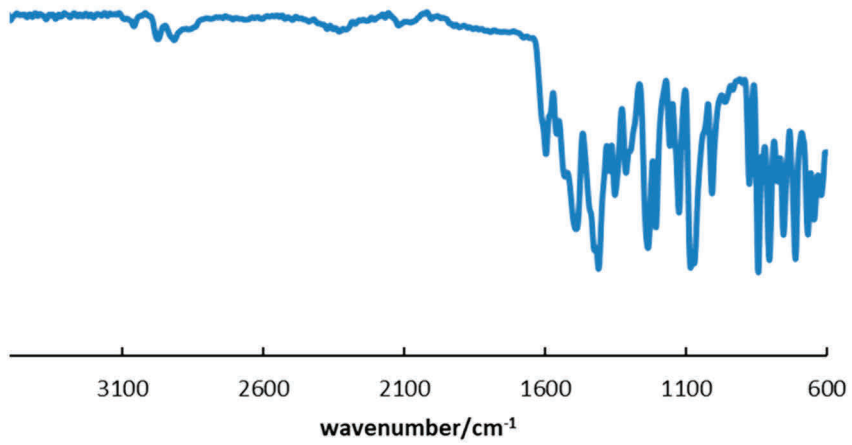


Figure A1-26b: FT-IR spectrum for $[Pt(phen)(L^{12}\text{-}\kappa S)_2]$.

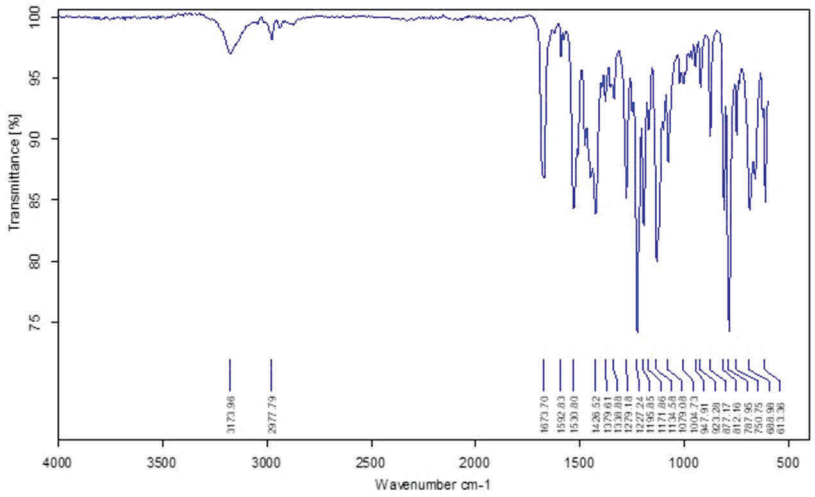


Figure A1-27a: FT-IR spectrum for HL[1].

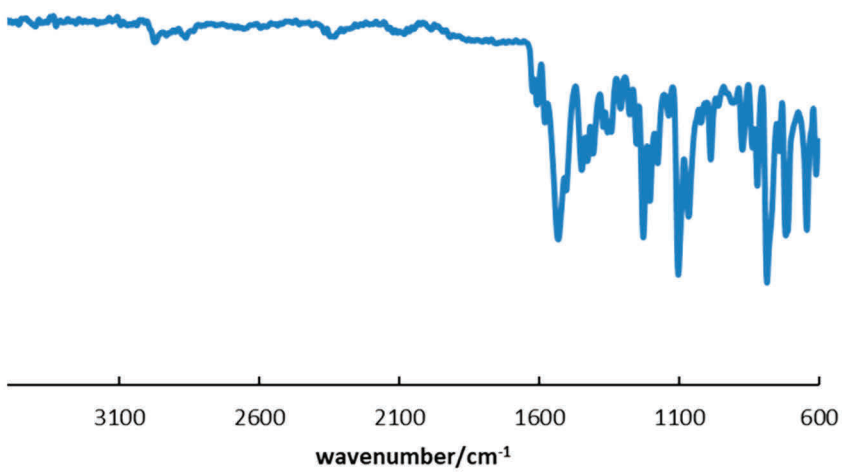


Figure A1-27b: FT-IR spectrum for [Pt(phen)(L[1]-κS)$_2$].

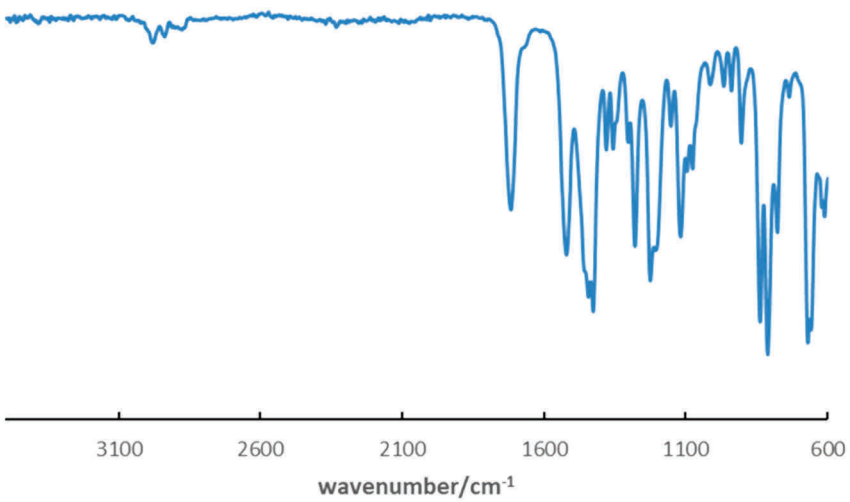


Figure A1-28a: FT-IR spectrum for HL[9].

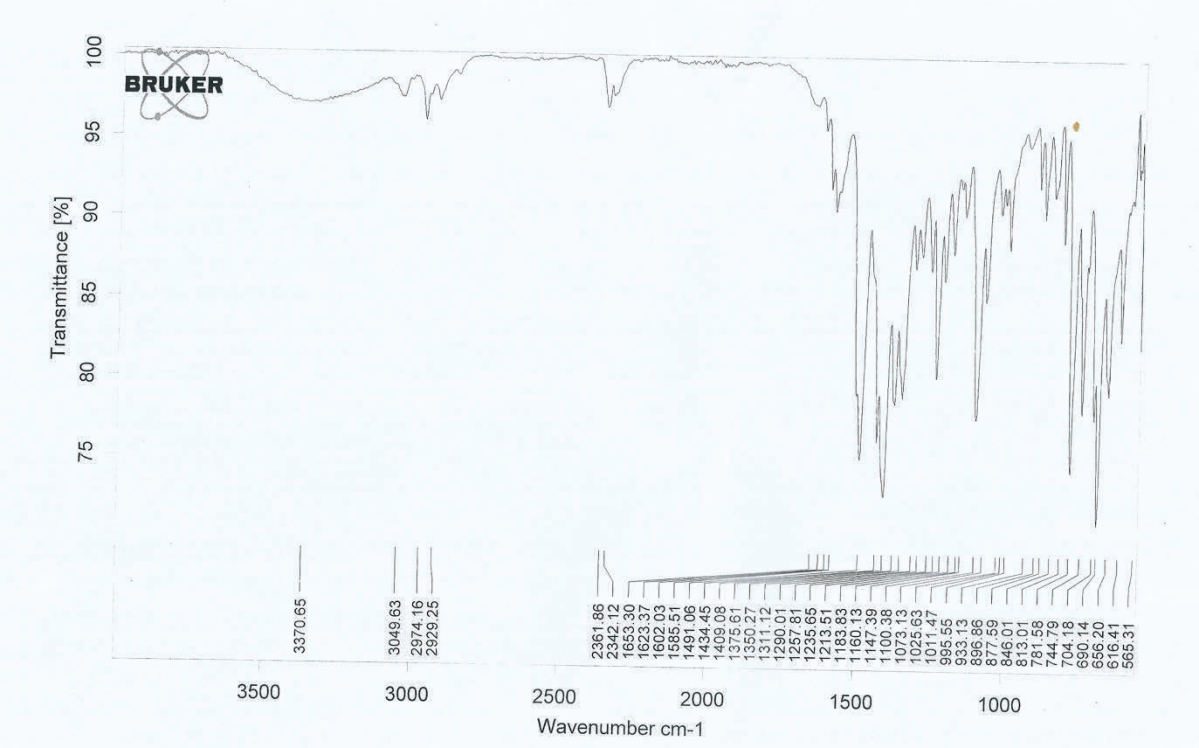


Figure A1-28b: FT-IR spectrum for [Pt(phen)(L^9-κS)$_2$].

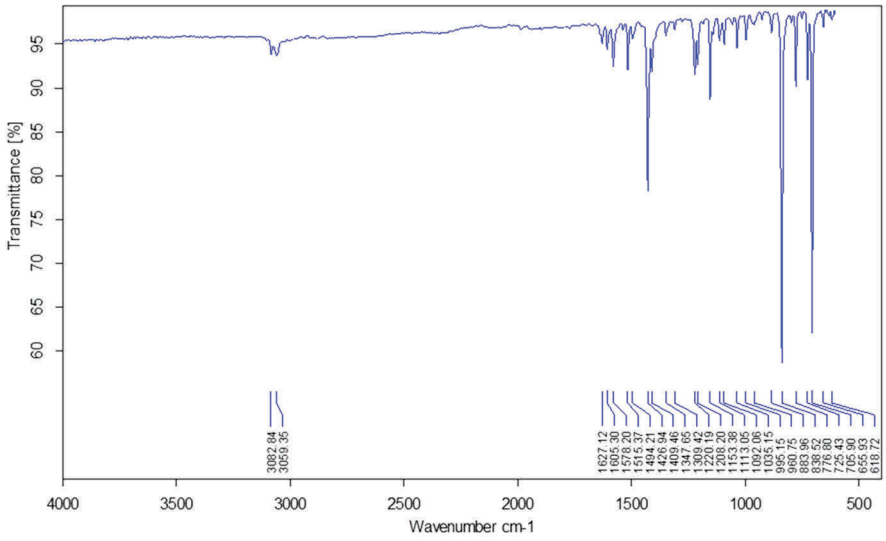


Figure 1A1-29: FT-IR spectrum for [PtCl$_2$(phen)].

Appendix 2. Uv-vis spectrophotometry and MS data for [Pt(phen)(L^n-κ*S*)$_2$] complexes

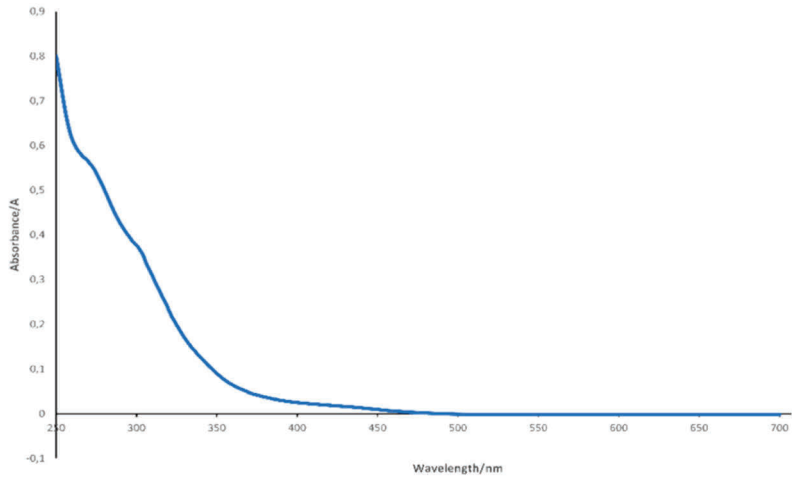


*Figure A2-1: Uv-vis spectrum for [Pt(phen)(L^{11}-κ*S*)$_2$] in methanol.*

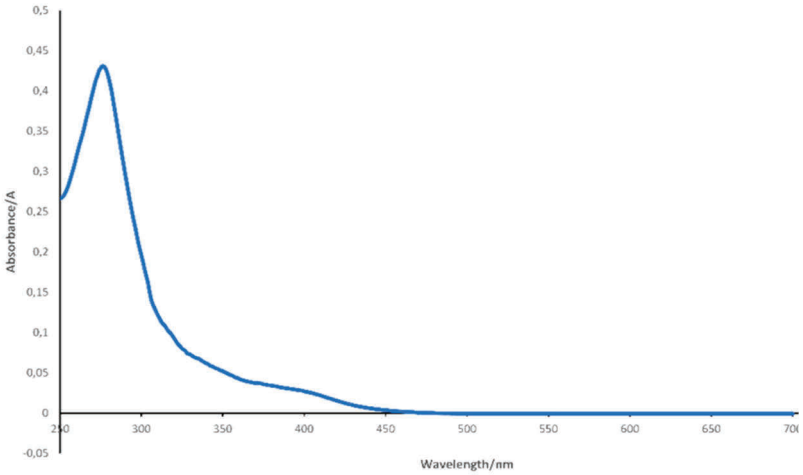


*Figure A2-2: Uv-vis spectrum for [Pt(phen)(L^6-κ*S*)$_2$] in methanol.*

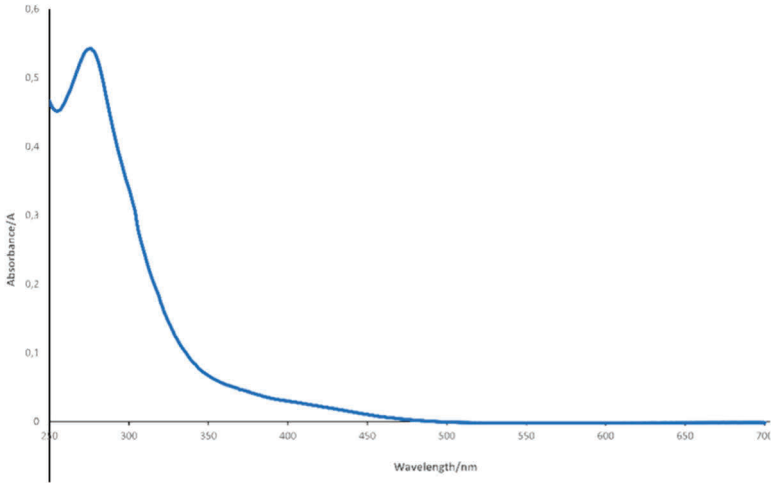


Figure A2-3: Uv-vis spectrum for [Pt(phen)(L^4-κS)$_2$] in methanol.

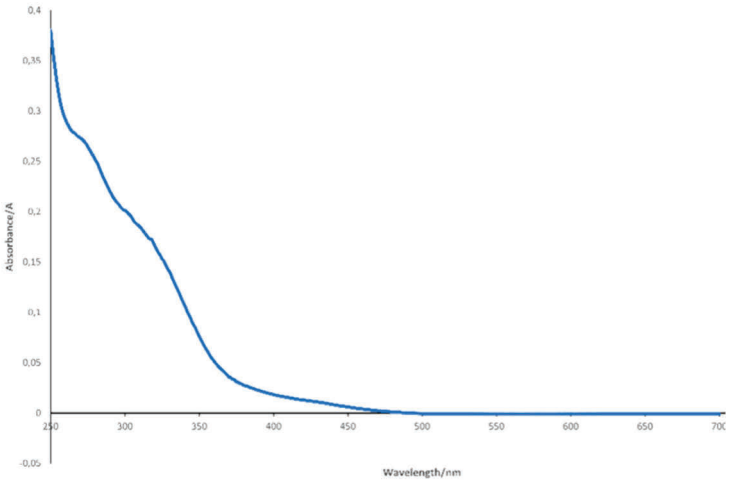


Figure A2-4: Uv-vis spectrum for [Pt(phen)(L^{15}-κS)$_2$] in methanol.

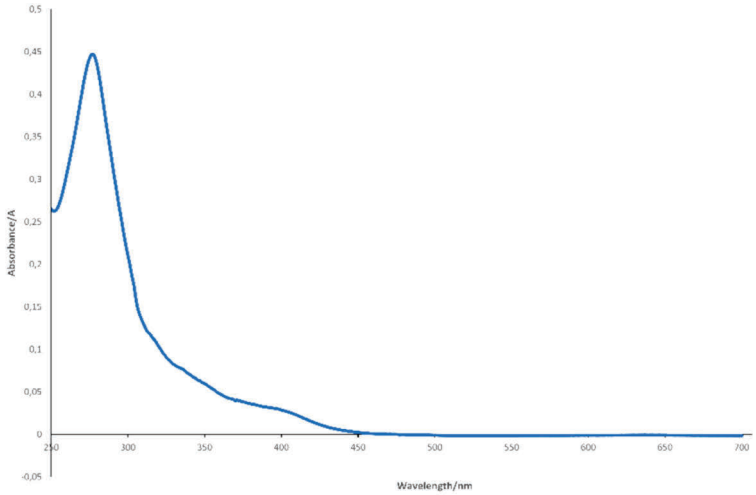


Figure A2-5: Uv-vis spectrum for [Pt(phen)(L^8-κS)$_2$] in methanol.

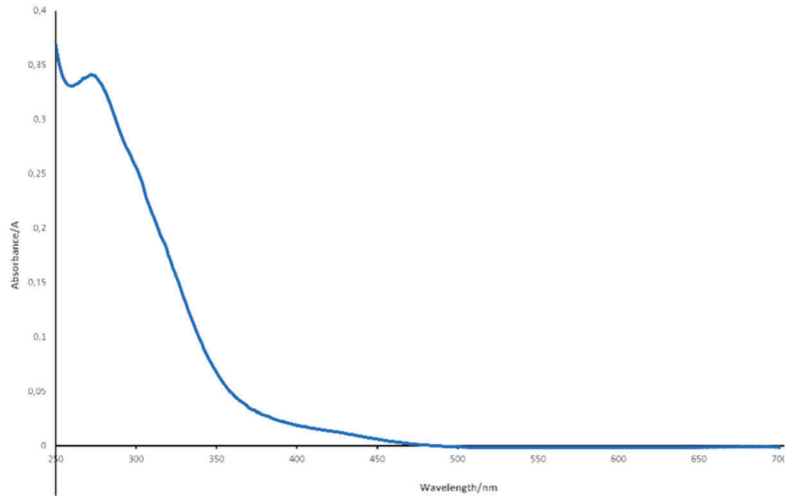


Figure A2-6: Uv-vis spectrum for [Pt(phen)(L^1-κS)$_2$] in methanol.

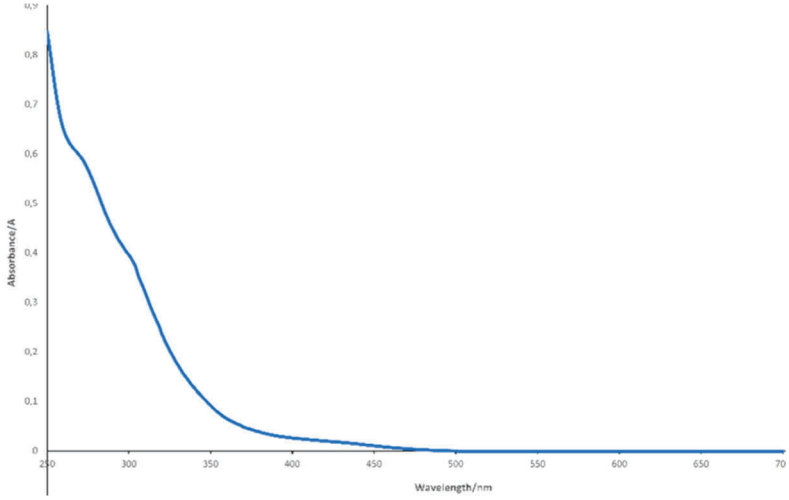


Figure A2-7: Uv-vis spectrum for [Pt(phen)(L^{10}-κS)$_2$] in methanol.

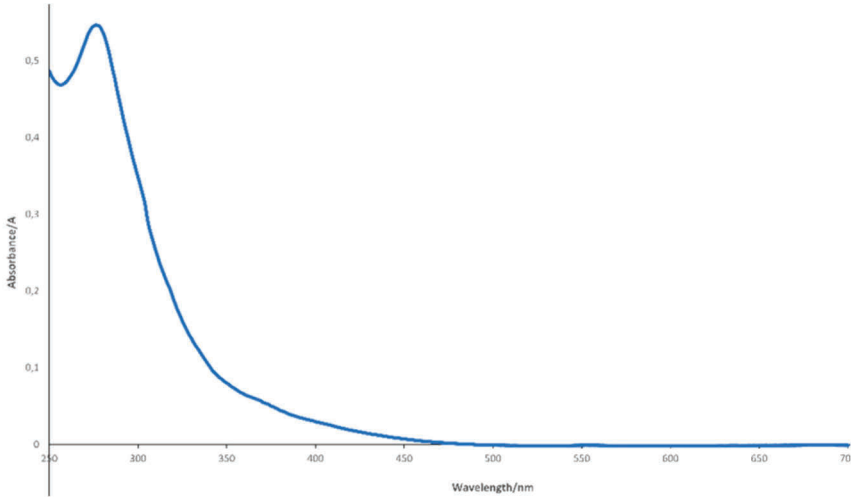


Figure A2-8: Uv-vis spectrum for [Pt(phen)(L^{12}-κS)$_2$] in methanol.

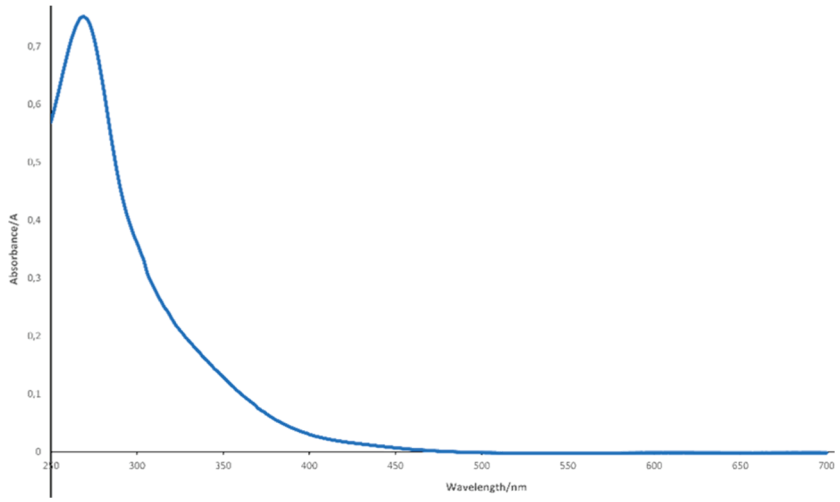


Figure A2-9: Uv-vis spectrum for [Pt(phen)(L^{14}-κS)$_2$] in methanol.

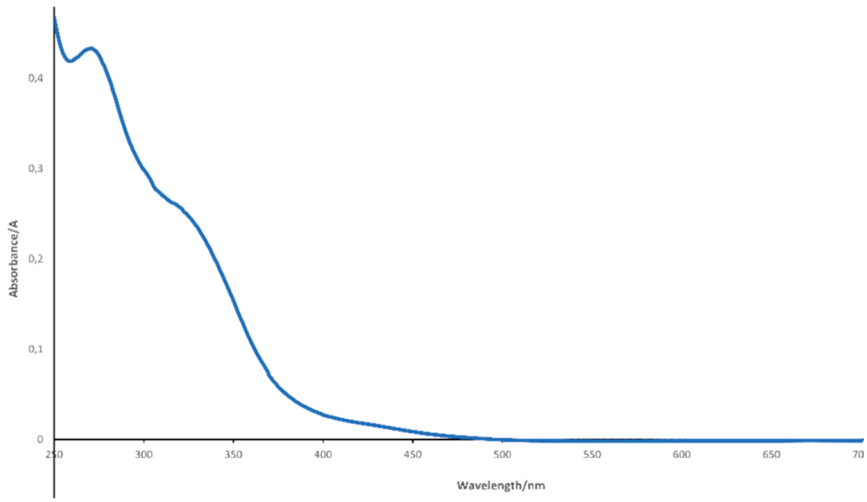


Figure A2-10: Uv-vis spectrum for [Pt(phen)(L^{16}-κS)$_2$] in methanol.

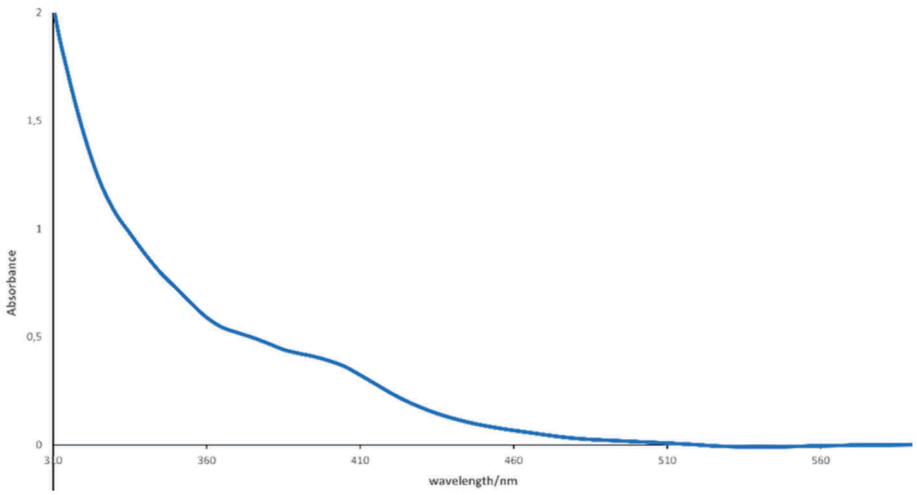


Figure A2-11: Uv-vis spectrum for [Pt(phen)(L^{7}-κS)$_2$] in methanol.

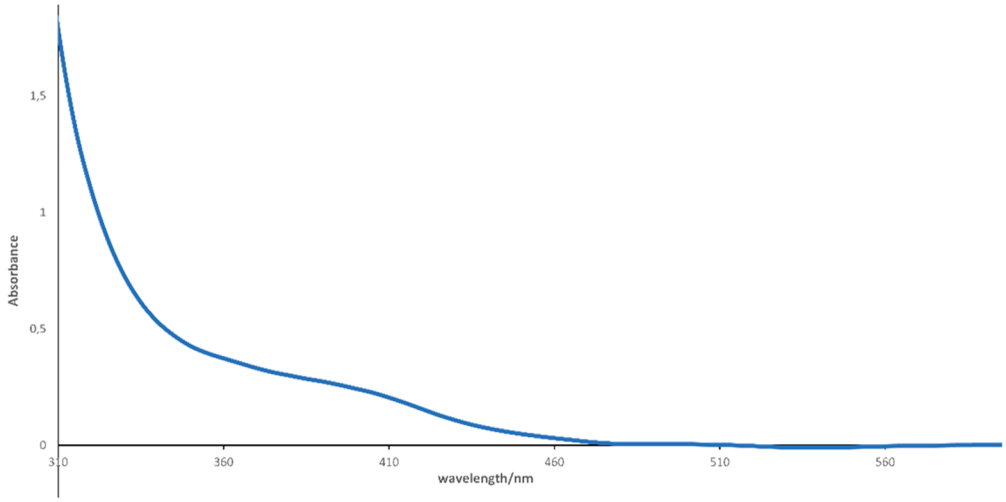


Figure A2-12: Uv-vis spectrum for [Pt(phen)(L^9-κS)$_2$] in methanol.

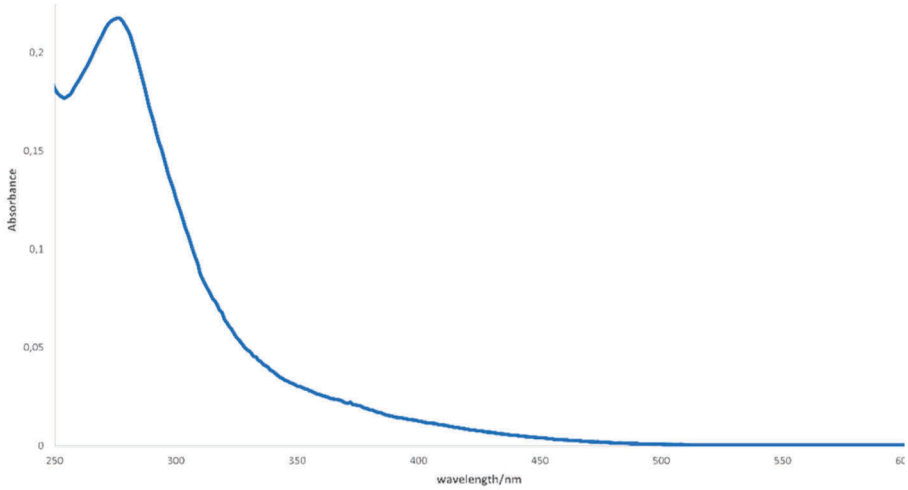


Figure A2-13: Uv-vis spectrum for [Pt(phen)(L^3-κS)$_2$] in methanol.

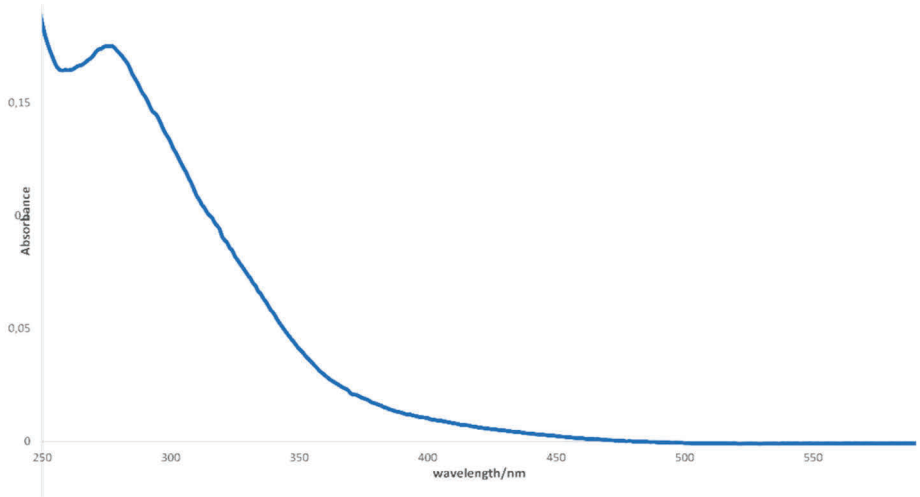


Figure A2-14: Uv-vis spectrum for [Pt(phen)(L^2-κS)$_2$] in methanol

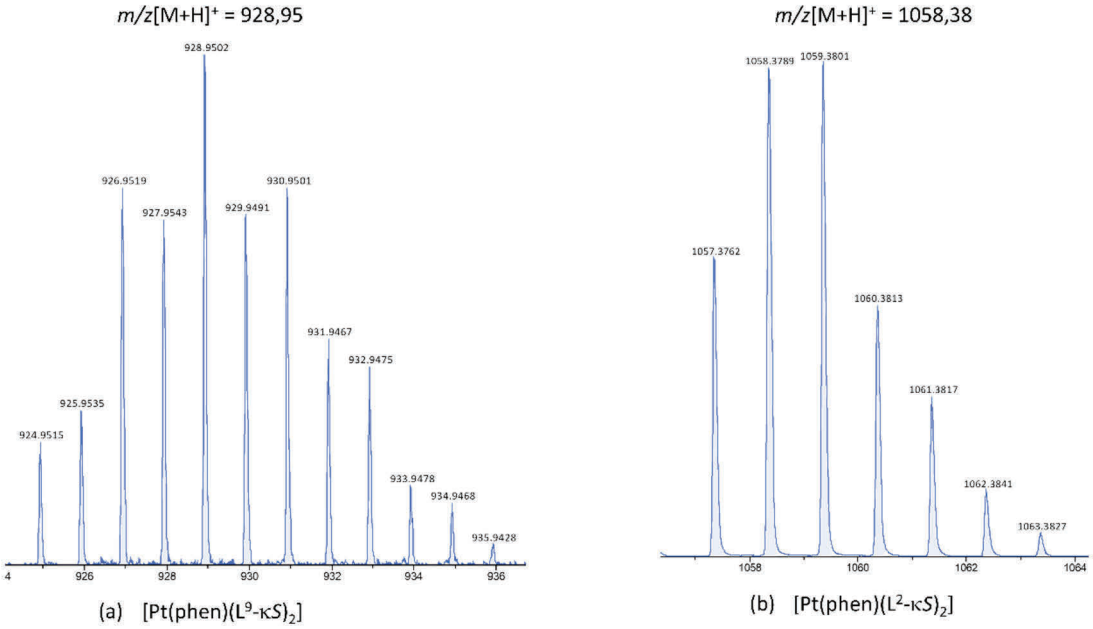


Figure A2-15: (+) ESI Mass spectra of [Pt(phen)(L^9-κS)$_2$], and [Pt(phen)(L^2-κS)$_2$] in methanol.

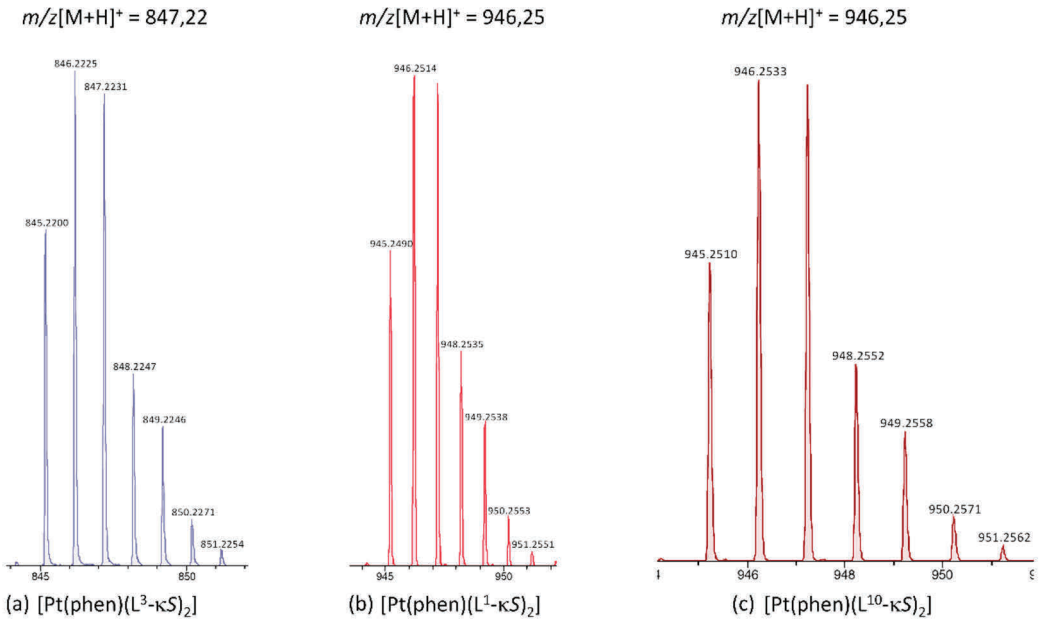


Figure A2-16: (+) ESI Mass spectra of [Pt(phen)(L^3-κS)$_2$], [Pt(phen)(L^1-κS)$_2$] and [Pt(phen)(L^{10}-κS)$_2$] in methanol.

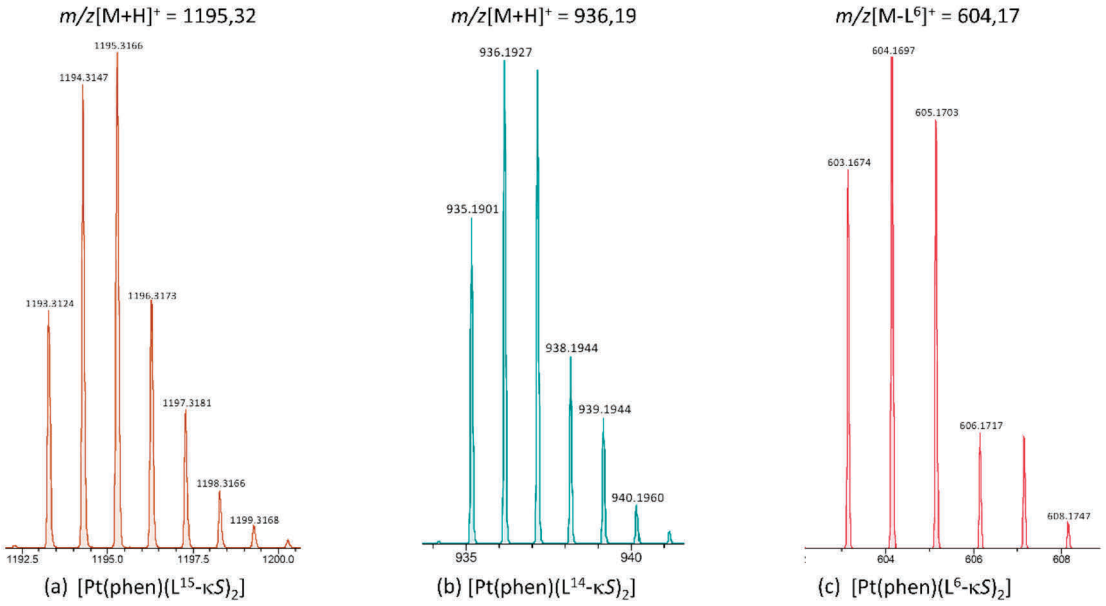


Figure A2-17: (+) ESI Mass spectra of [Pt(phen)(L^{15}-κS)$_2$], [Pt(phen)(L^{14}-κS)$_2$] and [Pt(phen)(L^{6}-κS)$_2$] in methanol.

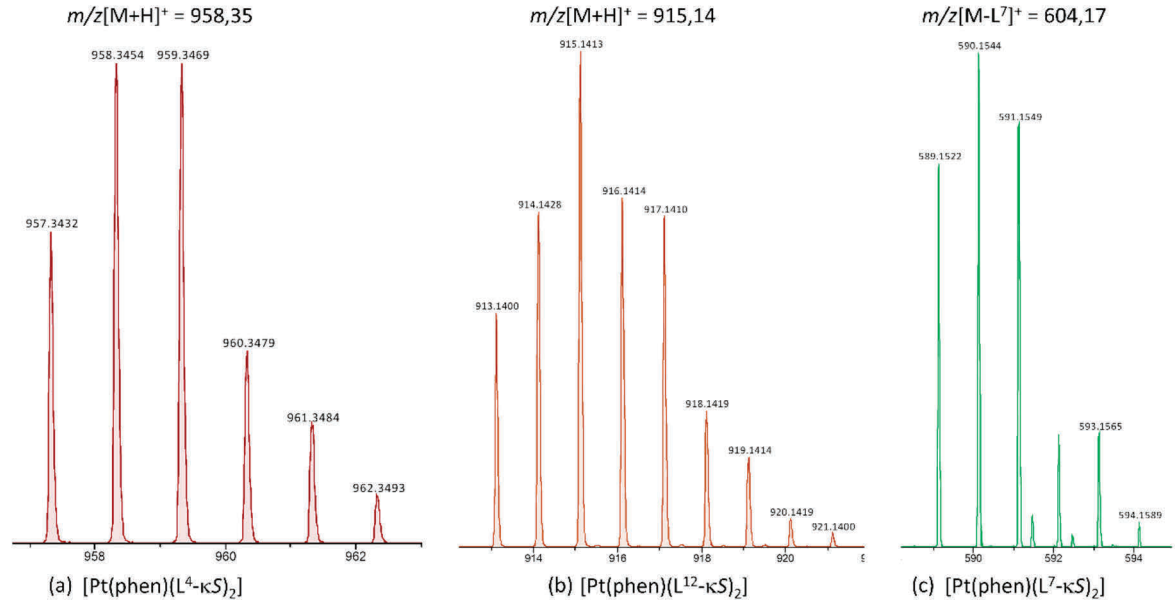


Figure A2-18: (+) ESI Mass spectra of [Pt(phen)(L^{4}-κS)$_2$], [Pt(phen)(L^{12}-κS)$_2$] and [Pt(phen)(L^{7}-κS)$_2$] in methanol.

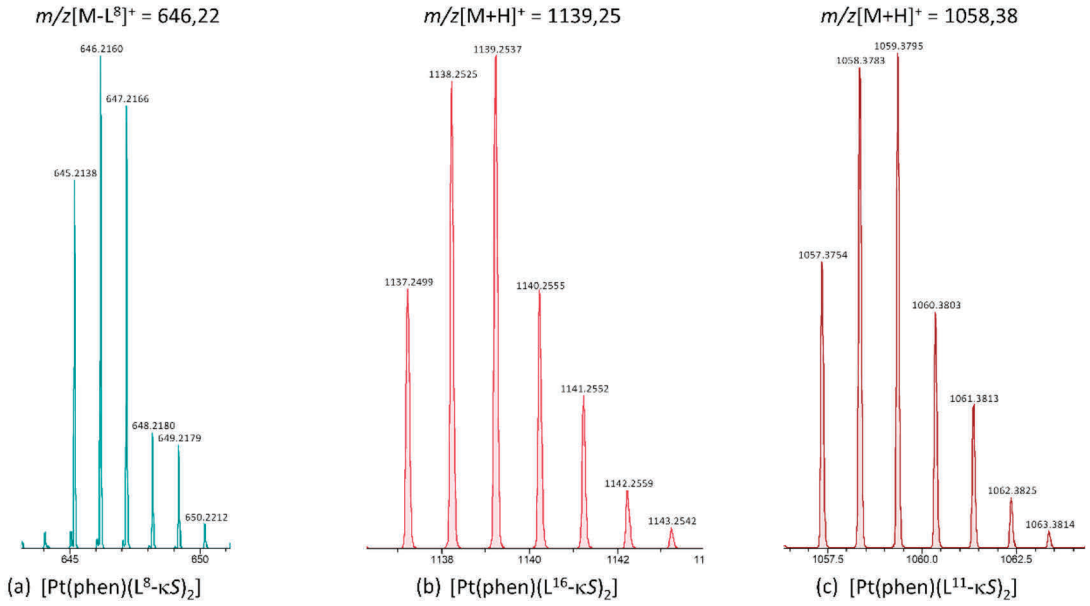


Figure A2-19: (+) ESI Mass spectra of [Pt(phen)(L^8-κS)$_2$], [Pt(phen)(L^{16}-κS)$_2$] and [Pt(phen)(L^{11}-κS)$_2$] in methanol.

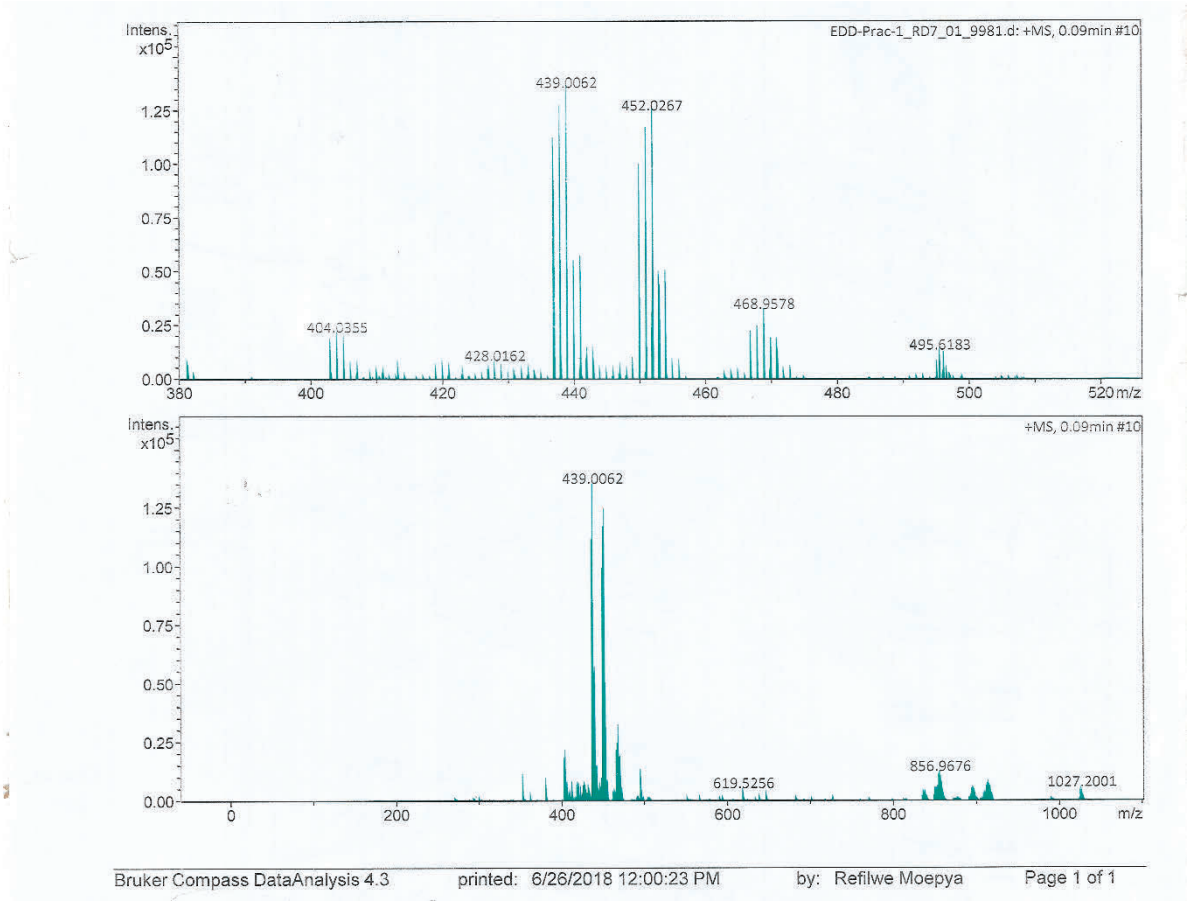


Figure A2-20: (+) ESI Mass spectrum of [PtCl$_2$(phen)] in methanol.

Appendix 3. Single crystal X-ray diffraction data for [Pt(phen)(L^n-κ*S*)$_2$] complexes

[Pt(phen)(L^1-κ*S*)$_2$]	Form I	Form II
Empirical formula	$C_{48}H_{50}N_6O_3PtS_2$	$C_{91}H_{98}N_{12}O_8Pt_2S_4$
Solvent(s)	(C_4H_8O)	(CH_3OH), H_2O
Formula weight	1018.15	2006.23
Crystal size [mm^{-3}]	0.1279 x 0.194 x 0.171	0.400 x 0.390 x 0.140
T [K]	173(2)	173(2)
System	Monoclinic	Monoclinic
Space group	$P2_1/n$	$P2_1$
a [Å]	13.9364(2)	12.1002(4)
b [Å]	18.6086(3)	21.8812(8)
c [Å]	16.7286(3)	16.8746(6)
α [°]	90	90
β [°]	94.5200(10)	109.1080(10)
γ [°]	90	90
V [A^{-3}]	4324.73(12)	4221.7(3)
Z	4	2
Density (calc.) [kg m^{-3}]	1.578	1.564
Absorption coeff.	3.474	3.391
Index ranges	$-18 \le h \le 18$	$-15 \le h \le 14$
	$-24 \le k \le 24$	$-27 \le k \le 27$
	$-22 \le l \le 22$	$-21 \le l \le 21$
Reflections collected	96 028	115 001
Independent reflections	10 442 [R_{int} = 0.0525]	18 416 [R_{int} = 0.0486]
Parameters	541	1071
Max./min. transmission	0.7334 and 0.4998	0.6619 and 0.3314
Goodness-of-fit on F^2	0.966	1.086
Largest difference peak and hole [e A^{-3}]	0.753 and -0.895	0.609 and -0.743
R_1 [$I > 2\sigma(I)$]	0.0225	0.0205
R_1 [all data]	0.0386	0.0219
wR_2 [$I > 2\sigma(I)$]	0.0425	0.0446
wR_2 [all data]	0.0450	0.0449

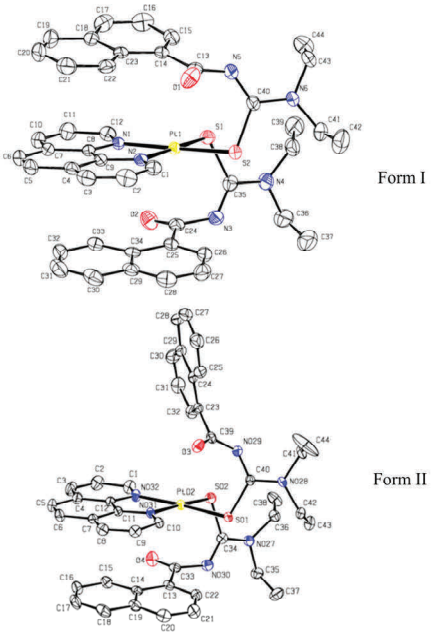


*Figure A3-1: X-ray crystallography data for [Pt(phen)(L^1-κ*S*)$_2$] form I and form II solvates.*

	[Pt(phen)(L^9-κ*S*)$_2$]	[Pt(phen)(L^{14}-κ*S*)$_2$]
Empirical formula	$C_{26}H_{28}Cl_6N_6O_2PtS_2$	$C_{36}H_{38}N_8O_7PtS_2$
Solvent(s)	n/a	H_2O
Formula weight	928.45	953.20
Crystal size [mm^{-3}]	0.309 x 0.108 x 0.038	0.482 x 0.149 x 0.138
T [K]	173(2)	173(2)
System	Triclinic	Monoclinic
Space group	*P -1*	*P 21/c*
a [Å]	9.8243(5)	16.6016(5)
b [Å]	12.7367(7)	15.7434(5)
c [Å]	15.0415(7)	14.2852(4)
α [°]	90.268(3)	90
β [°]	107.911(2)	97.4800(10)
γ [°]	111.533(2)	90
V [A^{-3}]	1651.16(15)	3701.89(19)
Z	2	8
Density (calc.) [kg m^{-3}]	1.867	1.712
Absorption coeff.	4.897	3.964
Index ranges	$-12 \le h \le 12$	$-21 \le h \le 21$
	$-16 \le k \le 16$	$-20 \le k \le 20$
	$-19 \le l \le 19$	$-18 \le l \le 18$
Reflections collected	34 442	40 862
Independent reflections	7936 [R_{int} = 0.1095]	8921 [R(int) = 0.0524]
Parameters	392	494
Max./min. transmission	0.8482 and 0.4124	0.7340 and 0.2746
Goodness-of-fit on F^2	0.952	1.000
Largest difference peak and hole [e A^{-3}]	2.977 and -2.037	0.912 and -0.527
R_1 [$I > 2\sigma(I)$]	0.0349	0.0225
R_1 [all data]	0.0511	0.0402
wR_2 [$I > 2\sigma(I)$]	0.0753	0.0458
wR_2 [all data]	0.0791	0.0622

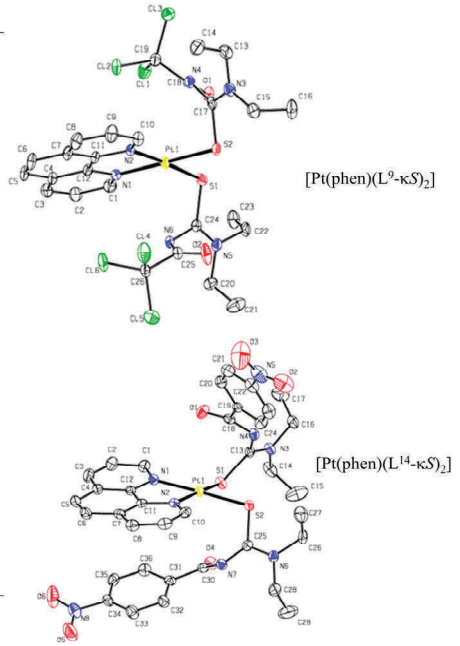


*Figure A3-2: X-ray crystallography data for [Pt(phen)(L^9-κ*S*)$_2$] and [Pt(phen)(L^{14}-κ*S*)$_2$] complexes.*

	[Pt(phen)(L^7-κ*S*)$_2$]	[Pt(phen)(L^3-κ*S*)$_2$]
Empirical formula	$C_{32}H_{50}N_6O_4PtS_2$	$C_{40}H_{50}N_6O_6PtS_2$
Solvent(s)	2(H_2O)	2(CH_3CH_2OH; H_2O)
Formula weight	841.99	974.11
Crystal size [mm^{-3}]	0.369 x 0.263 x 0.068	0.339 x 0.113 x 0.077
T [K]	173(2)	173(2)
System	Triclinic	Monoclinic
Space group	*P -1*	*P 2$_1$/c*
a [Å]	9.0104(3)	8.7448(2)
b [Å]	9.6554(4)	30.5493(6)
c [Å]	20.6529(8)	15.9872(3)
α [°]	94.167(2)	90
β [°]	92.638(2)	98.0830(10)
γ [°]	95.419(2)	90
V [A^{-3}]	1781.49(12)	4228.51(15)
Z	2	4
Density (calc.) [kg m^{-3}]	1.570	1.524
Absorption coeff.	4.099	3.469
Index ranges	$-11 \le h \le 11$ $-12 \le k \le 12$ $-27 \le l \le 27$	$-11 \le h \le 11$ $-40 \le k \le 40$ $-21 \le l \le 21$
Reflections collected	31 824	44 563
Independent reflections	8585 [R_{int} = 0.1017]	10509 [R_{int} = 0.1111]
Parameters	416	554
Max./min. transmission	0.7738 and 0.3483	n/a
Goodness-of-fit on F^2	0.865	0.970
Largest difference peak and hole [e A^{-3}]	1.430 and -1.673	2.924 and -1.698
R_1 [$I > 2\sigma(I)$]	0.0272	0.0486
R_1 [all data]	0.0336	0.0879
wR_2 [$I > 2\sigma(I)$]	0.0627	0.0921
wR_2 [all data]	0.0648	0.1010

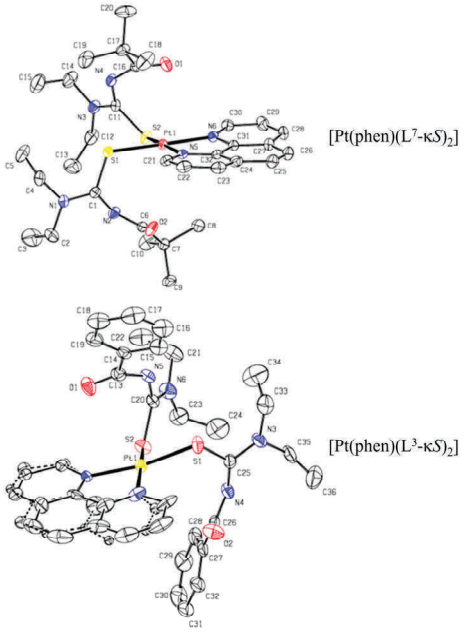


*Figure A3-3: X-ray crystallography data for [Pt(phen)(L^7-κ*S*)$_2$] and [Pt(phen)(L^3-κ*S*)$_2$] complexes.*

	[Pt(phen)(L^{12}-κ*S*)$_2$]	[Pt(bipy)(L^{10}-κ*S*)$_2$]
Empirical formula	$C_{36}H_{36}Cl_2N_6O_2PtS_2$	$C_{42}H_{42}N_6O_2PtS_2$
Solvent(s)	n/a	n/a
Formula weight	914.82	922.02
Crystal size [mm^{-3}]	0.445 x 0.068 x 0.047	0.301 × 0.294 × 0.273
T [K]	173(2)	173(2)
System	Monoclinic	Monoclinic
Space group	*P 2$_1$/n*	*P2$_1$/n*
a [Å]	18.7234(3)	9.6096(8)
b [Å]	9.72750(10)	13.7777(11)
c [Å]	20.5675(3)	28.903(2)
α [°]	90	90
β [°]	104.9750(10)	90.644(2)
γ [°]	90	90
V [A^{-3}]	3618.78(9)	3826.4(5)
Z	4	4
Density (calc.) [kg m^{-3}]	1.679	1.601
Absorption coeff.	4.183	3.821
Index ranges	$-24 \le h \le 24$ $-12 \le k \le 12$ $-27 \le l \le 27$	$-12 \le h \le 12$ $-18 \le k \le 18$ $-38 \le l \le 38$
Reflections collected	69 157	52 093
Independent reflections	8735 [R_{int} = 0.0621]	9543 [R_{int} = 0.0382]
Parameters	446	530
Max./min. transmission	0.8462 and 0.3810	n/a
Goodness-of-fit on F^2	0.906	1.099
Largest difference peak and hole [e A^{-3}]	0.739 and -0.520	1.54 and -0.61
R_1 [$I > 2\sigma(I)$]	0.0231	0.0228
R_1 [all data]	0.0399	0.0275
wR_2 [$I > 2\sigma(I)$]	0.0395	0.0496
wR_2 [all data]	0.0419	0.0511

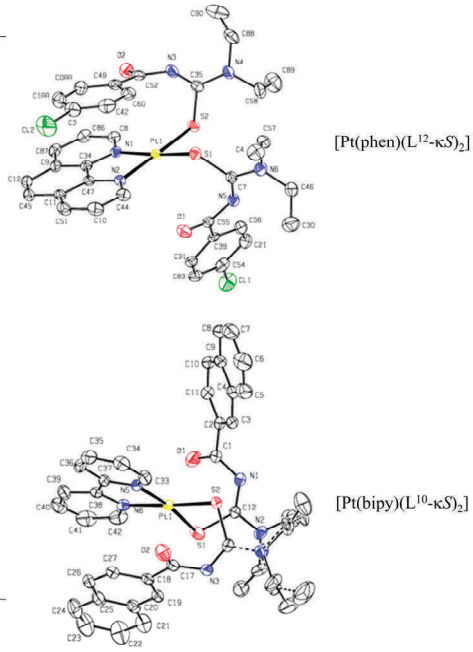


*Figure A3-4: X-ray crystallography data for [Pt(phen)(L^{12}-κ*S*)$_2$] and [Pt(phen)(L^{10}-κ*S*)$_2$] complexes.*

	[Pt(phen)(L^6-κ*S*)$_2$]	[Pt(phen)(L^4-κ*S*)$_2$]
Empirical formula	$C_{34}H_{50}N_6O_2PtS_2$	$C_{44}H_{54}N_6O_2PtS_2$
Solvent(s)	3(H_2O)	H_2O
Formula weight	888.05	976.15
Crystal size [mm^{-3}]	0.414 × 0.371 × 0.064	0.466 × 0.168 × 0.054
T [K]	173(2)	173(2)
System	triclinic	triclinic
Space group	*P-1*	*P-1*
a [Å]	8.0094(4)	9.5769(6)
b [Å]	10.8729(6)	10.5395(6)
c [Å]	23.3135(14)	21.8649(13)
α [°]	100.485(4)	79.4613(16)
β [°]	98.327(4)	78.8638(16)
γ [°]	92.747(4)	84.6404(17)
V [A^{-3}]	1969.56(19)	2125.0(2)
Z	2	2
Density (calc.) [kg m^{-3}]	1.497	1.526
Absorption coeff.	3.714	3.447
Index ranges	$-9 \le h \le 10$	$-12 \le h \le 12$
	$-13 \le k \le 13$	$-13 \le k \le 14$
	$-23 \le l \le 29$	$-28 \le l \le 29$
Reflections collected	17 507	31 642
Independent reflections	8111 [R_{int} = 0.0467]	10449 [R_{int} = 0.0319]
Parameters	609	512
Max./min. transmission	0.8794 and 0.4005	0.8616 and 0.4301
Goodness-of-fit on F^2	1.025	1.040
Largest difference peak and hole [e A^{-3}]	1.36 and -1.73	0.93 and -0.79
R_1 [$I > 2\sigma(I)$]	0.0681	0.0258
R_1 [all data]	0.1167	0.0329
wR_2 [$I > 2\sigma(I)$]	0.1715	0.0497
wR_2 [all data]	0.2017	0.0515

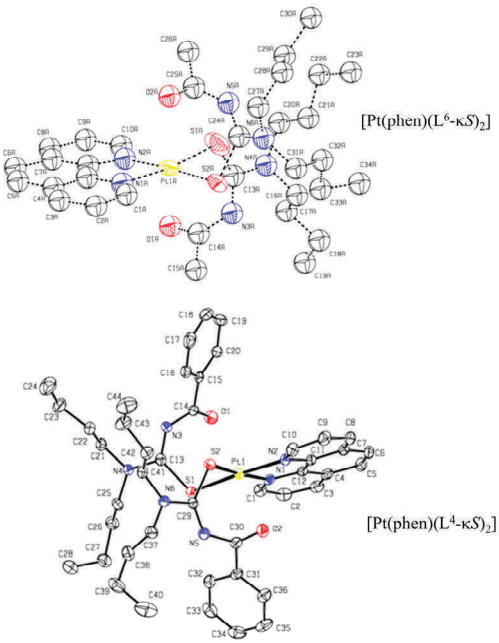


Figure A3-5: X-ray crystallography data for [Pt(phen)(L^6-κS)$_2$] and [Pt(phen)(L^4-κS)$_2$] complexes.

	[Pt(PPh$_3$)(L^1-κ*O*,*S*)(L^1-κ*S*)]	[Co(phen)(L^1-κ*O*,*S*)$_2$]
Empirical formula	$C_{50}H_{49}N_4O_2PPtS_2$	$C_{44}H_{42}CoN_6O_2S_2$
Solvent(s)	n/a	n/a
Formula weight	1028.11	809.88
Crystal size [mm^{-3}]	0.274 x 0.134 x 0.078	0.264 × 0.093 × 0.057
T [K]	173(2)	173(2)
System	Monoclinic	monoclinic
Space group	*P 2$_1$/c*	*P2$_1$/c*
a [Å]	10.4789(2)	17.1901(7)
b [Å]	14.1407(3)	11.6591(5)
c [Å]	29.9104(6)	21.3648(8)
α [°]	90	90
β [°]	91.8950(10)	113.358(2)
γ [°]	90	90
V [A^{-3}]	4429.67(15)	3931.0(3)
Z	4	4
Density (calc.) [kg m^{-3}]	1.542	1.368
Absorption coeff.	3.343	0.589
Index ranges	$-13 \le h \le 13$	$-20 \le h \le 20$
	$-18 \le k \le 18$	$-13 \le k \le 13$
	$-38 \le l \le 36$	$-25 \le l \le 25$
Reflections collected	74 008	28 163
Independent reflections	9677 [R_{int} = 0.0728]	6844 [R_{int} = 0.1119]
Parameters	545	496
Max./min. transmission	0.8252 and 0.4624	0.7457 and 0.6728
Goodness-of-fit on F^2	0.955	0.998
Largest difference peak and hole [e A^{-3}]	0.621 and -0.869	0.32 and -0.31
R_1 [$I > 2\sigma(I)$]	0.0234	0.0483
R_1 [all data]	0.0315	0.1144
wR_2 [$I > 2\sigma(I)$]	0.0479	0.0766
wR_2 [all data]	0.0493	0.0939

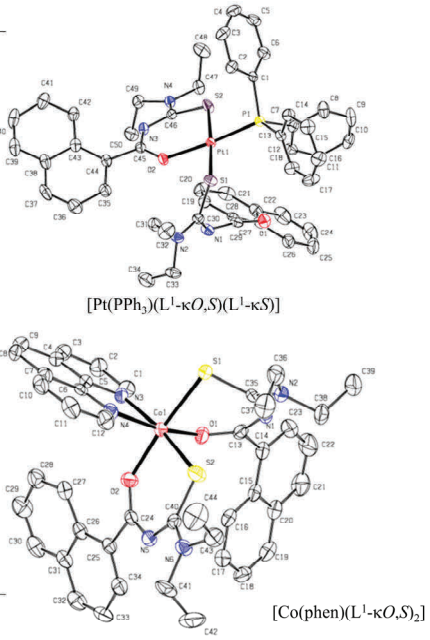


Figure A3-6: X-ray crystallography data for [Pt(PPh$_3$)(L^1-κO,S)(L^1-κS)] and [Co(phen)(L^1-κO,S)$_2$] complexes.